NASA CONTRACTOR REPORT

NASA CR-2785

POLLUTANT FORMATION IN FUEL LEAN RECIRCULATING FLOWS

Robert W. Schefer and Robert F. Sawyer

Prepared by
UNIVERSITY OF CALIFORNIA, BERKELEY
Berkeley, Calif. 94720
for Lewis Research Center

NATIONAL AERONAUTICS AND SPACE ADMINISTRATION • WASHINGTON, D. C. • DECEMBER 1976

TABLE OF CONTENTS

LIST OF FIGURES

LIST OF TABLES

NOMENCLATURE

A	pre-exponential factor
a	reaction order with respect to propane
b	reaction order with respect to oxygen
c_p	specific heat
D	combustor diameter, cm
d	effective thermocouple diameter, cm
D_i	mass diffusivity of ith specie
E	activation energy, cal/g mole
ΔH_f	heat of formation
h	stagnation enthalpy
$\overline{J}$	mass flux vector
K	constant in effective viscosity expression
k	reaction rate constant
k_G	combustion gas thermal conductivity
k_+	turbulent kinetic energy
L	length of flow field
ℓ	turbulent mixing length
m_i	mass fraction specie i
$\dot{m}$	mass flow rate
MW	molecular weight
N	number of iterations
Nu	Nusselt number
n	normal distance from wall
Pr	Prandtl number
p	pressure
q	heat flux vector

R_i	reaction rate species i
R_u	universal gas constant
Re	Reynolds number
r	radial distance
s	constant in velocity profile expression
T	temperature
T_{TC}	thermocouple temperature
T_G	combustion gas temperature
V	inlet velocity
ν	velocity
$\bar{\nu}$	time smoothed velocity
ν'	velocity fluctuation
z	axial distance
[	exchange coefficient
ε	emissivity
μ	viscosity
ρ	density
σ	Stefan-Boltzman constant
σ_i	Schmidt number specie i
σ_h	Prandtl number
τ	residence time
$\bar{\bar{\varepsilon}}$	stress tensor
Φ	equivalence ratio
ϕ	dependent variable
ω	vorticity
Ψ	stream function
α_{UR}	under-relaxation parameter

Subscripts

eff	effective
i	ith specie
h	enthalpy
j	jet stream
mix	mixture
p	primary stream
o	reference quantity
r	radial direction
z	z direction
ϕ	dependent variable ϕ

Superscripts

t	turbulent
l	laminar

CHAPTER 1

Introduction

Combustion of fossil fuels currently supplies more than 98% of the United States energy needs. While the development of alternative energy sources such as nuclear, solar, and geothermal should increase their importance in future years, it will be some time before fossil fuel combustion is replaced as our dominant source of energy. An estimate by Starr[1] indicates that by the year 2000 only 17% of the total United States energy needs will be supplied by these alternate sources. Unfortunately combustion processes involving fossil fuels are also major contributors to pollutant emissions. The fraction of total emissions attributable to combustion is shown in Table 1-1. Since it is unlikely that combustion will be eliminated as a major energy source in the near future it is imperative that methods of controlling pollutant formation in various combustion processes be developed.

TABLE 1-1. Contribution of Combustion Sources to Pollutant Emissions[2].

carbon monoxide	89%
hydrocarbons	89%
polynuclear aromatics	93%
oxides of nitrogen	98%
oxides of sulfur	76%
particulates	73%

Aircraft engines represent a relatively small contributor to the total air pollution problem (Table 1-2). On a local basis,

TABLE 1-2. Aircraft Contributions to Air Pollution, Percent of Total[3].

	CO	HC	NO_x	Particulate	SO_x
United States, 1968	2.4	0.9	1.7	0.1	0.03
New York City, 1968	0.6	0.6	0.2	0.2	-
Los Angeles, 1970	1.5	3.2	1.4	11.5	2.0
San Francisco, 1970	1.0	1.5	1.3	6.6	1.0
San Francisco, 1985	10.9	3.5	11.6	9.3	2.2

however, the growth of air traffic combined with control of other pollutant sources could make aircraft (which are primarily powered by gas turbine type combustors) a significant source of pollution. This is particularly applicable in the immediate vicinity of an airport and in urban air basins containing larger airports. The gas turbine engine has also been mentioned as an alternative power source for ground transportation and stationary power generation[4, 5]. Its development as such could significantly change its role as a minor source of air pollution.

The possible impact of high altitude aircraft emissions on the earth's ozone layer has recently been realized[6]. This ozone layer is responsible for filtering out harmful untraviolet radiation from the sun's rays. Some scientists have claimed that the addition of a relatively small amount of NO_x could result in a significant depletion of the ozone in the layer[7]. Crutzen[8] has proposed a catalytic cycle involving the following reactions

$$NO + O_3 \rightarrow NO_2 + O_2$$

$$\underline{NO + O \rightarrow NO + O_2}$$

$$\text{NET: } O_3 + O \rightarrow 2\,O_2$$

The net effect is the destruction of ozone while the total amount of NO_x is conserved. Under such considerations the control of NO_x emissions from gas turbine type engines takes on a special importance.

Typical exhaust emission data for a commercial jet engine are shown in Figure 1-1. Both unburned hydrocarbons (UHC) and CO are high at low power settings, whereas NO_x is highest during take-off. Inefficient combustion, as reflected by high levels of UHC and CO, is the result of inadequate burning rates in the primary combustion zone followed by thermal quenching of oxidation reactions involving intermediate hydrocarbon species and CO in cooler downstream regions and near the combustor walls. This thermal quenching at low power settings is primarily the result of 1) poor fuel atomization at low fuel flow rates, 2) low primary fuel-air ratios, and 3) low combustor inlet temperature and pressure[10]. Each can be reduced by providing sufficiently high temperatures and long residence times.

NO_x formation on the other hand is almost solely determined by maximum flame temperatures existing in the combustion zone. This strong dependence on flame temperature is shown in Figure 1-2. NO_x emissions from a number of different gas turbines are found to correlate quite well with the maximum local temperature in the combustor (assuming stoichiometric combustion). Residence time also has an effect, although somewhat smaller. Thus most attempts to control NO_x formation involve reductions in the flame temperature.

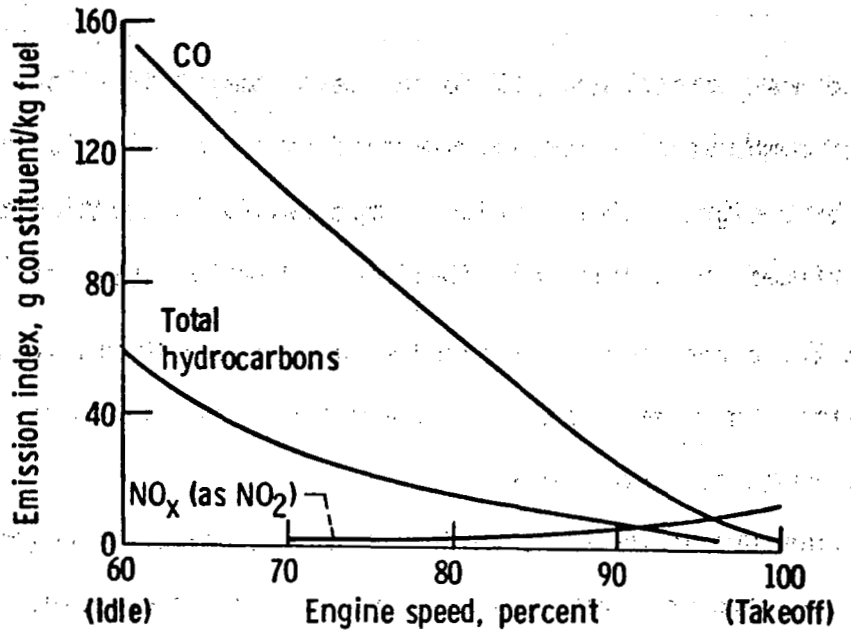

Figure 1-1. Typical engine emission characteristics. Engine pressure ratio, 13.4; fuel, JP-5.[9]

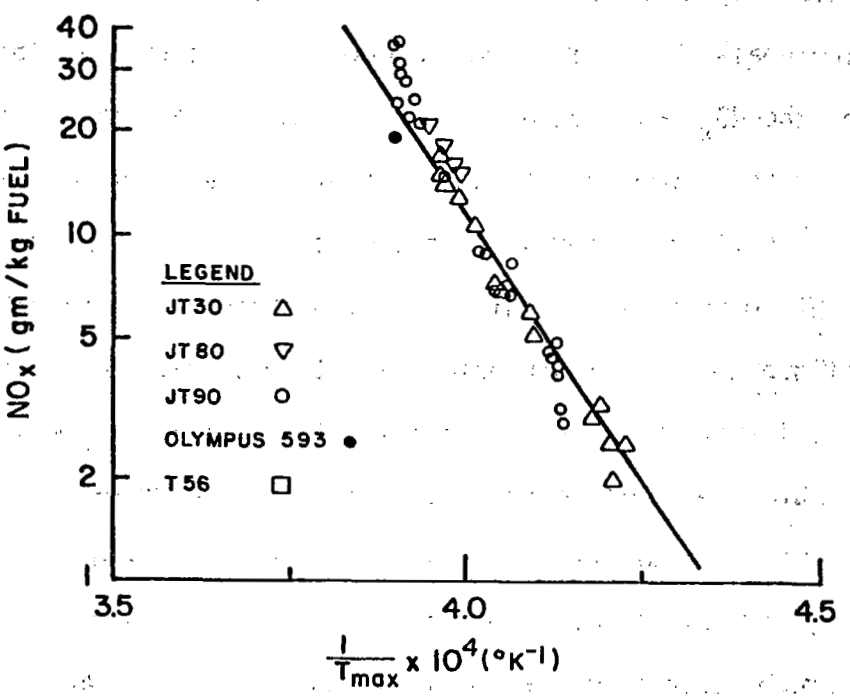

Figure 1-2. Arrhenius plot of oxides of nitrogen emissions index (reported as NO_2). Temperature refers to maximum local combustor temperature based on adiabatic, stoichiometric combustion.[11]

The most direct approach to the development of a low emission combustor is through minor modification of existing combustor designs. This involves improved fuel injection techniques, changes in airflow distribution, and water injection [12, 13]. The resulting design is a compromise with regard to the various pollutants and other aspects of combustor performance with a limited range for improvement.

A more promising approach is the development of new advanced design combustor concepts. These include variable geometry, staged combustion, and premixing of fuel and air[12]. Preliminary combustor designs incorporating these concepts under the NASA Clean Combustor Program have either achieved or closely approached idle emission goals for CO and UHC. However, all combustors failed to meet the NO_x emission goal of 15 g NO_2/kg fuel during takeoff[9].

A further problem with NO_x control can be expected for supersonic aircraft operating under cruise conditions. In subsonic flight NO_x emissions at cruise conditions are less than those at takeoff due to the low ambient temperature at high altitudes. This results in a low combustor inlet temperature and a low flame temperature. NO_x emissions at takeoff thus represent an upper limit on expected NO_x emissions. For supersonic aircraft however, combustor inlet temperature increases significantly with flight mach number and can result in an increase in NO_x emissions. Combustion efficiencies approaching 100% are commonly attained for both subsonic and supersonic aircraft under cruise conditions

Of the various advanced concepts being developed to reduce NO_x emissions perhaps those holding the greatest promise involve lean premixed combustion with fuel prevaporization[14]. Premixing and prevaporization provide a uniform mixture of fuel and air to the combustion zone. This eliminates locally fuel rich mixtures and low temperature regions associated with soot formation and high levels of UHC and CO. Also eliminated are locally stoichiometric mixtures and the associated high temperatures and NO production rates. Since high inlet temperatures are desirable to aid in fuel prevaporization and are necessary in the automotive application of gas turbines due to regeneration, low combustion temperatures and NO_x control are attained through lean inlet fuel air mixtures. In a premixed/prevaporized system no time is required for fuel vaporization and fuel-air mixing. Thus it should be possible to minimize the high temperature residence time without reducing combustor efficiency. This provides a further means of limiting NO_x production. A secondary advantage of premixed/prevaporized systems is a more uniform turbine inlet temperature, thus eliminating local hot spots on turbine blades. It is with this means of NO_x emission control, namely premixed lean combustion with elevated inlet temperatures, that the present investigation is concerned.

The effect of primary zone uniformity on nitric oxide production has been studied by Fletcher and Heywood[15] based on a statistical evaluation of the primary zone equivalence ratio distribution.

The greater control over NO_x emissions possible in a premixed system can be seen from Figure 1-3. Injection of liquid fuel as a spray into the combustion zone results in a wide variation in local fuel air ratio and a greatly reduced sensitivity of NO_x formation to overall equivalence ratio. By providing a uniform fuel-air mixture to the combustion zone a very strong dependence of NO_x formation on equivalence ratio is found. This results in a significantly greater potential to control NO_x emissions through stoichiometry than is possible with conventional combustors.

It should be noted a practical limit exists on the amount by which NO_x emissions can be reduced. The above combustor design concepts involve control of combustion temperature, and to a lesser extent combustor residence time, to minimize emissions at all operating conditions. As mentioned previously the oxidation rates of UHC and CO depend on temperature as does the NO formation rate. As a result for a given residence time, only a finite range of temperatures exist where both NO_x and CO can be maintained at relatively low levels. This is shown in Figure 1-4 for a hypothetical combustor. The limits for CO and NO_x shown in the graph correspond to 1977 automotive standards for a fuel consumption of 4.25 km/ℓ. UHC emissions closely follow the trends shown for CO.

The combustor chosen for this study is an opposed reacting jet (ORJ). The ORJ is shown in Figure 1-5. It consists of a main premixed stream of fuel and air, and a smaller stream of premixed fuel and air injected along the centerline and in a direction opposite to the main stream. The result is the formation of a

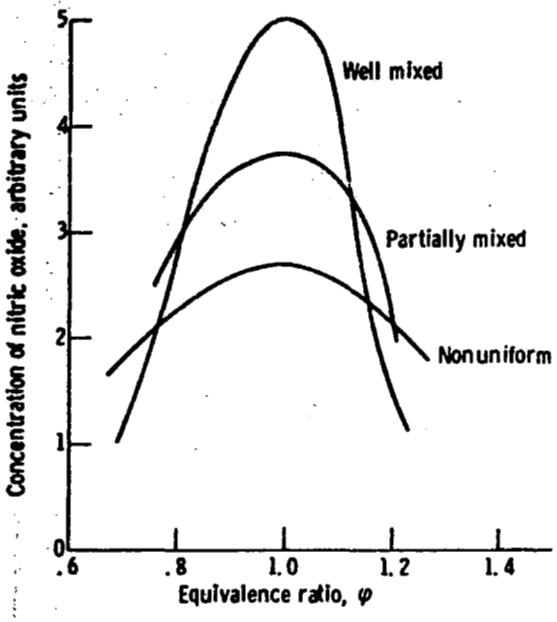

Figure 1-3. Variation of nitric oxide concentration with equivalence ratio distribution.[9]

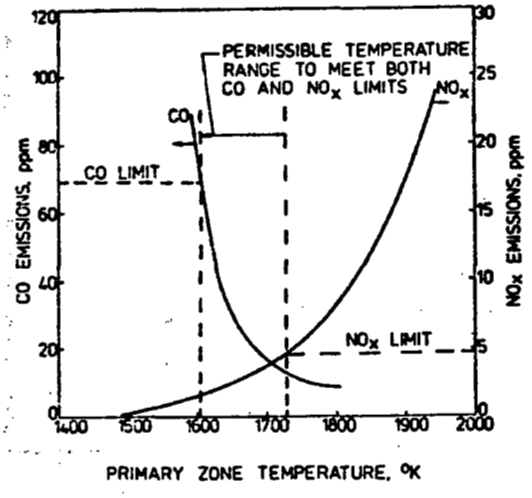

Figure 1-4. Influence of primary-zone temperature on CO and NO_x emissions.[12]

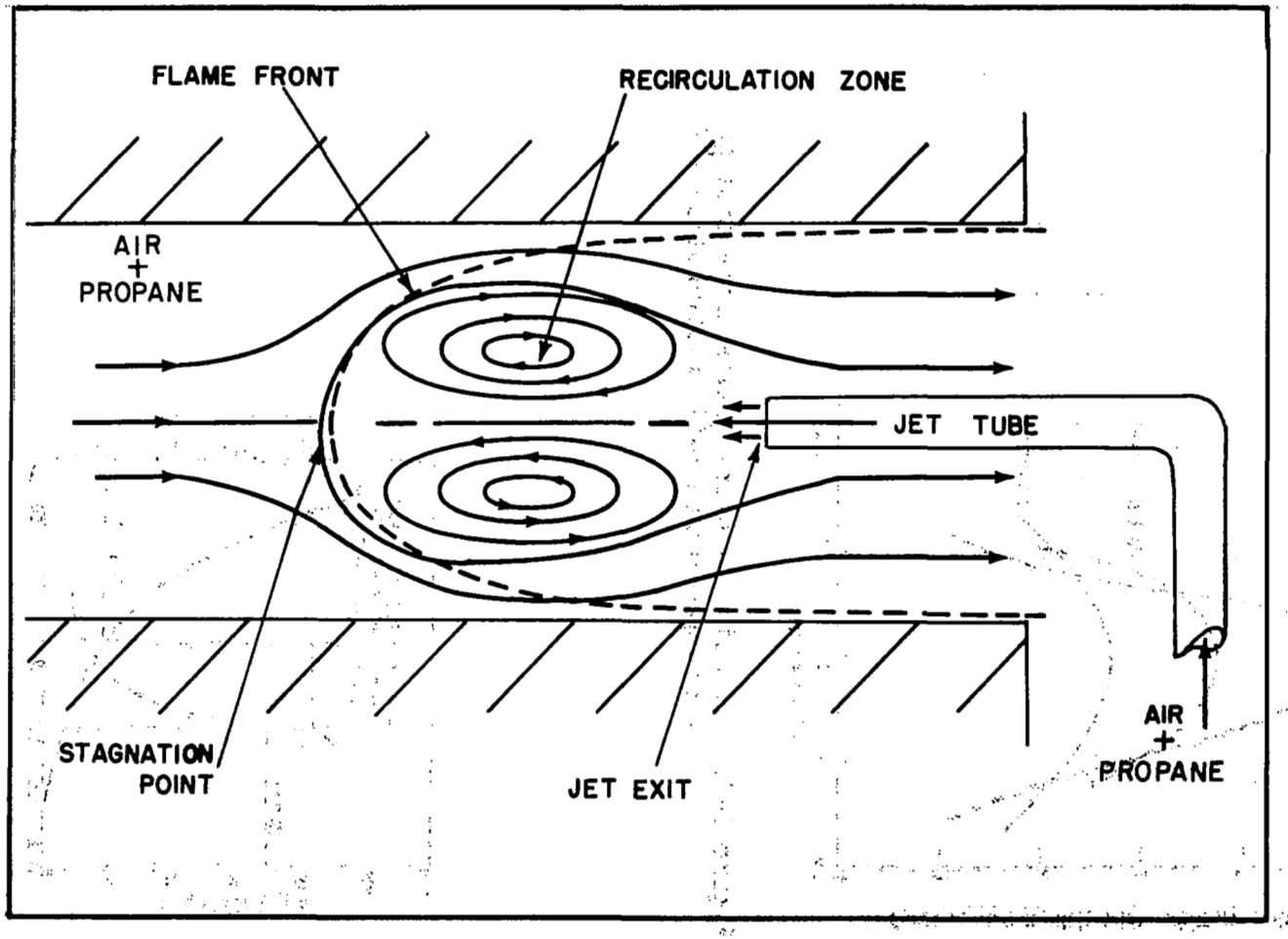

Figure 1-5. Opposed reacting jet flowfield.

stagnation region and a zone of strongly recirculating combustion gases. This recirculation of hot partially burned combustion gases back upstream into the flame zone allows stabilization of a flame at velocities significantly higher than the flame velocity associated with inlet conditions.

The ORJ has several advantages which make it adaptable to an investigation of the elementary processes governing pollutant formation. These are primarily due to the simplified geometry and flowfield it provides. In a more complex combustor configuration such as encountered in many full scale combustors separation of fluid mechanical and chemical kinetic aspects of the combustion process is extremely difficult. A model combustor such as the ORJ facilitates this process by providing greater control over those parameters which most affect pollutant formation. These include equivalence ratio, inlet temperature, and recirculation zone size. The axisymetric geometry of the ORJ also simplifies the specification of boundary conditions and the choice of a grid network for the numerical finite difference calculations which are discussed in Chapter 4.

The existence of a recirculation zone provides a relation between the ORJ and most real combustor systems. In a typical gas turbine type combustor recirculation into the primary combustion zone is controlled by secondary air injection through circumferentially located holes in the combustor walls, swirler vanes located at the upstream end of the combustor, or a combina-

tion of these. A schematic of the resulting flowfields for a conventional combustor and two advanced design combustors are shown in Figure 1-6. Most advanced combustor designs are provided with a capability for premixing fuel and air in an optimum ratio to limit pollutant formation, but flame stabilization in the primary combustion zone is still provided by recirculation. Thus a fundamental study of pollutant formation in a simplified recirculation zone such as that provided by the ORJ has direct application to most gas turbine type combustors.

Propane (C_3H_8) was selected as a fuel in the present investigation. This lead to difficulties in the kinetic modeling part of the investigation due to uncertainties in the high temperature propane oxidation mechanism. However, propane was felt to be more typical of the higher hydrocarbon constituents found in aircraft fuels such as JP-4 than perhaps methane which is better understood kinetically but less realistic as an aircraft fuel.

A comparison of operating conditions in the model ORJ combustor of the present investigation with those in several current and proposed gas turbine combustors is shown in Table 1-3. It can be seen that both the maximum combustor inlet temperature (600° K) used in the present investigation and the combustor exit temperatures attained are comparable to those encountered in full scale gas turbine combustors. Equivalence ratios given for the full scale combustors represent overall values, including dilution air, and are therefore not directly comparable with the values used in this investigation. Actual combustion in current full scale combustors occurs at more nearly stoichiometric conditions.

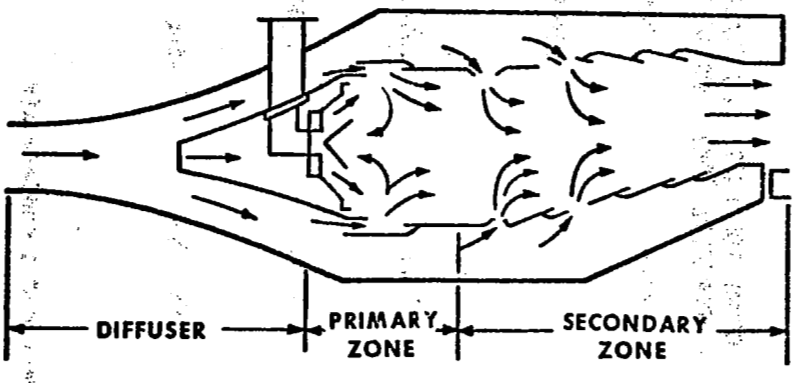

a) Conventional combustor

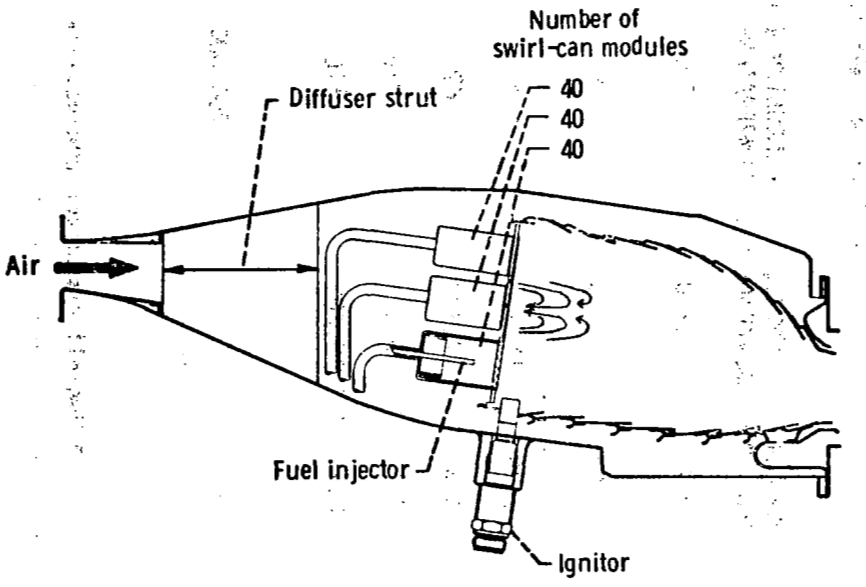

b) NASA modular swirl can combustor[8]

Figure 1-6. Typical gas turbine combustor schematic diagrams showing location of recirculation zones for flame stabilization.

TABLE 1-3. REPRESENTATIVE OPERATING CONDITION COMPARISON OF PRESENT AND PROPOSED GAS TURBINE COMBUSTORS[9].

COMBUSTOR	CRUISE MACH. NO.	CRUISE ALTITUDE (m)	COMBUSTOR INLET TEMPERATURE (°K)	COMBUSTOR INLET PRESSURE (atm)	COMBUSTOR EXIT TEMPERATURE (°K)	EQUIVALENCE RATIO, ϕ	FUEL
Pratt & Whitney JT9D	0.85	10,700	710	9.7	1410	.018*	JP-4
Future Turbofans (subsonic)	0.85	12,200	661	7.2	1540	.026*	JP-4
RB 211	0.85	10,670	703	10.1	-	-	JP-4
Olympus 593	2.0	17,700	824	6.5	1320	.0141*	JP-4
GE-4/J5P	2.7	19,810	866	5.4	-	-	JP-4
Future duct burning turbofans (supersonic)	2.7	19,800	810	4.7	1770	.0299*	JP-4
This study	-	-	300-600	1.0	1400-1900	0.45-0.625	Propane

* Overall combustor equivalence ratio, includes primary and secondary air

The pressure in the model ORJ combustor is significantly lower than in full scale combustors. However the primary effect of a higher inlet pressure on the combustion process is through an increase in flame temperature. Thus an increase in pressure could be expected to reduce both UHC and CO levels and increase the NO_x levels measured in this study. A premixed/prevaporized system achieves emission reductions primarily through combustion temperature control. As mentioned above, the temperature range investigated is similar to that which would be encountered in full scale gas turbine combustors. The effect of higher inlet pressures under actual operating conditions would be compensated for by a decrease in equivalence ratio and therefore emission levels could be expected to be similar in the model ORJ combustor and full scale premixed/prevaporized systems.

In Chapters 4 and 5 an analytical modeling technique is described and the predicted results from this model are compared with experimental results in an attempt to evaluate the usefulness of his model in predicting flowfield property and species concentration distributions. Combustor design development has usually involved somewhat of an empirical trial and error approach in which previous experience and experimental data on full scale combustors are used to modify existing designs until the desired results with respect to combustor performance or emission levels is achieved. Such an approach however can be quite time consuming and expensive.

Much of the time consuming experimental work associated with this approach can be eliminated by utilizing the predictions of analytical modeling techniques. This can be done only if such modeling techniques can be demonstrated to yield accurate predictions of combustor performance for the complicated flowfields characteristically found in practical gas turbine combustors.

CHAPTER 2

EXPERIMENTAL INVESTIGATION

The experimental part of this investigation deals with the measurement of detailed composition and temperature profiles in an opposed reacting jet combustor operating under fuel lean conditions. The present chapter describes the experimental equipment and procedures associated with this investigation. The combustor test facility is described in section 2.1. Section 2.2 discusses the selection and fabrication of analytical equipment associated with the composition and temperature measurements.

2.1. Experimental Facility

A schematic diagram of the experimental apparatus is shown in Figure 2-1. Air is supplied by the house air system. The humidity of the incoming air is measured continuously and found to remain constant at 0.00151 gm H_2O/gm air. Installation of six 6-Kw resistance heaters provide control over the reactant inlet temperature up to approximately 700 K. Propane and main stream are mixed upstream of the combustor test section in a venturi section. The flow then passes down a 1.0 meter long straightening section to assure a fully developed velocity profile and uniform composition. Measurements were made of the radial velocity profile at the test section inlet using a stagnation pressure probe in conjunction with a static pressure tap in the wall. The velocity profile indicated

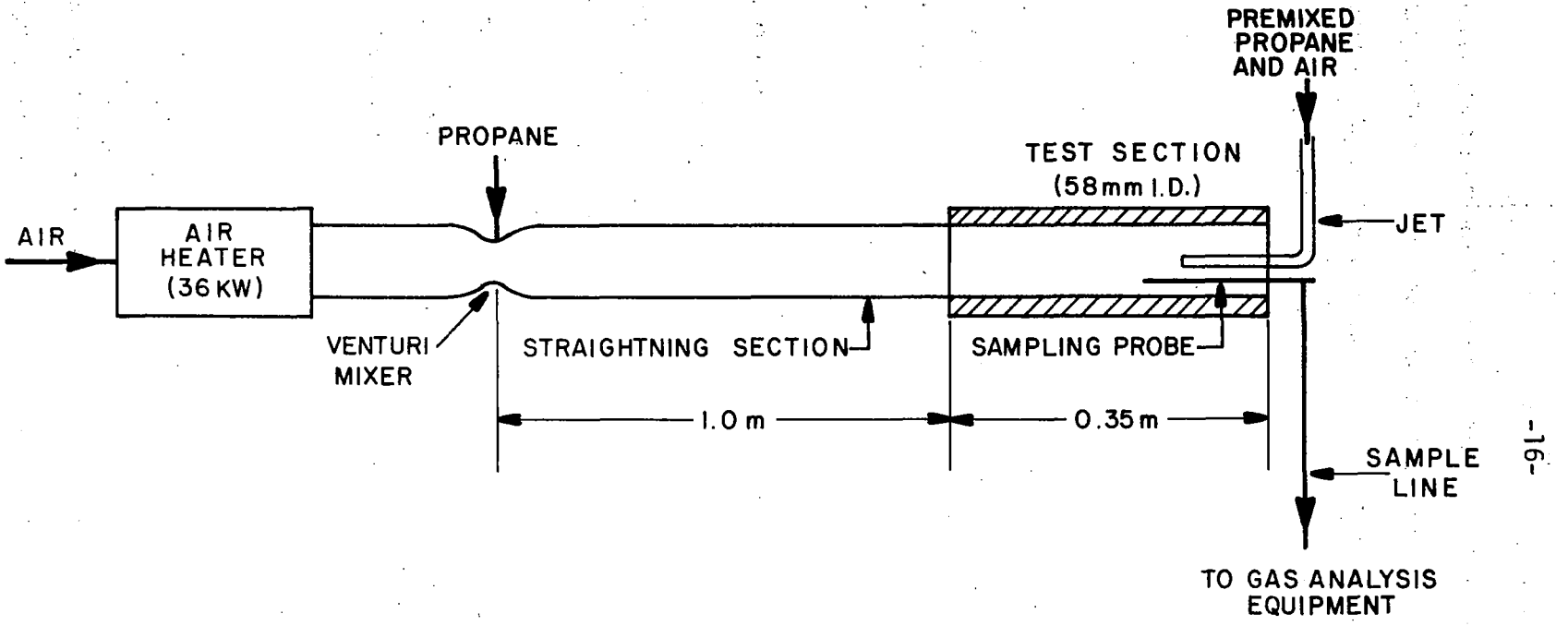

Figure 2-1. Experimental facility.

turbulent flow exists under the entire range of experimental conditions ($Re > 10^4$). Composition measurements using a quartz sampling probe and a mass spectrometer for analysis of N_2, O_2 and C_3H_8 showed that the venturi mixer is effective in producing a uniform composition profile at the test section inlet.

The combustor test section is shown in Figure 2-2. The test section consists of a 58 mm I.D. x 356 mm in length high temperature vycor liner. The test section is wrapped in 25.4 mm thick asbestos lagging to make the combustor more nearly adiabatic. Temperatures were measured at several locations inside the lagging to determine lagging effectiveness. The resulting temperature profiles indicated a heat loss of less than 0.3 percent of the total energy release due to combustion.

Jet air and propane are metered separately through rotometers and mixed in a mixing tee before passing into the jet injector. The stainless steel jet injector extends 63.5 mm into the test section. It has a 6.35 mm O.D. and a 3.97 mm I.D. at the jet exit the inner diameter is reduced to 1.59 mm through a converging nozzle. The injector is of standard triple wall construction to allow water cooling and operation of the ORJ at high combustion temperatures. The experimental facility is discussed in more detail in Appendix A.

2.2. Analytical Equipment

2.2.1. Composition Measurements

Two primary considerations must be dealt with when taking composition measurements in combustion systems. Any disturbance to the system being sampled from must be minimized and an accurate or representative sample must be transferred to the gas analysis equipment.

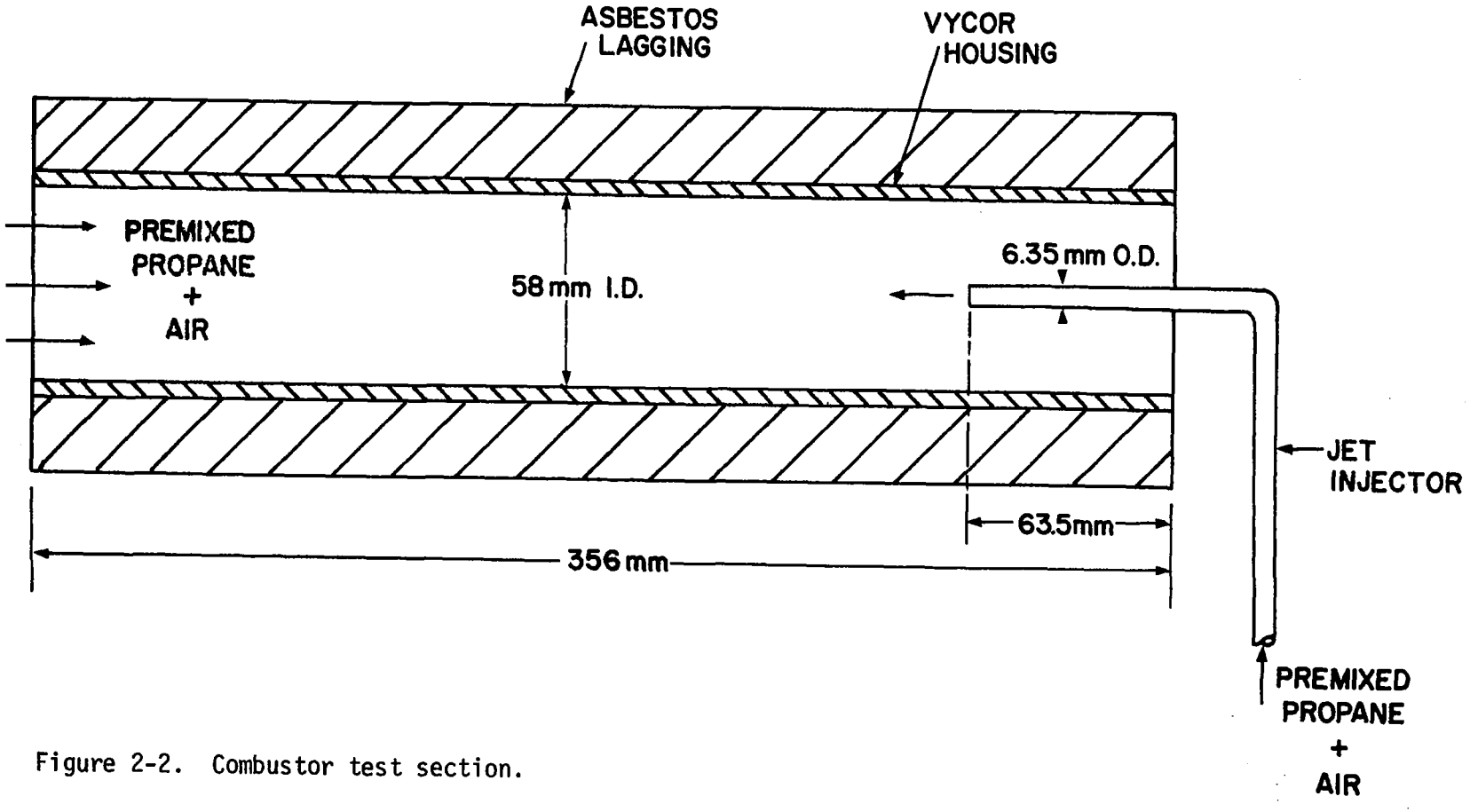

Figure 2-2. Combustor test section.

Three commonly used gas sampling probes are cooled stainless steel probes and cooled and uncooled quartz microprobes. In the case of the cooled probes, chemical reactions are quenched through a rapid reduction in temperature.[16] Additional quenching is often provided by expansion of the sample gases to a low pressure through a small diameter orifice located at the tip of the probe. A major disadvantage of the use of water cooled probes in recirculating flow systems is the possibility of disturbance to the system due to flow along the cold outer surface of the probe. In an effort to minimize this effect, it was decided to use a small diameter uncooled quartz probe designed according to recommendations by Fristrom and Westenberg.[19]

A comparison of NO_x measurements using a totally uncooled quartz probe and a water cooled quartz probe indicated that NO_x levels up to a maximum of 20% higher were obtained with the uncooled probe. These measurements were taken near the outer flame zone where the flow is predominantly downstream and the effect of the cooled probe walls on the combustion process was felt to be minimal. Thus the higher NO_x levels obtained with the uncooled probe were attributed to NO_x being formed in the probe. It was felt this was due to the high temperature of the probe walls resulting from the extended length (178 mm) of uncooled probe surface exposed to the hot combustion gases. This probe formation of NO_x was eliminated by enclosing all but that portion of the probe entering the recirculation region in a stainless steel cooling jacket.[18] The two probes used in the present investigation are shown in Figure 2-3. Both probes are identical except for the 45° bend in the lower probe.

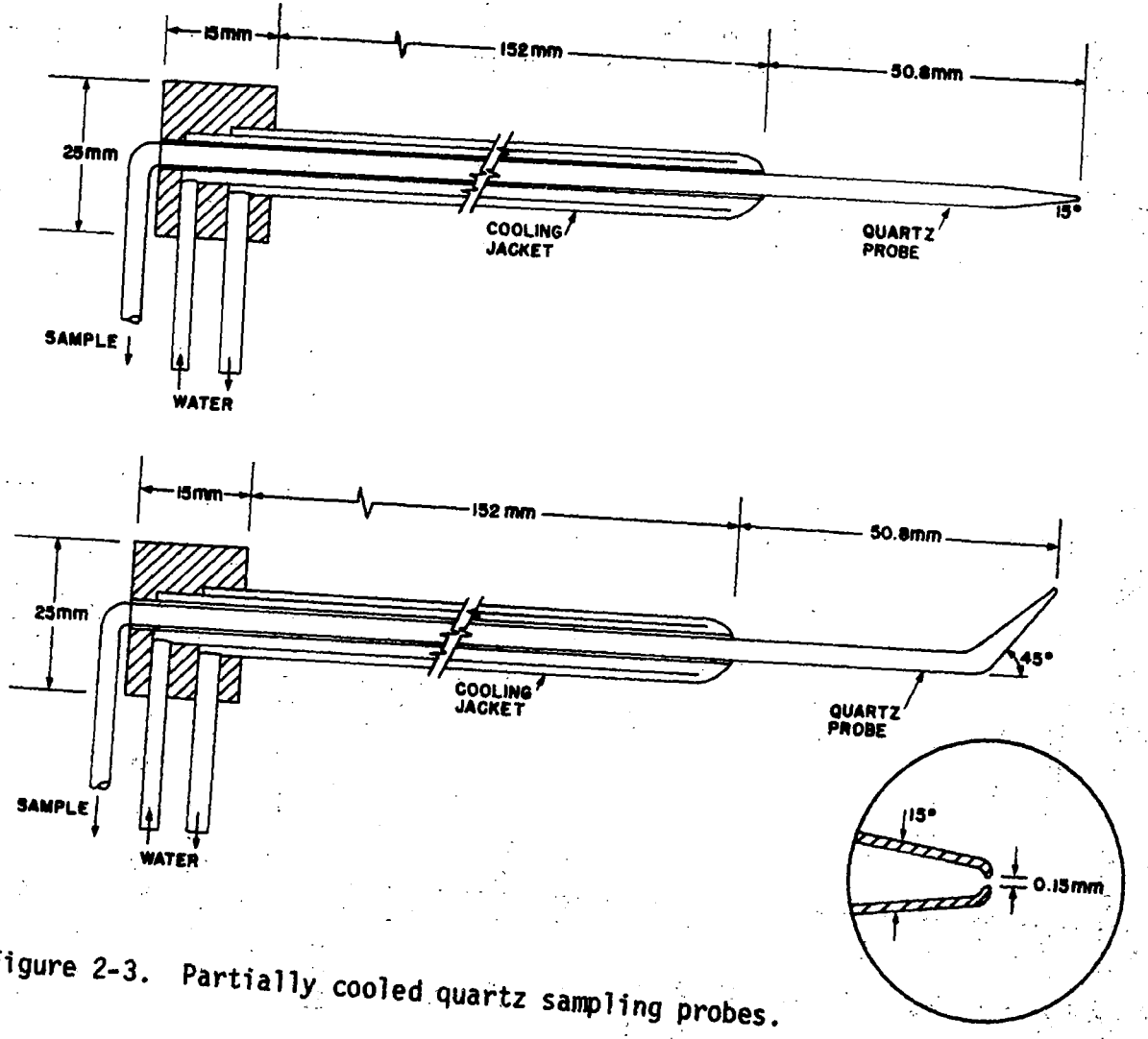

Figure 2-3. Partially cooled quartz sampling probes.

This bend made it possible to obtain measurements in the recirculation region up to the combustion centerline.

The probe is mounted on a specially built traversing mechanism which provides three degrees of freedom (Figures 2-4 and 2-5). With the probe inserted through the downstream end of the test section radial postion can be controlled to the nearest 0.025 mm using micrometers, while axial position can be controlled to the nearest 3.0 mm.

To determine the effectiveness of quenching, detailed kinetic calculations were made for temperature and pressure profiles in the probe which were felt to reasonably approximate the actual profiles. These calculations and the results are described in Appendix B. The probe was predicted to provide quenching for the stable species C_3H_8, CO, CO_2, H_2O, O_2, NO_x and N_2. However, as Allen[19] has pointed out, wall reactions in which NO can undergo recombination reactions with radicals (e.g. O, HO_2) to form NO_2 may be important in sampling probes. Wall reactions were not included in the above kinetic calculations, and no attempt was made to include reactions, involving conversion of NO to NO_2.

The sample passes through a 6.35 mm diameter teflon line to the gas analysis equipment after leaving the probe. This is shown in Figure 2-6. Carbon monoxide was measured using a Beckman Model 315A nondispersive infrared analyzer. The presence of water in the sample is known to interfere with CO measurements. However, at the concentrations of interest in the present work (less than 10 mole percent H_2O) this interference was negligible.

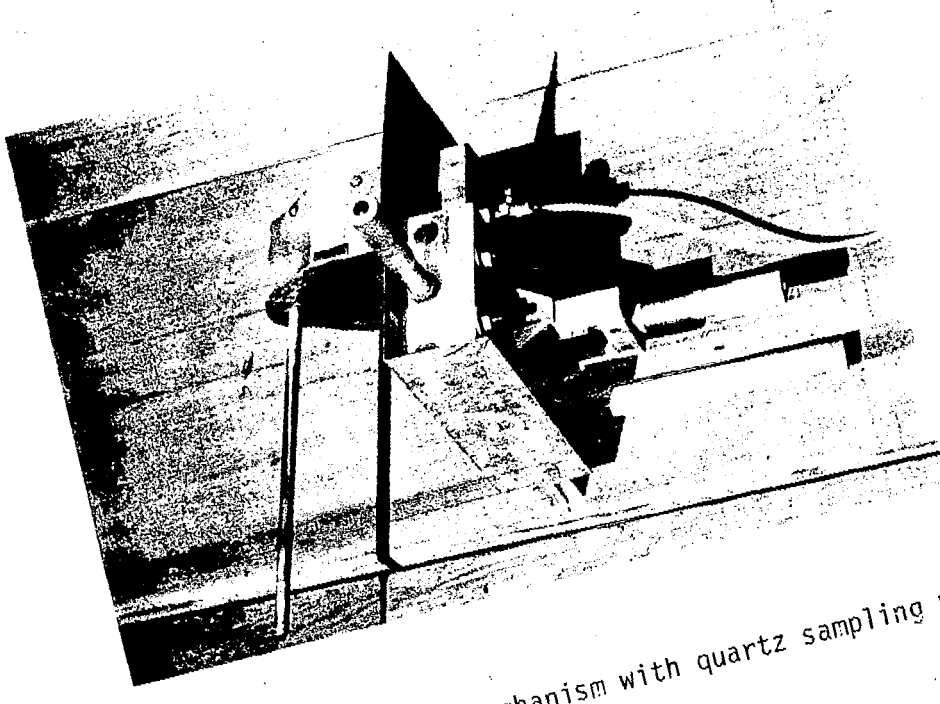

Figure 2-4. Traversing mechanism with quartz sampling probe.

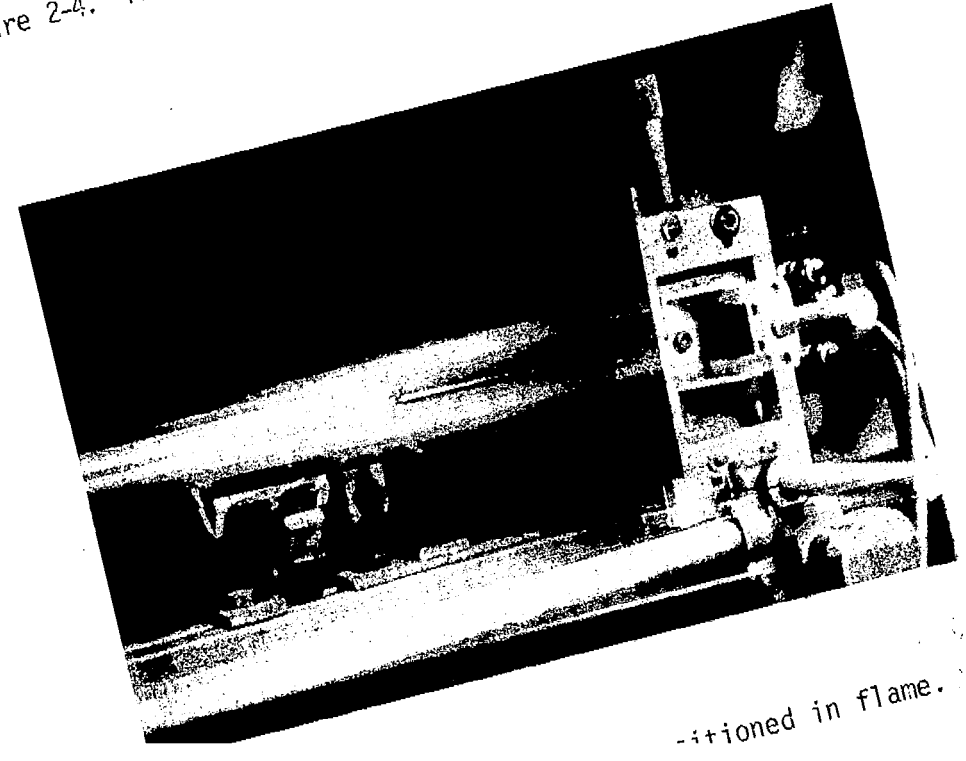

-itioned in flame.

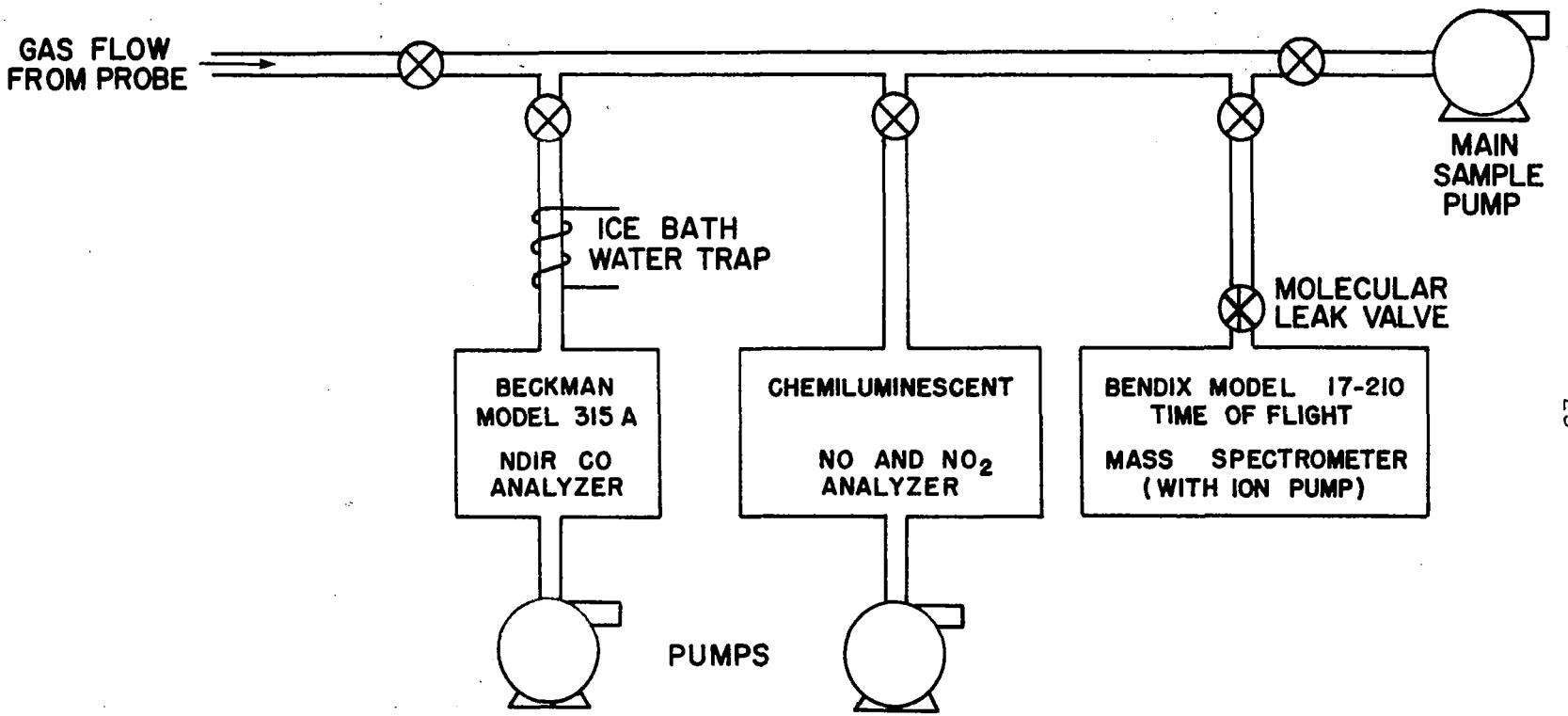

Figure 2-6. Gas analysis equipment.

NO and NO_2 were measured using a laboratory built chemiluminescent nitric oxide detector modified for the measurement of total NO_x by the addition of a heated length of molybdenum tubing[20, 21]. The heated molybdenum catalytically promotes the dissociation of NO_2 to NO. NO_2 is then taken as the measured difference between the total NO_x and the NO readings.

Several difficulties are encountered when measuring oxides of nitrogen. Tuttle, et al.[22] has pointed out that water condensation in the sample line is associated with significant NO_2 losses. This problem was solved by maintaining the sample line pressure at approximately 30 torr to prevent water condensation. A buildup of carbon particulate in the sample system has been shown[22] to result in adsorption of NO_2 and reduction of NO_2 to NO. However, because of the lean conditions of the present experiment, very little carbon was produced. This was verified by placing a particulate filter in the sample line. No carbon buildup was found to occur on the filter. Thus the presence of carbon in the sample line was not considered to be a source of error in composition measurements.

NO measurements using a chemiluminescence detector can also be affected by the presence of H_2O and CO_2 in the gas sample.[23, 24] This is due to the different third body efficiencies associated with the third body decay reaction

$$NO_2^* + M \rightarrow NO_2 + M \qquad (2\text{-}1)$$

Reaction (2-1) is in competition with the photorelaxation reaction

$$NO_2^* \rightarrow NO_2 + h\nu \qquad (2\text{-}2)$$

Thus variations in the concentrations of H_2O and CO_2 at different combustor locations can have an effect on measured NO_x readings. This effect was quantized through calibration and corresponding corrections were applied to the data (Appendix C). All NO_x measurements in this investigation were carried out at a pressure of 2.7 torr in the chemiluminescence detector. At this pressure the presence of 10 mole percent CO_2 in the N_2 carrier gas was found to result in NO readings approximately 5 percent too low. Interference corrections for H_2O were approximately 3 times those of CO_2. These values are in agreement with those of other investigators.[23, 24]

Other stable species were measured using a Bendix model 17-210 time-of-flight mass spectrometer. These species included H_2O, O_2, N_2, CO_2, and C_3H_8. In the case of H_2O and O_2, distinct mass spectra peaks free from any interfering species existed at mass numbers (m/e) of 17 and 18 for H_2O and 32 for O_2 and the concentrations were determined directly. N_2 (m/e = 14), CO_2 (m/e = 14, 44), and C_3H_8 (m/e = 14, 43, 44) had interfering peaks and a least mean squares computer program developed by McLean and Sawyer[25] was used to analyze the data. Note in the case of N_2 and C_3H_8 that secondary peaks, and not the primary or base peaks, were used to determine the their concentrations. Use of the above peaks was found to minimize interference between the various species and provide maximum reproducibility.

Hydrocarbon species other than propane most certainly exist at some point in the combustor. Investigations by Glassman, et al.[26] of propane in an adiabatic flow reactor indicate intermediate species C_3H_6, C_2H_4, CH_4, and C_2H_6 exist in measurable quantities

during the early oxidation phase of C_3H_8. However, examination of the mass spectra obtained in the present work indicated these species existed in negligible concentrations compared to other species of interest. Because of this the only unburned hydrocarbon species measured quantitatively was propane appropriate corrections were applied to the mass spectrometer data to account for the presence of CO.

2.2.2. Temperature Measurements

Temperatures were measured using a Pt/Pt-13% Rh fine wire thermocouple. The thermocouple and supporting ceramic stem are shown in Figure 2-7. A yttrium chloride-beryllium oxide coating developed by Kent[27] was used to reduce the possibility of catalytic reactions occurring on the thermocouple surface. The thermocouple probe was mounted on the same traversing mechanism as was used with the sampling probes.

Thermocouple measurements in the present combustion system involve measuring relatively high temperatures ($\sim$ 1800 K) in regions where steep temperature gradients often exist. Under such conditions both radiative and conductive heat losses from the thermocouple junction can be important. The use of 0.076 mm lead wires between the juction itself and the stronger 0.254 mm diameter support wires can be shown to make conduction losses negligible.[28] The lead wires are butt welded together to form a junction only slightly larger than the lead wire diameter (approximately a 0.114 mm diameter bead). Since readiative losses are proportional to bead size, this also acts to minimize radiative losses from the thermocouple junction. For a fine wire thermocouple the difference

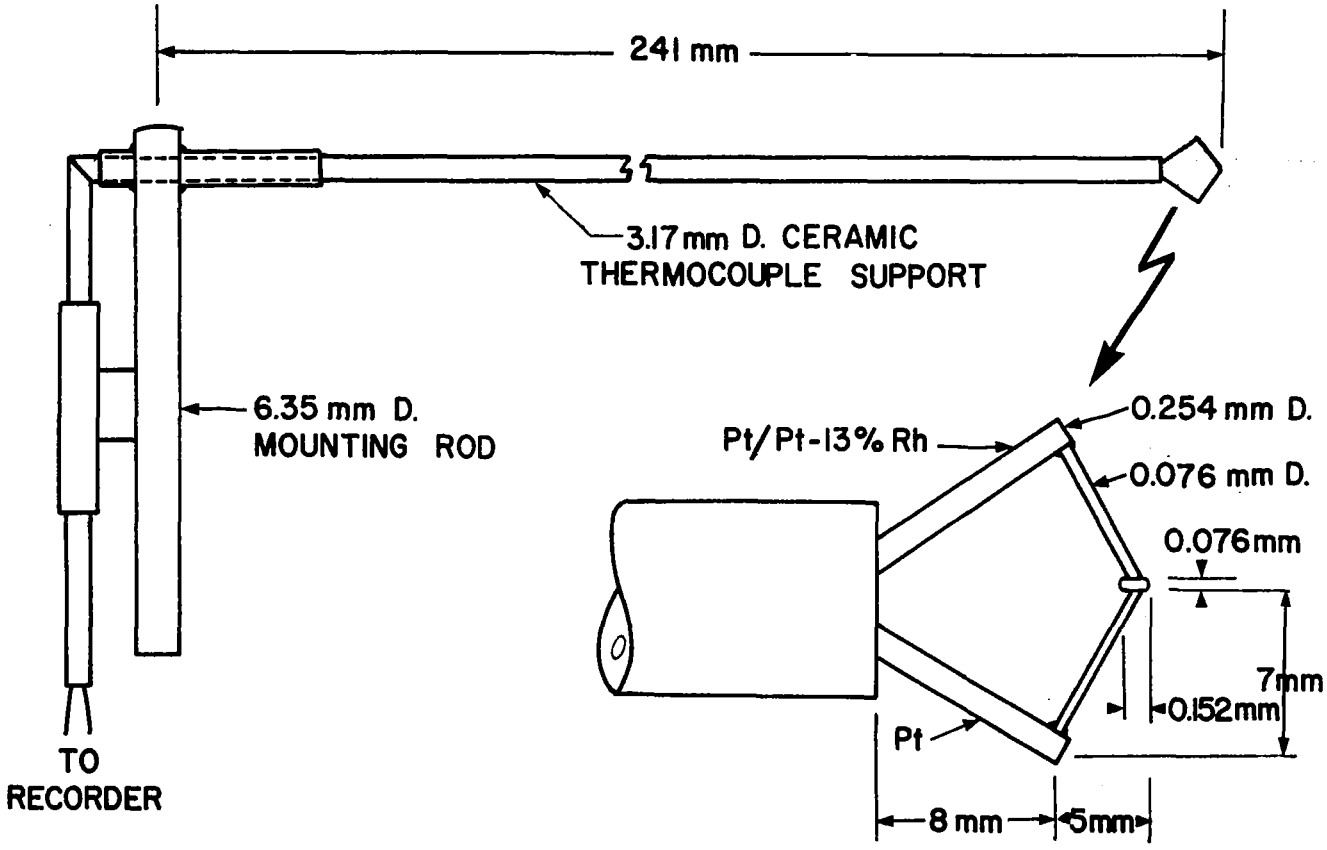

Figure 2-7. Thermcouple probe.

between the gas temperature and the measured thermocouple temperature can be estimated from the following relation

$$T_G - T_{TC} = \frac{\sigma\varepsilon}{h} (T_{TC}^4 - T_W^4) \qquad (2\text{-}4)$$

where

T_G = actual gas temperature

T_{TC} = measured thermocouple temperature

T_W = combustor wall temperature

σ = Stefan-Boltzman constant

ε = emissivity of the thermocouple junction

h = heat transfer coefficient

The heat transfer coefficient, h, can be obtained from the expression.[28]

$$Nu = \frac{hd}{k} \approx 0.42\ Pr^{0.2} \text{ to } 0.57\ Pr^{0.33}\ Re^{0.5} \qquad (2\text{-}5)$$

which is valid for $0.01 < Re_{TC} < 10000$. Here d is the thermocouple junction diameter and k is the gas thermal conductivity. Unfortunately the information needed to calculate thermocouple corrections from the above equations is largely unknown for the flowfield of the present investigation. Estimates can be made of the local gas properties for those cases in which complete composition and temperature measurements were taken. However velocity measurements which are needed to calculate the local Reynolds number were not made, and in a recirculating flow such as encountered here even an estimate of the velocity distribution would be difficult. Because of these difficulties radiation corrections to the thermocouple measurements

were not attempted. The maximum correction was estimated to be on the order of 200° K at a measured temperature of 1800° K. This represents an error approximately 10% in the temperature measurements.

CHAPTER 3

EXPERIMENTAL RESULTS

Chapter 2 discusses the experimental apparatus and describes the analytical equipment used in taking experimental data. This chapter presents the experimental results obtained for the opposed reacting jet. Experimentally determined lean stability limits of the ORJ and methods of increasing these stability limits are discussed in Section 3.1. Section 3.2 discusses operating point selection. Selected composition and temperature measurements are presented in Section 3.3. NO data are discussed in greater detail in Section 3.4. A complete set of experimental data for all operating conditions can be found in Appendix D.

3.1. Stability Limits

As was mentioned earlier, the purpose of this investigation is to examine the formation of pollutant species in a recirculating reacting flow under fuel lean conditions. Thus initial efforts were directed toward determining the lean stability limits of the opposed reacting jet and extending these limits to lower equivalence ratios.

The primary variables which affect the stability limits of the ORJ are jet stream equivalence ratio, jet stream flow rate, and main stream inlet temperature. Changes in jet stream inlet temperature when a premixed fuel/air jet was used were found by Noon[29] to have little effect on stability limits and were not considered. Figure 3-1 shows the effect of increasing jet stream equivalence ratio at a constant jet velocity. The main stream

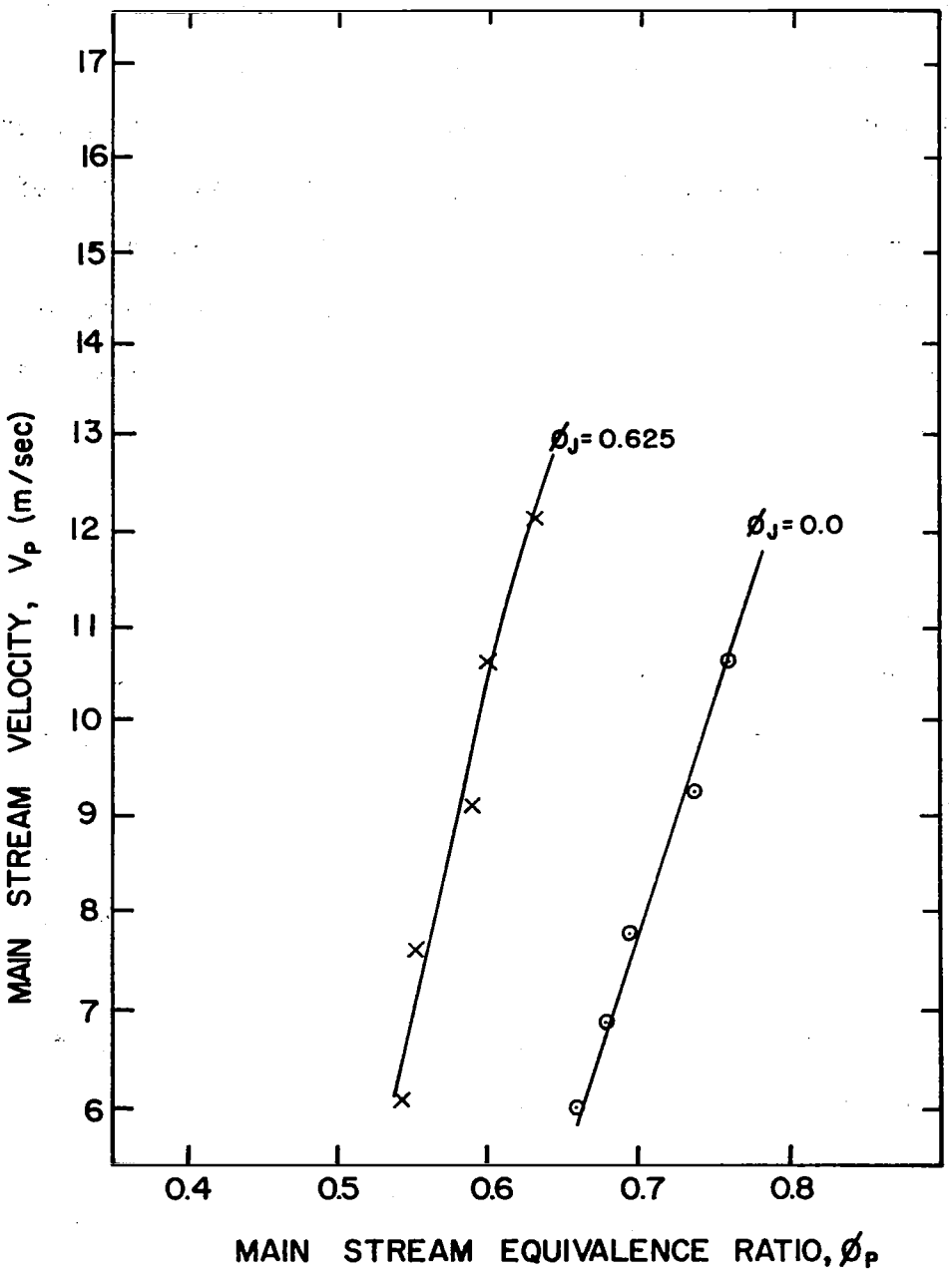

Figure 3-1. Effect of jet stream equivalence ratio on stability limits of opposed reacting jet combustor. T_p = 600 K; V_J = 95.9 m/s; T_J = 295 K.

equivalence ratio at blowout can be reduced only by increasing the jet stream equivalence ratio. The net result is little or no reduction in the equivalence ratio of the recirculation region. Indeed, Fuhs[30] has proposed that there may be one unique blowout curve of main stream velocity at blowout as a function of equivalence ratio in a small "critical" zone located at the upstream end of the recirculation region. A further consideration is that in the numerical calculations one species conservation equation can be eliminated by maintaining a uniform equivalence ratio throughout the flowfield. This can be accomplished by keeping the primary stream and jet stream equivalence ratios equal. Thus extending the stability limits to lower equivalence ratios through a variation in the jet stream composition does not appear useful in the current application.

Stable operation with both a lean primary and jet stream can be accomplished by increasing the jet exit velocity, as is shown in Figure 3-2. There is however a limit on increasing the jet velocity. The Mach number at the jet exit should be kept less than 0.5[31] to avoid compressibility effects. Compressibility effects threaten the convergence of the numerical solution and change the nature of the governing equations from elliptic to hyperbolic. A jet exit velocity of 168.4 m/s corresponds to $M_{JET\ EXIT} = 0.5$ and thus represents an upper limit.

With a jet exit velocity of 168.4 m/s the flame tip is located approximately 230 mm upstream of the jet exit. A shorter flame zone would be desirable for two reasons. First, probes of the

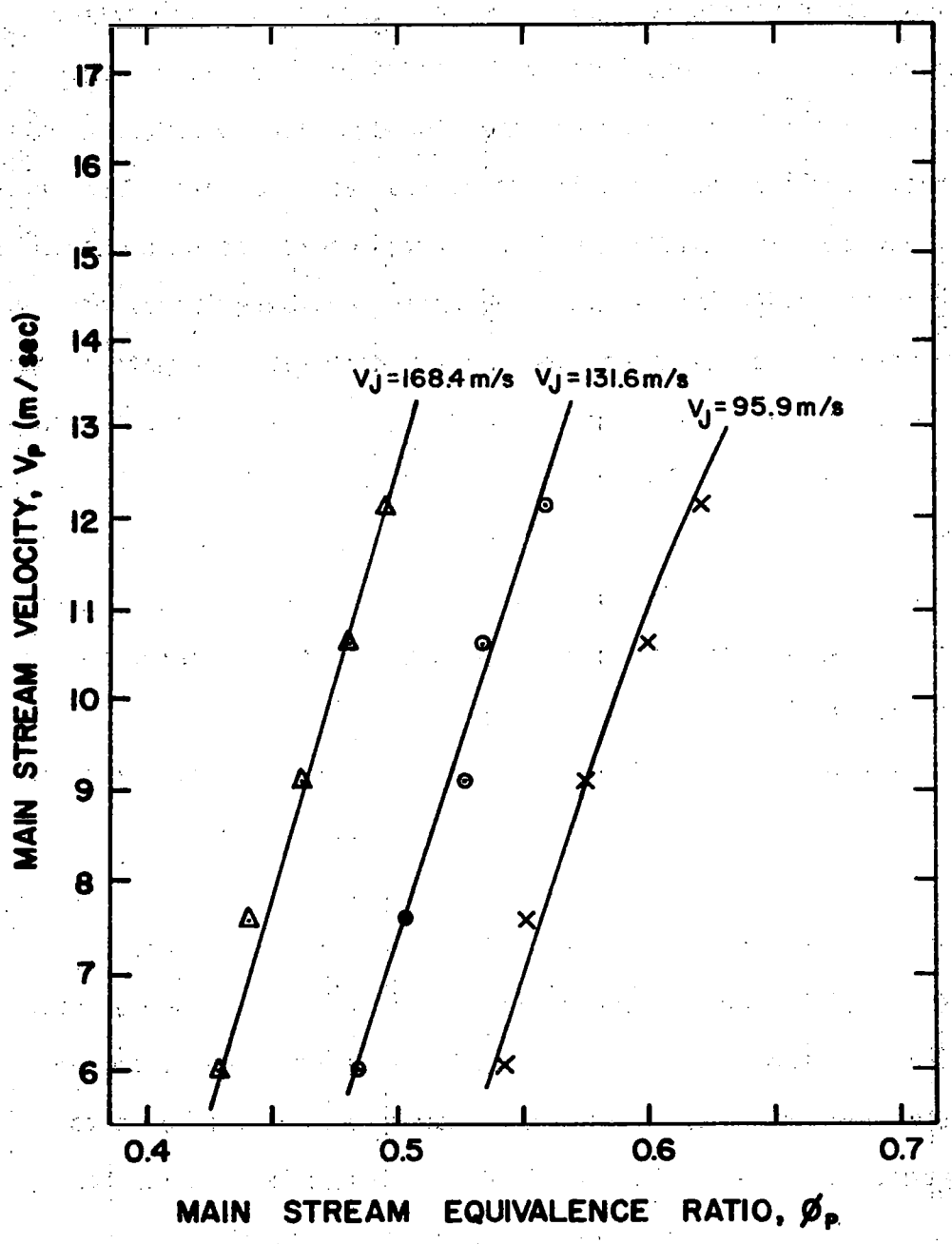

Figure 3-2. Effect of jet exit velocity on stability limits of opposed reacting jet combustor. T_p = 300 K; T_J = 295 K; ϕ_J = 0.625.

type used in this investigation (with a triple-wall water cooling jacket) become more difficult to construct as their length increases. Second, a longer flame zone requires a greater number of grid points to obtain an accurate numerical solution. This can significantly affect the time required to obtain a solution. For the composition and temperature measurements of the present investigation a jet exit velocity of 95.9 m/s was selected. This allowed a significant reduction in the number of grid points required (the maximum upstream position of the flamefront was approximately 152 mm) while at the same time providing a flame zone large enough to make possible good spatial resolution in the composition and temperature measurements.

The most effective way of increasing the lean stability limits of the ORJ was found to be an increase in primary stream inlet temperature. This is shown in Figure 3-3. For a jet exit velocity of 95.9 m/s and a primary stream velocity of 7.74 m/s, an inlet temperature of 600°K allowed stable operation to be maintained at an overall equivalence ratio as low as 0.45. An increase in jet velocity would of course reduce this stability limit further.

3.2. Operating Conditions

The operating variables affecting NO_x formation in the ORJ are 1) main stream inlet temperature, 2) equivalence ratio, and 3) main stream inlet velocity. The affect on NO_x formation occurs primarily through a resulting change in flame temperature and combustor residence time. Experimental composition and tempera-

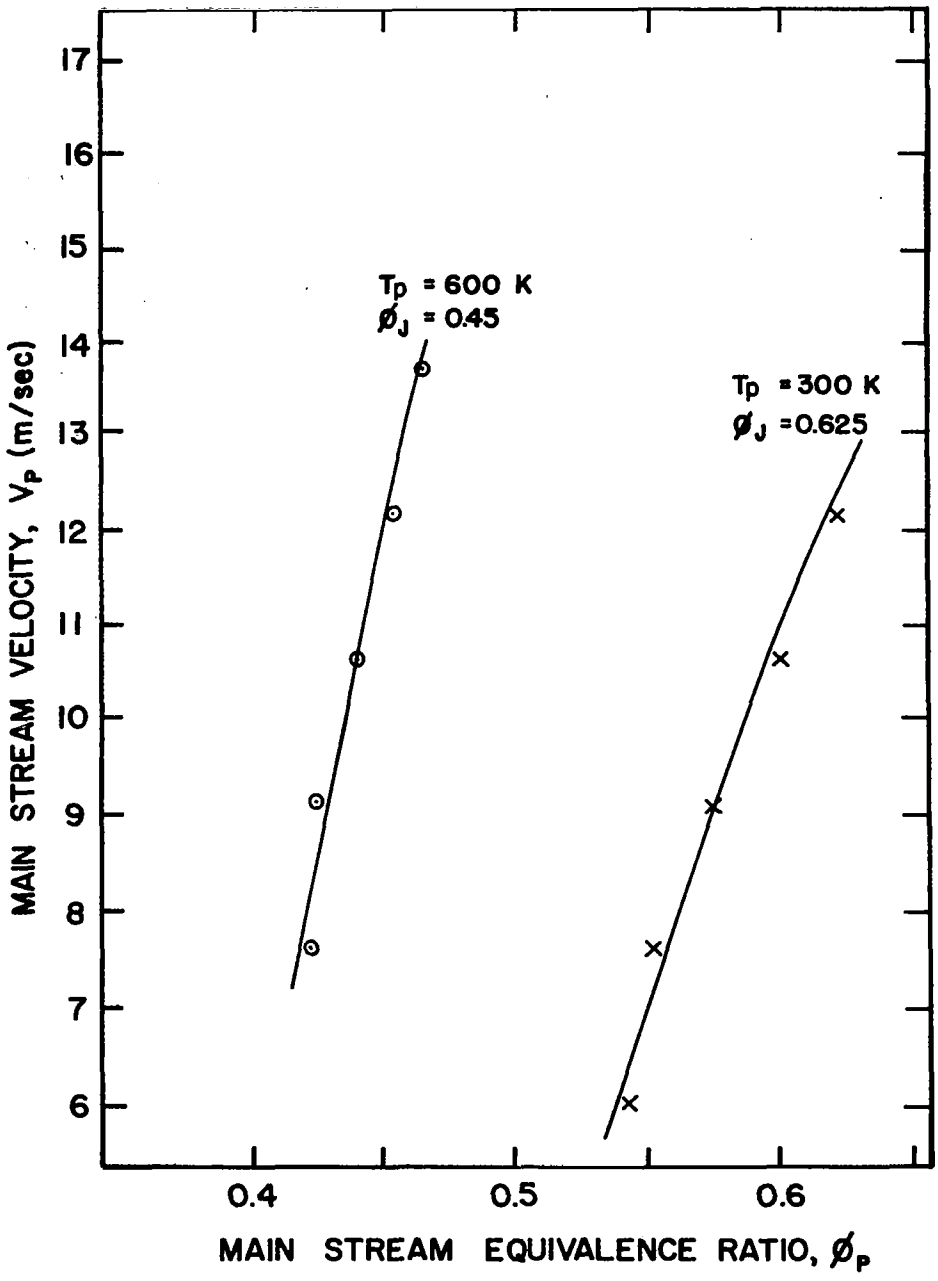

Figure 3-3. Effect of main stream inlet temperature on stability limits of opposed reacting jet combustor. V_J = 95.9 m/s; T_J = 295 K.

ture measurements were carried out over a range of these operating variables which would reflect their influence on NO_x production. The experimental conditions considered are shown in Table 3-1. In all cases, the jet stream velocity and temperature were maintained constant at 95.9 m/s and 295°K respectively. NO_x, NO and temperature profiles were measured at all conditions. O_2, CO_2, H_2O, CO, and unburned hydrocarbons were measured only for cases 1, 3, and 6.

TABLE 3-1. EXPERIMENTAL OPERATING CONDITIONS

CASE	EQUIVALENCE RATIO*	MAIN STREAM INLET TEMPERATURE (°K)	MAIN STREAM VELOCITY (m/sec)	ADIABATIC FLAME TEMPERATURE (°K)
1	0.625	300	7.74	1746
2	0.625	450	7.74	1857
3	0.625	600	7.74	1970
4	0.625	600	13.59	1970
5	0.550	600	7.74	1838
6	0.450	600	7.74	1649

*Jet and main flow equivalence ratios are equal in all cases reported.

3.3. Composition and Temperature Measurements

In this section representative axial and radial profiles are presented and discussed. For clarity, the section is divided into three subsections, 3.3.1, 3.3.2, and 3.3.3, in which cases 1, 3, and 6 are discussed individually. Emphasis is placed on the hydrocarbon system, although profiles for oxides of nitrogen presented as total NO_x are also presented. The effect of operating conditions on NO_x formation and measurements of NO and NO_2 are discussed in more detail in Section 3.4.

3.3.1. Case 1: $\phi = 0.625$, $T_p = 300$ K, $V_p = 7.74$ m/s.

Selected axial concentration and temperature profiles for case 1 are shown in Figures 3-4 through 3-6 at radial positions of 19.2, 11.6, and 1.4 mm from the centerline, respectively. It should be noted no temperature measurements were taken at the 1.4 mm position due to probing limitations. The profiles of Figure 3-4 (r = 19.2 mm) show that CO begins increasing approximately 110 mm upstream of the combustor exit. The low temperatures encountered at this radial location ($T < 800°K$) indicate this is probably the result of diffusion from the inner combustion region since little pyrolysis of C_3H_8 would be expected at these temperatures. The same considerations would also apply to the apparent buildup of other combustion products such as CO_2 farther downstream.

Axial concentration and temperature profiles at a radial position of 11.6 mm from the combustor centerline are shown in Figure 3-5. A difference is immediately apparent between the turbulent combustion encountered in the ORJ and atmospheric

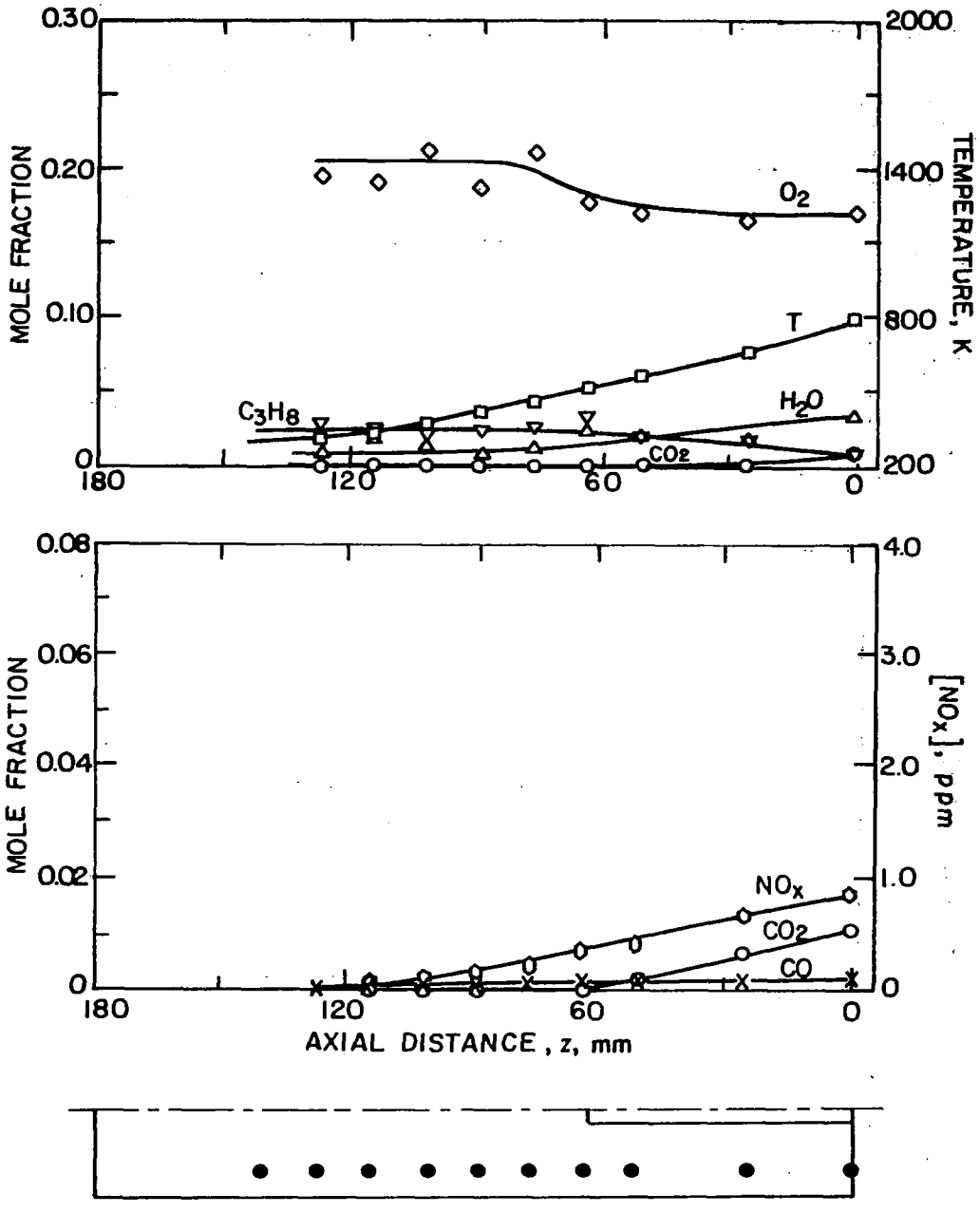

Figure 3-4. Axial concentration and temperature distributions at a radial location of 19.2 mm from the combustor centerline. Experimental case 1. T_p = 300 K; ϕ = 0.625; V_p = 7.74 m/s; V_J = 95.9 m/s.

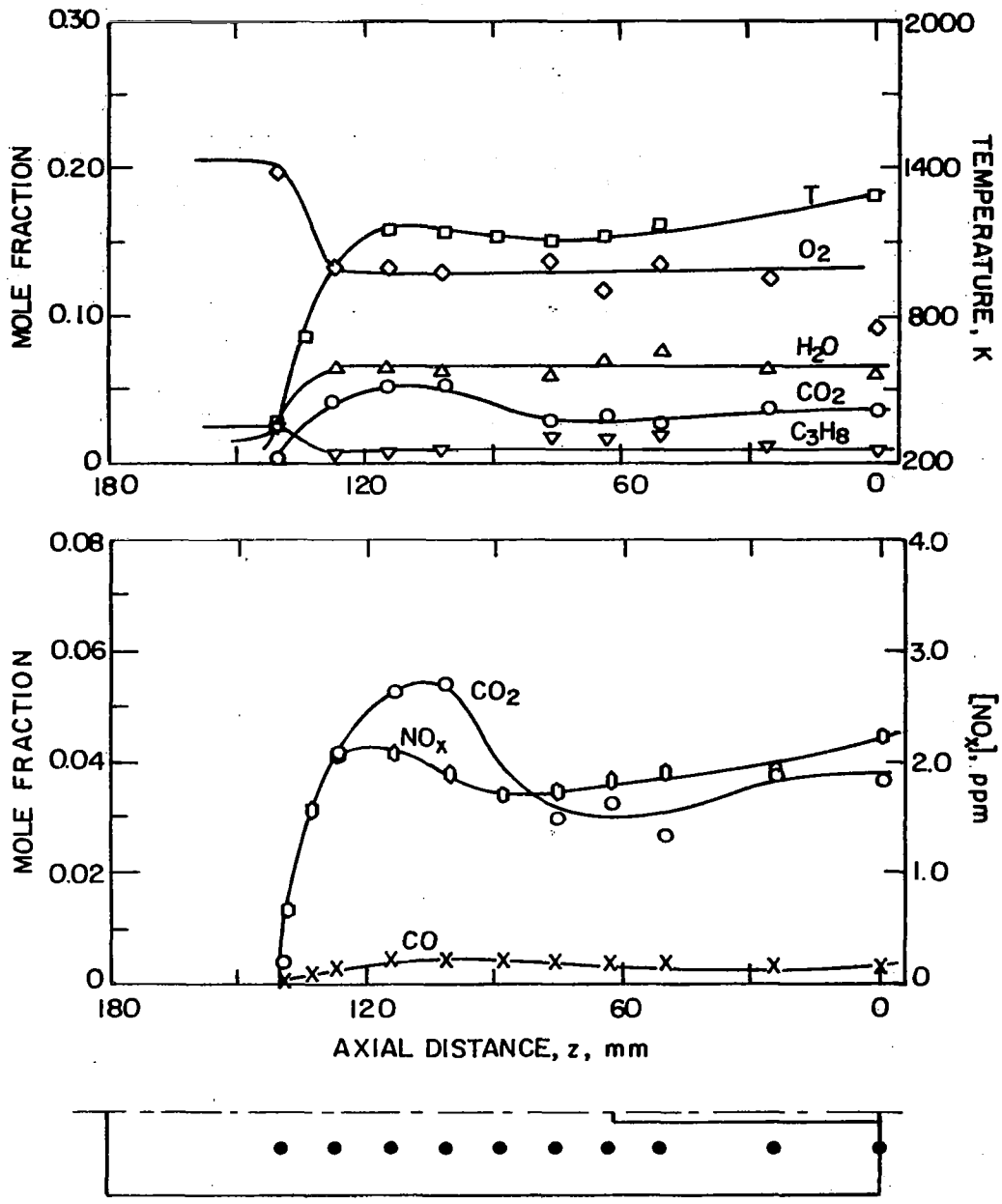

Figure 3-5. Axial concentration and temperature distributions at a radial location of 11.6 mm from the combustor centerline. Experimental case 1. T_p = 300 K; ϕ = 0.625; V_p = 7.74 m/s; V_J = 95.9 ^{p}m/s.

laminar flames in which the flamefront extends over a distance of only several millimeters. As can be seen in Figure 3-5 the flamefront extends over a much greater axial distance (approximately 20 mm) due to the turbulent unsteady nature of the flowfield. The decrease in C_3H_8 and H_2O is accompanied by a rapid rise in temperature to approximately 1200 K as the flamefront is crossed. In agreement with laminar flame studies[17, 26] H_2O forms more rapidly than does CO_2. This is due to the more rapid kinetics associated with H_2O formation.

The absence of maximum CO at the flamefront can be seen in Figure 3-5. CO levels in fuel lean systems are controlled by a balance between the primary CO formation and destruction reactions

$$HCO + OH \rightarrow CO + H_2O \qquad (3\text{-}1)$$

$$CO + OH \rightarrow CO_2 + H \qquad (3\text{-}2)$$

The absence of an initial maximum in CO indicates that under the conditions existing at this radial location the rates of reactions (3-1) and (3-2) are comparable. Rate constants for these reactions have been given as

$$\log k_1 = 10^{13.7} \quad [32]$$

$$\log k_2 = 10.83 + 3.94 \times 10^{-4} T \quad [33]$$

Note that k_1 is independent of temperature and, for temperatures greater than 1200 K, k_2 is a strongly increasing function of temperature. The ratio of the rates of production and destruction of CO via reactions (3-1) and (3-2) can then be written

$$\frac{R_2}{R_1} = \frac{[CO]}{[HCO]} \quad 10^{2.87 + 3.94 \times 10^{-4} T}$$

Thus on the basis of temperature only, a maximum in CO could be expected at lower temperatures ($R_1 >> R_2$). This is contrary to the results of the present investigation. A maximum in CO was found to occur only in high temperature regions (see for example Figure 3-6). It therefore appears that the presence (or lack) of a maximum in CO is attributable to the more rapid formation of HCO via propane oxidation at higher temperatures. Uncertainties in the propane oxidation mechanism make it difficult to draw any further conclusions

Fenimore and Moore[34] have shown that for temperatures greater than 1300 K and sufficiently low post-combustion gas cooling rates ($-dT/dt < 3.4 \times 10^5 T^2 \exp(-19790/T)$ K/sec) reaction (3-2) is in partial equilibrium. These conditions appear to be true here once the initial flamefront (as characterized by a rapid rise in temperature) has been traversed. Thus in the downstream region of Figure 3-5 the relative concentrations of CO and CO_2 are governed by the partial equilibrium expression

$$\frac{[CO]}{[CO_2]} = \frac{1}{K_2} \frac{[H]}{[OH]} \qquad (3\text{-}3)$$

where K_2 is the equilibrium constant for reaction (3-2). Since the temperature is relatively constant from the initial flamefront to the exit, it appears that the ratio $[CO]/[CO_2]$ is primarily controlled by the relative radical concentrations, in particular $[H]/[OH]$.

Figure 3-6 shows concentration profiles at r = 1.4 mm from the combustor centerline. The flamefront is now located approximately 150 mm upstream of the combustor exit. The

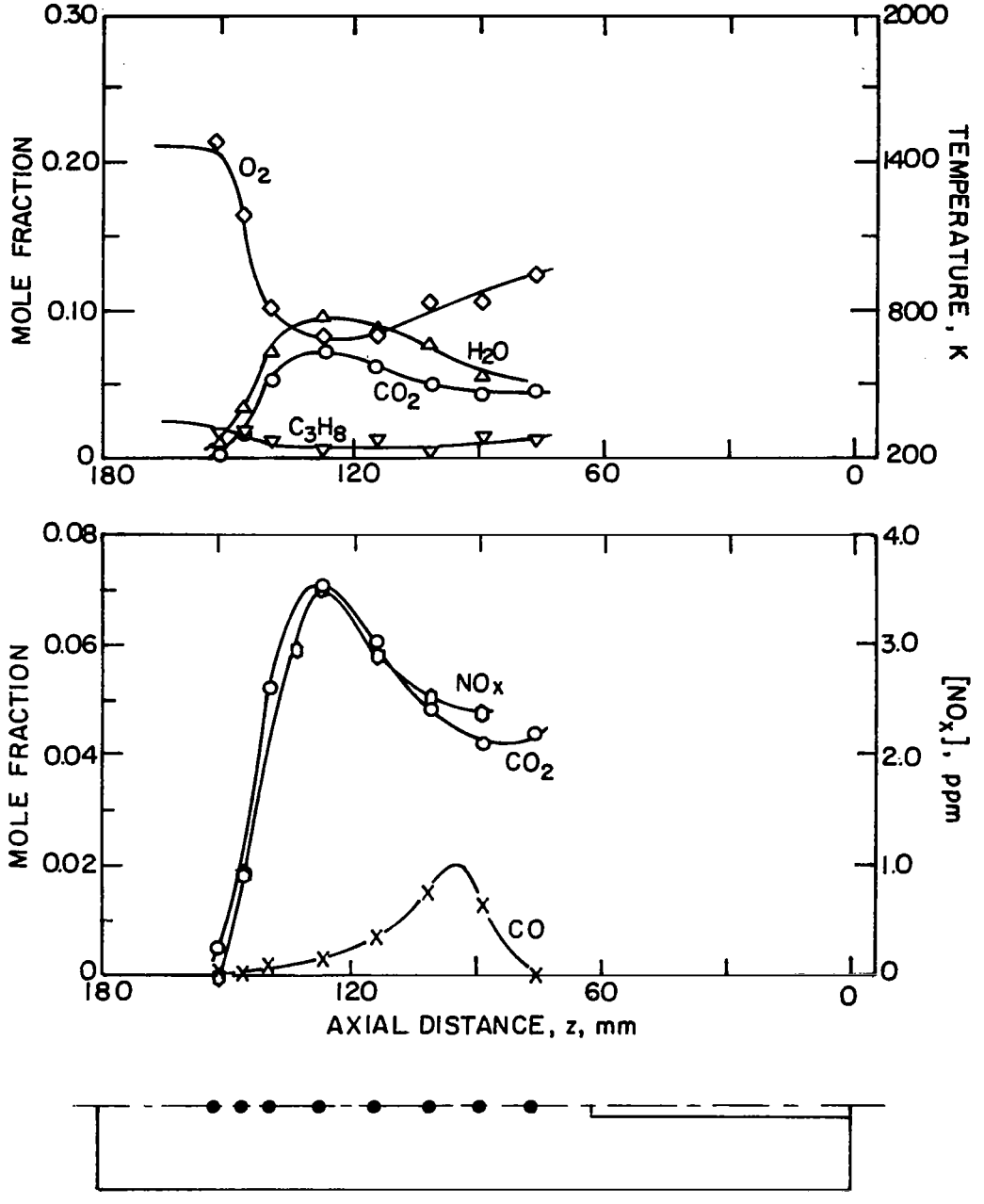

Figure 3-6. Axial concentration and temperature distributions at a radial location of 1.4 mm from the combustor centerline. Experimental case 1. T_p = 300 K; ϕ = 0.625; V_p = 7.74 m/s; V_J = 95.9 m/s.

relatively high levels of CO_2 and H_2O indicate more complete combustion occurring in the intensely mixed recirculation zone upstream of the jet exit due to the relatively long residence time and high temperatures in the recirculation zone. The maximum mole fractions for H_2O and CO_2 of 0.093 and 0.072 compare closely with equilibrium values of 0.093 and 0.0747.

The CO and CO_2 profiles appear at first surprising, with a peak in CO_2 appearing upstream of the CO. A possible explanation of this result can be found in the recirculating nature of the flowfield, with the flow at this radial position moving upstream due to the high jet velocity. This peak in CO is probably associated with the oxidation of jet injected C_3H_8.

Some general observations can be made concerning NO_x formation based on the results shown in Figures 3-4 through 3-6. The strong dependence of NO_x on temperature and residence time is apparent, with NO_x increasing as one moves radially inward higher temperature and downstream toward the combustor exit (longer residence time). Maximum NO_x levels occur in the recirculation zone (3.2 PPM) where relatively high temperatures and long residence times occur.

Typical radial profiles for case 1 are shown in Figures 3-7 through 3-9. At the combustor exit (Figure 3-7) the low temperature and combustion product concentrations near the Vycor wall indicate the flamefront has not yet reached the outer Vycor wall. Moving radially inward a buildup of H_2O, CO, and CO_2 occur with a corresponding decrease in C_3H_8 and O_2. The maximum

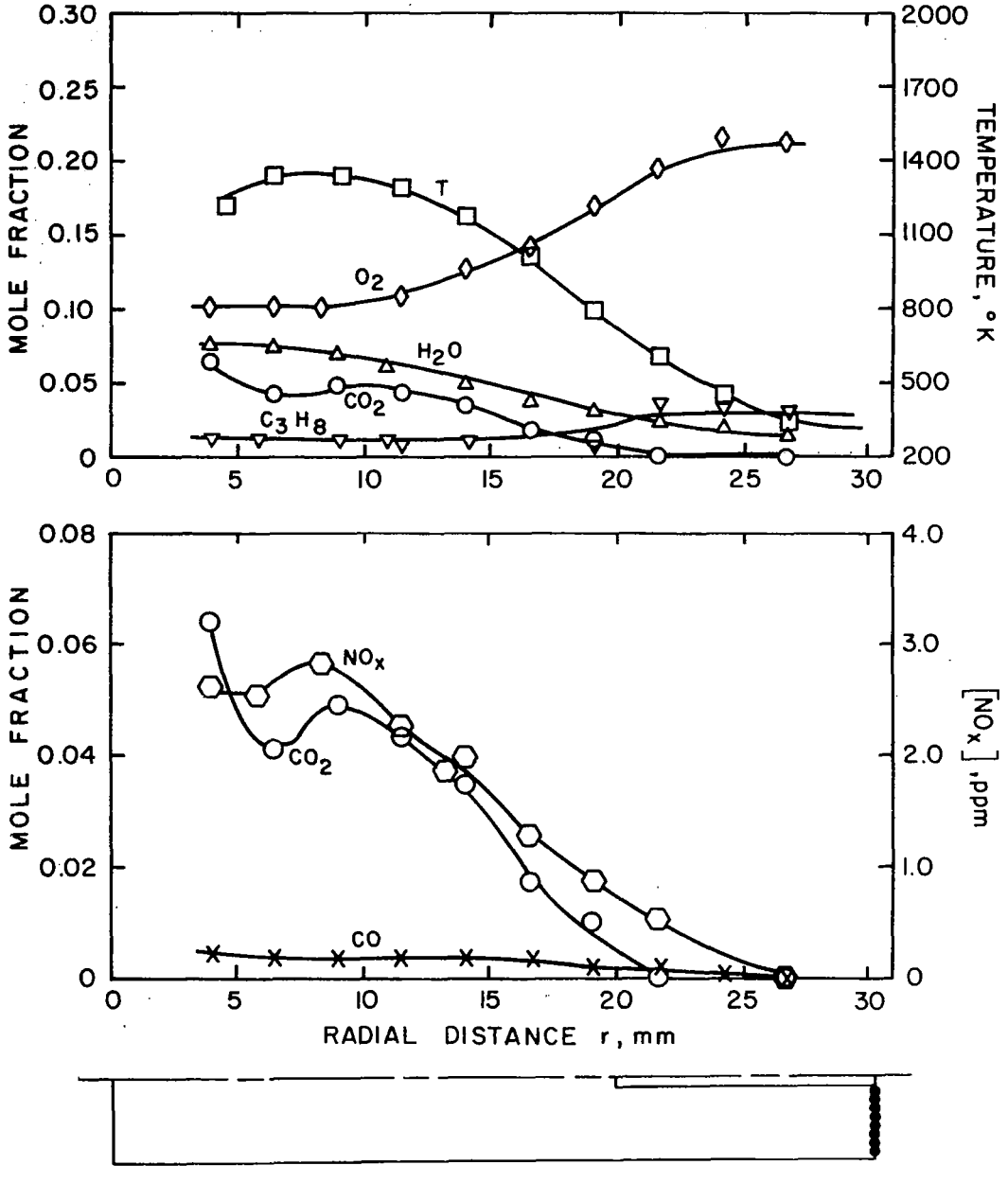

Figure 3-7. Radial concentration and temperature distributions at the combustor exit. Experimental case 1. T_r = 300 K; ϕ = 0.625; V_D = 7.74 m/s; V_a = 95.9 m/s.

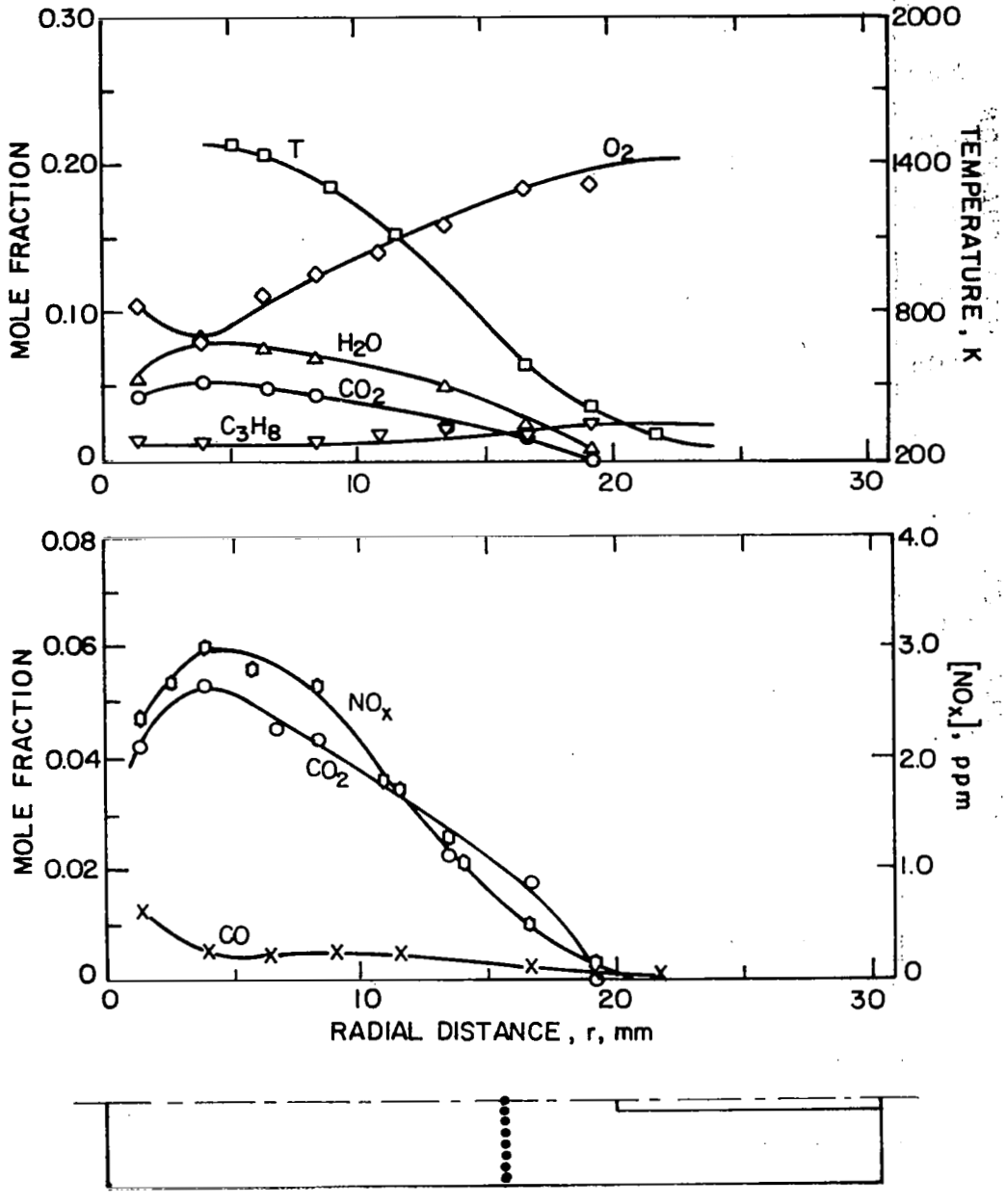

Figure 3-8. Radial concentration and temperature distributions at a axial location of 88.9 mm upstream of the combustor exit. Experimental case. T_p = 300 K; ϕ = 0.625; V_p = 7.74 m/s; V_J = 95.9 m/s

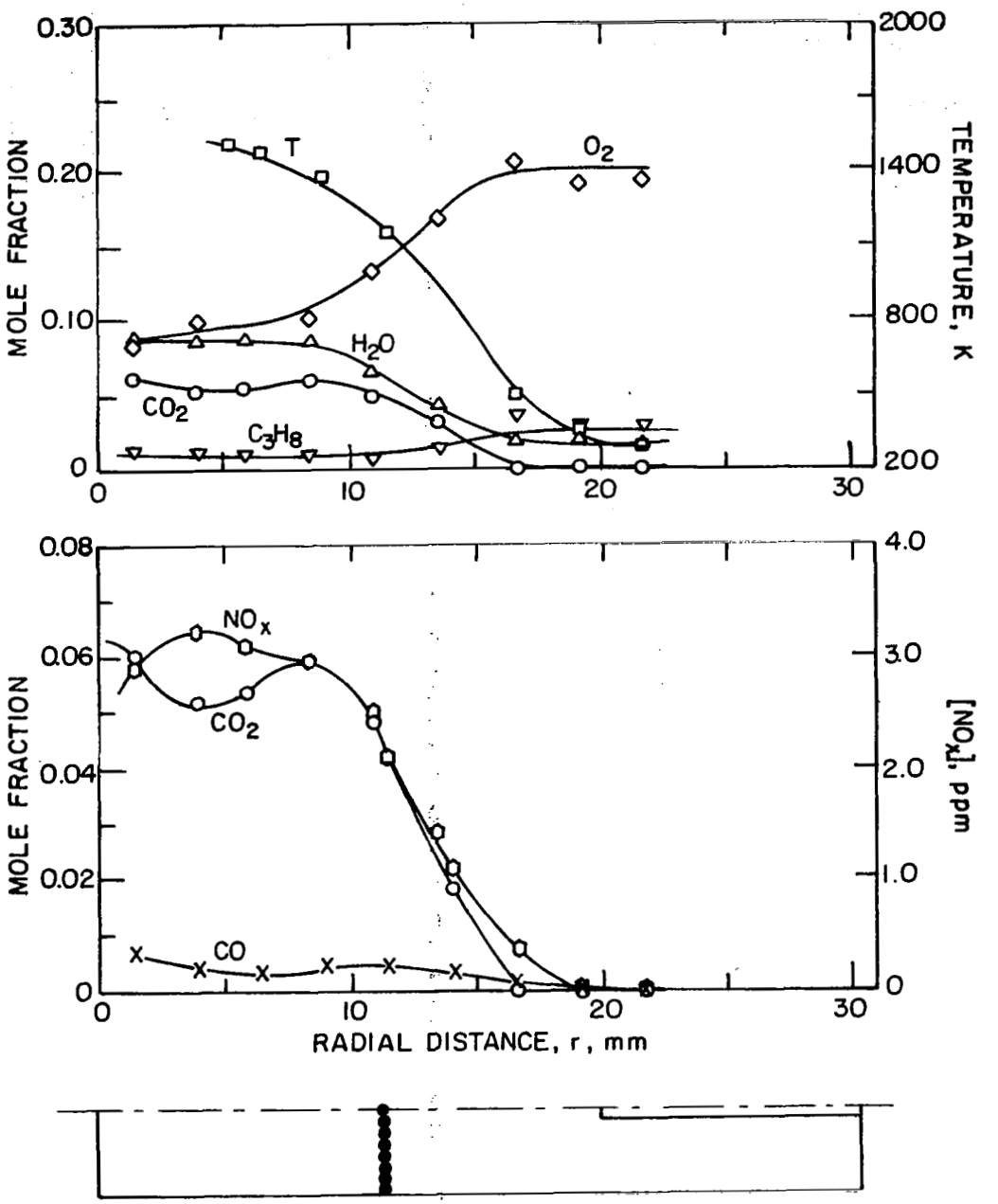

Figure 3-9. Radial concentration and temperature distributions at an axial location of 114.3 mm upstream of the combustor exit. Experimental case 1. T_p = 300 K; ϕ = 0.625; V_p = 7.74 m/s; V_J = 95.9 m/s.

temperature attained of 1380 K compares with an adaibatic flame temperature of 1740 K, reflecting both radiative losses from the thermocouple and incomplete combustion. Using Equation (2-4) the radiative losses can be calculated to be approximately 200 K at the combustor exit.

A relatively rapid increase in CO_2 can be seen as the jet wall is approached even though the temperature appears to be decreasing. This can be accounted for by the downstream transport of the large quantities of CO_2 existing in the recirculation region as opposed to any increase in the local oxidation rate of CO.

The NO_x concentration profiles again closely follow the temperature profile, reaching a maximum of 2.4 PPM in the high temperature combustion region. The effects of radial diffusion are apparent in the finite quantities of NO_x existing as the Vycor wall is approached even though the temperature has decreased to a relatively low value.

Figure 3-8 presents radial profiles of the same species at an axial position of 88.9mm upstream of the combustor exit. The flamefront has moved inward toward the combustor centerline. The effect of the jet injector is characterized by an increase in O_2 and a decrease in H_2O and CO_2 as the centerline is approached. The rapid increase in CO accompanied by a relatively low level of C_3H_8 as the centerline is approached indicates a rapid oxidation of jet injected C_3H_8 to CO.

At a distance of 114.3mm from the combustor exit (Figure 3-9) the effects of jet injected reactants have almost entirely disappeared. The concentrations of O_2, H_2O, CO, and C_3H_8 have become fairly uniform over the entire recirculation region. The CO_2 concentration is also relatively uniform across this region with the exception of a dip between the centerline and the outer flame-front. Once again, since conditions are such in the recirculation zone that partial equilibrium of reaction (3-2) would be expected, this reflects the interaction of relative radical concentrations (specifically H and OH) and temperature and their effect on this partial equilibrium via Equation (3-3).

3.3.2. Case 3: $\phi = 0.625$, $T_p = 600$ K, $V_p = 7.74$ m/s

Experimental results for case 3 are shown in Figures 3-10 through 3-14. The axial profile shown in Figure 3-10 for a radial position of r = 11.6 mm from the centerline reflects the influence of the elevated inlet temperature. The sharp initial peak in CO that was characteristic only of the high temperature recirculation zone in case 1 is present here at all radial locations. This maximum in CO is followed by much more rapid conversion of CO to CO_2 than was found in case 1. As the combustor exit is approached C_3H_8 and CO mole fractions decrease to much lower values, accompanied by much higher concentrations of CO_2.

NO_x concentrations have increased by nearly a factor of 4 over those obtained in case 1. This is primarily a result of the higher combustion temperatures and the larger region over which these temperatures are maintained. Maximum concentrations are

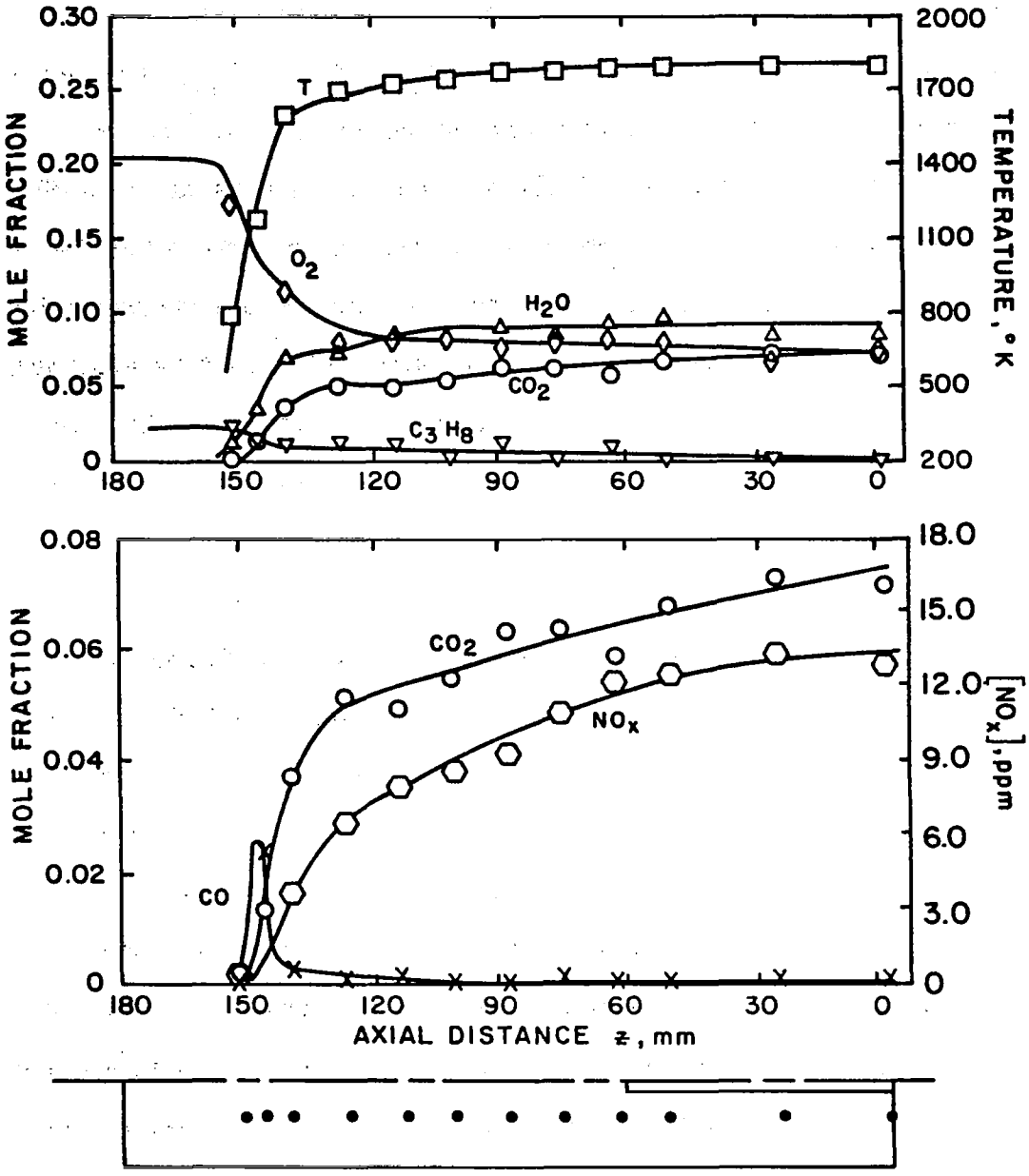

Figure 3-10. Axial concentration and temperature distributions at a radial location of 11.6 mm from the combustor centerline. Experimental case 3. T_D = 600 K; ϕ = 0.625; V_D = 7.74 m/s; V_J = 95.9 m/s.

obtained at the combustor exit. This reflects the linear dependence of NO formation on residence time since temperature is maintained at relatively high values across much of the combustor.

At a radial distance of 1.4 mm from the combustor centerline (Figure 3-11) the flamefront has become quite steep due to the effect of the elevated inlet temperature. The mole fractions of H_2O and CO_2 rise abruptly and remain approximately constant as the jet exit is approached. A sharp peak occurs in the CO at the upstream flamefront. The rise in CO at the two points nearest the jet exit indicates the possibility of a second peak due to the oxidation of jet injected propane just after the jet exit.

Radial profiles at the combustor exit are shown in Figure 3-12. Due to the higher inlet temperature the flamefront has spread out much farther into the main stream flow than in case 1. Significant combustion occurs almost entirely across the combustor exit. The primary combustion products are H_2O and CO_2 with very little of the C_3H_8 and CO remaining. Mole fractions of H_2O, CO_2, and CO correspond closely to the equilibrium values of 0.099, 0.0744, and 0.0003, respectively. The average temperature is in excess of 1700 K (uncorrected) over most of the combustor exit. This compares with an adiabatic flame temperature of 1970 K.

Radial profiles at an axial distance 88.9mm upstream of the combustor exit are shown in Figure 3-13. While the effects of the jet injector were readily apparent in case 1 as a decrease in CO_2 and H_2O and a sharp increase in CO near the combustor centerline, such effects are significantly reduced here. Only a small

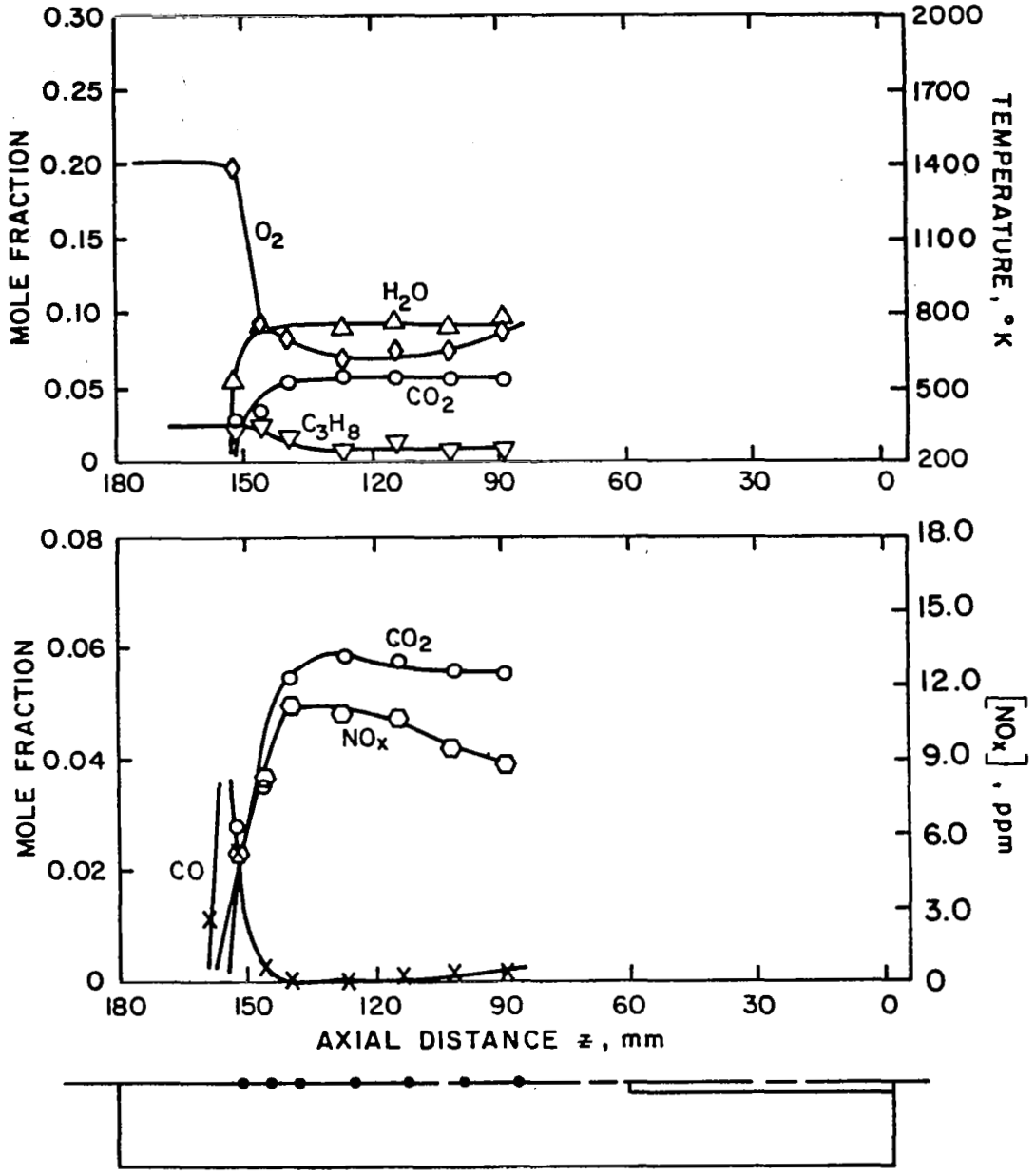

Figure 3-11. Axial concentration and temperature distributions at a radial location of 1.4 mm from the combustor centerline. Experimental case 3. T_p = 600 K; ϕ = 0.625; V_p = 7.74 m/s; V_J = 95.9 m/s.

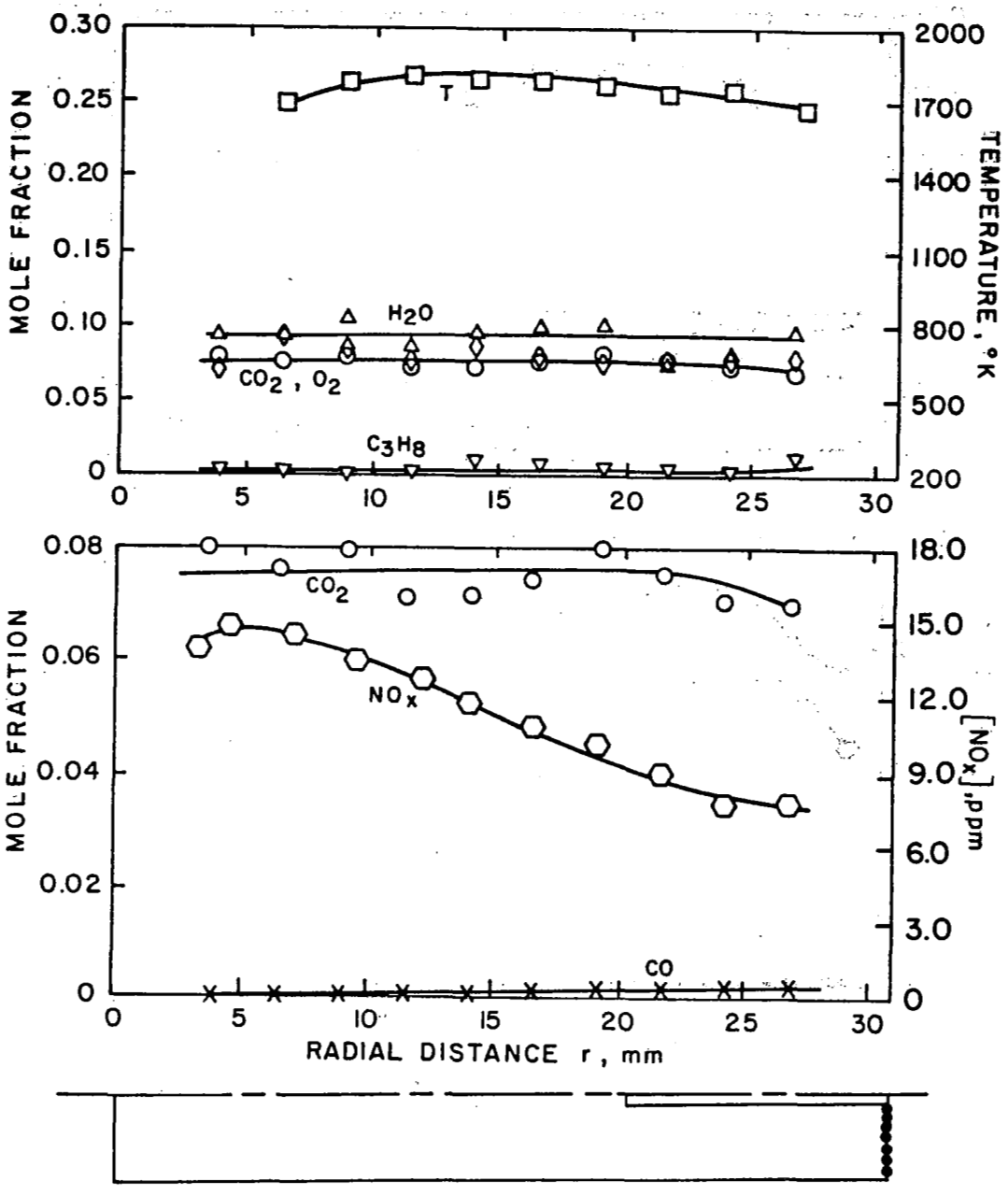

Figure 3-12. Radial concentration and temperature distributions at the combustor exit. Experimental case 3. T_p = 600 K; ϕ = 0.625; V_p = 7.74 m/s; V_J = 95.9 m/s.

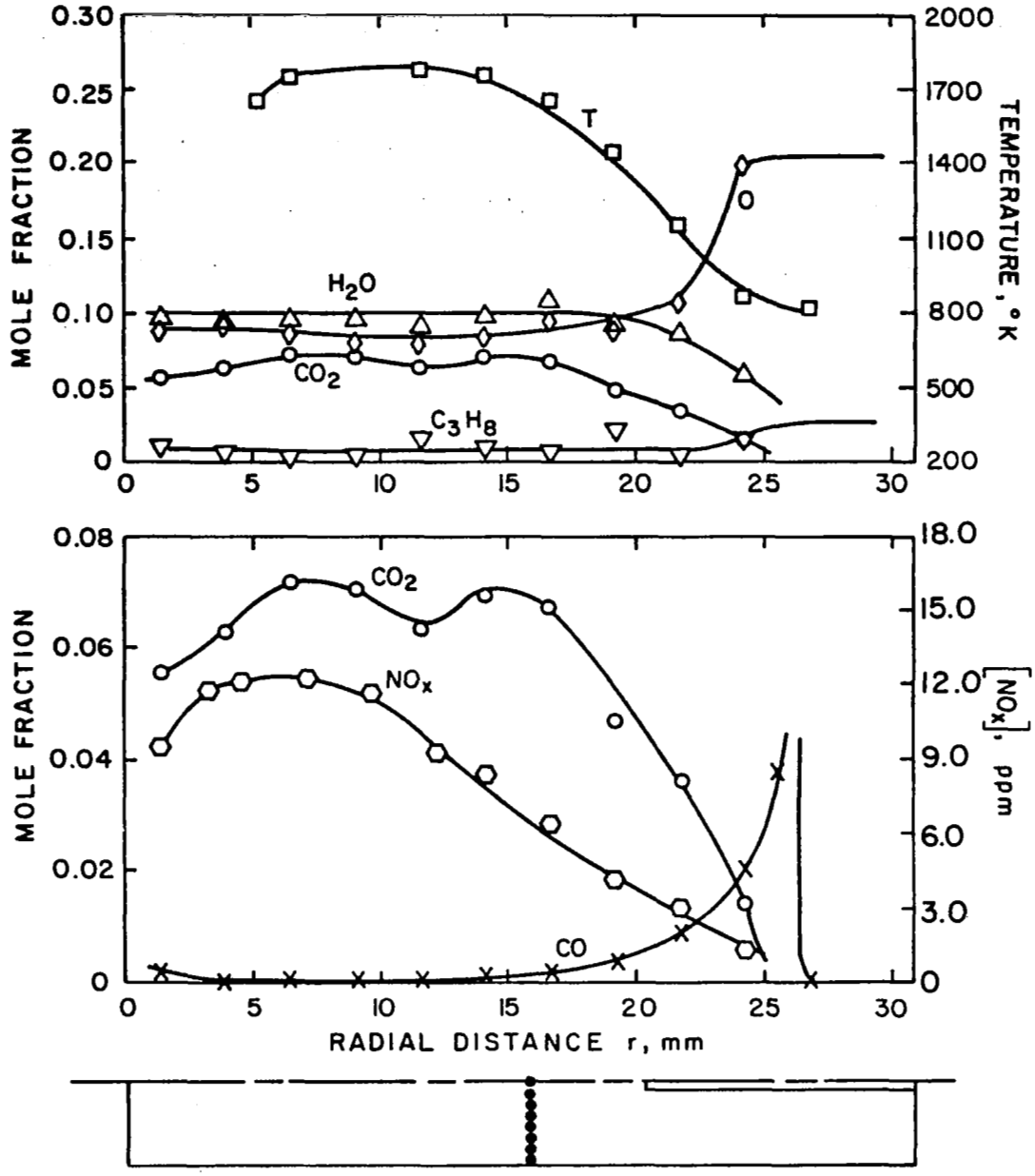

Figure 3-13. Radial concentration and temperature distributions at an axial location of 88.9 mm upstream of the combustor exit. Experimental case 3. T_p = 600 K; ϕ = 0.625; V_p = 7.74 m/s; V_J = 95.9 m/s.

decrease in CO, and a slight rise in CO can be seen in Figure 3-15 as the centerline is approached. This again reflects the more rapid oxidation of C_3H_8 and CO at the higher combustion temperatures of case 3. A region of relatively uniform composition appears to exist out to approximately 20.0 mm from the combustor centerline. Such uniform radial profiles were found to be typical in the recirculation region of case 3.

3.3.3. Case 6: $\phi = 0.45$, $T_p = 600$ K, $V_p = 7.74$ m/s

Axial profiles for case 6 are shown in Figure 3-14 and 3-15. The general characteristics of these profiles are quite similar to those of case 1. At a radial position of 11.6mm from the centerline the flamefront is fairly well defined, with abrupt changes in temperature and species concentrations. No initial peaks in CO exist. This behavior was also characteristic of the lower temperature regions in case 1. The temperature increases to a value of approximately 1400 K and remains relatively constant as the exit is approached. This compares with a maximum temperature for the same axial profile of 1300 K in case 1. Since the adiabatic flame temperature is lower for the present case (1649 K versus 1746 K for case 1), an explanation would seem to lie in the more complete combustion attained in case 6.

Figure 3-15 shows concentration and temperature profiles at a radial distance of 1.4 mm from the combustor centerline. The flamefront has become very abrupt, as indicated by the rapid rise in H_2O and CO_2. As the jet exit is axially approached the influence of jet injected reactants again becomes apparent as an

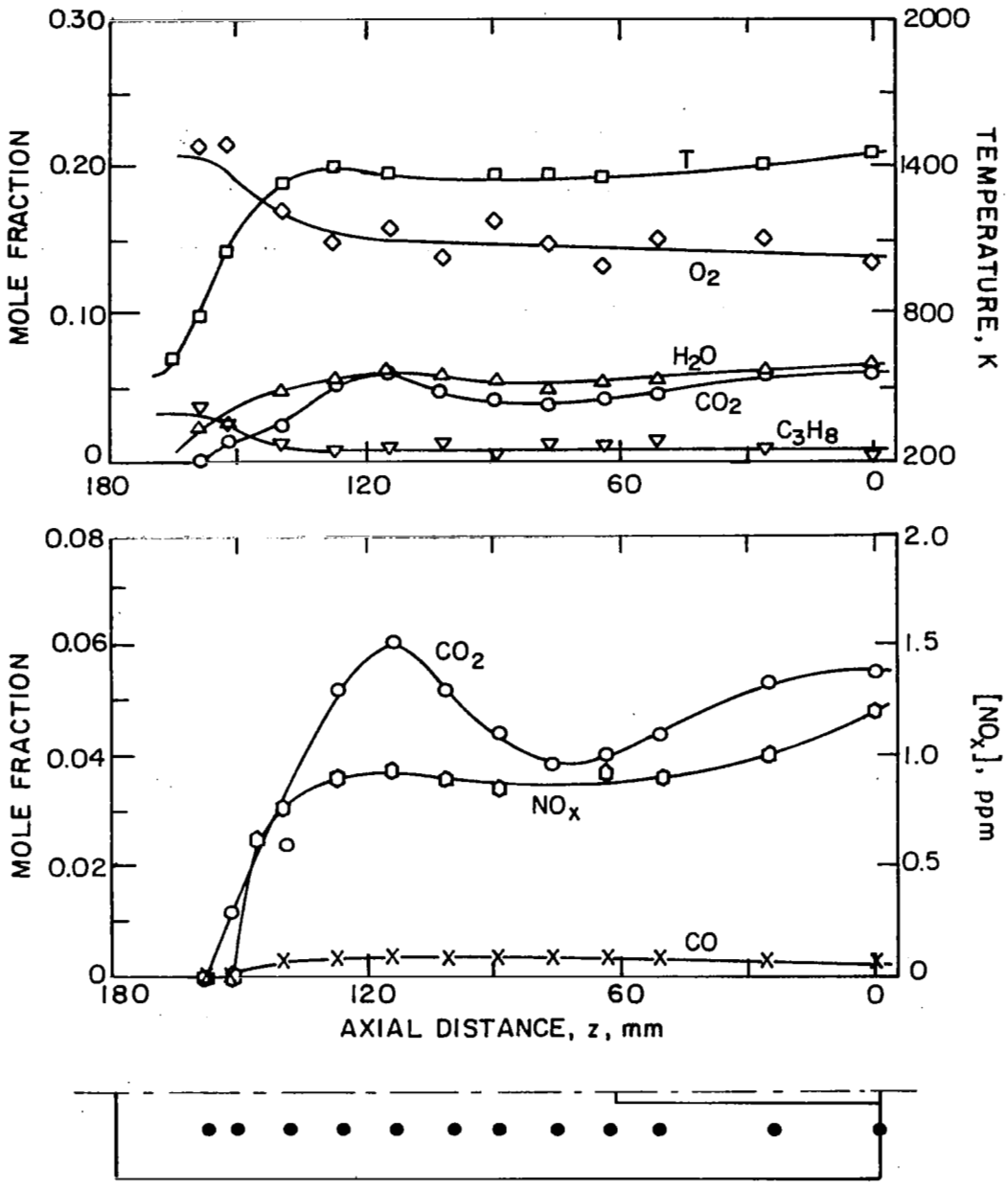

Figure 3-14. Axial concentration and temperature distributions at a radial location of 11.6 mm from the combustor centerline. Experimental case 6. T_p = 600 K; ϕ = 0.45; V_p = 7.74 m/s; V_J = 95.9 m/s.

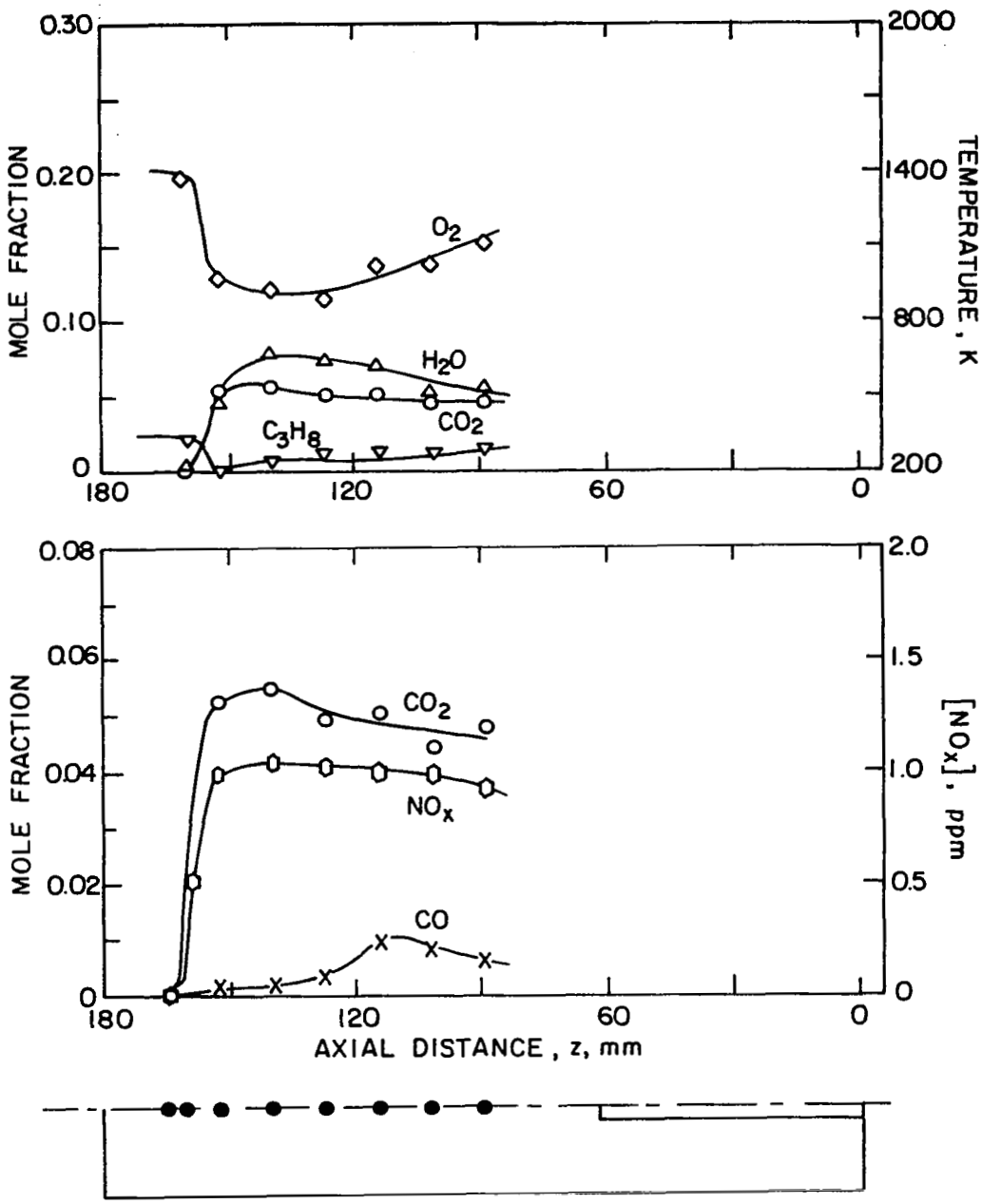

Figure 3-15. Axial concentration and temperature distributions at a radial location of 1.4 mm from the combustor centerline. Experimental case 6. T_p = 600 K; ϕ = 0.45; V_p = 7.74 m/s; V_J = 95.9 m/s

increase in O_2 and C_3H_8. As with case 1 the mole fractions associated with H_2O and CO_2, 0.075 and 0.054 respectively, compare quite closely with the equilibrium values of 0.073 and 0.055.

A comparison of Figure 3-15 with the corresponding axial profile for case 1 (Figure 3-6) indicates a peak in the CO concentration in both cases. However this peak occurs closer to the jet exit and is significantly higher in case 1, indicating more rapid conversion of C_3H_8 to CO. This primarily reflects the effect of increased equivalence ratio on the C_3H_8 oxidation rate since the jet temperature is the same in both cases.

An examination of the experimental data reveals that the flamefront in case 6 extends farther out into the main stream than in case 1. Thus it appears that differences between cases 6 and 1 can be explained by the existence of two regions in which either equivalence ratio or inlet temperature exerts the dominant influence. Near the combustor centerline since the jet inlet temperature is the same in both cases, the effect of a higher equivalence ratio for case 1 results in a higher local temperature and a more rapid oxidation of C_3H_8 to CO and of CO to CO_2. In the outer regions of the combustor the effect of an increased inlet temperature in case 6 compensates for the decrease in equivalence ratio. The result is a flamefront extending farther out into the mainstream and farther upstream (i.e., greater flame velocity) and a higher flame temperature being achieved in the outer regions of the combustor.

Radial profiles at the combustor exit are shown in Figure 3-16 for case 6. The maximum NO_x level achieved is 1.26 PPM. This is less than half the maximum value of 2.9 PPM obtained in case 1 in spite of a 300 K increase in inlet temperature. Comparison of the NO_x profile at the combustor exit with that of case 1 (Figure 3-7) shows that NO_x concentrations in the present case are less than those of case 1 over the entire combustor exit. This is surprising in that temperatures in the outer regions of the combustor were found to be higher in case 6. Two explanations can be proposed for this. First, due to the higher apparent temperatures in the recirculation region for case 1 greater quantities of NO_x would be expected to form in this region (a maximum of 3.5 PPM was found in the recirculation region for case 1 versus 1.4 PPM for case 6). Through radial mixing the NO_x levels attained in the recirculation zone will effect those levels obtained away from the combustor centerline, especially downstream as the combustor exit is approached. NO_x formation is also dependent on O atom concentration. Thus a difference in O atom concentration profiles yields a second possible explanation. Unfortunately O atom concentrations were not measured and therefore no conclusions can be drawn about the validity of this explanation. As in the recirculation zone, both H_2O and CO_2 approach their equilibrium values as the jet wall is approached.

Radial profiles for case 6 at axial distances of 114.3 mm and 139.7 mm from the combustor exit are shown in Figures 3-17 and 3-18 respectively. These profiles are similar to the corres-

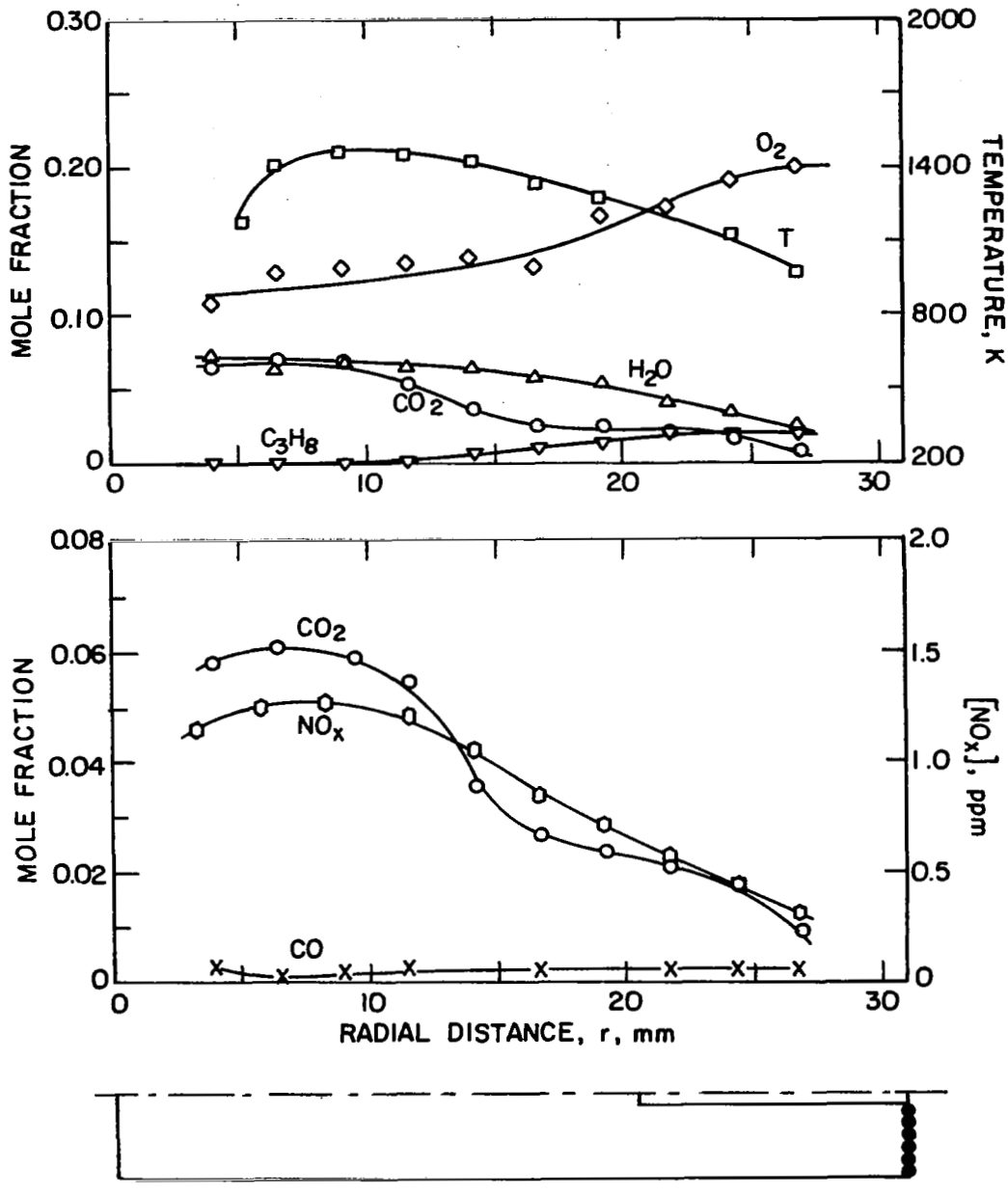

Figure 3-16. Radial concentration and temperature distributions at the combustor exit. Experimental case 6. T_p = 600 K; ϕ = 0.45; V_p = 7.74 m/s; V_J = 95.9 m/s.

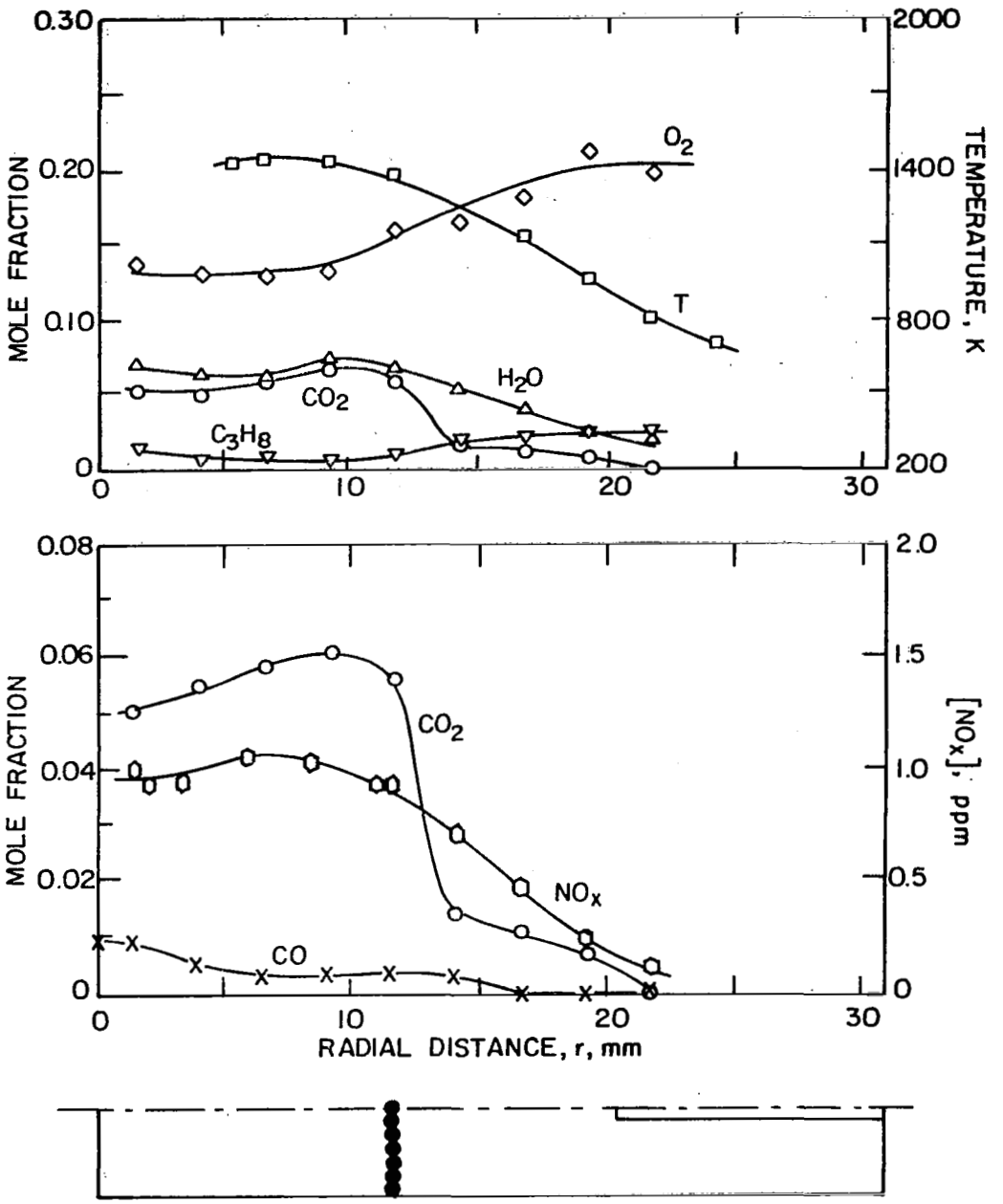

Figure 3-17. Radial concentration and temperature distributions at an axial location of 114.3 mm upstream of the combustor exit. Experimental case 6. T_p = 600 K; ϕ = 0.45; V_p = 7.74 m/s; V_J = 95.9 m/s.

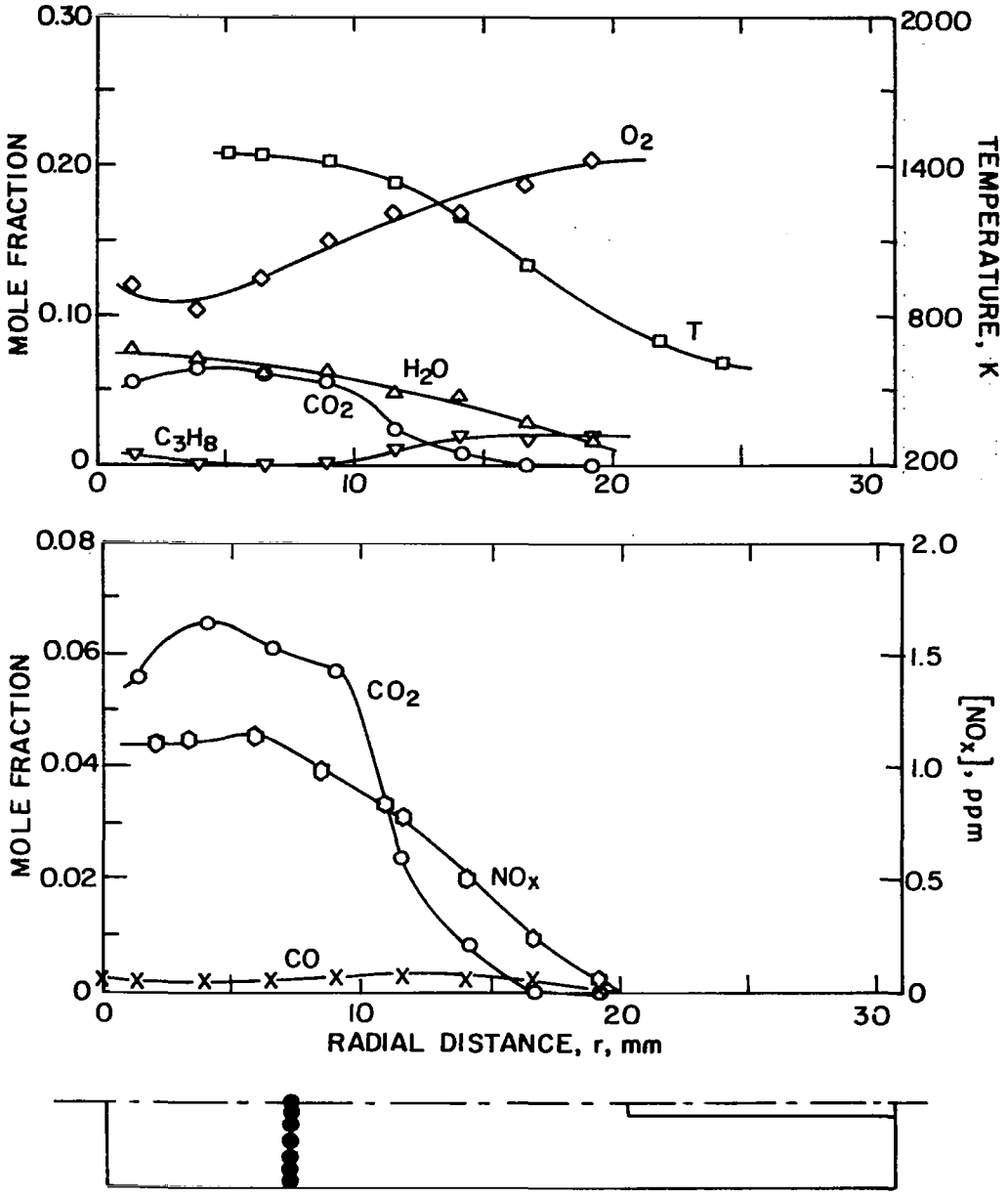

Figure 3-18. Radial concentration and temperature distributions at an axial location of 139.7 mm upstream of the combustor exit. Experimental case 6. T_p = 600 K; ϕ = 0.45; V_p = 7.74 m/s; V_J = 95.9 m/s.

ponding profiles for case 1. Again the composition is quite uniform across the entire recirculation region. The mole fractions of both H_2O and CO_2 are approximately equal to their respective equilibrium values. The dip in the CO_2 profile near the centerline is due to the slower rate of CO oxidation upstream of the jet exit.

3.3.4. Summary

The results of this section emphasize several important aspects of combustion in the ORJ. Most apparent is the existence of a well mixed region corresponding to the recirculation zone upstream of the jet exit in which species concentrations are quite uniform once the effect of jet injected reactants has disappeared. In all cases the mole fractions of H_2O existing in this zone approach those that would be expected at equilibrium. The ratio of CO to CO_2 is at a value somewhat higher than would be expected at total equilibrium. At the relatively high temperatures existing in the recirculation zone the primary CO_2 producing reaction $CO + OH \rightleftharpoons CO_2 + H$ is in partial equilibrium and the ratio $[CO]/[CO_2]$ is governed by relative radical concentrations and temperature through Equation (3-3).

It would be desirable to compare emission levels obtained in the present investigation with those obtained in typical aircraft combustors. Emission levels are frequently presented in terms of an "emission index" (grams of pollutant per kilogram of fuel burned) to normalize emissions on the basis of fuel flow. The emission index was calculated for cases 1, 3, and 6 of the present

investigation based on average UHC, CO, and NO_x concentrations at the test section exit. In cases 1 and 6 the flamefront did not extend across the entire combustor. Therefore to make any comparisons more realistic, a local emission index was calculated based on concentration measurements in that portion of the exiting gases which had undergone combustion. The results are shown in Table 3-2 along with calculated combustion efficiencies. Combustion efficiency is related to the CO and UHC emission index values by the following expression[35]:

$$1 - \eta_c = [0.232\ (EI_{CO}) + EI_{UHC}] \times 10^{-3} \qquad (3\text{-}4)$$

where η_c = combustion efficiency, EI_i = emission index of species i.

TABLE 3-2. POLLUTANT EMISSION LEVELS

	EI_{UHC} (g CH_2/kg fuel)	EI_{CO} (g CO/kg fuel)	EI_{NO_2} (g NO_2/kg fuel)		η_c
Case 1	11.4	76.7	0.11	(1.75)	0.97
Case 3	6.8	5.2	0.58	(3.22)	0.99
Case 6	1.2	85.1	0.07	(0.34)	0.98
*JT9D, cruise	0.1 - 0.3	0.2 - 0.8	16-23		1.0
*Olympus 593, cruise	<1	1 - 5	18-19		1.9

* Reference [9].

Also shown in the table are emission levels for two typical jet aircraft engines operating at cruise conditions, the JT9D for subsonic aircraft and the Olympus 593 turbojet engine for supersonic aircraft. The NO_2 emission index values in parentheses

represent values corrected to typical inlet conditions at cruise for the Olympus 593 engine (see Table 1-3). A correlation equation developed by Niedzwiecki and Jones[77] for application to swirl can and other lean combustors was used to correct the experimental data of the present invesitgation:

$$\frac{\left(EI_{NO_x}\right)_1}{\left(EI_{NO_x}\right)_2} = \frac{\left(P_3^{1/2}\right)_1 \left(e^{T_3/288}\right)_1}{\left(P_3^{1/2}\right)_2 \left(e^{T_3/288}\right)_2}$$

where P_3 and T_3 refer to combustor inlet pressure and temperature, respectively.

In case 1 (Tp = 300 K, ϕ = 0.625) the emission index for oxides of nitrogen (presented as NO_2) of 0.11 was significantly less than found in the jet engine combustors. However unacceptably high levels of UHC and CO were obtained due to the low resulting flame temperatures and insufficient residence time. Cases 3 (Tp = 600 K, ϕ = 0.625) and 6 (Tp = 600 K, ϕ = 0.45) resulted in combustion efficiencies only slightly below those attained in both jet engine combustors, with NO_2 emission index values significantly reduced. An emission index less than 1 kg NO_2/kg fuel was also attained by Anderson[36] in a lean premixed propane air experimental burner operating at conditions comparable to turbojet combustors and by Roffe and Ferri[37] in a laboratory burner using premixed-prevaporized JP-5 fuel.

As noted above, UHC and CO emission levels were slightly higher than those found in aircraft engines operating at cruise conditions. Anderson[36] has shown in a lean premixed system that a tradeoff exists between combustion efficiency and NO_x pro-

duction which effectively puts a limit on minimum NO_x emission levels attainable in such a system. Under conditions encountered in typical gas turbine combustors NO_x production is proportional to combustor residence time. Limiting high temperature residence time is an effective means of reducing NO emissions. However, as residence time is reduced insufficient time becomes available to completely oxidize unburned fuel and CO. More favorable UHC and CO emission levels could be obtained in the present investigation, with some increase in NO_x emissions, by providing slightly longer residence times in the exit portion of the combustor test section. In the study by Anderson an emission index for oxides of nitrogen as low as 0.3 g NO_2/kg fuel was measured at a combustion efficiency greater than 99 percent. Thus fuel lean premixed combustion does appear to be an effective means of reducing NO_x emissions while at the same time maintaining high combustion effieiencies.

3.4.1. NO_x Formation

The primary variables effecting NO_x formation are temperature, equivalence ratio, and residence time. In this section the effect of these variables on NO_x formation will be discussed. In all cases NO_x concentrations will be presented uncorrected for H_2O and CO_2 interference in the chemiluminescent detector since these species were not measured in all cases presented.

Figure 3-19 shows radial NO_x and temperature profiles at the combustor exit for main stream inlet temperatures of 300 K, 450 K, and 600 K. The operating points represented correspond to cases 1, 2, and 3 in Table 2-1 in which main stream velocity and equi-

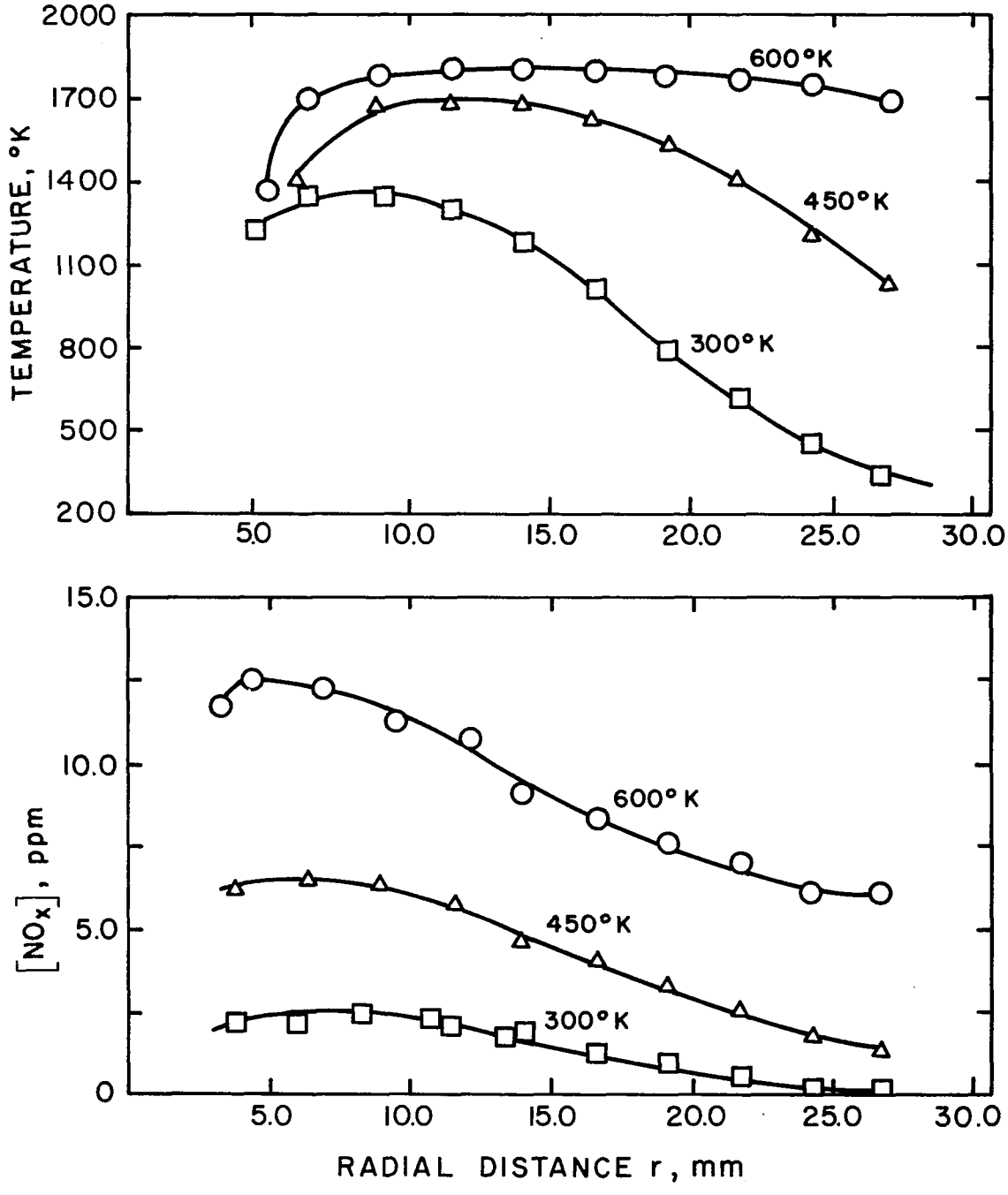

Figure 3-19. The effect of main stream inlet temperature on oxides of nitrogen and temperature distributions at the combustor exit. $\phi_p = 0.625$; $V_p = 7.74$ m/s; $\phi_J = 0.625$; $V_J = 95.9$ m/s.

valence ratio are maintained constant at 7.74 m/s and 0.625 respectively. The strong effect of flame temperature on NO_x production is apparent. An increase in inlet temperature by a factor of two results in approximately a factor of five increase in average NO_x concentration at the exit from 2 ppm for an inlet temperature of 300 K to 10.5 ppm for an inlet temperature of 600 K. While this large increase in NO_x is predominantly the result of an increase in flame temperature, residence time could also play a role. For the 600 K inlet temperature case the concentration and temperature profiles discussed in Section 3.3.1 reveal a larger combustion zone with the flame front moving both upstream and outward toward the Vycor wall. Thus combustion gases would have a longer residence time in this high temperature combustion zone before reaching the exit.

The effect of equivalence ratio is shown in Figure 3-20. In all cases the main stream and jet stream equivalence ratios were equal. An increase in equivalence ratio from 0.45 to 0.625 results in over an order of magnitude increase in average NO_x at the combustor exit (from 0.9 ppm to 10.5 ppm). Once again this can be explained in terms of the resulting change in flame temperature. Cernansky, et al[11] and Lipfert[38] have shown that NO_x emissions from different gas turbine combustors can be correlated over a range of operating conditions with the maximum flame temperature (assumed to be equal to the adiabatic flame temperature for stoichiometric combustion). Figure 3-21 shows a similar plot of average NO_x concentration at the combustor exit as a function of adiabatic flame temperature for the cases presented in Figures 3-19

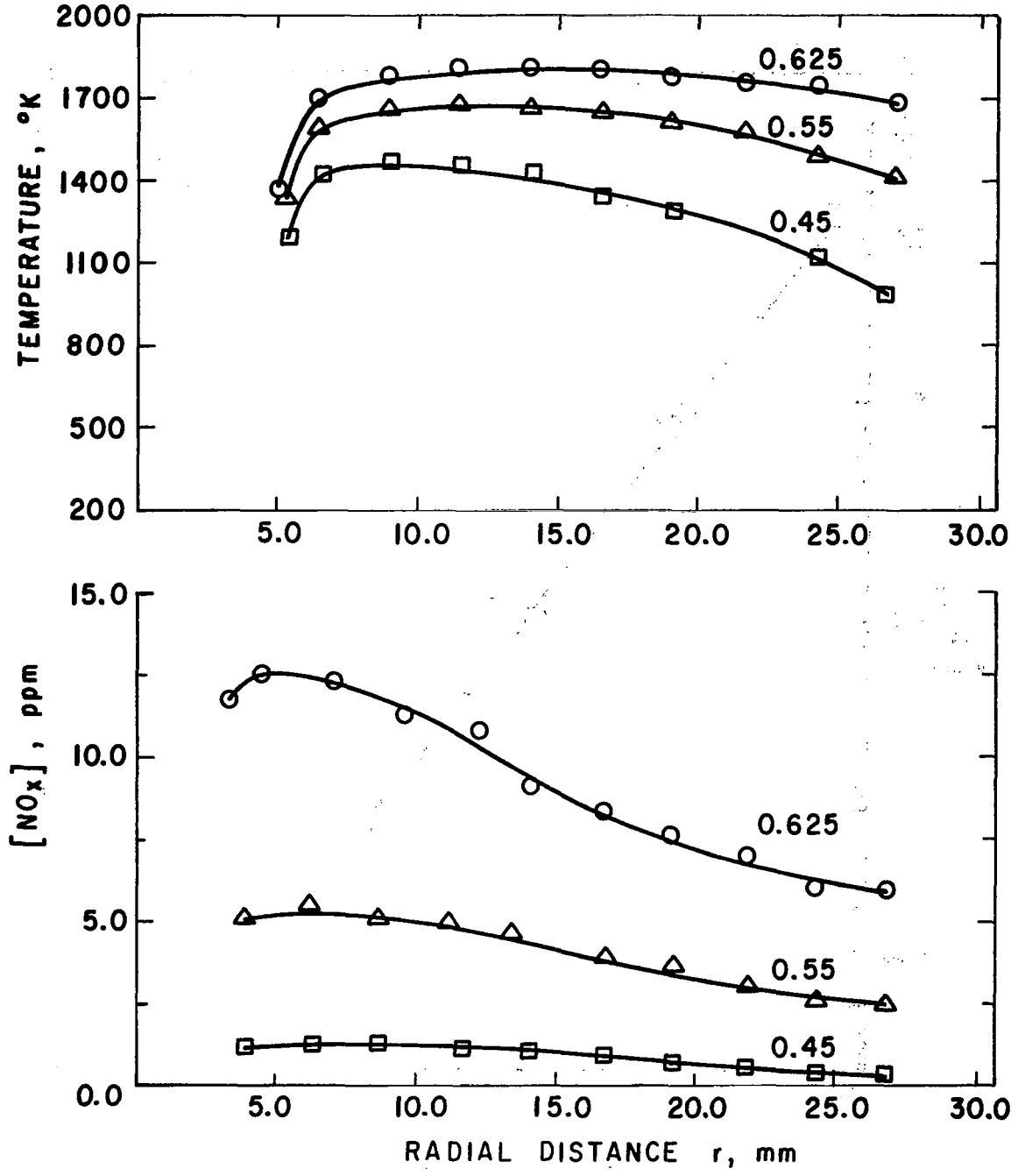

Figure 3-20. The effect of equivalence ratio on oxides of nitrogen and temperature distributions at the combustor exit. V_p = 7.74 m/s; T_p = 600 K; V_J = 95.9 m/s.

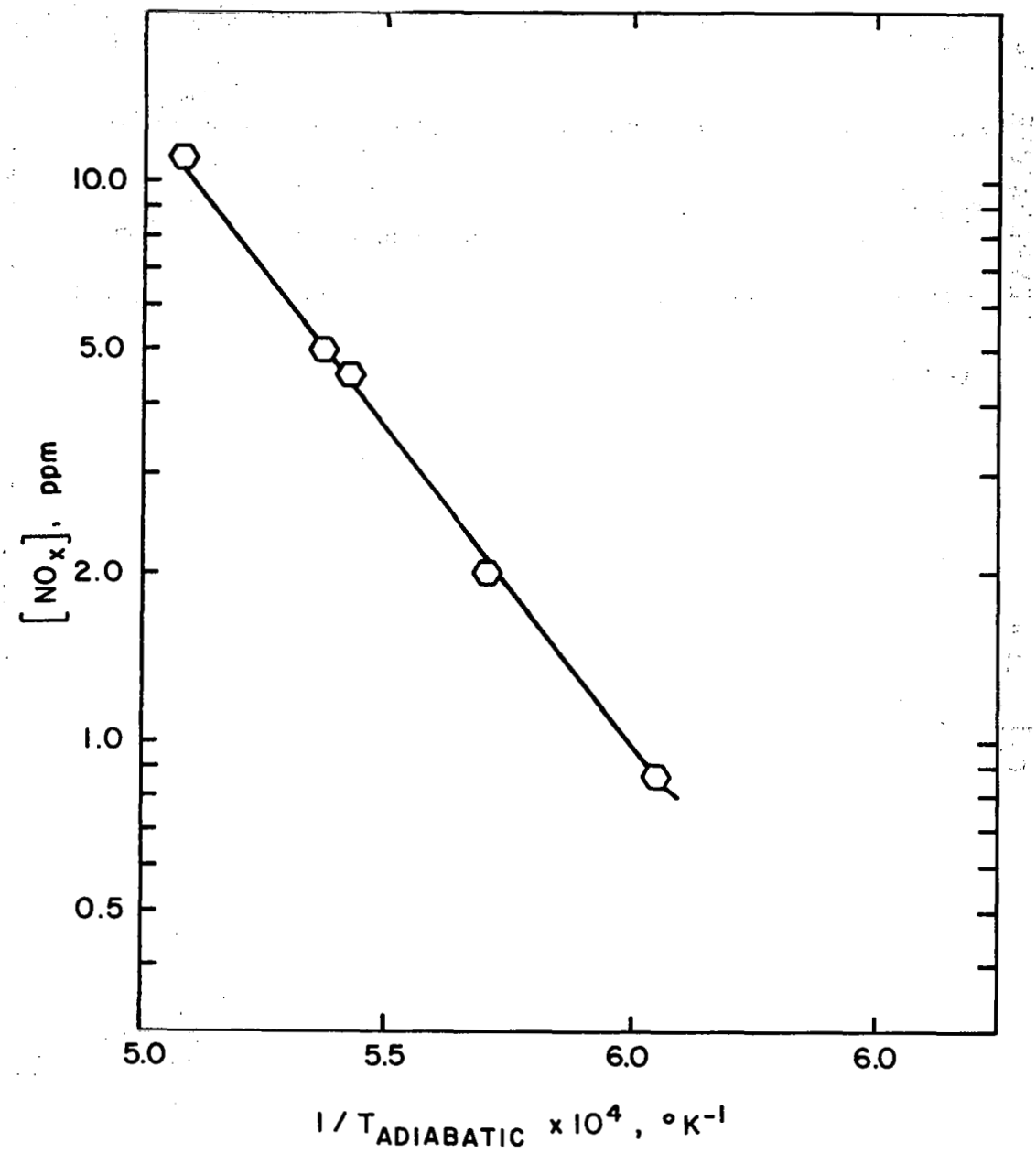

Figure 3-21. Arrhenius plot of average oxides of nitrogen concentration at the combustor exit.

and 3-20. The correlation is quite good. NO_x formation thus appears to be exponentially dependent on flame temperature as would be expected from the discussion of NO_x kinetics presented in Chapter 4, and the effect of changes in inlet temperature and equivalence ratio on NO_x production is primarily through their effect on flame temperature.

Figure 3-22 shows the effect of increasing main stream inlet velocity on NO_x formation. The trend is much as would be expected due to the linear dependence of NO_x formation on residence time. The average value of NO_x at the combustor exit can be seen to decrease from 10.5 PPM at an inlet velocity of 13.59 m/s to 9.5 PPM at a velocity of 7.74 m/s. Since changes in inlet velocity were found to effect both residence time (through increased mass flow rate) and temperature distribution in the combustor, quantitatively it would be difficult to evaluate the effect of residence time on NO_x formation from the present experimental results.

Oxides of nitrogen emission index values were calculated for all experimental cases based on average test section exit concentrations. These are summarized in Table 3-3.

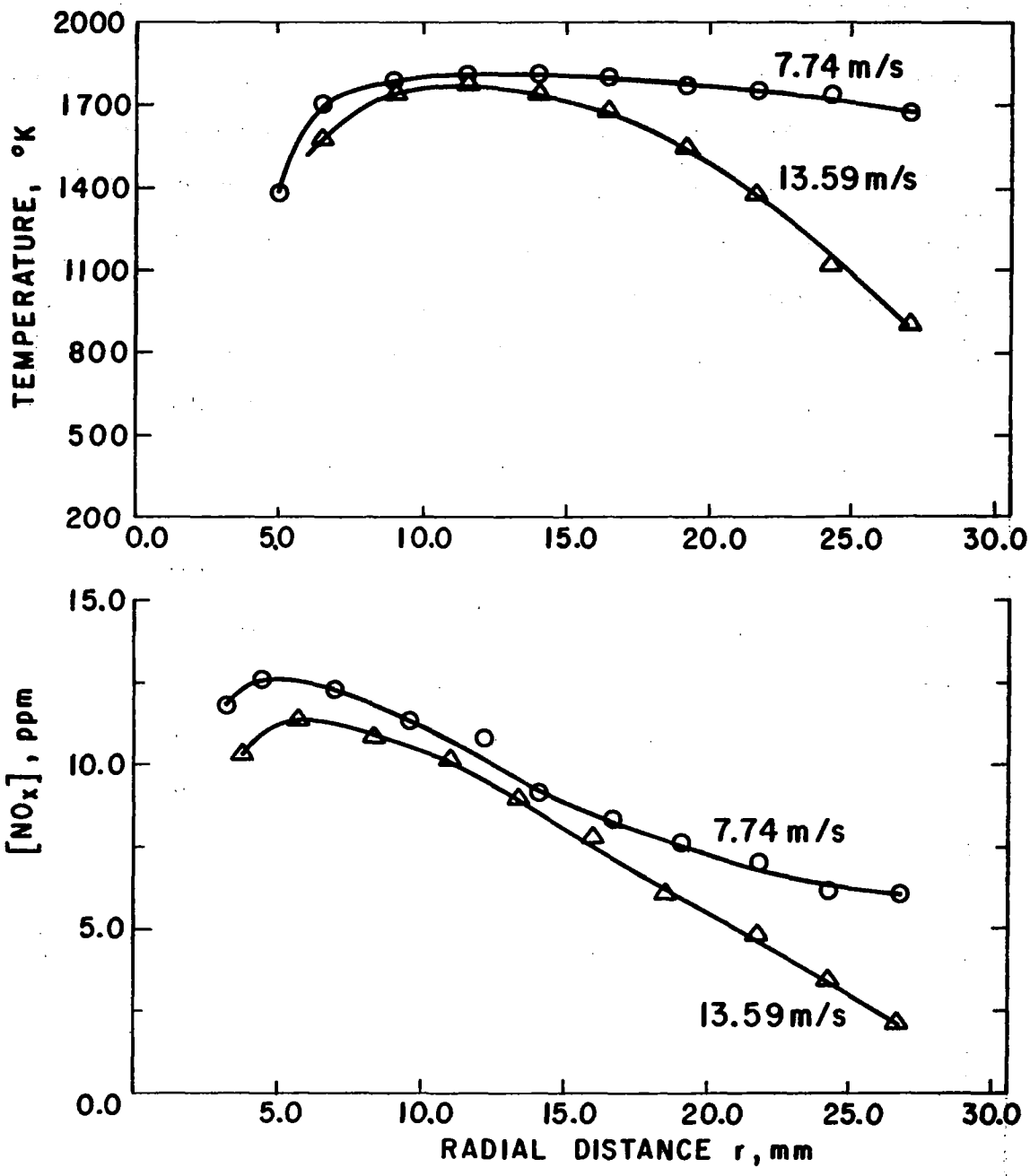

Figure 3-22. Radial distributions of oxides of nitrogen at the combustor exit for different main stream inlet velocities. $\phi_p = 0.625$; $\phi_J = 0.625$; $V_J = 95.9$ m/s.

TABLE 3-3. OXIDE OF NITROGEN EMISSION INDEX VALUES

Case	EI_{NO_2} (g NO_2/kg fuel)
1	0.11
2	0.21
3	0.58
4	0.40
5	0.21
6	0.07

The oxides of nitrogen emission index values obtained in this investigation and in similar studies[36,37] on the use of premixed/prevaporized systems to limit NO_x emissions emphasize the feasibility of achieving low NO_x emission levels through advanced combustor design.

An informative comparison can be made between the ORJ and an idealized well stirred reactor. The well stirred reactor is a constant volume steady flow reactor in which mixing is assumed to occur instantaneously between cold incoming reactants and reacting gases existing in the reactor. Thus the composition within the reactor is homogeneous and the combustion process is kinetically limited. A well stirred reactor represents the limiting case of a turbulent, premixed recirculating flow system.

Experimental NO_x emission index values obtained in this investigation for cases 3 through 6 (T_p = 600 K) were compared with the concentrations predicted in an idealized well stirred reactor. The governing equations were solved using a computer program developed by Pratt and Bowman.[39] Propane was assumed to be

prepyrolized to H_2 and CO, since predicted NO_x production was found to be insensitive to the propane oxidation mechanism used. A detailed kinetic mechanism described in Section 4.5 was used for the subsequent oxidation of CO and H_2, and the Zeldovich mechanism (reactions (4-38) and (4-39)) was used to predict NO formation. An inlet temperature and pressure of 600 K and 1 atm were assumed for the calculations. Residence time in the reactor was assumed to be equal to the estimated residence time in the recirculation zone of the ORJ for the above experimental cases (2 msec). The results are shown in Figure 3-23. Experimental emission index values agree quite well with the well stirred reactor predictions, and are significantly less than would be expected at equilibrium. These results show that NO_x emission levels approaching the limiting values of a well stirred reactor are indeed possible in premixed combustors. Comparable studies[35] on the use of premixed/prevaporized systems to limit NO_x emissions have yielded similar conclusions.

3.4.2. NO and NO_2 Formation

Recent controversy has arisen surrounding the formation of NO_2 in combustion systems. Theoretical studies involving both chemical equilibrium considerations and chemical kinetic calculations have generally predicted that NO_2 should constitute a negligible fraction of the total oxides of nitrogen emitted from gas turbine type combustors. [40, 41] However, recent experimental emission studies in both gas turbine exhaust[42] and model laboratory combustors [16, 43] involving gas sampling have yielded relatively large quantities of NO_2.

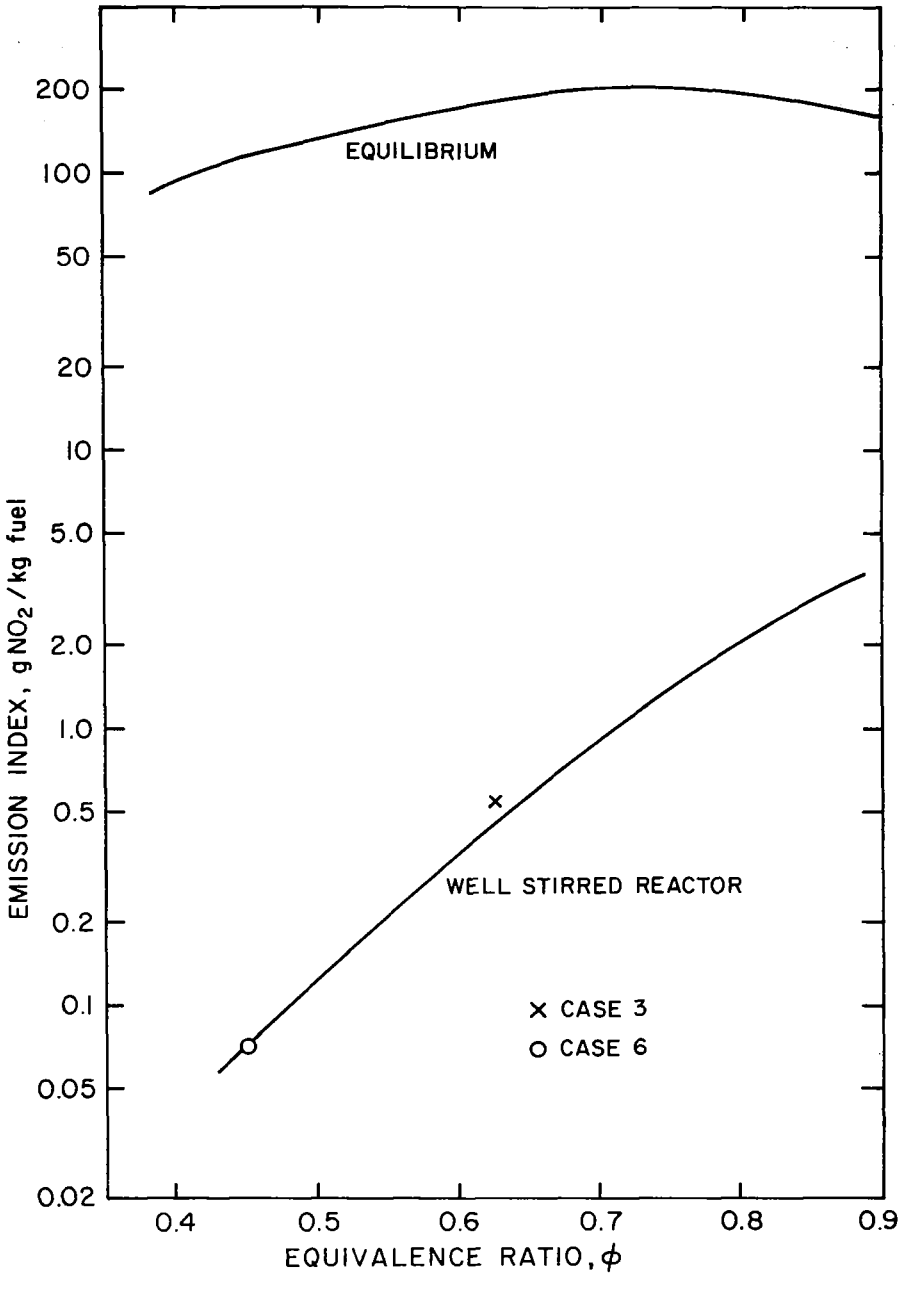

Figure 3-23. Comparison between experimental and predicted nitrogen oxides emissions. Well stirred reactor residence time is 2 msec. T = 600 K; P = 1 atm (101325 N/m^2).

Experimentally measured NO_x and NO distribution for the ORJ used in the present study are shown in Figures 3-24 through 3-36 for experimental cases 1, 3, and 6. Also shown are the corresponding temperature distributions. NO_2 is taken as the difference between NO_x and NO. It is apparent that in all cases NO_2 is the predominant oxide of nitrogen found. In cases 1 and 3 NO_2 constitutes from 50 to 100 percent of the total NO_x. In case 6 100 percent of the total NO_x exists as NO_2.

Some general observations can be drawn from an examination of these results. Measurable quantities of NO were only found to exist in higher temperature regions. In case 1 NO was measured only in the recirculation zone where the temperature was in a range greater than 1400° K to 1500° K (uncorrected for radiation). In case 3 relatively large quantities of NO were found in both the recirculation zone and over much of the downstream region of the combustor. Once again however measurable amounts of NO existed only in those regions where the temperature was greater than approximately 1400° K to 1500° K. The presence of NO in the cool region near the jet wall is probably associated with downstream convection of NO from higher temperature regions. In case 6 the maximum measured temperature was 1450° K and no NO was measured.

In summary large quantities of NO_2, in some instances constituting up to 100 percent of the total NO_x, were measured in the present investigation. Only in higher temperature regions in which the uncorrected temperature was greater than approximately 1400° K to 1500° K was any NO measured. In a recent experimental investi-

a) NO_x concentration, ppm

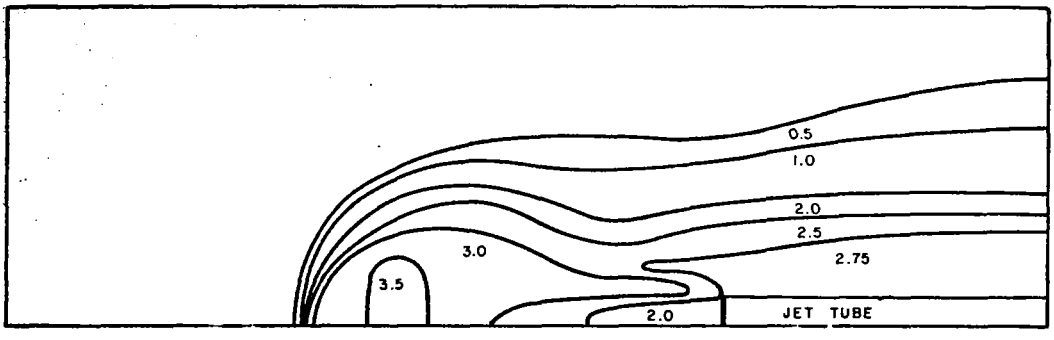

b) NO concentration, ppm

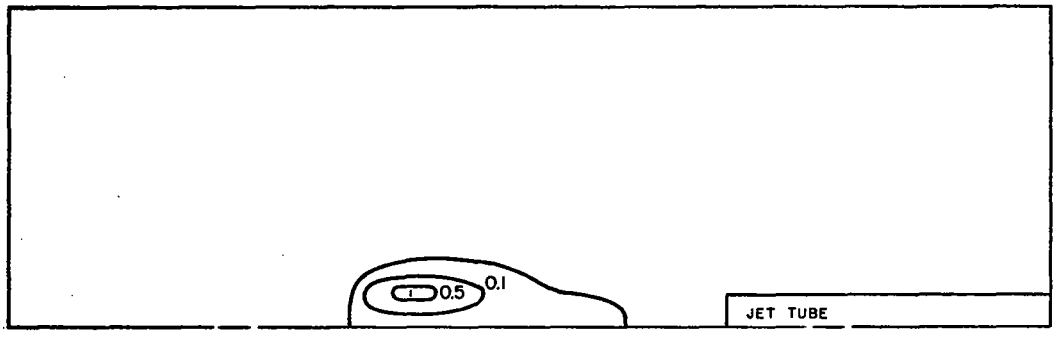

c) Temperature, °K

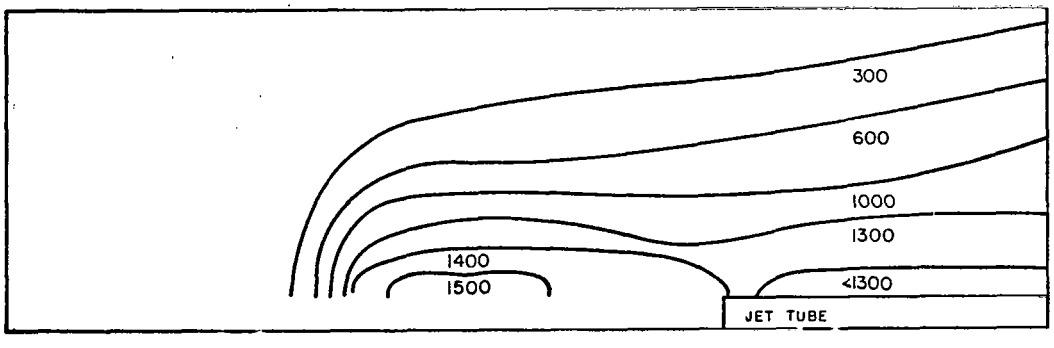

Figure 3-24. Experimental distributions of NO_x, NO, and temperature for case 1. T_p = 300 K; ϕ = 0.625; V_p = 7.74 m/s.

a) NO_x concentration, ppm

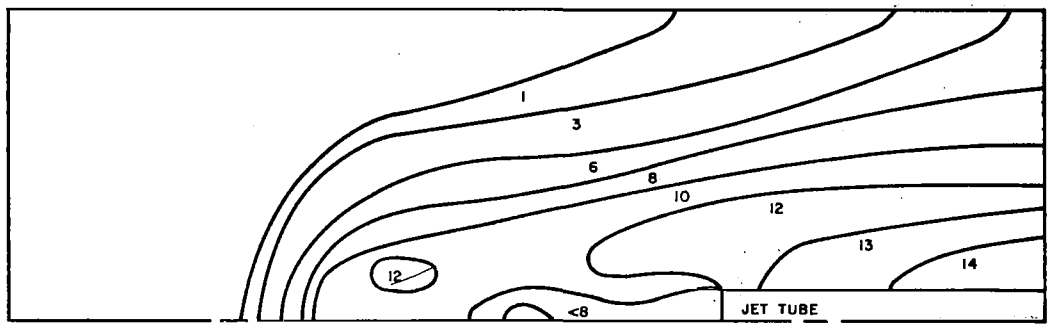

b) NO concentration, ppm

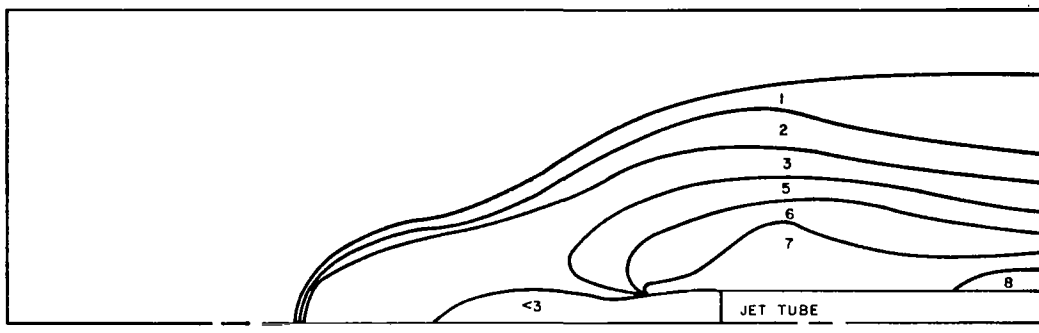

c) Temperature, °K

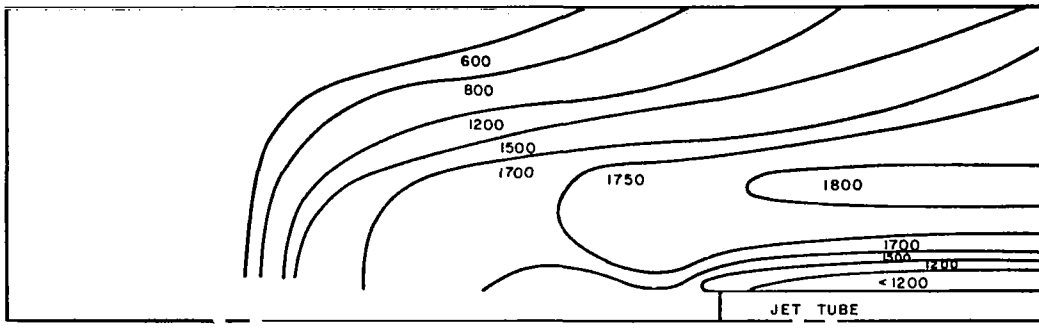

Figure 3-25. Experimental distributions of NO_x, NO, and temperature for case 3. T_p = 600 K; ϕ = 0.625; V_p = 7.74 m/s.

a) NO_x concentration, ppm

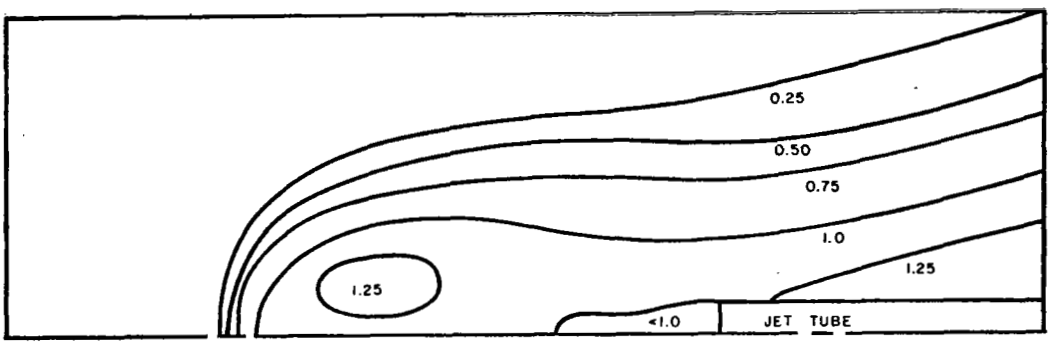

b) Temperature, °K

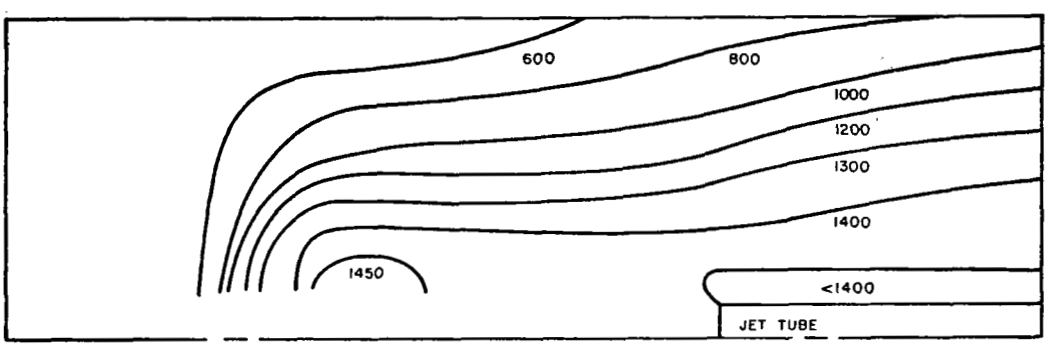

Figure 3-26. Experimental distributions of NO_x and temperature for case 6. T_p = 600 K; ϕ = 0.45; V_p = 7.74 m/s.

gation by Merrymann and Levy[44] on a flat flame premixed methane-air burner significant quantities of NO_2 were found early in the flame zone. The data were consistent with the following reaction mechanism

$$CN + O_2 \rightleftharpoons NO + CO \qquad (3\text{-}4)$$

$$NH + O_2 \rightleftharpoons NO + OH \qquad (3\text{-}5)$$

$$NO + HO_2 \rightleftharpoons NO_2 + OH \qquad (3\text{-}6)$$

$$NO_2 + O \rightleftharpoons NO + O_2 \qquad (3\text{-}7)$$

In the above mechanism NO formed in the flame zone by reactions (3-4) and (3-5) is rapidly converted to NO_2 via reaction (3-6). Subsequent conversion of NO_2 to NO is assumed to occur in the early postflame region by reaction (3-7) due to a rapid increase in O atom concentration. Under fuel lean conditions approximately 60 percent of the NO_2 was reconverted to NO.

In the above mechanism NO_2 exists primarily as a transient species due to the presence of O atoms. It is probable, however, than in turbulent systems such as encountered in this investigation rapid mixing between hot and cold regions occurs. Cernansky[43] has shown under fuel lean conditions that if the resulting cooling of hot combustion gases is rapid enough radicals such as H, O, and OH which favor NO_2 destruction fall to low levels and significant conversion of NO to NO_2 can occur via reaction (3-6). Thus maximum $[NO_2]/[NO]$ ratios would be expected in cooler regions of the combustion zone and near the flame front where rapid mixing between hot and cold gas mixtures occurs. This is precisely where maximum levels of NO_2 were found in the present

investigation. A typical radial temperature traverse taken using the thermocouple probe described in Chapter 2 is shown in Figure 3-27. It is unlikely that the time response of the thermocouple probe is rapid enough to quantitatively follow the turbulent fluctuations occurring, but the data presented do give a qualitative idea of the temperature fluctuations occurring even in a premixed system such as the ORJ. As expected maximum fluctuations occur in the outer regions of the combustor near the flamefront. In the recirculation region near the combustor centerline the temperature fluctuations are relatively small.

While it appears that the proposed mechanism involving conversion of NO to NO_2 by HO_2 radicals is consistent with the experimental results, unfortunately the same conditions which can explain the formation of NO_2 in combustion systems also exist in typical sampling probes due to the rapid decrease in gas temperature resulting from aerodynamic expansion and water cooling. Further kinetic calculations by Cernansky[43] carried out for an idealized sampling probe at a pressure of 80 torr indicate that reactions involving NO_2 are possible. Allen[19] has pointed out the possible importance of probe wall reactions such as

$$NO + O \xrightarrow{\text{probe wall}} NO_2$$

and

$$H \text{ (or } O) + O_2 \xrightarrow{\text{probe wall}} HO_2 \text{ (or } O_3)$$

followed by

$$NO + HO_2 \text{ (or } O_3) \rightarrow NO_2 + OH \text{ (or } O_2)$$

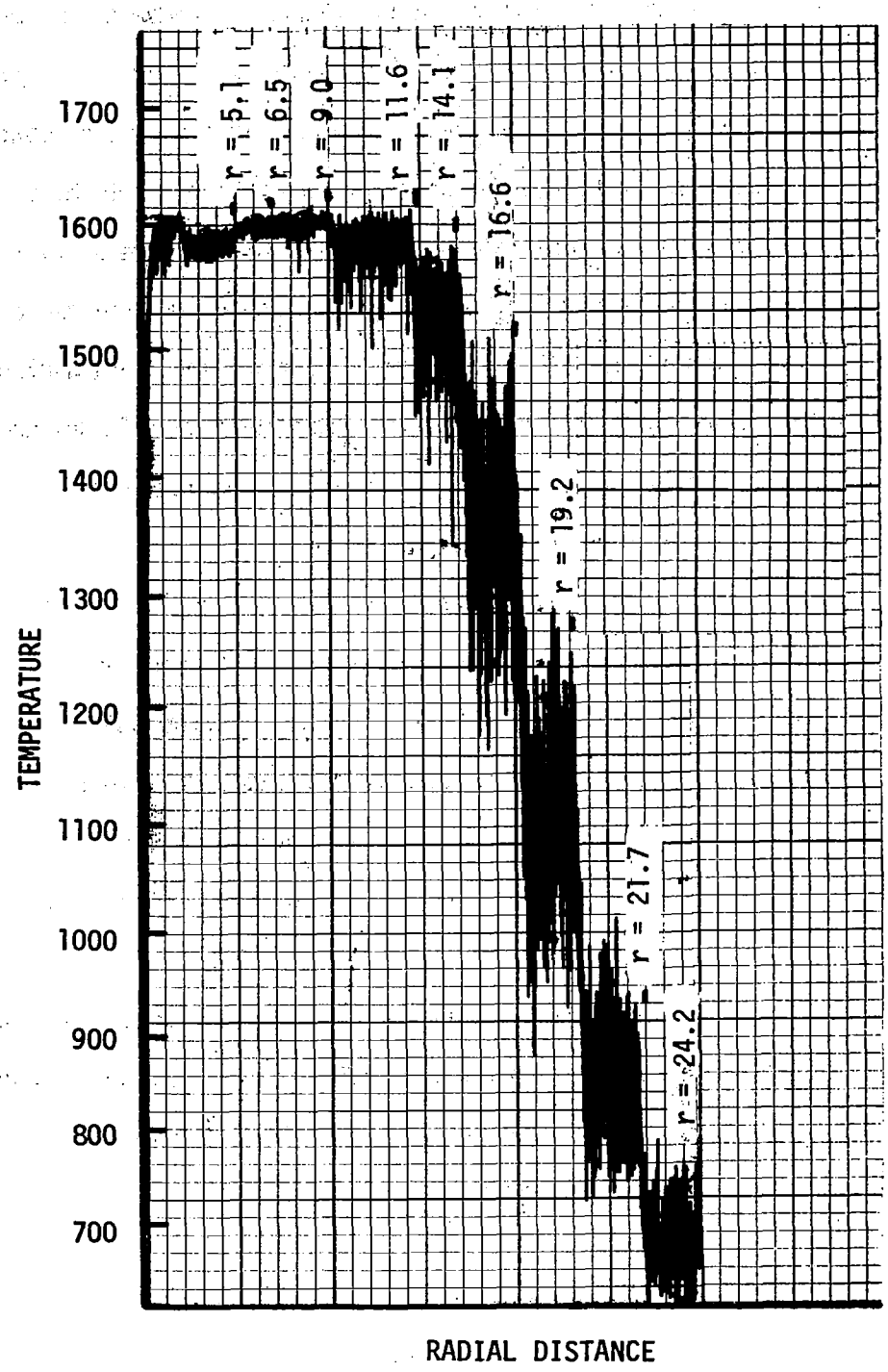

Figure 3-27. Experimentally recorded radial temperature data at an axial position of 114.3 mm upstream from the combustor exit.

Thus, it appears the only conclusion which can be drawn at this time regarding whether NO_2 is formed in the combustion system itself, in the sampling system, or perhaps in both is that much more study is needed to resolve the question.

CHAPTER 4

ANALYTICAL INVESTIGATION

4.1. Introduction

An analytical model for predicing point by point properties and concentration distributions in the combustor configuration of the present investigation was developed. This model is based on a numerical procedure developed by Gosman, et al[44] for the solution of the governing set of elliptic non-linear differential equations which describe recirculating flows of this nature.

The governing differential equations and boundary conditions reguirements are presented in Sections 4.2 and 4.3. Section 4.4 discusses the necessary physical inputs and simplifying assumptions. The kinetic model is developed in Section 4.5. The computational procedures are discussed in Section 4.6.

4.2. Numerical Calculations

4.2.1. Governing Differential Equations

The governing partial differential equations for a turbulent steady flow system in the absence of combustion are the conversation of mass and the conservation of momentum. The conservation of energy and a conservation equation for each species must be considered when dealing with a nonisothermal chemically reacting system.

These equations in their most general form are shown below in tensor notation.[45]

Conservation of Mass:

$$\frac{\partial}{\partial t}\rho = -(\nabla \cdot \rho\vec{v}) \tag{4.1}$$

Conservation of Momentum:

$$\frac{\partial}{\partial t}\rho\vec{v} = -(\nabla \cdot \rho\vec{v}\vec{v}) - \nabla p - (\nabla \cdot \bar{\bar{\tau}}) \tag{4.2}$$

Conservation of Energy:

$$\frac{\partial}{\partial t}\rho h = -(\nabla \cdot \rho\vec{v}h) - (\nabla \cdot \vec{q}) - (h\nabla \cdot \vec{J}_i) - (\bar{\bar{\tau}} : \nabla\vec{v}) \tag{4.3}$$

Conservation of species:

$$\frac{\partial}{\partial t}\rho m_i = -(\nabla \cdot \rho\vec{m}_i) - (\nabla \cdot \vec{J}_i) - R_i = 0 \tag{4.4}$$

Here $\bar{\bar{\tau}}$, $\vec{q}$, and $\vec{J}_i$ represent the flux of momentum, energy, and mass respectively and are given by the well known relations

$$\bar{\bar{\tau}} = \mu(-\tfrac{2}{3}\nabla \cdot \vec{v} + \text{def}\,\vec{v}) \tag{4.5a}$$

$$\vec{q} = -k\nabla T \tag{4.5b}$$

$$\vec{J}_i = -\rho D_i \nabla m_i \tag{4.5c}$$

R_i represents a source term for species i due to chemical reaction.

Note than in general the dependent variables $\vec{v}$, h, and m_i are instantaneous values and are functions of time as well as space since turbulence is characterized by unsteady fluctuations in these quantities. Theoretically, at least it would be possible to solve the above system of equations for the instantaneous values of the dependent variables if adequate computer facilities were available. Unfortunately the excessive computer facilities required made such a solution economically unfeasible.

A more common approach to the problem is the introduction of time averaged quantities.[31] For velocity this time average becomes becomes

$$\vec{v} = \frac{1}{t_o} \int_t^{t+t_o} v\,dt$$

Here the integration is taken over a sufficient period of time, t_o, to make the average value independent of time. The instantaneous velocity can then be written as the sum of the average value and a velocity fluctuation v'

$$v = \vec{v} + v' \tag{4-6}$$

A similar derivation can be made for the other fluctuating variable. Substitution of these equations into the conservation equations (4-1) through (4-4) yields the time smoothed conservation equations:

Conservation of Mass:

$$-(\nabla \cdot \rho v) = 0 \tag{4-7}$$

Conservation of Momentum:

$$-\rho - [\nabla \cdot \rho \vec{v}\vec{v}] - (\nabla \cdot \bar{\bar{\tau}}) - [\nabla \cdot \bar{\bar{\tau}}_{(t')}] = 0 \tag{4-8}$$

Conservation of Energy:

$$-[\nabla \cdot \rho \vec{v} h] - [\nabla \cdot \vec{q}] - [\nabla \cdot \vec{q}^{\,t}] - [h\nabla \cdot \vec{J}] - [h\nabla \cdot \vec{J}^{\,t}] -$$

$$-(\tau : \nabla \vec{v}) - (\tau : \nabla \vec{v})^{t} = 0 \tag{4-9}$$

Conservation of Species:

$$-[\nabla \cdot \rho \vec{v} m_i] - [\nabla \cdot \vec{J}] - [\nabla \cdot \vec{J}^{\,t}] - R_i = 0 \tag{4-10}$$

Note in the above equations the appearance of a series of turbulent flux transport terms of the form

$$q_i^{t} = \rho c_p \overline{v_i' T} \tag{4-11a}$$

$$\tau^t_{ij} = \overline{v'_i v'_j} \qquad (4\text{-}11b)$$

$$J^t_i = - \overline{v'_i m'_i} \qquad (4\text{-}11c)$$

Much of the difficulty in dealing with turbulent flows lies in adequately modeling these turbulent flux terms.

An early proposal,[45] in analogy with laminar transport laws (see Equations 4-5 through 4-7), was to assume a similar dependence of heat, momentum, and species fluxes on average temperature velocity, and concentration gradients respectively, and replace the corresponding transport coefficients by effective transport coefficients. These new coefficients are no longer constants but become functions of the intensity and scale of turbulence. Thus the above turbulent flux equations can be written

$$\bar{\bar{\tau}} = \mu_{eff} \left(\vec{\bar{v}}\bar{\bar{I}} + \text{def } \vec{\bar{v}}\right) \qquad (4\text{-}12a)$$

$$\bar{\bar{\tau}} = \mu_{eff} \left(2/3 \cdot \vec{\bar{v}}\bar{\bar{I}} + \text{def } \vec{\bar{v}}\right) \qquad (4\text{-}12b)$$

$$q = - k_{eff} \nabla \bar{T} \qquad (4\text{-}12c)$$

$$\bar{T}_i = \rho D_{i_{eff}} \nabla \bar{m}_i \qquad (4\text{-}12d)$$

This is the approach adopted in the present investigation. Further discussion of these effective transport terms can be found in Section 4.4.

For that part of the flow away from the wall the turbulent diffusivities are much greater than the corresponding molecular diffusivities, i.e.,

$$\mu \ll \mu_{eff}$$

$$k \ll k_{eff}$$

$$D \ll D_{eff}$$

and therefore the molecular transport terms in the conservation equations can be neglected. In a region very near the wall, however, the turbulent and molecular diffusivities transport mechanism become comparable. It can be shown for the conditions of the present investigation that molecular transport is important only in a region within 1 mm of the outer combustor wall. Since this region is not likely to have a significant effect on the overall combustion process, molecular transport was neglected in the solution of the conservation equations.

This time averaged approach has been useful[44] in predicting convective patterns in steady flow combustors. However, as more experimental data are obtained, the limitations of this approach are becoming apparent. As stated by Pratt,[46] "The most serious shortcoming of this approach is the inability to deal directly with the effect of coupled species concentration and temperature fluctuations, which are ultimately required for correct prediction of combustion stability limits and formation of temperature-sensitive pollutants such as NO_x." Even in the present premixed system temperature fluctuations of several hundred degrees were apparent near the outer flame zone as was shown in Figure 3-27. Concentration fluctuations are also almost certain to occur. By dealing with time average properties the entire process by which relatively cold large scale eddies containing unburned fuel-air mixtures break down into smaller scale eddies where molecular mixing between reactants and reactive combustion products occurs is being substantially simplified. It is felt that only through comparisons

with experimental data as is done in the present investigation can those possible shortcomings in numerical techniques be brought out and improvements made.

4.2.2. Finite Difference Formulation

For the purposes of numerical calculations the above system of governing differential equations can be written in a common form. This involves the introduction of two additional variables, the vorticity and stream function.

The vorticity, ω, is defined as

$$\omega = \frac{\partial v_r}{\partial z} - \frac{\partial v_z}{\partial r}$$

Introduction of the vorticity allows the removal of pressure from the conservation equations and reduces the number of momentum equations to be solved from two to one.

For two dimensional axisymetric flow the stream function, ψ, is defined as

$$v_z = \frac{1}{r} \frac{\partial \psi}{\partial r} \quad ; \qquad v_r = -\frac{1}{r} \frac{\partial \psi}{\partial z}$$

Introduction of the stream function automatically satisfies the continuity equation and eliminates velocity from the conservation equations. Thus for two dimensional axisymetric flow the above set of conservation equations can be written as[44]

$$a_\phi \frac{\partial}{\partial z}\left(\phi \frac{\partial \psi}{\partial r}\right) - \frac{\partial}{\partial r}\left(\phi \frac{\partial \psi}{\partial z}\right) - \frac{\partial}{\partial z} b_\phi \frac{\partial}{\partial z}\left(c_\phi \phi\right) - \frac{\partial}{\partial r} b_\phi \frac{\partial}{\partial r}\left(c_\phi \phi\right) + d_\phi = 0 \qquad (4\text{-}13)$$

where the functions a_ϕ, b_ϕ, c_ϕ, and d_ϕ are given in Table 4-1.

TABLE 4-1.

ϕ	a_ϕ	b_ϕ	c_ϕ	d_ϕ
Ψ	0	$\frac{1}{\rho}$	1	$-\omega$
ω/r	r^2	r^3	μ_{eff}	$-r^2 \frac{\partial}{\partial z}\left(\frac{v_z^2 + v_r^2}{2}\right) \cdot \frac{\partial \rho}{\partial r}$ $- \frac{\partial}{\partial r}\left(\frac{v_z^2 + v_r^2}{2}\right) \cdot \frac{\partial \rho}{\partial z}$
h	1	$r\Gamma_{h,eff}$		$-\frac{\partial}{\partial z}\left(\mu_{eff} r\{(1 - \frac{1}{\sigma_h}) \frac{\partial v^2/2}{\partial z}\right.$ $+ \Sigma \left(\frac{1}{\sigma_i} - \frac{1}{\sigma_h}\right) h_i \frac{\partial m_i}{\partial z} - \frac{\partial}{\partial r}[\mu_{eff} r$ $\left.(1 - \frac{1}{\sigma_h}) \frac{\partial v^2/2}{\partial r} + \sum_i \left(\frac{1}{\sigma_i} - \frac{1}{\sigma_h}\right) h_i \frac{\partial m_i}{\partial r}\}\right]$
m_i	1	$r\Gamma_{i,eff}$	1	$-rR_i$

Here σ_h and σ_i refer to the effective Prandtl and Schmidt numbers. $\Gamma_{h,eff}$ and $\Gamma_{i,\,eff}$ are the effective exchange coefficients for heat and mass transfer. These are defined by the following expressions.

$$\sigma_h = \frac{\mu_{eff}\, c_p}{k_{eff}} = \frac{\mu_{eff}}{\Gamma_{h,\,eff}} \; ; \quad \sigma_i = \frac{\mu_{eff}}{\rho D_{i,\,eff}} = \frac{\mu_{eff}}{\Gamma_{i,\,eff}}$$

The effective Prandtl and Schmidt numbers are treated further in Section 4.3. Once the effective viscosity is estabilished, all the transport properties are known.

Equation (4-13) represents a system of simultaneous non-linear differential equations for the dependent variables ω/r, Ψ, h, and m_i. An approach to the solution of this system of equations was proposed by Gosman, et al[44] in which attention is confined to the solution of Equation (4-13) at a finite number of nodal grid points. The above system of equations is then reduced to a set of simultaneous algebraic finite difference equations in which the values of the variables at a particular node are related to the values of variables at adjacent nodes. Details on the derivation of these finite difference equations can be found in reference [44].

4.3. Boundary Conditions

The above set of equations are elliptic in nature and therefore require that boundary conditions be specified for each dependent variable at all points surrounding the flowfield. These boundary conditions are generally of three types: 1) specification of the dependent variable value along a particular boundary, 2) specification of the gradient of the variable normal to the boundary, 3) specification of an algebraic relation which connects the value of the variable at the boundary to the normal velocity component at that boundary. The boundary conditions used in the present investigation are consistent with the following descrip-

tion of the ORJ test section being modeled. Details on the finite difference form of the resulting boundary conditions can be found in the computer program listing in Appendix E.

Inlet conditions were based on experimentally measured values. The main stream inlet velocity profile is shown in Figure 4-1. Main stream inlet composition and temperature profiles were found to be uniform. For the experimental case being modeled (case 3) these were taken as corresponding to an inlet equivalence ratio of 0.625 and an inlet temperature of 600° K. Velocity, temperature, and composition profiles at the jet exit were also assumed to be uniform. For case 3 the velocity at the jet exit was 95.9 m/sec and the composition corresponded to an equivalence ratio of 0.625. Since the jet injector was water cooled, a jet inlet temperature of 300° K was assumed.

The outer Vycor wall is assumed to be adiabatic and impermeable to mass fluxes. Thus gradients in mass fraction and enthalpy normal to the wall are equal to zero. The same considerations apply to the axis of symmetry at the centerline. An assumed parabolic distribution in the dependent variable of interest was used to calculate its value at the wall from the value at the two nodes adjacent to the wall. Since the velocity normal to a wall or the centerline is zero, the stream function takes on a constant value along these boundaries.

At the exit plane the streamlines are assumed to be parallel to the axis. This is valid if the walls at the exit are parallel to the centerline and if the recirculation zone is reasonably far upstream. Subject to the same constraint, gradients in mass

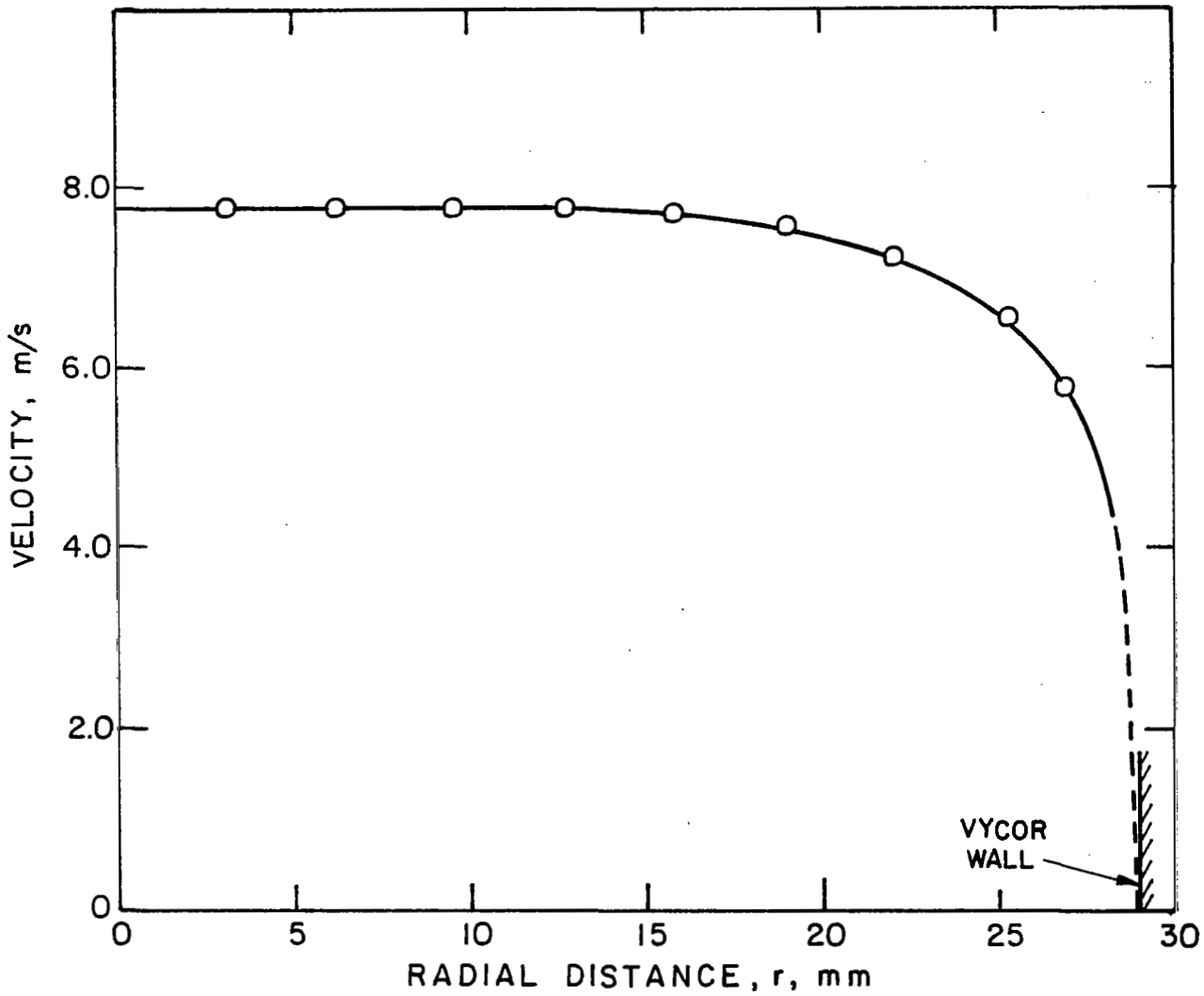

Figure 4-1. Main stream inlet velocity distribution.

fractions and enthalpy were also assumed to be zero at the exit plane. Subsequent experimental results showed this assumption to be valid.

Vorticity presents a problem since neither vorticity along a wall nor the vorticity gradient normal to the wall are known initially. An equation for vorticity at the wall was derived by Samuelsen[47] based on the following assumptions:

1. The flow between the wall and the node adjacent to the wall is parallel to the wall ($v_r = 0$) and the velocity varies according to the $\frac{1}{6}$ power of the distance between the two points. Thus for a horizontal wall (constant r)

$$v_z = s \frac{n}{n_1}^{\frac{1}{6}}$$

where

s = a constant

n = normal distance from wall

n_1 = normal distance from wall to adjacent node

2. The density varies linearly between the wall and the adjacent node. An expression for the wall vorticity can then be derived through integration of the vorticity stream function relation using a finite difference approximation.

Since the jet injector is water cooled, the outer wall of the jet is non-adiabatic and the temperature must be specified. More detailed radial temperature profiles were taken in the region

of the jet wall, and extrapolation of these profiles indicated a wall temperature of 700° K.

4.4. Thermodynamic Properties

The required inputs to the numerical program are density, transport coefficients, and specific heat.

Density: The ideal gas equation of state is used to relate density to the pressure and temperature. Thus

$$\rho = \frac{P(MW_{mix})}{R_u T}$$

where the molecular weight of the mixture is computed from the species mass fractions using the relation

$$MW_{mix} = \frac{1}{\sum_i m_i/MW_i}$$

Specific Heat: The specific heat is used to compute the temperature from the relation

$$h = \int_{To}^{T} (\Sigma c_{p_i} m_i)\, dT + \sum_i \Delta H_{F_i} m_i \qquad (4\text{-}15)$$

where

h = stagnation enthalpy of mixture

c_{p_i} = constant pressure specific heat of species i

ΔH_{F_i} = heat of formation of species i

m_i = mass fraction of species i

To = reference temperature

Since c_{p_i} is a nonlinear function of temperature, the determination of T from Equation (4-15) would require a more extensive iteration procedure. Thus it was found desirable in the numerical calculations

to assume a constant value for specific heat. A value was chosen which would give an adiabatic flame temperature for complete combustion (products CO_2 and H_2O) in agreement with that calculated using JANAF thermochemical data.[48] Calculations yielded a value for specific heat of 1.22 J/gm °K. Introduction of a constant specific heat was estimated to introduce a maximum error of approximately 4.0% in flame temperature calculations.

Effective Viscosity: A simplified viscosity model developed by Pun and Spalding[49] and Odlozinski[50] was used in the present calculations. This is given by

$$\mu_{eff} = KD^{\frac{2}{3}}L^{\frac{1}{3}}\rho^{\frac{2}{3}}[(mv^2)_p + (mv^2)_J]^{\frac{1}{3}} \qquad (4\text{-}16)$$

where

K = constant (0.012)

D = combustor diameter

L = combustor length

ρ = density

mv^2 = incoming kinetic energy

Derivation of Equation (4-16) is based on the observations that:

1. μ_{eff} increases with local density
2. μ_{eff} increases with the incoming kinetic energy rate
3. μ_{eff} decreases with an increase in chamber length and increases with chamber diameter.

It should be noted that currently more advanced turbulence models are available or are being developed.[51] Most of these

involve the solution of additional equations for a turbulent kinetic energy k_t and mixing length l. As originally proposed by Prandtl the effective viscosity can be calculated from an equation of the type

$$\mu_{eff} = \rho l v_t$$

where v_t is related to the turbulence kinetic energy

$$v_t \propto \sqrt{k_t}$$

Such a model would almost certainly result in a more realistic prediction of turbulence properties. However, such models are still in the developmental stage and involve some degree of empiricism. Because of these considerations and the approximations necessary in the kinetic model, it was concluded that the additional expense and complexity did not warrant the use of a more advanced viscosity model in this investigation.

Effective Prandtl and Schmidt Numbers: The effective Prandtl and Schmidt Numbers were defined previously as

$$\sigma_h = \frac{\mu_{eff} c_p}{k_{eff}} \quad ; \quad \sigma_i = \frac{\mu_{eff}}{\rho D_{i,\,eff}} \tag{4-17}$$

For gases in turbulent flows, the effective Prandtl and Schmidt numbers are near 0.7[52]. In the present investigation their values were taken as equal to 1.0. Referring to Table 4-1 one can see that this has the effect of considerably simplifying the source terms in the energy conservation equation. Once μ_{eff} is known the other transport coefficients can be determined from Equation (4-17).

4.5. Chemical Kinetics

4.5.1. Introduction

Uncertainties exist in both the mechanism and the rates for the high temperature oxidation of higher hydrocarbons and the

resulting intermediates. The complexity involved makes the modeling of even a relatively simple hydrocarbon such as methane quite difficult. Recent work by Glassman, et al[26] in an adiabatic flow reactor has identified the presence of a number of intermediate hydrocarbon species during the oxidation of higher paraffin hydrocarbons such as propane. These include C_3H_8, C_2H_4, CH_4, and C_2H_6. Further oxidation of these species would require consideration of a large number of additional species and a complicated set of largely unknown reaction steps.

The high temperature mechanism for CO oxidation is fairly well known. The principal CO oxidation reaction in hydrocarbon flames[53] is

$$CO + OH \rightleftharpoons CO_2 + H \qquad (4\text{-}18)$$

Thus, to predict CO oxidation rates a knowledge of OH and H concentrations is necessary. In the initial flame zone, radical concentrations are determined by the bimolecular reactions[54]

$$H + O_2 \rightleftharpoons OH + O \qquad (4\text{-}19)$$

$$O + H_2 \rightleftharpoons OH + H \qquad (4\text{-}20)$$

$$H_2 + OH \rightleftharpoons H_2O + H \qquad (4\text{-}21)$$

$$OH + OH \rightleftharpoons H_2O + O \qquad (4\text{-}22)$$

At some later point in the combustion zone the relatively slow thermolecular recombination reactions

$$O + O + M \rightleftharpoons O_2 + M \qquad (4\text{-}23)$$

$$H + H + M \rightleftharpoons H_2 + M \qquad (4\text{-}24)$$

$$H + O + M \rightleftharpoons OH + M \qquad (4\text{-}25)$$

$$H + OH + M \rightleftharpoons H_2O + M \qquad (4\text{-}26)$$

also become important in determining overall radical levels. Rate constants for the above reactions are presented in Table 8-1.

It can be seen from the above discussion that any detailed mechanism describing propane oxidation will consist of a large number of species and reaction steps. Since each species considered involves the introduction of an additional species conservation equation, the use of any detailed reaction mechanism in the numerical solution used in the present investigation leads to excessive computer times and costs. Thus an overall or global reaction kinetic concept was employed. This involves the assumption that a detailed reaction mechanism involving a number of elementary steps can be described in terms of a few main reactants and overall reaction steps. Such an approximation entirely neglects any reactions occurring between hydrocarbon intermediates or radicals. As a result global modeling can, at most, be expected to describe only spatial energy release rates and reactant/final product concentration distributions. As stated by Glassman, et al[26] "Under what circumstances such an overall (global) correlation is usable is largely dependent on both the kinetic mechanism to which it is applied and the physical environment in which the process is occurring. Where a particular rate-determining step or sequence in the true chemical reaction mechanism occurs and the physical circumstances of the application are similar to those in which the expression was derived, the overall approximation is a valid and vastly simplifying idea. However, extension of such a correlation to experimental conditions outside the range studied should never be done without some reservation."

4.5.2. Propane Oxidation

Two global approximations for propane oxidation have been used in the past. The first and simplest assumes an infinitely fast oxidation of propane to H_2 and CO.[54] Such an approach however offers no possibility of predicting unburned hydrocarbon levels. The second, perhaps a somewhat better approach, is the use of a finite rate global expression for the oxidation of the hydrocarbon based on overall experimental observations in a particular system. Edelman and Fortune[55] derived such an expression for the oxidation of a parrafin hydrocarbon based on shock tube ignition delay times. For propane, they wrote the overall reaction as

$$C_3H_8 + \frac{3}{2} O_2 \quad 3\ CO + 4\ H_2$$

and gave the global rate as

$$R = \frac{5.52 \times 10^8}{p^{.825}} \quad (C_3H_8)^{1/2} \quad (O_2)\ T \exp\left(-\frac{12{,}200}{T}\right) \frac{\text{moles}}{\text{cm}^3 \text{sec}} \qquad (4\text{-}27)$$

As mentioned above caution should be exercised whenever a global reaction rate derived for one combustion configuration is used for another. In two such different systems as a shock tube, where low radical concentrations are present during the initial stages of hydrocarbon oxidation, and a strongly backmixed system such as a well stirred reactor where high radical concentrations are present throughout the combustion process, it is probable that both the important reaction paths and the rate will be different.

To determine the feasibility of using the above mechanism to model propane oxidation in the present system, experimental propane disappearance rates based on average estimated residence

times and average measured species concentrations in the combustion zone were compared with rates predicted from Equation (4-27). From the experimental results of Chapter 4 and Appendix G it can be seen that C_3H_8 and O_2 concentrations and temperature are relatively uniform in the region upstream of the plane of the jet exit once the initial flamefront has been traversed. This is due to the intense turbulent mixing characteristic of the recirculation region of the ORJ. Any rates derived from experimental measurements should thus be more representative of the chemistry of the system as opposed to mixing phenomena. Such an analysis likens the upstream region of the ORJ to a perfectly stirred reactor. Average residence time τ was computed from the relation

$$\tau = \frac{\rho V}{\dot{m}} \qquad (4\text{-}28)$$

The volume V was taken as that region upstream of the jet exit in which the concentrations had achieved 95% of their maximum or minimum value. The density was calculated from the ideal gas law using average properties in the combustion zone. The mass flow rate m was assumed equal to that portion of the flow which passes through the flamefront upstream of the jet exit plane. It should be noted this approximation neglects different residence times encountered by gases entering the flamefront at different locations. Table 4-2 shows a comparison of predicted (Equation (4-27)) and experimental propane disappearance rates.

TABLE 4-2. EXPERIMENTAL AND PREDICTED PROPANE DISAPPEARANCE RATES

Case	$R_{C_3H_8}$ EXP, $\frac{moles}{cc\text{-}sec}$	$R_{C_3H_8}$ PRED, $\frac{moles}{cc\text{-}sec}$
1	7.17×10^{-5}	5.6×10^{-2}
2	6.34×10^{-5}	9.9×10^{-2}
3	3.08×10^{-5}	3.8×10^{-2}

Predicted propane disappearance rates are approximately two orders of magnitude greater than those experimentally determined. Similar calculations were made based on concentration profiles for propane combustion in an adiabatic flow reactor.[26] The findings were in agreement with those of Table 4-2, with predicted disappearance rates approximately two orders of magnitude to fast. This again emphasizes the difficulty encountered in applying a global reaction rate to predict the characteristics of a system for which it was not derived.

At this point it was felt a more representative rate for propane oxidation in the ORJ could be derived from the experimental measurements of the present investigation. The experimental propane disappearance rates of Table 4-2 together with average O_2, temperature, and propane concentrations were correlated with a rate expression of the form

$$\frac{d\,[C_3H_8]}{dt} = A \exp(-E/RT)\,[C_3H_8]^a\,[O_2]^b$$

The unknown coefficients were determined using a nonlinear regression analysis program[56], and the final rate expression was found to be

$$\frac{d\,[C_3H_8]}{dt} = 4.97 \exp(-9195/RT)\,[C_3H_8]^{0.5} \qquad (4\text{-}29)$$

Note that the rate was found to be independent of O_2 concentration due to the lean equivalence ratios being considered. A plot of the correlated data is shown in Figure 4-2. An activation energy of 9195 cal/mole appears to be low when compared to those found by other investigators for higher hydrocarbons.[57,58] This is attributable to the limited conditions over which the experimental data were considered.

4.5.3. Carbon Monoxide Oxidation

Several levels of approximation have been used to model CO oxidation. Two of these are the H_2/O_2 partial equilibrium and total equilibrium models. Each of these provides a means of estimating radical concentrations in terms of more easily measured species.

At temperatures of interest in most post flame combustion zones the biomolecular reations (4-19) through (4-22) can be considered in a state of partial equilibrium. Under such conditions it can be shown[59] that the concentrations of OH, H, and O are related to the concentrations of the more stable species H_2, H_2O, and O_2 as follows

$$[OH] = (K_{19}K_{20})^{1/2}[H_2]^{1/2}[O_2]^{1/2} \qquad (4\text{-}30)$$

$$[O] = K_{19}K_{21}\frac{[H_2][O_2]}{[H_2O]} \qquad (4\text{-}31)$$

$$[H] = K_{21}(K_{19}K_{20})^{1/2}\frac{[H_2]^{3/2}[O_2]^{1/2}}{[H_2]} \qquad (4\text{-}32)$$

where K_i is the equilibrium constant for the i th reaction. Substitution of Equations (4-30) through (4-32) into the rate expression for CO oxidation from Equation (4-18) yields

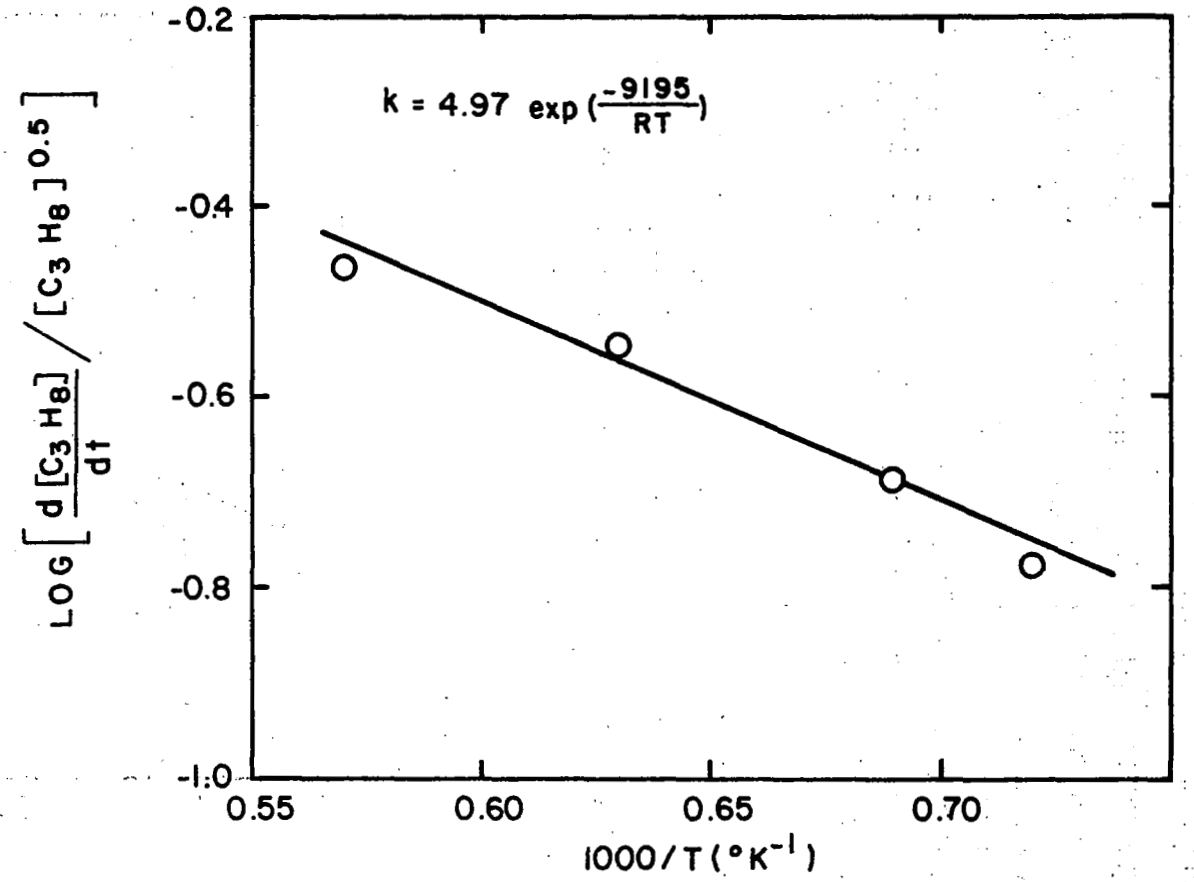

Figure 4-2. Arrhenius plot of propane disappearance rate.

$$\frac{d[CO]}{dt} = k_{18F}[CO][OH] - k_{18R}[CO_2][H]$$

$$= k_{18F}(K_{19}K_{20})^{1/2}[CO][H_2]^{1/2}[O_2]^{1/2}$$

$$-k_{18R}K_{21}(K_{19}K_{20})^{1/2}[CO_2][H_2]^{3/2}$$

$$[H_2O]^{-1}[O_2]^{1/2} \qquad (4\text{-}33)$$

Here the equilibrium constants K_{19}, K_{20}, K_{21} can be evaluated from curve fits of JANAF thermochemical data.[60]

The total equilibrium model assumes reactions (4-19) through (4-26) are in equilibrium. Then, from reactions (4-22) and (4-23)

$$\frac{[H_2O][O]}{[OH]^2} = K_{22}$$

$$\frac{[O_2]}{[O]^2} = K_{23}$$

Elimination of [O] yields, after some rearrangement

$$[OH] = (K_{22}K_{23}^{1/2})^{-1/2}[H_2O]^{1/2}[O_2]^{1/4}$$

Considering only the forward direction of reaction (4-18)

$$\frac{d[CO]}{dt} = k_{18F}(K_{22}K_{23}^{1/2})^{-1/2}[CO][H_2O]^{1/2}[O_2]^{1/4} \qquad (4\text{-}34)$$

Several investigators have experimentally determined values for the rate constant term $k_{18F}(K_{22}K_{23}^{1/2})^{-1/2}$. These are presented in Table 4-3.

While both of the above models are approximations, the partial equilibrium approach would appear to be more physically realistic than the total equilibrium approach. The bimolecular H_2/O_2 propagation reactions (4-19) through (4-22) would be expected to be in equilibrium much earlier in the flame zone and over a larger

TABLE 4-3. OVERALL CO OXIDATION RATES

-d [CO]/dt (mole/cm^3 sec)	Temperature (°K)	Equiv. Ratio	Fuel	Method	Ref.
$1.3 \times 10^{14}[CO]\,[O_2]^{0.5}[H_2O]^{0.5}\,\exp(-15.10/T)$	840-2360	OVERALL CORRELATION OF SEVERAL STUDIES			61
$5.6 \times 10^{14}\,[CO]\,[O_2]^{0.25}\,[H_2O]^{0.5}\,\exp(-21.64/T)$	1030-1230	0.04-0.5	CH_4	Flow Reactor	62
$1.8 \times 10^{13}\,[CO]\,[O_2]^{0.5}[H_2O]^{0.5}\,\exp(-12.58/T)$	1450-1750	0.5-0.8	CH_4	Well-Stirred Reactor	63
$2.9 \times 10^{10}\,[CO]\,[O_2]^{0.35}\,[H_2O]^{0.4}\,\exp(-7.55/T)$	1400-1900	0.5-9.5	C_3H_8	Well-Stirred Reactor	64

range of conditions than the relatively slow termolecular recombination reactions (4-23) through (4-26). Additionally, as equilibrium is approached the reverse reaction $CO_2 + H \rightarrow CO + OH$ should be considered as is done in Equation (4-33). A problem was anticipated however in applying the H_2/O_2 partial concept to the early flame region where temperatures are relatively low (< 1100°K) and radical buildup is still occurring.

The partial equilibrium approach was investigated using the idealized well stirred reactor program of Pratt and Bowman[38] described in Section 3.4.1. Assuming propane is prepyrolized to H_2 and CO, predicted radical concentrations based on a detailed reaction scheme for H_2 and CO oxidation (reactions

(4-18) through (4-26)) were compared with those obtained using the partial equilibrium approximations presented above. Under the fuel lean conditions considered, in applying the partial equilibrium approach the primary H_2O producing reaction was found to be

$$OH + H + M \rightleftarrows H_2O + M \qquad (4\text{-}26)$$

CO oxidation was assumed to occur via the rate limiting step

$$CO + OH \rightleftarrows CO_2 + H \qquad (4\text{-}18)$$

Radical concentrations for the above reactions were computed from the partial equilibrium relations (4-30) through (4-32).

The results are shown in Figure 4-3, where radical concentrations are plotted as a function of residence time in the reactor. At short residence times the partial equilibrium scheme significantly overpredicts radical concentrations. Since the H_2/O_2 partial equilibrium concept is valid only at higher temperatures, such a result is not entirely unexpected.

Considering the above problems, it was decided to use a two step global reaction mechanism in which propane reacts to form CO and H_2O followed by the oxidation of CO to CO_2

$$C_3H_8 \rightarrow CO + H_2O \qquad (4\text{-}36)$$

$$CO \rightarrow CO_2 \qquad (4\text{-}37)$$

The experimentally determined rate for propane oxidation, Equation (4-29) was used for reaction (4-36).

The choice of CO and H_2O as the products in the one step global reaction for C_3H_8 oxidation was based on the results of both flat flame[17] and adiabatic flow reactor studies[26] of hydrocarbon oxidation. Species concentration profiles in these studies

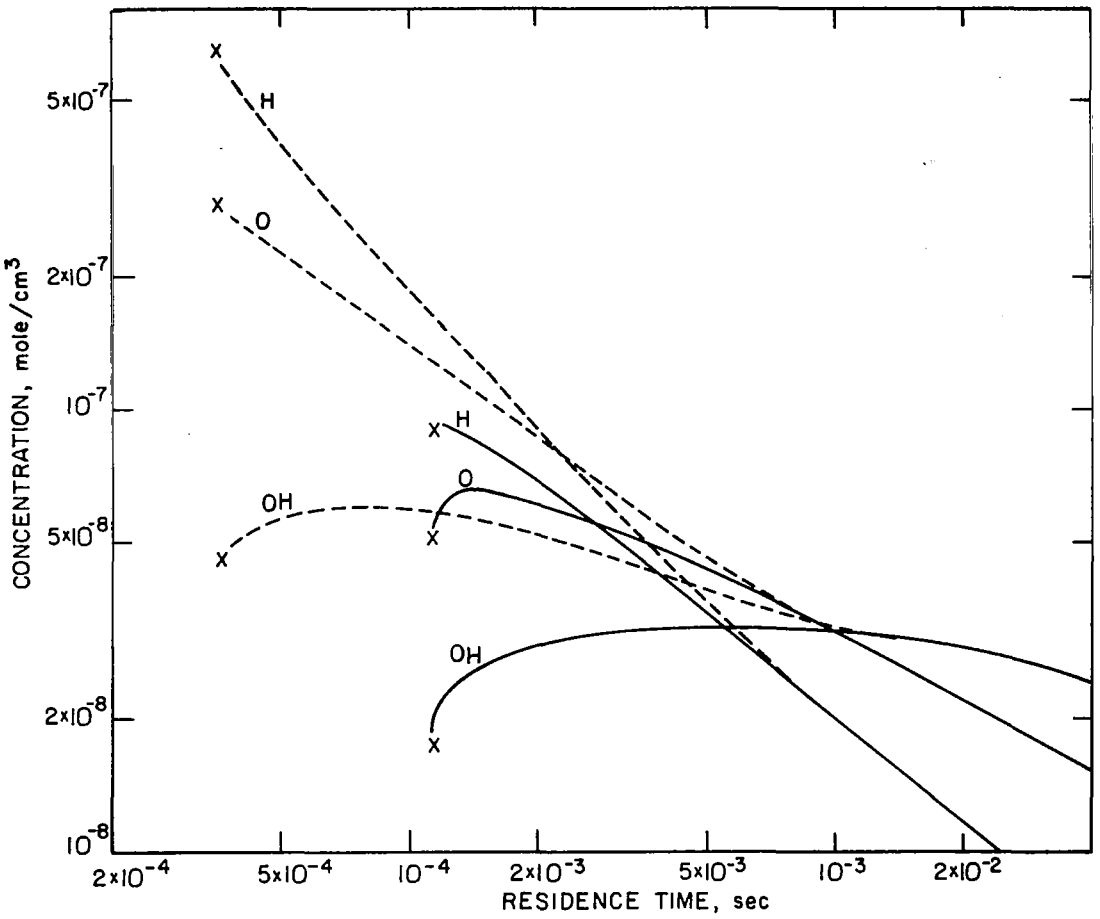

Figure 4-3. Radical concentration as a function of residence time based on an adiabatic well stirred reactor model. ϕ = 0.625; T_{INLET} = 600 K; P = 1.01 x 10^5 N/m^2. ——, detailed kinetic mechanism; ---, partial equilibrium model.

H_2O and CO were then computed from H and C atom conservation equations. Because the equivalence ratio is everywhere uniform, the O_2 mass fraction at any point can be determined from the initial C_3H_8 mass fraction and an O atom conservation equation.

4.5.4. NO Formation

Under fuel lean conditions NO formation is governed by the Zeldovich mechanism[76]

$$O + N_2 \rightleftarrows NO + N \tag{4-38}$$

$$N + O_2 \rightleftarrows NO + O \tag{4-39}$$

Invoking the steady state assumption for N atoms, it can be shown that initially (i.e., for $[NO] \ll [NO]_{EQ}$) the NO formation rate is given by[65]

$$\frac{d[NO]}{dt} = 2\, k_{38f}\, [O]\, [N_2] \tag{4-40}$$

It remains to determine the O atom concentration.

Three approximations have generally been used. The most straightforward approach is to assume O_2/O equilibrium. Then

$$[O] = K_o\, [O_2]^{1/2} \tag{4-41}$$

In typical combustion systems, several recent studies [22, 66, 67] have indicated O atom concentrations at least an order of magnitude greater than that predicted by Equation (4-41).

A second approach is provided by the H_2/O_2 partial equilibrium assumption presented in Section 4.4.3. The O atom concentration can then be calculated from Equation (4-31).

$$[O] = K_{19}K_{21}\, \frac{[H_2]\, [O_2]}{[H_2O]} \tag{4-31}$$

indicate a rapid increase in both CO and H_2O occurring simultaneously with the hydrocarbon disappearance. H_2 appears only as an intermediate species at relatively low concentrations. This indicates a rapid oxidation of H_2 to H_2O. The oxidation of CO to CO_2 does not appear to be significant until later in the flame zone.

Referring to Table 4-3 for overall CO oxidation rates, both the rates from References [61] and [64] were used in the numerical calculations. Global rate expressions would be expected to be somewhat dependent on fuel type, system, and stoichiometry. Therefore it was initially decided to use the rate derived by Hottel, et al [64] since the conditions for which this rate was derived appear to most closely approximate those of the present investigation. The results of subsequent numerical calculations showed poor agreement between experimental and predicted CO_2 and CO profiles. This was primarily a result of the low activation energy associated with this rate. Since the temperature ranges associated with the rates from References [62] and [63] fall below those encountered in the case being modeled (average temperatures in combustion zone for case 3 were greater than 1700 K, uncorrected for radiation), the over all correlation rate given by Reference [26] was used to obtain the final results presented in Chapter 5.

The above two equation reaction scheme ((4-36) and (4-37)) considers 5 species; C_3H_8, O_2, CO, H_2O, CO_2. The required number of species conservation equations can be reduced however. The mass fractions of C_3H_8 and CO_2 were selected as dependent variables (requiring 2 species conservation equations). Mass fractions of

Sarofim and Pohl[67] obtained agreement with experimentally measured maximum NO production rates, on a flat flame burner using methane, within a factor of 5 using Equation (4-31) to predict O atom concentrations. This expression however requires knowledge of the H_2 concentration. The kinetic model used in the present investigation only considers the product species N_2, O_2, CO, CO_2.

Iverach, et al[68] has suggested partial equilibrium of the reaction

$$CO + OH \rightleftarrows CO_2 + H \tag{4-18}$$

in addition to the H_2/O_2 partial equilibrium scheme. Then

$$\frac{[CO]}{[CO_2]} = K_{18}\frac{[H]}{[OH]}$$

Substitution of the partial equilibrium expressions for [H] and [OH] (Equations (4-30) and (4-32) into the above expression yields

$$\frac{[H_2]}{[H_2O]} = \frac{K_{18}}{K_{21}}\frac{[CO]}{[CO_2]} \tag{4-42}$$

Substitution of Equations (4-31) and (4-42) into (4-40) gives the following expression for NO formation

$$\frac{d\,[NO]}{dt} = 2\,k_{38f}K_{18}K_{19}\frac{[N_2]\,[CO]\,[O_2]}{[CO_2]} \tag{4-43}$$

In the present investigation k_{38f} was taken from the rate data of Baulch, et al [69].

$$k_{38f} = 1.36 \times 10^{14} \exp(-37947/T)$$

The equilibrium constants K_{18} and K_{19} were taken from a curve fit of JANAF thermochemical data. Substitution of these values into Equation (4-43) yields the final rate expression for NO formation

$$\frac{d[NO]}{dt} = 1.7 \times 10^{13} \exp(-34088/T)\frac{[N_2][CO][O_2]}{[CO_2]}$$

4.6 Computational Procedure

As was discussed in the previous two sections the numerical computations consist of solving the finite difference form of a set of simultaneous governing partial differential equations at the nodal points of a grid network covering the flowfield. In the present investigation this involves the solution of six equations for six dependent variables:

Stream function, Ψ

Vorticity variable, ω/r

C_3H_8 mass fraction, $m_{C_3H_8}$

CO_2 mass fraction, m_{CO_2}

NO mass fraction, m_{NO}

Stagnation enthalpy, h

The grid network used is shown in Figure 4-4. This is the same grid as used in a previous study of the ORJ by Samuelsen[47]. The grid is nonuniform in both radial and axial directions to provide a finer mesh in those regions containing the steepest gradients. Minimum spacing in the radial (J) direction is 0.4064 mm (at the combustor centerline) and 5.08 mm in the axial (I) direction as the jet exit is approached

Primary interest was in obtaining a numerical solution corresponding to the conditions of experimental case 3. However a solution was also obtained for a cold flow case (no combustion) in which CO was introduced through the jet injector. In the latter case three dependent variables were considered: the stream function, the vorticity variable, and the CO mass fraction. Inlet conditions for

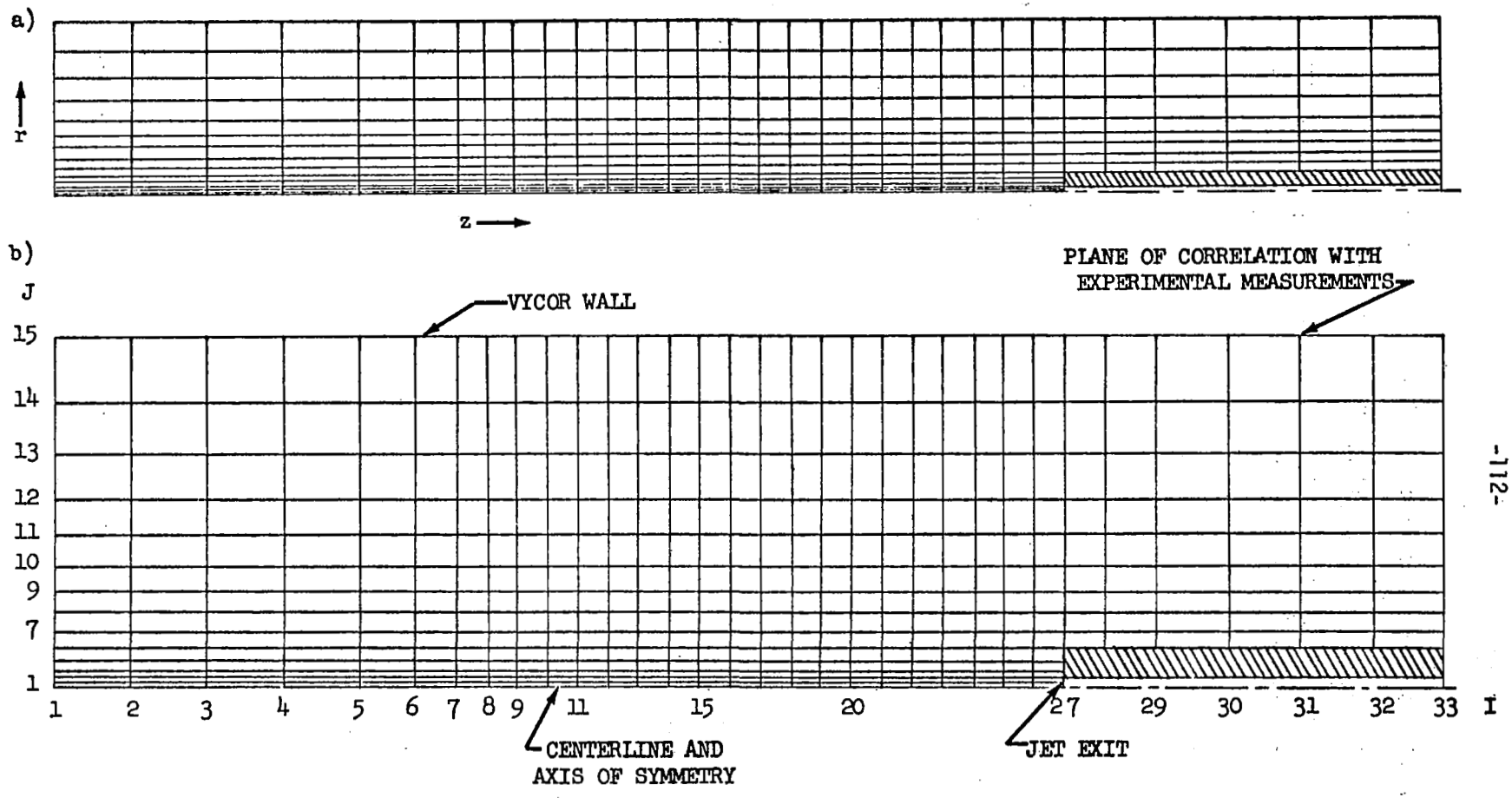

Figure 4-4. Grid for numerical calculations.

a) Actual size
b) Radial direction expanded (X2)

the cold flow and hot flow case are shown in Table 4-4.

TABLE 4-4 COLD FLOW INLET CONDITIONS

VARIABLE	MAIN STREAM	JET STREAM
Velocity, m/s	7.74	95.9
Temperature, °K	295	295
"Air" Mass Fraction	1.0	0.973
CO Mass Fraction	0.0	0.027

The CO distribution was measured experimentally in the ORJ operating under the conditions of Table 4-4 in a cold flow mode using the sampling probe and NDIR CO analyzer described in Chapter 2. It was felt a comparison of the experimental and numerical results would provide a partial validation of the viscosity model and numerical technique. The vorticity and streamfunction distributions calculated in the cold flow case were then used as initial guesses for the case with combustion added. Inlet conditions for the case with combustion are shown in Table 4-5.

TABLE 4-5 HOT FLOW INLET CONDITIONS

VARIABLE	MAIN STREAM	JET STREAM
Velocity, m/s	7.74	95.9
Temperature, °K	600	300
Equivalence ratio	0.625	0.625

In numerical calculations of the present type, the solution is considered to have converged when the fractional change in the value of each dependent variable from one iteration (N-1) to the next (N) is less than a certain prescribed value. This value was taken as 0.005[44]. Thus the convergence criteria can be written as

$$\frac{|\phi_N - \phi_{N-1}|}{\phi_N} < 0.005$$

It has been pointed out[44] that divergence can occur if variation in any of the terms of the finite difference equations is large. No problems were encountered with the cold flow solution. Convergence problems did occur however when combustion was added. This was remedied by under-relaxing several of the variables. The expression used for under-relaxation is given by

$$\phi = \phi_{N-1} + \alpha_{UR} \left(\phi_N - \phi_{N-1} \right)$$

where ϕ_{N-1} is the value of the variable which was computed on the (N-1) the iteration, ϕ_N is the value which would be computed in the normal way on the Nth iteration, α_{UR} is the under-relaxation parameter, and ϕ is the value which is actually used for the Nth iteration. Values of α_{UR} used in the calculations were as follows

VARIABLE	α_{UR}
Ψ	1.0
ω/r	0.75
$m_{C_3H_8}$	0.2
m_{CO_2}	0.2
h	1.0

From the standpoint of computer time, it was found advantageous to divide the hot flow solution into two parts. Since the flowfield properties are almost entirely determined by the hydrocarbon system, a solution was first obtained while neglecting NO formation. NO kinetics were then superimposed on the hydrocarbon system as a separate problem.

The cold flow solution with CO injection took 160 iterations to converge (30 seconds central processing time on a CDC 7600). Using the cold flow solution for ω/r and Ψ as an initial guess the solution for the hydrocarbon system with combustion took 1100 iterations (5 minutes computing time). Superimposing the NO system kinetics on the hydrocarbon solution required an additional 70 iterations to obtain a final solution.

CHAPTER 5

ANALYTICAL RESULTS AND DISCUSSION

In this chapter the results of the analytical modeling are presented. Two cases were studied. The results for cold flow CO injection are presented in Section 5.1 and results for the case with combustion included (corresponding to experimental case 3) can be found in Section 5.2. The results are discussed and a comparison with the experimental findings is made.

5.1. Cold Flow CO Injection

Predicted stream function and CO mole fraction distributions for the case of cold flow CO injection through the jet are shown in Figures 5-1a and 5-1b. Also shown in Figure 5-1c is the experimentally determined CO distribution. Although some discrepancies exist, agreement between the experimental and predicted CO distributions is quite good. The primary discrepancies are near the outer Vycor wall where the predicted axial rate of increase in CO is too rapid, and along the combustor centerline where the predicted CO level decreases too rapidly as one moves upstream from the jet exit.

The inlet conditions corresponding to this case are inlet velocities of 7.94 m/s and 95.9 m/s in the main stream and jet streams respectively, and an inlet temperature of 295°K. To determine the effect of experimental uncertainty on the results, inlet velocities and compositions were varied by $\pm$ 5%. It was found that

a) Predicted stream function distribution (x 10^3)

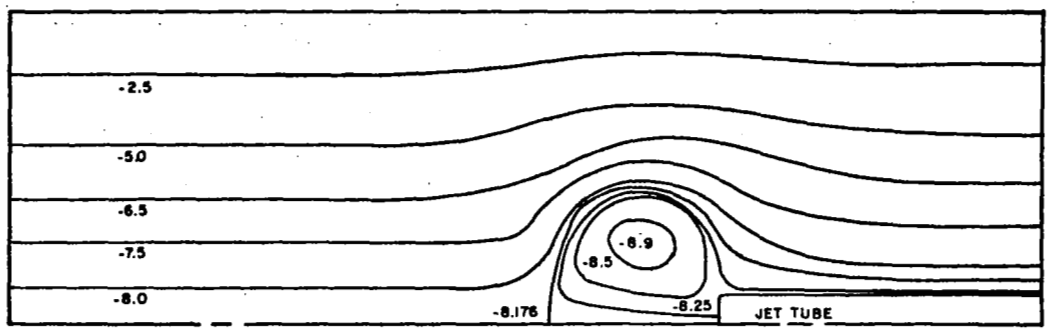

b) Predicted CO mole fraction

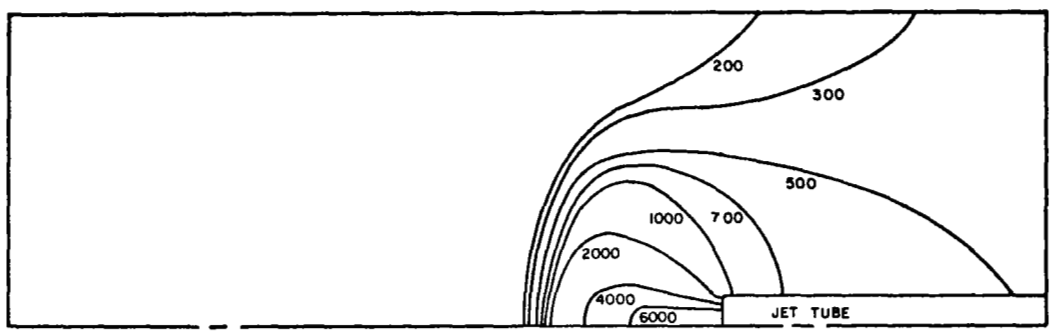

c) Experimental CO mole fraction

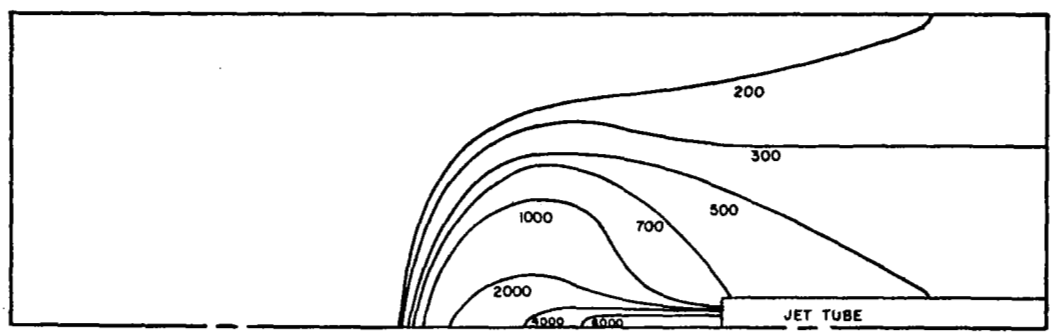

Figure 5-1. Flowfield property distributions for cold flow CO injection.

such a variation could not account for the observed discrepancy. Thus it would appear that the observed disagreement between experimental and predicted CO distributions is due to the simplicity of the turbulence model being used to describe what is a very complex turbulent flow system. The effect of a variation in effective viscosity is shown in Figures 5-2 and 5-3. Figure 5-2 shows a comparison between measured and predicted CO centerline profiles. Figure 5-3 compares measured and predicted radial CO profiles at an axial distance of 88.9 mm from the combustor exit. Predicted profiles are presented for two values of effective viscosity; an effective viscosity as calculated from Equation (4-16) (used to determine the predicted distributions in Figure 5-1), and a second value representing a 25% reduction in μ_{eff}. While agreement with experimental results for the latter value of μ_{eff} is somewhat improved, remaining differences between experimental and predicted profiles represent a limit on the accuracy of the proposed viscosity model.

5.2. Solution with Combustion

5.2.1. Hydrocarbon System

Predicted and experimental flowfield distributions are presented in Figures 5-4 through 5-11. Inlet conditions correspond to those of experimental case 3. The two step C_3H_8 and CO oxidation scheme represented by Equations (4-36) and (4-37) was used in conjunction with the global CO oxidation rate of Howard, et al[61]. The predicted stream function distribution is shown in Figure 5.4. For the cold flow case the stagnation point was located approximately 100 mm upstream of the jet exit (Figure 5-1). With combustion the stagnation point has moved to approximately 146 mm upstream

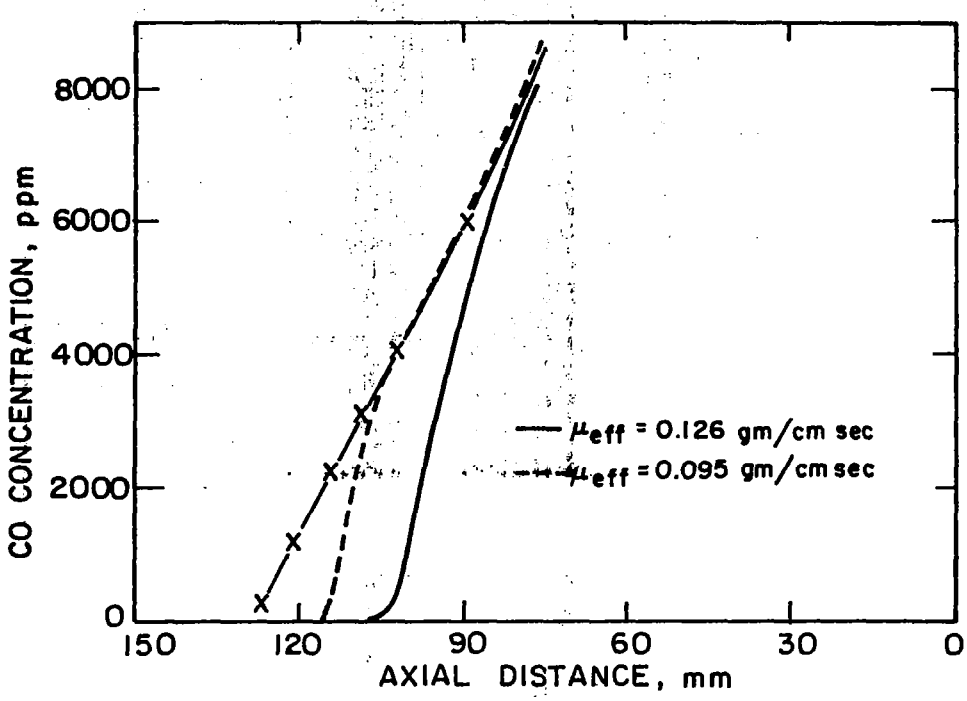

Figure 5-2. Comparison of measured and predicted CO centerline profiles for cold flow CO injection.

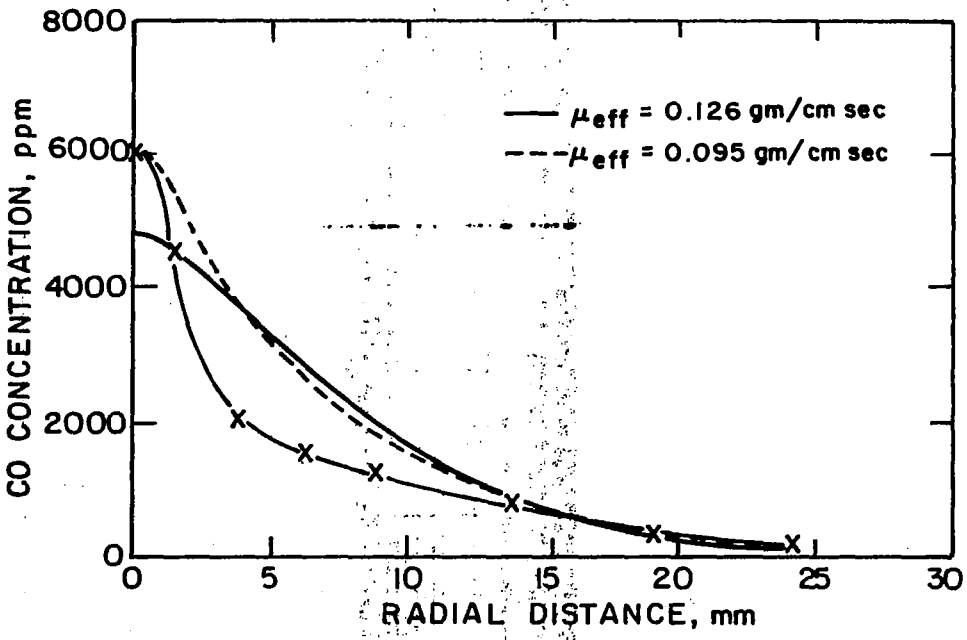

Figure 5-3. Comparison of measured and predicted radial CO profiles at an axial distance of 88.9 mm from the combustor exit for cold flow CO injection.

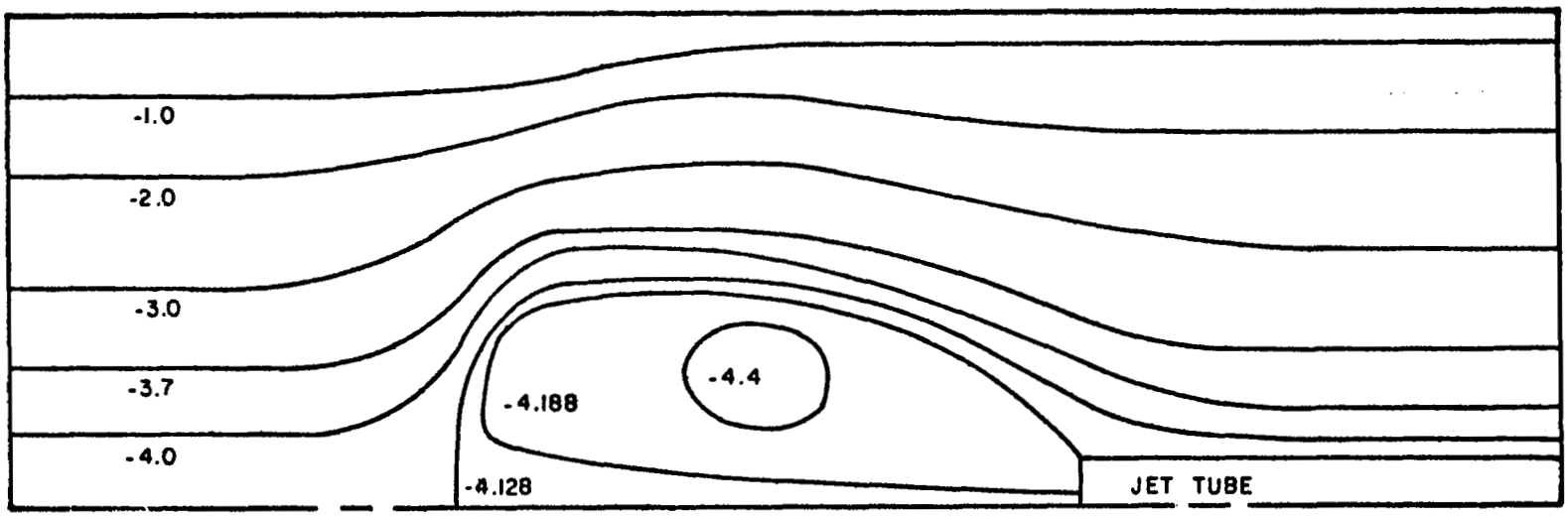

Figure 5-4. Predicted stream function distribution (x 10^3) for flow with combustion.

of the jet exit. Since the jet velocities are the same in both cases, this is a result of the expansion of the hot combustion gases.

Predicted and experimental C_3H_8 mole fraction distributions are shown in Figure 5-5. Qualitatively agreement is fair. Near the centerline experimental C_3H_8 mole fractions begin to decrease 15 mm farther upstream than predicted values. In the lower temperature regions near the outer Vycor wall the predicted C_3H_8 mole fractions begin decreasing farther upstream than the experimental. This is a similar behavior to that found in the previous section for CO distributions in the cold flow case, and can partially be accounted for by the simplified viscosity model employed.

Perhaps a more direct cause of the predicted behavior in the lower temperature outer regions would be the use of the experimentally derived rate for C_3H_8 oxidation

$$\frac{d\,[C_3H_8]}{dt} = 4.97 \exp(-9195/RT)\,[C_3H_8]^{0.5} \qquad (4\text{-}29)$$

This rate was based on average concentration and temperature measurements taken over a limited range of conditions in the high temperature recirculation zone. For example, the temperature range used in the derivation extended only from 1450° K to 1750° K. Extrapolation of this rate expression to lower temperature regions of the combustor could not be expected to yield accurate predictions throughout the combustion zone. The trends shown in Figure 5-5 indicate a predicted rate which is too fast at lower temperatures. This is directly attributable to the low activation energy associat-

a) Experimental C_3H_8 mole fraction

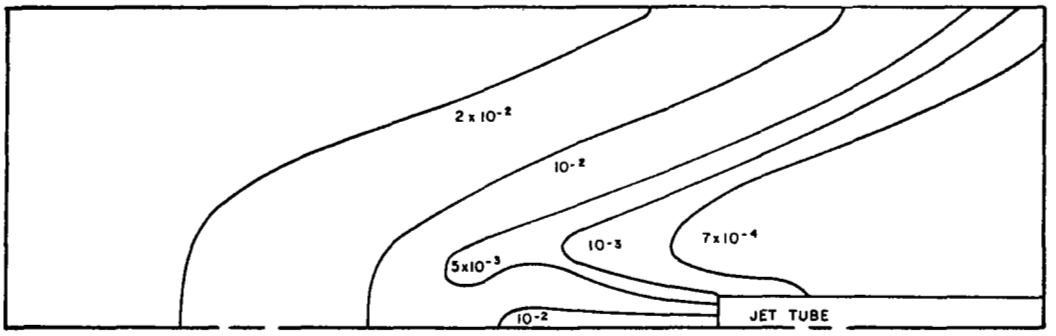

b) Predicted C_3H_8 mole fraction

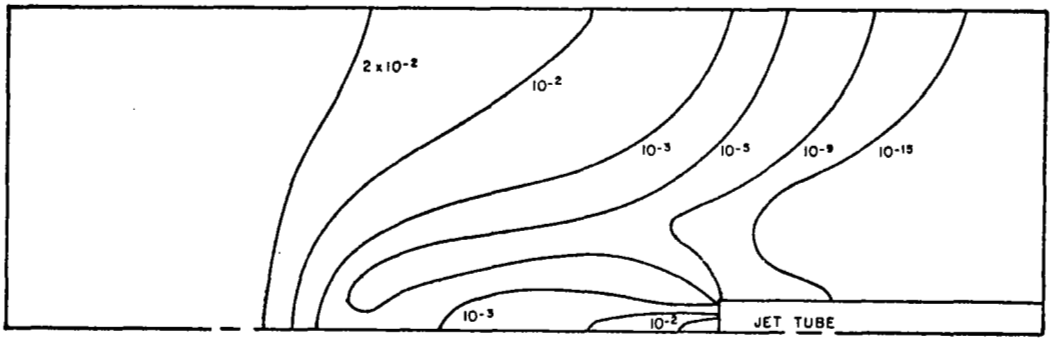

Figure 5-5. Experimental and predicted C_3H_8 mole fraction distributions.

ed with Equation (4-29). Predicted C_3H_8 concentrations are also seen to decrease to much lower values downstream of the initial flamefront. Again this is a result of using the above propane oxidation rate over a range of conditions for which it was not derived.

Predicted and experimental H_2O distributions are shown in Figures 5-6. Again the apparent disagreement between the predicted and experimental results can be explained in terms of the above discussion of the experimentally derived propane oxidations rate. Due to the assumption of a one step oxidation of C_3H_8 to H_2O via reaction (4-36)

$$C_3H_8 \rightarrow CO + H_2O$$

the H_2O appearance rate is directly related to the C_3H_8 disappearance rate. Thus the early predicted C_3H_8 disappearance is accompanied by an early increase in H_2O, especially in the lower temperature regions of the combustor.

The effect of the additional kinetic approximation introduced by assuming a one step oxidation of CO to CO_2 can be seen through a comparison of predicted and experimental CO distributions in Figure 5-7. As expected, in the upstream region of the flamefront the predicted initial buildup occurs farther upstream than is found experimentally. This is more clearly shown in Figure 5-8 where a comparison between predicted and experimental axial CO profiles at a radial distance of 13.2 mm from the combustor centerline is presented. The initial rise in CO occurs approximately 35 mm upstream of that found experimentally although the peak in CO concentration occurs at the same location This peak

a) Experimental H_2O mole fraction

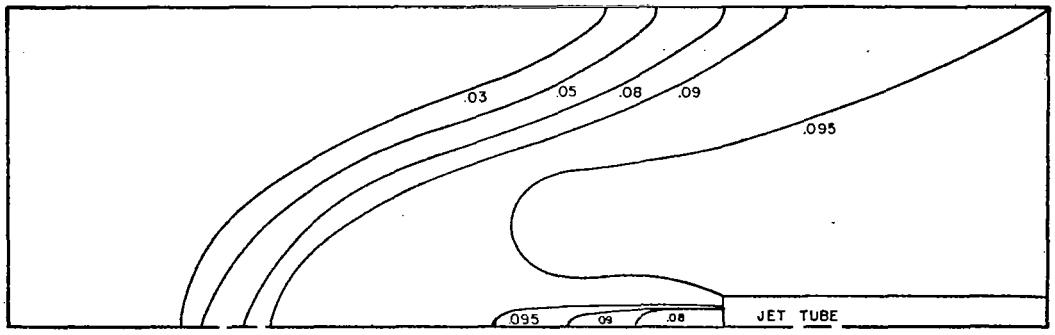

b) Predicted H_2O mole fraction

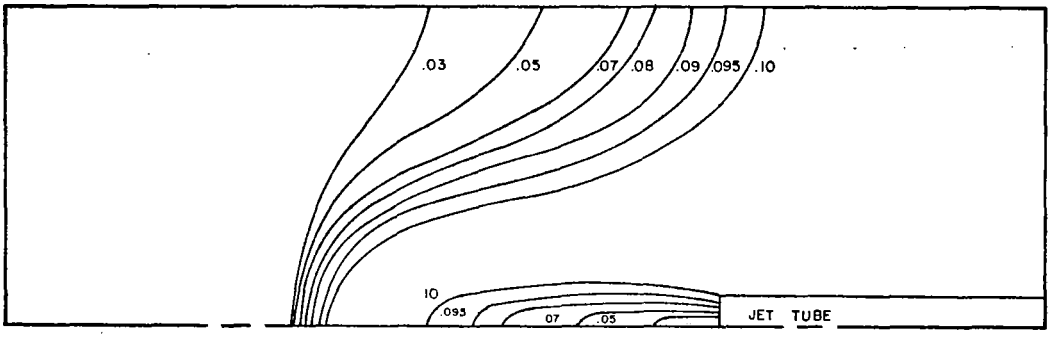

Figure 5-6. Experimental and predicted H_2O mole fraction distributions.

a) Experimental CO mole fraction

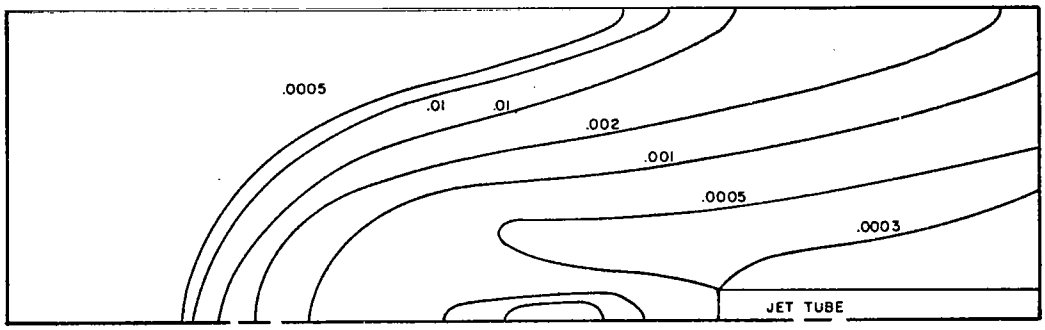

b) Predicted CO mole fraction

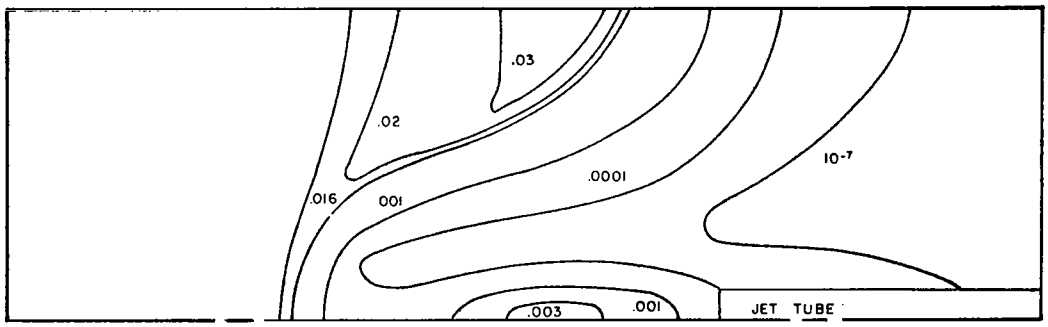

Figure 5-7. Experimental and predicted CO mole fraction distributions.

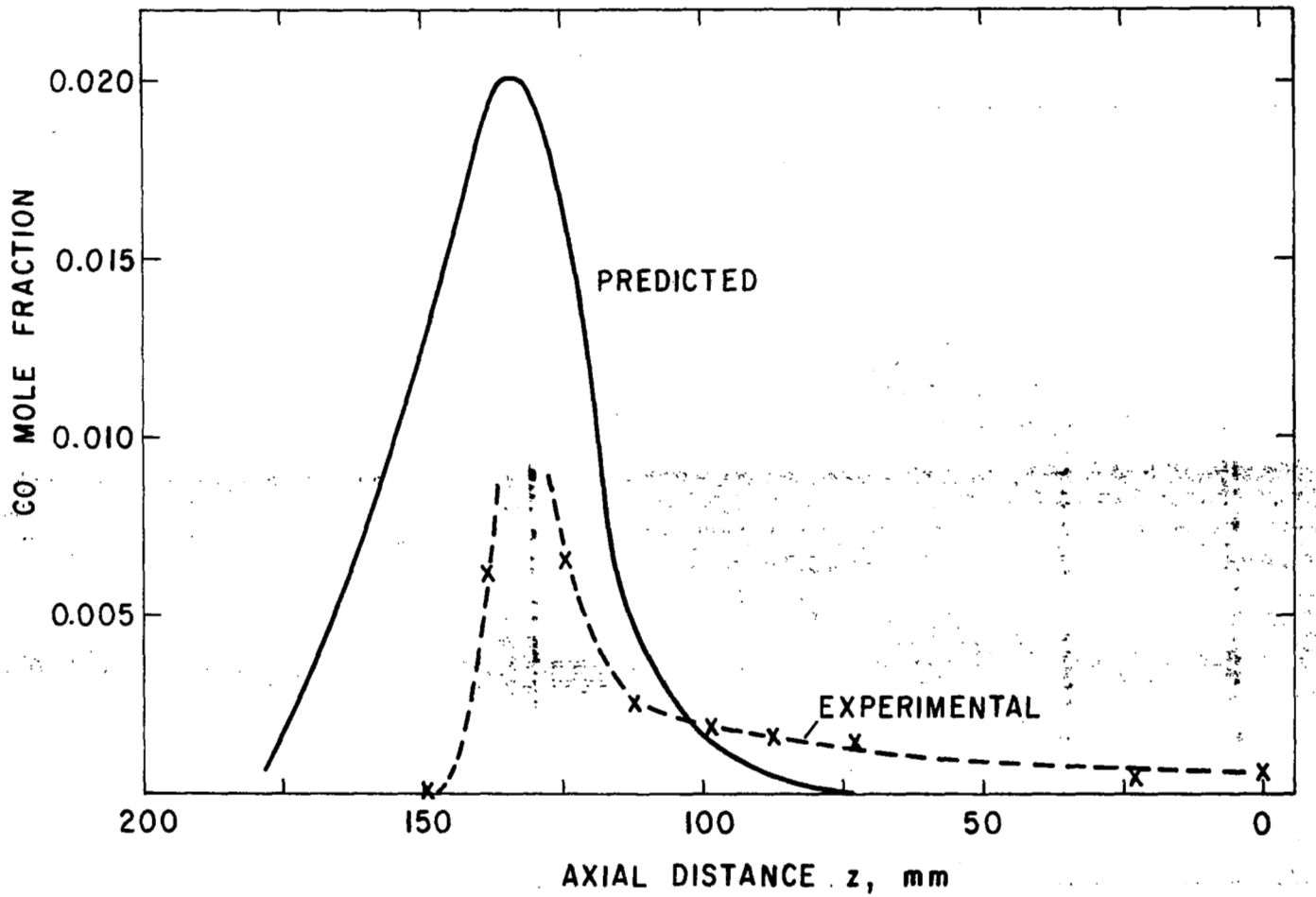

Figure 5-8. Predicted and experimental CO profiles at a radial position of 13.2 mm from the combustor centerline.

corresponds to a calculated temperature of 1200° K and represents the point at which the oxidation of CO to CO_2 becomes faster than the production of CO from C_3H_8 oxidation.

Subsequently, as one moves downstream toward the combustor exit, the predicted levels of CO decrease to values considerably below those found experimentally. This can also be seen in Figure 5-7 to be true across the entire combustor once the initial flamefront has been traversed. As has been pointed out by Howard, et al.[61], the CO rate expression used to obtain the results of the present section can be expected to give rates up to an order of magnitude fast when applied late in the postflame region where the back reaction $CO_2 + H \rightarrow OH + CO$ becomes important. Such appears to be the case here.

The theoretical well stirred reactor discussed in Section 4.4.3 was used to compare species concentration profiles using a detailed mechanism for CO oxidation and the global one step reaction given by Howard, et al.[61] Inlet conditions were taken to be the same as those of experimental case 3 (T_{IN} = 600°K, ϕ = 0.625), and an infinite propane oxidation rate was assumed. The results are shown in Figure 5-9 where $[CO]/[CO_2]$ and T are plotted as a function of reactor residence time. For increasing residence time the ratio of CO to CO_2 decreases much more rapidly when Howard's global rate is used than when using a detailed mechanism. For the range of residence times expected in the ORJ combustor (1-5 m sec) operating under the present conditions, CO levels predicted using the global approximation are up to a factor of 3 lower than those predicted using the detailed mechanism. Calculations also show that the back

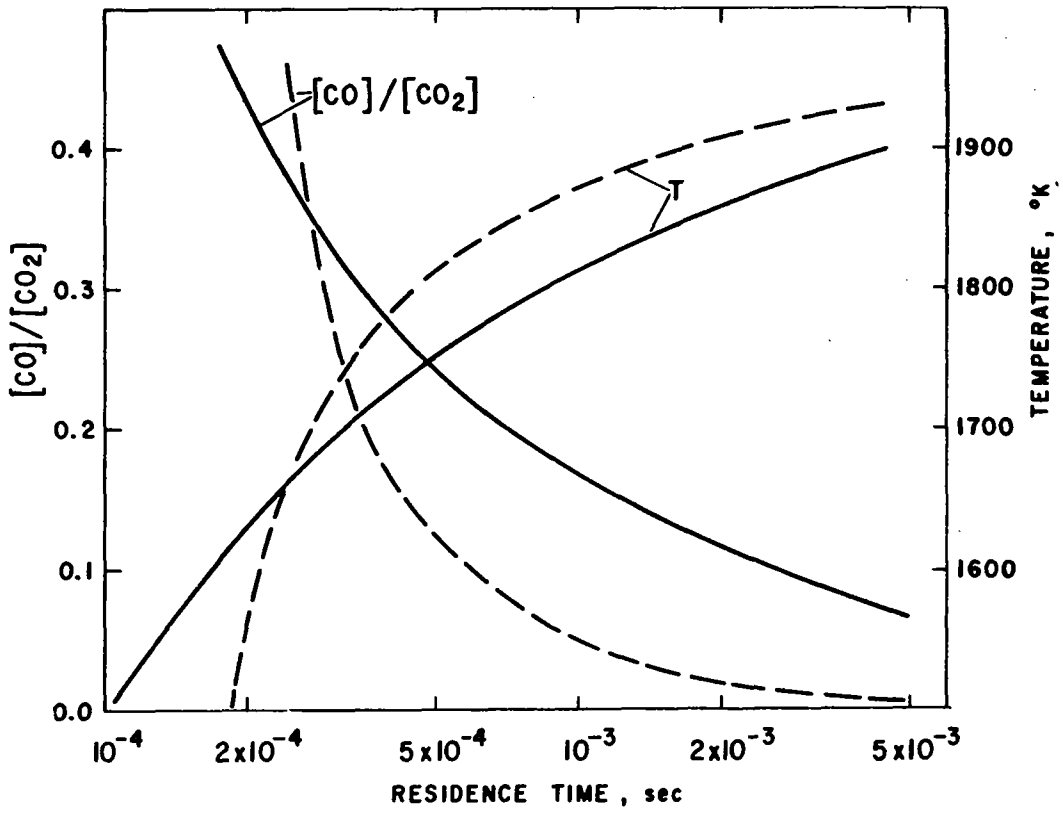

Figure 5-9. Composition and temperature based on adiabatic well stirred reactor model. ϕ = 0.625; T_{INLET} = 600 K; P = 1.01 x 10^5 N/m^2. ——, detailed CO oxidation mechanism; ---, global rate for CO oxidation (Howard, et al [61]).

reaction $CO_2 + H \rightleftharpoons CO + OH$ becomes important for residence times greater than 1 msec. While this comparison between the well stirred reactor and an ORJ is only an approximation, it should be noted that overall concentrations of the species and temperatures are in agreement for the two systems and general observations made in one system should hold in the other.

If the above explanation of the low predicted CO levels were indeed true then one would expect predicted CO_2 formation rates to be greater than those found experimentally. Examination of Figure 5-10 show this to be the case, with the maximum CO_2 mole fraction of 0.074 being attained much sooner and over a larger portion of the combustor in the predicted distribution. In the following section the smaller predicted ratio of $[CO]/[CO_2]$ in the high temperature regions of the combustor will have a significant effect on predicted NO levels.

Predicted and experimental temperature distributions are shown in Figure 5-11. The experimental temperatures are uncorrected for thermocouple radiative losses and thus could be expected to be somewhat lower than predicted values. As discussed in Section 2.2.2 typical thermocouple corrections are on the order of 200 K, indicating agreement in the maximum levels attained. Since the temperature is computed from the local enthalpy and species concentrations, the difference in predicted and experimental distributions is a direct result of the differences in concentration distributions discussed previously.

5.2.2. NO System

Once the flowfield was established for the hydrocarbon system,

a) Experimental CO_2 mole fraction

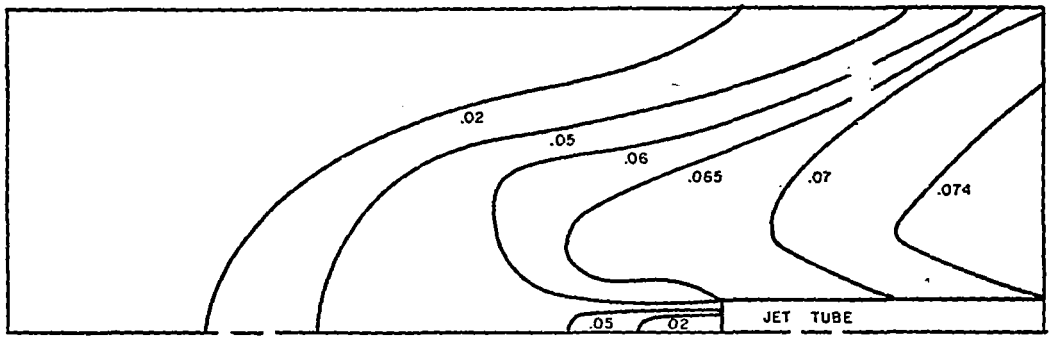

b) Predicted CO_2 mole fraction

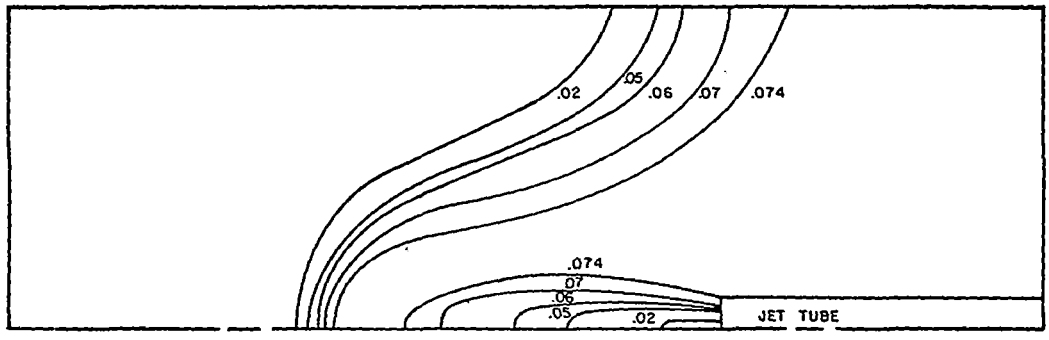

Figure 5-10. Experimental and predicted CO_2 mole fraction distributions.

a) Experimental temperature (°K)

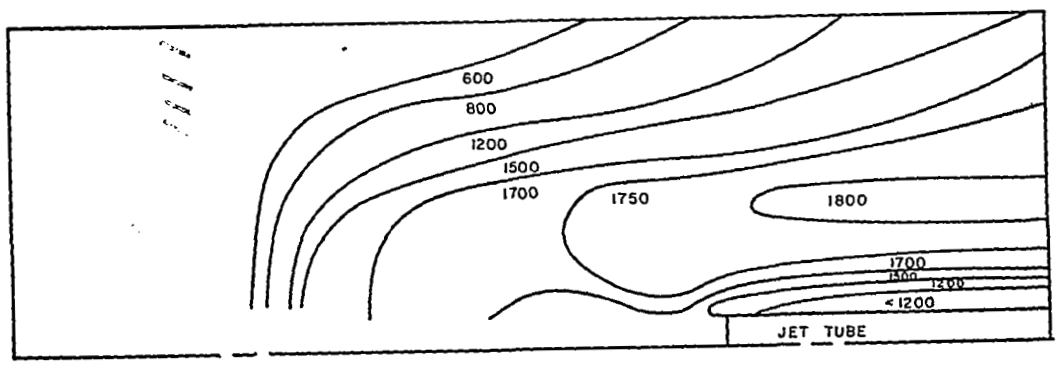

b) Predicted temperature (°K)

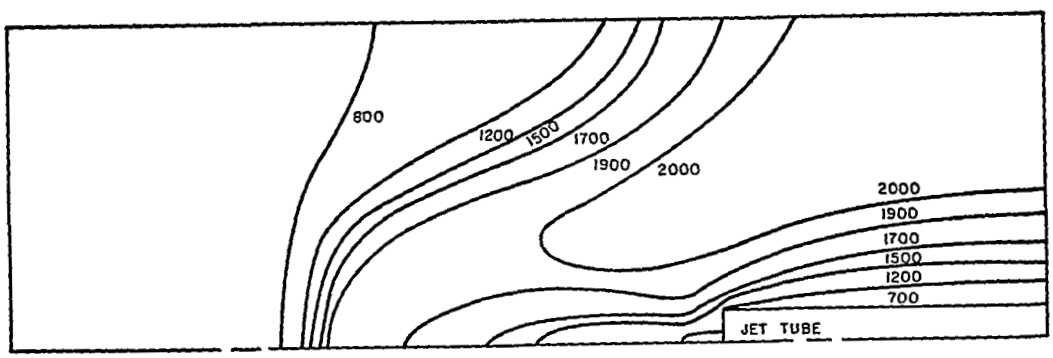

Figure 5-11. Experimental and predicted temperature distributions.

the resulting temperature and species concentration distributions were used in conjunction with the simplified nitric oxide formation rate (Equation 4-42) to obtain the corresponding NO distribution. The predicted and experimental results are shown in Figure 5-12. Note that experimental results are presented as total oxides of nitrogen (NO_x) whereas predicted values are for NO. These concentrations should be comparable since all proposed schemes for the production of NO_2 in high temperature flames involve conversion of the initially formed NO.

It is immediately apparent that predicted NO levels are significantly lower (up to 50% at the combustor exit). There are several explanations for this discrepancy, mostly related to simplifications used in the kinetic scheme.

Pratt and Malte [70] have proposed that N_2O may play an important role as an intermediate in NO production in low temperature fuel lean systems. The proposed mechanism is as follows

$$N_2 + O + M \rightleftarrows N_2O + M \qquad (5\text{-}1)$$

$$N_2O + O \rightleftarrows NO + NO \qquad (5\text{-}2)$$

$$N_2O + O \rightleftarrows N_2 + O_2 \qquad (5\text{-}3)$$

$$N_2O + H \rightleftarrows N_2 + OH \qquad (5\text{-}4)$$

To determine the possible importance of this mechanism in NO production under the conditions of the present investigation theoretical well stirred reactor calculations were carried out for an equivalence ratio of 0.625 and an inlet temperature of 600 K. In one case only the Zeldovich mechanism was used (Equations (4-38) and (4-39)) and in the other the above N_2O mechanism was added. The results are shown in Figure 5-13. Approximately a 30% increase

a) Experimental NO_x distribution (ppm)

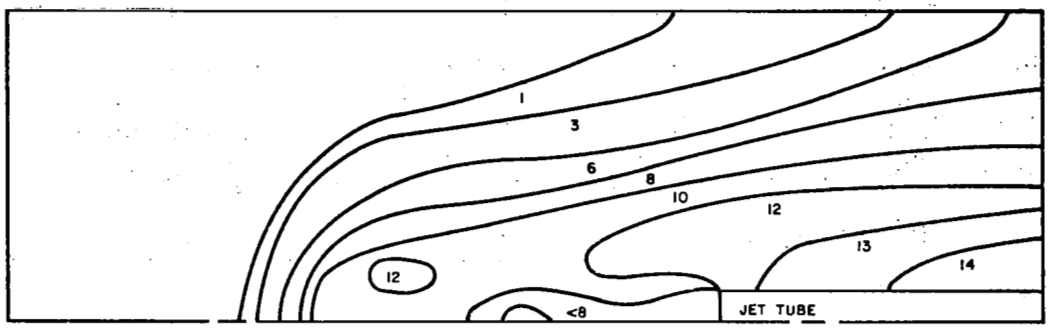

b) Predicted NO distribution (ppm)

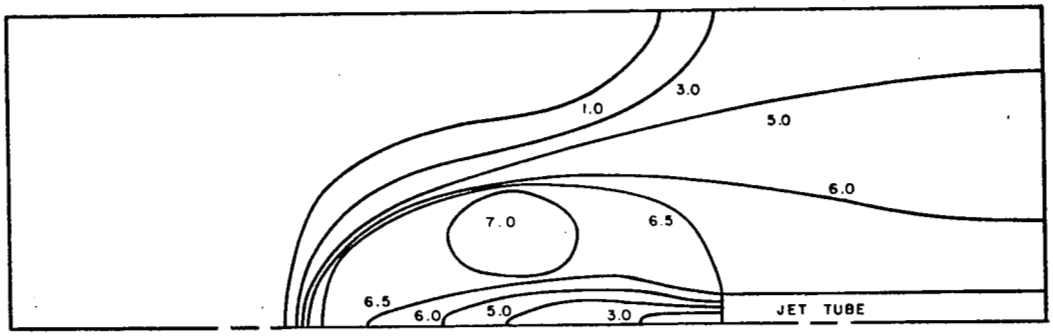

Figure 5-12. Predicted and experimental NO_x distributions.

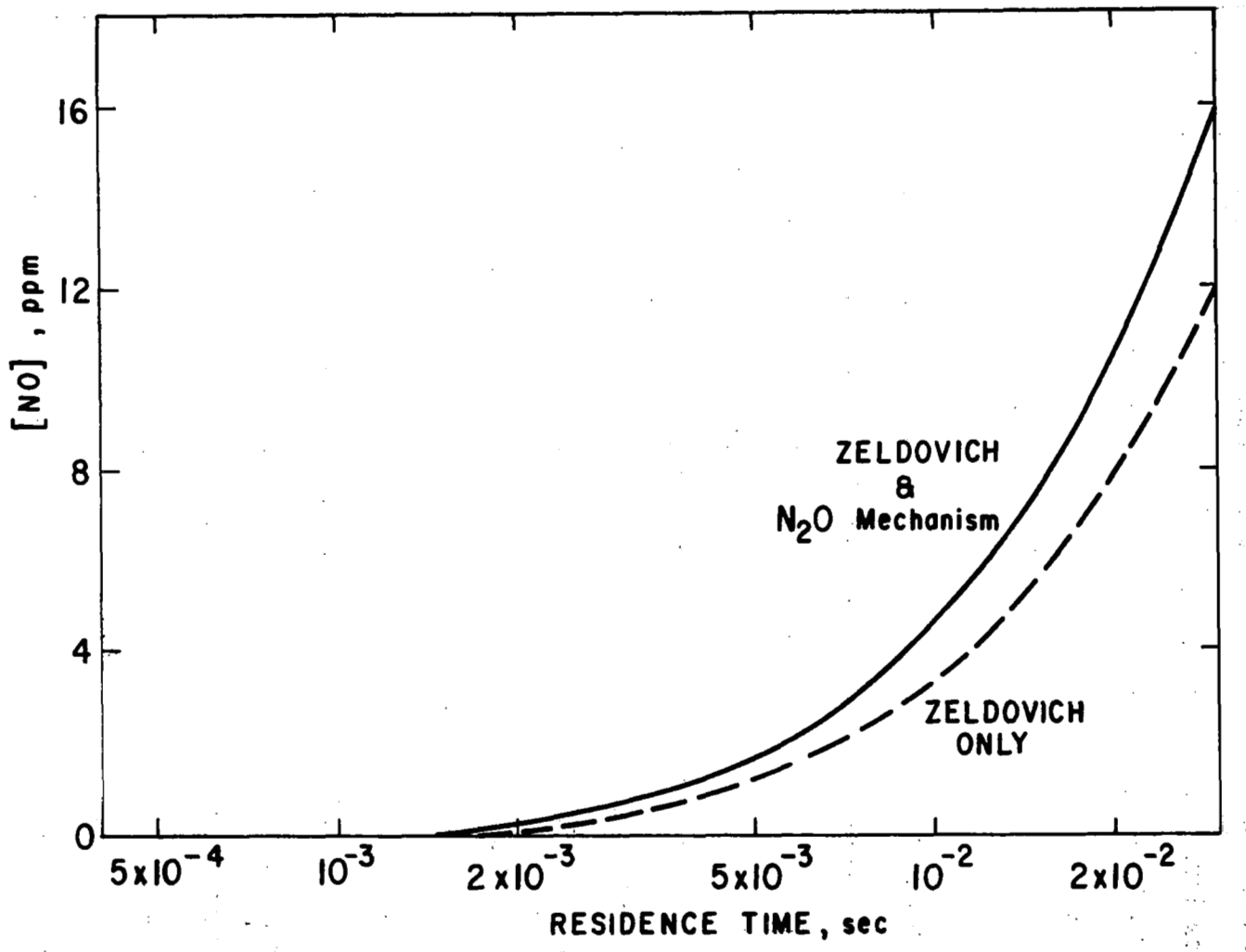

Figure 5-13. Predicted NO concentrations based on adiabatic well stirred reactor model. $\phi = 0.625$; $T_{IN} = 600$ K; $P = 1.01 \times 10^5$ N/m^2.

in NO occurs with the addition of the N_2O mechanism. Thus it appears possible that neglecting the N_2O contribution to NO production in the numerical calculations could partially account for the low levels of predicted NO.

The NO formation rate used in the numerical calculations is given by

$$\frac{d\,[NO]}{dt} = 2\,k_{38f}K_{18}K_{19}\frac{[N_2]\,[CO]\,[O_2]}{[CO_2]} \qquad (4\text{-}42)$$

The concentrations of N_2 and O_2 are relatively constant across the high temperature region of the combustor. Therefore the predicted NO formation rate becomes primarily a function of $[CO]/[CO_2]$ and T. Typical radial variations in the experimental and predicted values of these variables are shown in Figure 5-14. Considering that the experimental temperature profiles are uncorrected for radiative thermocouple losses the agreement in temperature profiles appears to be quite good. Note however, especially in the high temperature region where maximum NO_x is formed, the predicted $[CO]/[CO_2]$ ratio is anywhere from a factor of 2 to an order of magnitude less than the experimental value. Thus the inability of the one step CO oxidation scheme to correctly predict $[CO]/[CO_2]$ ratios in high temperature regions seems to be the primary cause for the inability of the model to predict NO_x concentrations.

This conclusion is verified by the theoretical well stirred reactor results for NO presented in Figure 5-15. Corresponding values for $[CO]/[CO_2]$ and temperature were shown in Figure 5-9. Note that when the CO/CO_2 partial equilibrium scheme [Equation 4-43) is used for NO formation together with a detailed mechanism

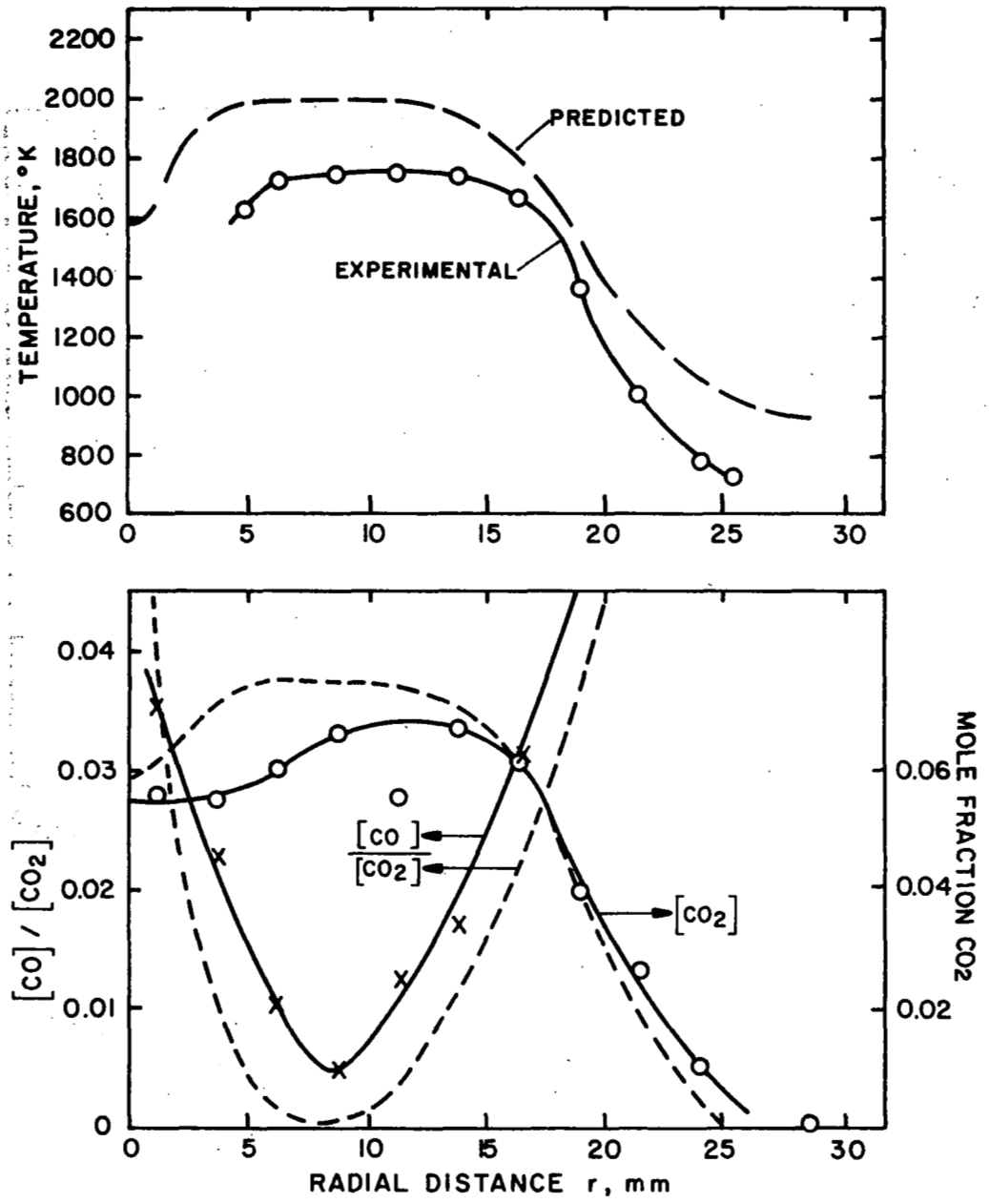

Figure 5-14. Predicted and experimental radial composition and temperature profiles at an axial position of 101.6 mm from the combustor exit.

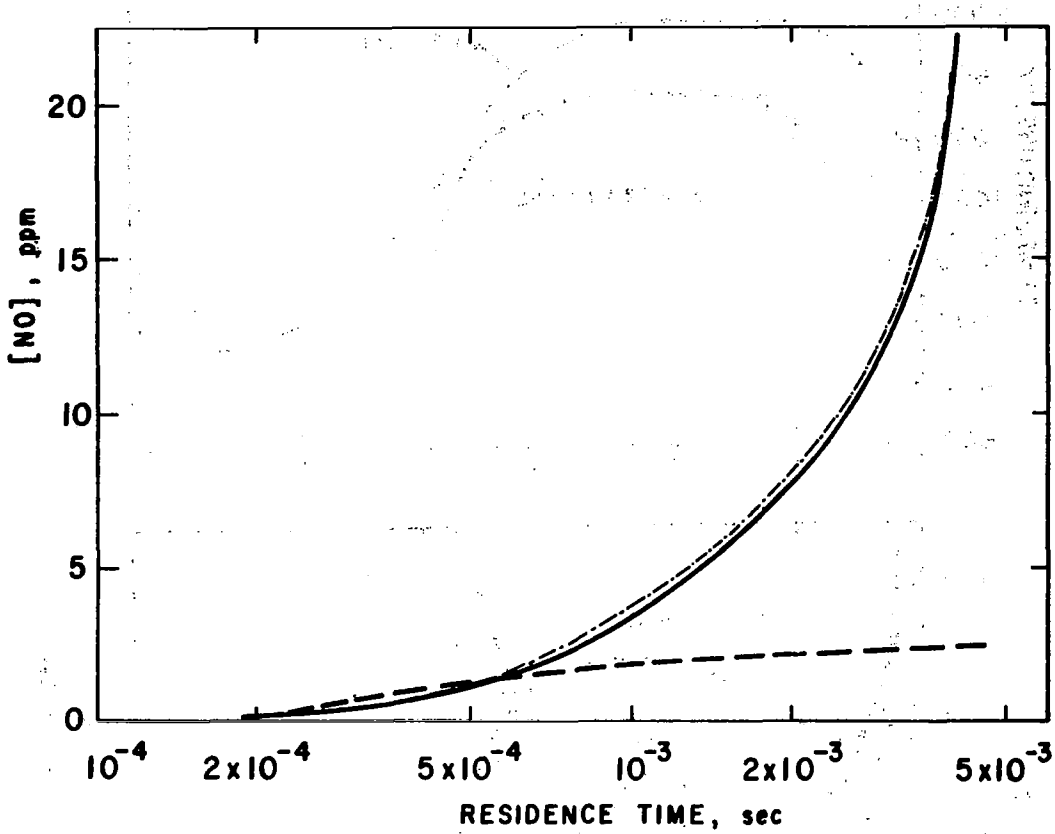

Figure 5-15. Predicted NO concentrations based on adiabatic well stirred reactor model. ϕ = 0.625; T_{IN} = 600 K; P = 1.013 x 10^5 N/m^2; ——, detailed kinetic mechanism for CO and NO (Zeldovich); ---, detailed CO oxidation mechanism, partial equilibrium CO/CO_2 mechanism for NO (Eqn. 4-43); ---, global rate (Howard, et al[31]) for CO oxidation, partial equilibrium CO/CO_2 mechanism for NO (Eqn. 4-43).

for CO oxidation, good agreement is obtained with NO concentrations predicted using the Zelodovich mechanism. However when Howard's global rate for CO oxidation is used the partial equilibrium model underpredicts NO concentrations by an amount comparable with that found in the numerical calculations of Figure 5-12.

5.3 Summary

A comparison between experimentally measured and predicted properties in a turbulent recirculating flow with and without combustion has been presented. In the case of cold flow with CO injection through the jet the resulting distributions indicated a strong dependence of the results on the turbulence model. A comparison of the results obtained here with a more sophisticated turbulence model would be informative in bringing out the shortcomings of the present model.

In the case of flow with combustion shortcomings in both the turbulence and kinetic models were found. Due to the interaction between fluid mechanics and chemistry however it is not possible to isolate the relative effects. Agreement between experimental and predicted species distributions for the hydrocarbon system was fair. The major discrepancy was found in low temperature regions at the initial flamefront and near the outer Vycor wall where the experimentally derived rate for propane oxidation was being applied outside of the temperature range for which it was derived. In high temperature regions a more complete oxidation of CO to CO_2 was predicted than found experimentally. This was due to the importance of the back reaction $CO_2 + H \rightarrow CO + OH$ which was neglected in the simplified CO oxidation scheme.

Predicted NO levels were up to 50% lower than experimental. It was proposed that this was the result of the low ratio of $[CO]/[CO_2]$ in the high temperature regions in which NO is formed. The NO formation rate used in the calculations is proportional to this ratio. Neglecting N_2O as an intermediate in NO formation was also shown to have a possible effect. Finally, predicted NO levels are subject to the limitations inherent in the use of a time averaged approach. Such an approach neglects turbulent fluctuations in temperature and concentration which are likely to effect local chemical kinetic rates. This is especially true in the case of a strongly temperature sensitive pollutant such as NO_x. Investigations are needed into the effect of turbulent fluctuations on kinetic rates.

CHAPTER 6

CONCLUSION

An investigation of pollutant formation under fuel lean conditions in an opposed reacting jet model combustor was undertaken. The intense mixing achieved in the ORJ allows stabilized combustion to be maintained at overall equivalence ratios as low as 0.45. Detailed concentration and temperature measurements over a range of equivalence ratios from 0.625 to 0.45 and at inlet temperautres from 300°K to 600°K have been presented.

Fuel lean premixed combustion is concluded to be an effective means of achieving low pollutant emission levels. NO_x levels in the ORJ were found to approach those of a theoretical well stirred reactor model. This represents a significant reduction over NO_x levels measured in conventional gas turbine combustors. Unburned hydrocarbon and CO levels were somewhat high due to the limited residence times available in the experimental configuration used. Efficiencies approaching 100% should be possible, with a relatively small increase in NO_x emissions, through the use of longer residence times.

Significant levels of NO_2 were measured. Under conditions promoting lower flame temperatures NO_2 constituted up to 100% of the total NO_x. At higher temperatures this percentage decreased to a minimum of 50%. These experimental observations are consistent with a mechanism involving conversion of NO to NO_2 by the HOO

radical. Rapid mixing of hot and cold regions of the combustor appears necessary to quench NO_2 destruction reactions involving O, H and OH radicals.

An analytical model for predicting point by point properties of the opposed reacting jet flowfield was developed. Agreement with experimental results was fair. Discrepancies were found to be the result of the simplified kinetic and fluid mechanic approximations.

REFERENCES

1. Starr, C., Energy and Power, W.H. Freeman, San Francisco (1972).

2. Battelle Memorial Institute, "The Federal R & D Plan for Air Pollution Control by Combustion Process Modification," EPA, Contract CPA 22-69-147 (1971).

3. Sawyer, R.F., "Atmospheric Pollution by Aircraft Engines and Fuels-A Survey," AGARD Advisory Report No. 40, NATO (1972).

4. White, D.J., Roberts, P.B. and Compton, W.A., "Low Emission Variable Area Combustor for Vehicular Gas Turbines," ASME Paper No. 73-GT-19 (1973).

5. Sternlicht, B., "Which Automotive Engines in the Future," Mechanical Engineering, 96, 11 (1974).

6. Johnston, H.S., "Reduction of Stratospheric Ozone by Nitrogen Oxide Catalysts from SST Exhaust," Science, 173, 517 (1971).

7. Hoffert, M.I. and Stewart, R.W., "Stratospheric Ozone-Fragile Shield?," Astronautics and Aeronautics, 42-55 (October 1975).

8. Crutzen, P.J., "The Influence of Nitrogen Oxide on the Atmospheric Ozone Content," Quant. J. Roy. Meterol. Soc., 320-325 (1970).

9. Grobman, J. and Ingebo, R.D., "Forecast of Jet Engine Exhaust Emissions of High-Altitude Commericial Aircraft Projected to 1990," Propulsion Effluents in the Stratosphere, CIAP Monograph 2, Chapter 5, (September 1975).

10. Grobman, J.S., "Effect of Operating Variables on Pollutant Emissions from Aircraft Turbine Engine Combustors," Emissions from Continuous Combustions Systems, W. Cornelius and W.G. Agnew, Eds., Plenum, 123 (1972).

11. Sawyer, R.F., Cernansky, N.P. and Oppenheim, A.K., "Factors Controlling Pollutant Emissions from Gas Turbine Engines," AGARD Conference Proceedings No. 125 on Atmospheric Pollution by Aircraft Engines, AGARD-CP-125, Section 22 (April 1973).

12. Lefebvre, A.H., "Pollution Control in Continuous Combustions Engines," Fifteenth Symposium (International) on Combustion, 229, The Combustion Institute, Tokyo, Japan (1974).

13. Sawyer, R.F., "Aircraft," Combustion Sources of Air Pollution and their Control, Continuing Education in Engineering, University Extension and the College of Engineering, University of California, Berkeley (1973).

14. Sawyer, R.F. and Blazowski, W.S., "Fundamentals of Pollutant Formation," Propulsion Effluents in the Stratosphere, CIAP Monograph 2, Chapter 3 (September 1975).

15. Fletcher, R.S. and Heywood, J.B., "A Model for Nitric Oxide Emissions from Aircraft Gas Turbine Engines," AIAA Paper 71-123, presented at AIAA 9th Aerospace Sciences Meeting, New York, January (1971).

16. Schefer, R.W., Matthews, R.D., Cernansky, N.P., and Sawyer, R.F., "Measurement of NO and NO_2 in Combustion Systems," Paper No. WSCI 73-31, presented at the 1973 Fall Meeting, Western States Section of the Combustion Institute, El Segundo, California (1973).

17. Fristrom, R.M. and Westenberg, A.A., Flame Structure, McGraw-Hill, New York (1965).

18. Cernansky, N.P., "Private Communication," Department of Mechanical Engineering, University of California, Berkeley (1974).

19. Allen, J.D., "Probe Sampling of Oxides of Nitrogen from Flames," Combustion and Flame, 24, 133 (1975).

20. Patterson, J.A., McElroy, M.W., Sawyer, R.F., and Singh, T., "A Prototype Chemicluminescent NO Analyzer," Report No. TS-70-9, Department of Mechanical Engineering, University of California, Berkeley (1970).

21. Matthews, R.D., "Distributions of NO, NO_2, and NO_x in a Model Gas Turbine Combustor," M.S. Thesis, Department of Mechanical Engineering, University of California, Berkeley (1973).

22. Tuttle, J.H. Shisler, R.A. and Mellor, A.M., "Nitrogen Dioxide Formation in Gas Turbine Engines: Measurements and Measurement Methods," Environmental Protection Agency Grant No. R-801284, Report No. PURDUE-CL-73-06 (1973).

23. Maahs, H.G., "Interference of Oxygen, Carbon Dioxide and Water Vaport on the Analysis for Oxides of Nitrogen by Chemiluminescence," NASA TM X-3229 (August 1975).

24. Allen, J.D., Billingsly, R. and Shaw, J.T., "Evaluation of the Measurement of Oxides of Nitrogen in Combustion Products by the Chemiluminescence Method," J. Institute of Fuel (December 1974).

25. McLean, W.J. and Sawyer, R.F., "Mass Spectrometer Data Reduction and Error Analysis," Report No. TS-67-4, Department of Mechanical Engineering, University of California, Berkeley (1967).

26. Glassman, I., Dryer, F.L. and Cohen, R., "Combustion of Hydrocarbons in an Adiabatic Flow Reactor: Some Considerations and Overall Correlations of Reactions Rate," presented at Joint Meeting of the Central and Western States Sections of the Combustion Institute, The Combustion Institute, San Antonio (1975).

27. Kent, J.A., "A Noncatalytic Coating for Platinum-Rhodium Thermocouples," Combustion and Flame, 14, 279 (1970).

28. Bradley, D. and Matthews, K.J., "Measurement of High Gas Temperatures with Fine Wire Thermocouples," J. Mech. Engr. Sci., 10, 4, p. 299 (1968).

29. Noon, A.W., "Investigation of Jet Flameholders, Part II," WADC TN 56-316 (1957).

30. Fuhs, A.E., "Spectroscopic Studies of Reverse Jet Flame Stabilization," ARS Journal, 30, 238 (1960).

31. Schlichting, H., Boundary Layer Theory, 6th edition, McGraw-Hill Book Company, New York (1958).

32. Bowman, C.T., Seery, D.J., "Investigation of NO Formation Kinetics in Combustion Processes: The Methane-Oxygen-Nitrogen Reaction," Emissions from Continuous Combustion Systems, W. Cornelius and W.G. Agnew, Plenum, 123 (1972).

33. Baulch, D.L. and Drysdale, D.D., "An Evaluation of Rate Data for the Reaction CO + OH CO_2 + H," Combustion and Flame, 23, 215 (1974).

34. Fenimore, C.P. and Moore, J., "Quenched Carbon Monoxide in Fuel-Lean Flame Gas," Combustion and Flame, 22, 343 (1974).

35. Blazowski, W.S. and Henderson, R.E., "Aircraft Exhaust Pollution and Its Effect on the U.S. Air Force," AFAPL-TR-74-64, Air Force Aero-Propulsion Lab, Wright-Patterson Air Force Base, Ohio (1974).

36. Anderson, D.N., "Effects of Equivalence Ratio and Dwell Time on Exhaust Emissions from an Experimental Premixing Prevaporizing Burner," NASA TM X-71592 (1975).

37. Roffe, G. and Ferri, A., "Prevaporization and Premixing to Obtain Low Oxides of Nitrogen in Gas Turbine Combustors," NASA CR-2495 (1975).

38. Lipfert, F.W., "Correlation of Gas Turbine Emissions Data," ASME 72-GT-60 (1972).

39. Pratt, D.T. and Bowman, B.R., PSR-A "Computer Program for Calculation of Combustion Reaction Kinetics in a Micromixed Perfectly Stirred Reactor," Circular 43, Engineering Extension Service, Washington State University, Pullman, Washington (1972).

40. Marteney, P.J., "Analytical Study of the Kinetics of Formation of Nitrogen Oxide in Hydrocarbon-Air Combustion," Combustion Science and Technology, 1, 461 (1970).

41. Mellor, A.M., "Current Kinetic Modeling Techniques for Continuous Flow Combustors," Emissions from Continuous Combustion Systems, Plenum Press, New York (1972).

42. Anonymous, "Exhaust Emissions Test," AiResearch Aircraft Propulsion and Auxillary Power Gas Turbines, AiResearch Co. Report GT-8747-R (1971).

43. Cernansky, N.P., "Formation of NO and NO_2 in a Turbulent Propane/Air Diffusion Flame, Ph.D. Dissertation, University of California, Berkeley, California (1974).

44. Gosman, A.D., Pun, W.M., Runchal, A.K., Spalding, D.B. and Wolfshtein, M., Heat and Mass Transfer in Recirculating Flows, Academic Press, London (1969).

45. Bird, R.B., Stewart, W.E. and Lightfoot, E.M., Transport Phenomena, John Wiley & Sons, Inc., New York (1960).

46. Pratt, D.T., "Theories of Mixing in Continuous Combustion," Fifteenth Symposium (International) on Combustion, 1339, The Combustion Institute (1975).

47. Samuelsen, G.S., "Analytical and Experimental Investigation of an Ammonia-Air Opposed Reacting Jet," Ph.D. Dissertation, University of California, Berkeley (1970).

48. JANAF Thermochemical Data, The Dow Chemical Company, Midland, Michigan (1960).

49. Pun, W.M. and Spalding, D.B., "A Procedure for Predicting the Velocity and Temperature Distributions in Confined, Steady, Turbulent, Gaseous Diffusion Flames," Imperial College, Mechanical Engineering Department, SF/TN/11, (1967).

50. Odlozinski, G., "A Procedure for Predicting the Distribution of Velocity and Temperature in a Flame Stabilized Behind a Bluff Body," Imperial College, Department of Mechanical Engineering, EF/R/G/2 (1968).

51. Launder, B.E. and Spalding, D.B., Mathematical Models of Turbulence, Academic Press, London (1972).

52. Shapiro, A.H., The Dynamics and Thermodynamics of Compressable Fluid Flow, The Ronald Press, New York (1954).

53. Caretto, L.S., "Modeling Pollutant Formation in Combustion Processes," Fourteenth Symposium (International) on Combustion, 803, The Combustion Institute, Pittsburgh, Pennsylvania (1973).

54. Hammond, D.C. and Mellor, A.M., "Analytical Calculations for the Performance and Pollutant Emissions of Gas Turbine Combustors," Combustion Sci. Tech., 4, 3, 101 (1971).

55. Edelman, R. and Fortune, O., "A Quasi-Global Chemical Kinetic Model for the Finite-Rate Combustion of Hydrocarbon Fuels," AIAA Paper 69-86 (1969).

56. Marks, M., "Nonlinear Regression Analysis Program," Air Force Rocket Propulsion Laboratory, Edwards AFB, California (1974).

57. Kydd, P.H. and Foss, W.I., "Combustion of Fuel-Lean Mixtures in Adiabatic Well Stirred Reactors, " Tenth Symposium (International) on Combustion, 101, The Combustion Institute (1965).

58. Clarke, A.E. and Odgers, J., Stringer, F.W. and Harrison, A.J., "Combustion Processes in a Spherical Combustor," Tenth Symposium (International) on Combustion, 1151, The Combustion Institute (1965).

59. Leonard, P.A., Lester, T.W., Clancy, M.G., Laurendeau, N.M. and Mellor, A.M., "Nitric Oxide Formation in Hydrocarbon/Air Flames," Report No. PURDU-CL-73-04, Purdue University, West Lafayette, Indiana (1973).

60. Kondratiev, V.M., Rate Constants of Gas Phase Reactions, National Technical Information Service No. COM-72-10014 (1972).

61. Howard, J.B., Williams, G.C., and Fine, D.H., "Kinetics of Carbon Monoxide Oxidation in Postflame Gases," Fourteenth Symposium (International) on Combustion, 975, The Combustion Institute, Pittsburgh, Pennsylvania (1973).

62. Dryer, F.L. and Glassman, I., "High Temperature Oxidation of CO and CH_4," Fourteenth Symposium (International) on Combustion, 987, The Combustion Institute, Pittsburgh, Pennsylvania (1973).

63. Williams, G.C., Hottle, H.C. and Morgan, A.C., "The Combustion of Methane in a Jet-Mixed Reactor," Twelfth Symposium (International) on Combustion, 913, The Combustion Institute (1969).

64. Hottel, H.C., Williams, G.C., Nerheim, N.M., and Schneider, G.R., "Kinetic Studies in Stirred Reactors: Combustion of Carbon Monoxide and Propane," Tenth Symposium (International) on Combustion, 111, The Combustion Institute (1965).

65. Laurendeau, N.M., "The Thermal Decomposition of Nitric Oxide and Nitrogen Dioxide," Ph.D. Thesis, Report No. TS-72-4, Department of Mechanical Engineering, University of California, Berkeley (1972).

66. Thompson, D., Brown, T.D., and Beer, J.M., "NO_x Formation in Combustion," Combustion and Flame, 19, 69 (1972).

67. Sarofim, A.F., and Pohl, J., "Kinetics of Nitric Oxide Formation in Premixed Laminar Flames," Fourteenth Symposium (International) on Combustion, 739, The Combustion Institute (1973).

68. Iverach, D. Basden, K.S. and Kirov, N.Y., "Formation of Nitric Oxide in Fuel-Lean and Fuel-Rich Flames," Fourteenth Symposium (International) on Combustion, 767, The Combustion Institute (1973).

69. Baulch, D.L., Drysdale, D.D. and Lloyd, A.C., "Critical Evaluation of Rate Data for Homogeneous, Gas Phase Reactions of Interest in High Temperature Systems," Nos. 1 and 2, Department of Phys. Chem., The University of Leeds, England (1968).

70. Malte, P.C. and Pratt, D.C. "Oxides of Nitrogen Formation for Fuel-Lean, Jet Stirred Carbon Monoxide Combustion," Paper 73-37, presented at the Fall Meeting, Western States Section of the Combustion Institute, El Segundo, California (1973).

71. Cunningham, R.D., "Orifice Meters with Supercritical Compressable Flow," Trans. Am. Soc. Mech. Engr., 73, 625 (1951).

72. Baulch, D.L., Drysdale, D.D., Horne, D.G. and Lloyd, A.C., Evaluated Kinetic Data for High Temperature Reactions, Butterworths, London (1972).

73. Garvin, D. and Hampson, R.F., "Chemical Kinetics Data Survey VII. Tables of Rate and Photochemical Data for Modeling the Stratosphere (Revised)," Report No. NBSIR-74-430, National Bureau of Standards, Washington, D.C. (1974).

74. Nickerson, G.R. and Frey, H.M., GKAP - "Generalized Kinetic Analysis Program," Ultrasystems, Irvine, California (1971).

75. Merryman, E.L. and Levy, A., "Nitrogen Oxide Formation in Flames: The Roles of NO_2 and Fuel Nitrogen," Fifteenth Symposium (International) on Combustion, 1073, The Combustion Institute (1975).

76. Bowman, C.T., "Kinetics of Nitric Oxide Formation in Combustion Processes," Fourteenth Symposium (International) on Combustion, 729, The Combustion Institute (1973).

77. Niedzwiecki, R.W. and Jones, R., "Parametric Test Results of a Swirl Can Combustor," NASA TM X-68247 (1973).

APPENDIX A

Experimental Facility

A.1. Introduction

A brief description of the combustor and combustor test section was given in Chapter 3. In this appendix details of the experimental facility and related support equipment are presented. A schematic of the experimental facility is shown in Figure A-1. The fuel and air supply systems, metering of the fuel and air, and design of the facility are discussed below.

A.2. Main Fuel and Air

Main air is supplied from the house compressed air system which is maintained at a nominal pressure of 1.48×10^6 N/m^2. A 50.8 mm line is used to supply the experimental system. The pressure is reduced to 4.46×10^5 N/m^2 prior to metering. The main air is metered with a standard 15.24 mm diameter ASME orifice (with flange pressure tops) designed in accordance with ASME codes (ASME; 1961; Cunningham[71]). The pressure ratio across the orifice was read in inches of water on a manometer. Upstream static pressure is measured with a Boudon gage and the temperature of the flow is measured using a thermocouple. The orifice calibration was checked against a positive displacement meter.

The main air flow is controlled by means of a 12.7 mm needle metering valve. The 50.8 mm line is reduced to a 12.7 mm line to accomodate the valve. After the control valve air preheat is provided by a General Electric air circulation heater utilizing six 6-KW stages, one of which has a Chromalox (Model CIPD73-6C) solid

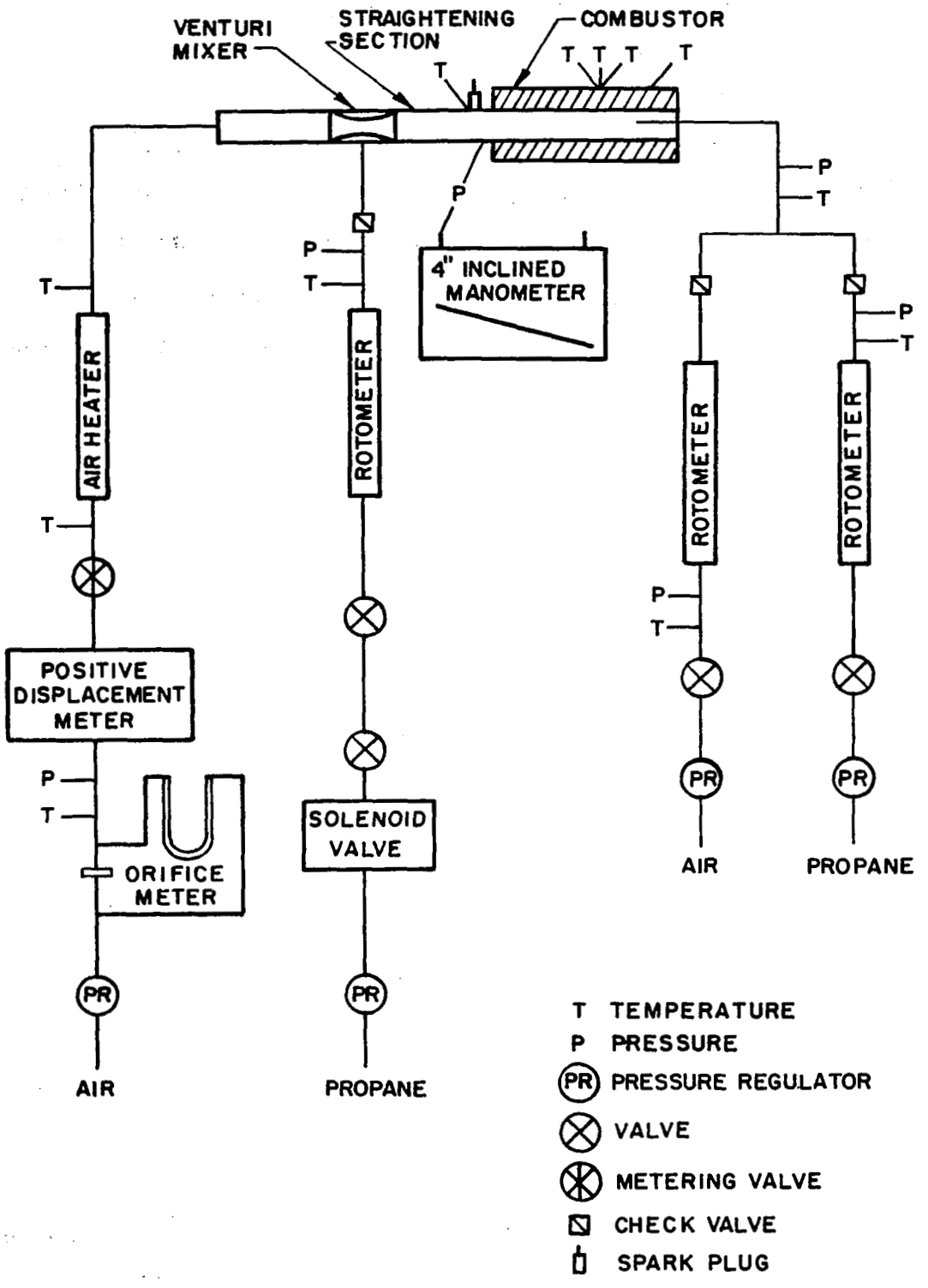

Figure A-1. Schematic of combustor test facility.

state proportional temperature controller. Air preheated to a maximum of 812°K at the heater exit can be maintained. Due to unavoidable heat losses in the lines, this corresponds to a maximum test section inlet temperature of 650°K at the flow rates of interest in the present investigation.

The propane fuel used is Matheson Co. commercial grade supplied from pressurized tanks. Minimum purity of the propane is 99.0 mole percent, with a typical analysis as follows: 99.4% propane, 0.05% ethane, 0.50% isobutane, and 0.05% propylene.

The main fuel is metered in a Fisher-Porter Stable-Vis Rotometer (tube B3A-25, float BSX-33-55) which was calibrated with a wet test meter. Pressure and temperature of the fuel is measured at the rotometer to enable calculation of the fuel mass flow rate. A fast response solenoid shut off valve located in the fuel line provides rapid shut off of the fuel.

The main stream fuel and air are mixed upstream of the combustor test section in a venturi section designed by Samuelsen[47]. The fuel is injected radially into the airstream at a 22.86 mm diameter throat through four nozzles evenly spaced about the circumference. The fuel and air mixture then passes down a one meter long, 57.15 mm diameter straightening section before entering the Vycor test section (described in Section 2.4). The pressure and temperature of the main stream are measured just prior to the test section inlet through taps in the straightening section walls. The fuel and air mixture is ignited by a spark plug (Champion H-14Y) located diametrically opposite to the pressure and temperature taps at the end of the straightening section.

A.3. Jet Fuel and Air

Propane for the jet injector is tapped off the main propane line just downstream of the solenoid valve. The jet fuel is metered in a Matheson ball rotometer (tube 602) which was calibrated with a wet test meter. Jet air is tapped off the main air line upstream of the orifice meter, and subsequently metered in a Fisher-Porter Stable-Vis rotometer (tube B3A-25, float BSX-33-55). Both rotometers were individually calibrated prior to use with a wet test meter.

The jet fuel and air are mixed in a 6.35 mm Swedgelok tee section approximately 1.2 m upstream of the jet injector. Temperature and pressure of the jet stream are measured just downstream of the mixing tee. Because the jet air was tapped off the main air line upstream of the air heater, no preheat was provided to the jet injected reactants.

APPENDIX B

Probe Calculations

B.1 Introduction

In the use of combustion gas sampling probes a major problem is to obtain a representative sample of combustion gases. As was discussed in Chapter 2 quenching of chemical reactions in the sampling probe can best be accomplished through a rapid decrease in both gas temperature and pressure. The partially water cooled probe used in the present investigation utilizes expansion of the sample gas to a low pressure through a critical flow orifice located at the probe tip to quench reactions in the initial uncooled portion of the probe, followed by a water cooled section in which an additional degree of quenching is obtained through a decrease in the gas temperature.

In this appendix a simplified theoretical analysis is described in which an attempt was made to determine whether the partially cooled probe used in this investigation did indeed provide adequate quenching of chemical reactions in the sample gases.

B.2 Probe Analysis

The dimensions of the probe used in the analysis are shown in Figure B-1a. Pressure and temperature were measured at the probe exit while sampling from the opposed jet reactor operating under the conditions of case 3 (ϕ = 0.625, T_{INLET} = 600° K). The sample gas temperature was found to be approximately 530° K at this point. The relatively high back pressure of 35 torr

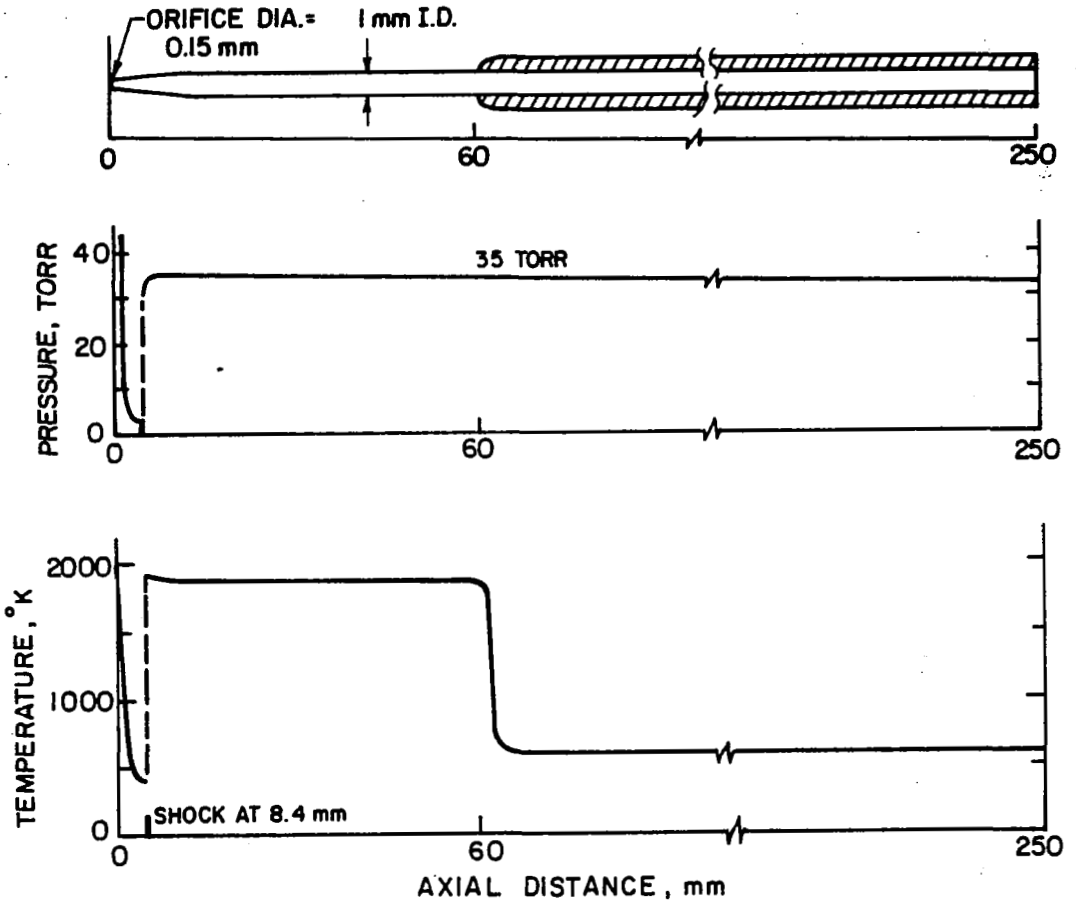

Figure B-1. Pressure and temperature distributions in an idealized partially cooled quartz sampling probe.

(a result of the long sample line) compared to what would be obtained during isentropic expansion indicated that a shock must be present in the probe. Calculations were made using the experimentally measured pressure, and the required position of the shock was found to be 9.4 mm downstream of the probe inlet. The resulting pressure profile along the probe is shown in Figure B-1b. The pressure drop due to friction downstream of the shock was found to be on the order of 10^{-4} torr/cm length and therefore was neglected. Isentropic flow was assumed in that portion of the nozzle before the shock. Downstream of the shock heat transfer calculations were used to compute the temperature profile. In the uncooled portion of the probe a wall temperature of 1860° K was assumed. As discussed below this corresponds to the flame temperature for the sample case studied. It should be noted that this temperature is quite close to the softening temperature of quartz which is 1900° K and thus represents an upper limit on the probe wall temperature. The resulting sample gas temperature profile is shown in Figure B-1c.

It was necessary to make several simplifying assumptions for the numerical calculations. A constant pressure of 35 torr and a constant temperature of 1860° K were assumed in the region preceeding the shock. Neglecting the pressure and temperature drop during the expansion preceeding the shock should represent a worst case with regard to reactions occurring in the probe. One dimensional flow was also assumed, thus radial concentration and velocity gradients in the probe were neglected. Possible effects of this assumption will be discussed in the next section.

To determine probe inlet conditions, sampling was assumed to occur from an idealized well stirred reactor operating at inlet conditions equivalent to those of case 3 (ϕ = -.625, T_{INLET} = 600°K, p = 1.013 x 10^5 N/m^2). It was felt this would provide more representative radical concentrations than if equilibrium conditions were assumed. An operating point for the well stirred reactor ($\dot{m}/V$) was chosen which gave a flame temperature and NO_x concentration approximately equal to those encountered experimentally in the ORJ. The sampling conditions are summarized in Table B-1. These concentrations were take as the probe inlet conditions. The corresponding flame temperature is 1860°K.

TABLE B-1. Probe Inlet Species Concentrations

Species	Mole Fraction
O_2	8.4×10^{-2}
CO	8.5×10^{-3}
CO_2	7.3×10^{-2}
H_2O	9.3×10^{-2}
H_2	2.3×10^{-3}
OH	6.2×10^{-3}
H	1.7×10^{-3}
O	3.9×10^{-3}
N_2	8.2×10^{-1}
N	1.8×10^{-9}
NO	1.05×10^{-5}

B.3. Reaction Scheme

The reaction scheme used for the calculations is shown in Table B-2. Due to the uncertainties discussed in Chapter 3 with

regard to probe reactions between NO and NO_2 attention was confined to the formation of total oxides of nitrogen via the Zeldovich mechanism[39]. An excellent discussion of possible probe reactions involving interconversion of NO and NO_2 is presented by Cernansky[43].

TABLE B-2. Reaction Scheme

	Reaction	Forward Rate Constant	Reference
1.	$OH + H_2 \leftrightharpoons H + H_2O$	$10^{13.342}\exp(-2.59/T)$	72
2.	$H + O_2 \leftrightharpoons OH + O$	$10^{14.342}\exp(-8.44/T)$	72
3.	$O + H_2O \leftrightharpoons OH + OH$	$10^{13.833}\exp(-9.24/T)$	72
4.	$O + H_2 \leftrightharpoons OH + H$	$10^{10.255}T'\exp(-4.48/T)$	72
5.	$H + H + M \leftrightharpoons H_2 + M$	$10^{17.806}T^{-1}$	72
6.	$O + O + M \leftrightharpoons O_2 + M$	$10^{18.139}T^{-1}\exp(0.17/T)$	73
7.	$O + H \quad M \leftrightharpoons OH + M$	$10^{15.86}$	73
8.	$H + OH + M \leftrightharpoons H_2O + M$	$10^{16.788}\exp(0.25/T)$	70
9.	$H + HO_2 \leftrightharpoons OH + OH$	$10^{14.398}\exp(-0.95/T)$	72
10.	$H + O_2 + M \leftrightharpoons HO_2 + M$	$10^{15.176}\exp(0.50/T)$	72
11.	$H_2 + O_2 \leftrightharpoons H + HO_2$	$10^{13.740}\exp(-29.08/T)$	72
12.	$CO + OH \leftrightharpoons CO_2 + H$	$10^{11.748}\exp(-0.54/T)$	69
13.	$CO + O + M \leftrightharpoons CO_2 + M$	$10^{14.00}\exp(-1.26/T)$	69
14.	$CO_2 + O \leftrightharpoons CO + O_2$	$10^{13.279}\exp(-27.24/T)$	69
15.	$N + NO \leftrightharpoons N_2 + O$	$10^{13.204}$	69
16.	$N + O_2 \leftrightharpoons O + NO$	$10^{9.806}T'\exp(-3.15-T)$	69

---

*Units - k: $(cm^3mole^{-1})^{n-1}sec^{-1}$ where n is reaction order;

Because of uncertainties associated with a reaction mechanism for propane under these conditions no attempt was made to include

propane in the calculations. Wall reactions were also neglected.

The kinetic calculations were carried out using the Generalized Kinetic Analysis Program developed by Nickerson and Frey[74].

B.4. Results

The results are shown in Figure B-2. It can be seen that quenching is adequate for all major species of interest. As expected obtaining representative concentrations of the radical species O, OH and H is not feasible with the present probe due to inadequate quenching.

It was mentioned in the previous section that one dimensional flow was assumed in the probe. The primary effect of a parabolic velocity distribution is a longer residence time for that part of the flow nearest the wall. In an effort to determine the effect of this assumption on the results, the above calculations were repeated with the residence time in the uncooled section of the probe being increased by a factor of 2. No change was found in the results.

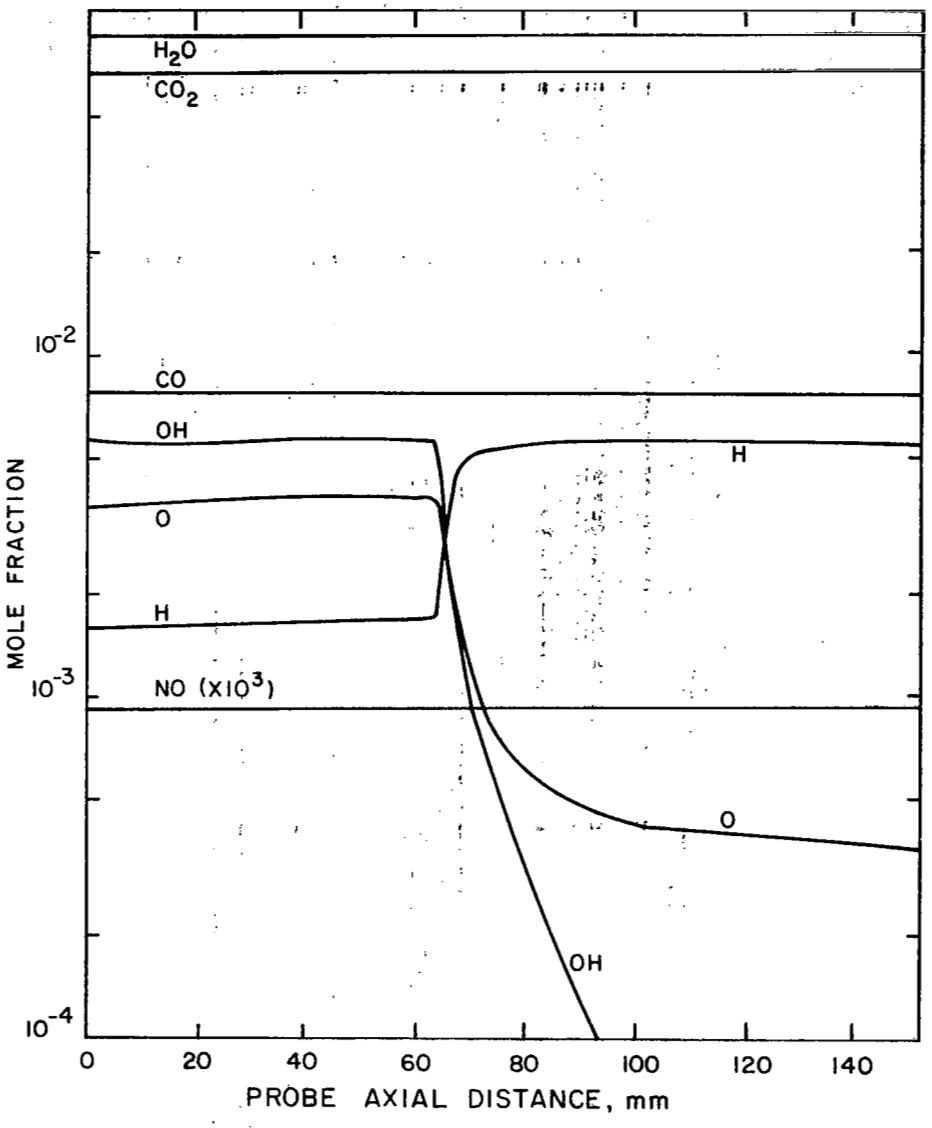

Figure B-2. Predicted axial concentration distributions for idealized partially cooled quartz sampling probe.

APPENDIX C

Chemiluminescent Detector Interference

C.1. Introduction

NO_x concentrations were measured in the combustor using a chemiluminescent nitric oxide detector. It has been pointed out by several investigators that under certain conditions the presence of H_2O and CO_2 can have a significant effect on the measured levels of NO. Both of these gases occur in the present system in sufficient quantities to warrant consideration.

C.2. Third Body Efficiency Effect

The reactions of importance in the chemiluminescent detector are[20]

$$NO + O_3 \rightarrow NO_2^* + O_2 \qquad \text{(C-1)}$$

$$NO + O_3 \rightarrow NO_2 + O_2 \qquad \text{(C-2)}$$

$$NO_2^* \rightarrow NO_2 + h\nu \qquad \text{(C-3)}$$

$$NO_2^* + M \rightarrow NO_2 + M \qquad \text{(C-4)}$$

Interference by H_2O and CO_2 is due to the different third body efficiencies of these molecules associated with the NO_2^* quenching reaction C-4. CO_2 has been found by Clough and Thrush[23] to have an efficiency of 2.2 in this reaction. Although no quenching efficiencies could be found for H_2O, a quenching efficiency of approximately 3 times that of CO_2 was estimated by Allen, et al.[24] These values compare with a quenching efficiency of 1.0 for O_2 and N_2.

It can be shown that the intensity of chemiluminescence from the above system of reactions is given by the expression

$$I = \frac{K_3 K_1 [NO][O_3]}{K_4[M]} \qquad \text{(C-5)}$$

For gases with differing third body efficiencies, [M] can be replaced by

$$[M] = \frac{P}{RT} \sum_i x_i \eta_i \qquad \text{(C-6)}$$

where x_i and η_i are the mole fraction and quenching efficiency, respectively of the i th species. Thus for a system containing gases of different third body efficiencies the fractional reduction in intensity due to the presence of these gases can be calculated from

$$\frac{I_{\eta=1}-I}{I_{\eta=1}} = 1 - \frac{1}{\sum x_i \eta_i} \qquad \text{(C-7)}$$

$I_{\eta=1}$ is the measured intensity from a system in which all third body efficiencies are 1.0.

C.3. Interference Correction Factors

While Equation C-7 allows one to calculate the effect of H_2O and CO_2 on measured concentrations of NO_x, a more straight forward approach was used in which the chemiluminescent detector was calibrated with gas mixtures containing known quantities of N_2, NO, H_2O, and CO_2. The concentration of NO was maintained constant while N_2 was replaced by H_2O and CO_2 in concentrations typical of those found in the present investigation. Pressure in the detector reaction chamber was 2.7 torr in all cases. The fractional decrease in measured NO concentrations as a function of H_2O and CO_2 mole fraction is shown in Figure B-1.

These results are similar to those of Allen, et al[24], who found a 1.5% reduction in detector signal per 10% CO_2 addition at an organized oxygen to sample flow rate ratio of 6, up to a 7% reduction per 10% CO_2 for a ratio of 0.5. Figure C-1 shows

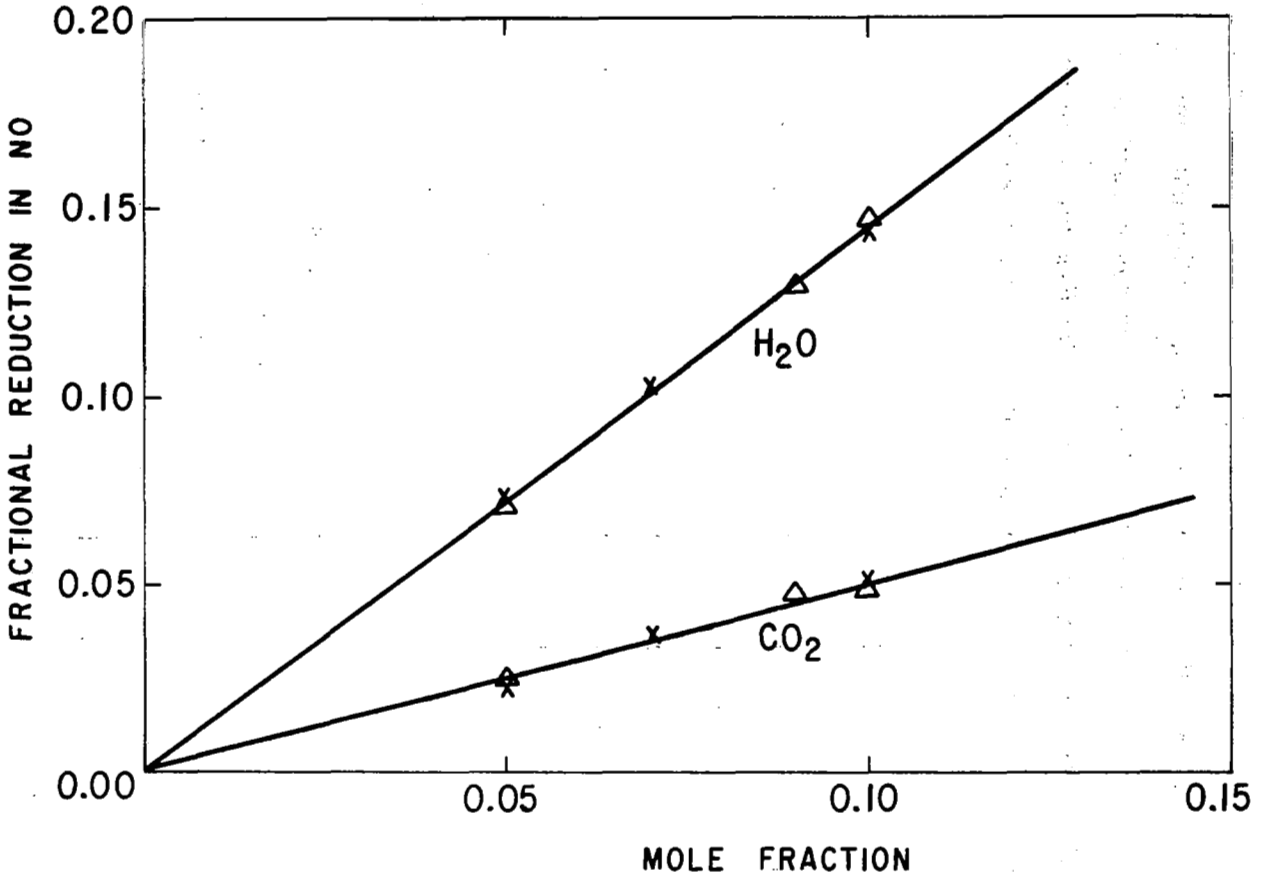

Figure C-1. The effect of H_2O and CO_2 interference on NO measurements in a chemiluminescent detector; x - 10 ppm NO; Δ - 20 ppm NO.

TABLE D-1 MASS SPECTROMETER, CO, AND TEMPERATURE DATA

DATA FOR CASE 1 TEMP= 300.0 EQIV= .6250 VEL= 7.240

Z(I)	R(J)	NOX	NO	Z(I)	R(J)	NOX	NO
0.	26.80	.06	0.	63.5	5.84	2.44	0.
0.	24.26	.22	0.	63.5	3.94	2.50	0.
0.	21.72	.53	0.	63.5	1.40	-.00	-.00
0.	19.18	.87	0.	76.2	26.80	-.00	-.00
0.	16.64	1.25	0.	76.2	24.26	-0.	-0.
0.	14.10	1.91	0.	76.2	21.72	.04	0.
0.	13.46	1.81	.06	76.2	19.18	.25	0.
0.	11.56	2.13	-0.	76.2	16.64	.63	0.
0.	10.92	2.21	.06	76.2	14.10	1.25	0.
0.	8.38	2.68	.06	76.2	13.46	1.31	0.
0.	5.84	2.38	.06	76.2	11.56	1.76	-0.
0.	3.94	2.44	.06	76.2	10.92	1.80	0.
0.	1.40	-.00	-.00	76.2	8.38	2.19	.06
25.4	26.80	0.	0.	76.2	5.84	2.50	.06
25.4	24.26	.10	0.	76.2	3.94	2.88	0.
25.4	21.72	.35	0.	76.2	1.40	-0.	-0.
25.4	19.18	.69	0.	88.9	26.80	-.00	-.00
25.4	16.64	1.19	0.	88.9	24.26	-.00	-.00
25.4	14.10	1.47	0.	88.9	21.72	-.00	-.00
25.4	13.46	1.56	.06	88.9	19.18	.17	0.
25.4	11.56	1.97	-0.	88.9	16.64	.50	0.
25.4	10.92	2.06	.06	88.9	14.10	1.06	0.
25.4	8.38	2.52	.06	88.9	13.46	1.25	0.
25.4	5.84	2.50	.06	88.9	11.56	1.73	-0.
25.4	3.94	2.25	.06	88.9	10.92	1.81	0.
25.4	1.40	-.00	-.00	88.9	8.38	2.50	0.
50.8	26.80	-0.	-0.	88.9	5.84	2.81	.04
50.8	24.26	0.	0.	88.9	3.94	2.80	.06
50.8	21.72	.19	0.	88.9	1.40	2.25	.25
50.8	19.18	.44	0.	101.6	26.80	-.00	-.00
50.8	16.64	.94	0.	101.6	24.26	-.00	-.00
50.8	14.10	1.45	0.	101.6	21.72	-.00	-.00
50.8	13.46	1.56	0.	101.6	19.18	.13	0.
50.8	11.56	1.92	-0.	101.6	16.64	.47	0.
50.8	10.92	2.09	0.	101.6	14.10	1.00	0.
50.8	8.38	2.31	0.	101.6	13.46	1.30	.04
50.8	5.84	2.44	0.	101.6	11.56	1.91	-0.
50.8	3.94	2.50	0.	101.6	10.92	2.10	.04
50.8	1.40	-.00	-.00	101.6	8.38	2.52	0.
63.5	26.80	-.00	-.00	101.6	5.84	2.75	.06
63.5	24.26	-0.	-0.	101.6	3.94	2.88	.15
63.5	21.72	.13	0.	101.6	1.40	2.36	.10
63.5	19.18	.38	0.	114.3	26.80	-.00	-.00
63.5	16.64	.75	0.	114.3	24.26	-.00	-.00
63.5	14.10	1.25	0.	114.3	21.72	-0.	-0.
63.5	13.46	-0.	-0.	114.3	19.18	-0.	-0.
63.5	11.56	1.85	-0.	114.3	16.64	.40	0.
63.5	10.92	1.69	0.	114.3	14.10	1.13	0.
63.5	8.38	2.38	0.	114.3	13.46	1.44	0.

TABLE D-1 (Continued)

Z(I)	R(J)	NOX	NO
114.3	11.56	2.10	-0.
114.3	10.92	2.38	0.
114.3	8.38	2.75	0.
114.3	5.84	2.88	.25
114.3	3.94	3.00	.50
114.3	1.40	2.69	.20
127.0	26.80	-.00	-.00
127.0	24.26	-.00	-.00
127.0	21.72	-0.	-0.
127.0	19.18	0.	0.
127.0	16.64	.13	0.
127.0	14.10	.69	0.
127.0	13.46	1.23	0.
127.0	11.56	2.08	-0.
127.0	10.92	2.31	0.
127.0	8.38	3.04	0.
127.0	5.84	3.04	.31
127.0	3.94	3.04	.90
127.0	1.40	3.19	.19
133.3	26.80	-.00	-.00
133.3	24.26	-.00	-.00
133.3	21.72	-.00	-.00
133.3	19.18	-.00	-.00
133.3	16.64	.03	0.
133.3	14.10	.31	0.
133.3	13.46	.75	0.
133.3	11.56	1.60	-0.
133.3	10.92	1.75	0.
133.3	8.38	2.44	0.
133.3	5.84	2.75	0.
133.3	3.94	3.06	.60
133.3	1.40	2.94	.10
139.7	26.80	-.00	-.00
139.7	24.26	-.00	-.00
139.7	21.72	-.00	-.00
139.7	19.18	-.00	-.00
139.7	16.64	-0.	-0.
139.7	14.10	-.00	-.00
139.7	13.46	.25	0.
139.7	11.56	.70	-0.
139.7	10.92	.81	0.
139.7	8.38	1.63	0.
139.7	5.84	2.19	0.
139.7	3.94	2.69	0.
139.7	1.40	2.88	0.
146.0	26.80	-.00	-.00
146.0	24.26	-.00	-.00
146.0	21.72	-.00	-.00
146.0	19.18	-.00	-.00
146.0	16.64	-.00	-.00
146.0	14.10	-.00	-.00
146.0	13.46	-.00	-.00
146.0	11.56	-.00	-.00
146.0	10.92	-.00	-.00
146.0	8.38	.13	0.
146.0	5.84	.38	0.
146.0	3.94	.74	0.
146.0	1.40	.90	0.
152.4	26.80	-.00	-.00
152.4	24.26	-.00	-.00
152.4	21.72	-.00	-.00
152.4	19.18	-.00	-.00
152.4	16.64	-.00	-.00
152.4	14.10	-.00	-.00
152.4	13.46	-.00	-.00
152.4	11.56	-.00	-.00
152.4	10.92	-.00	-.00
152.4	8.38	-0.	-0.
152.4	5.84	0.	0.
152.4	3.94	-0.	-0.
152.4	1.40	0.	0.

TABLE D-1 (Continued)

DATA FOR CASE 2 TEMP= 450.0 EQIV= .6250 VEL= 7.240

Z(I)	R(J)	NOX	NO	Z(I)	R(J)	NOX	NO
0.	26.80	1.31	0.	76.2	14.10	3.25	.19
0.	24.26	1.81	0.	76.2	11.56	4.31	0.
0.	21.72	2.55	0.	76.2	9.02	5.00	.13
0.	19.18	3.31	0.	76.2	6.48	5.50	.22
0.	16.64	4.00	.13	76.2	3.94	6.00	.13
0.	14.10	4.69	.13	76.2	1.40	-.00	-.00
0.	11.56	5.75	.81	88.9	26.80	-.00	-.00
0.	9.02	6.44	1.06	88.9	24.26	-.00	-.00
0.	6.48	6.56	1.44	88.9	21.72	.69	0.
0.	3.94	6.31	3.25	88.9	19.18	1.25	0.
0.	1.40	-.00	-.00	88.9	16.64	2.31	0.
25.4	26.80	-.00	-.00	88.9	14.10	3.31	.15
25.4	24.26	1.25	0.	88.9	11.56	4.50	.03
25.4	21.72	2.00	0.	88.9	9.02	4.88	.06
25.4	19.18	3.00	.13	88.9	6.48	5.81	.25
25.4	16.64	3.56	.13	88.9	3.94	5.44	.06
25.4	14.10	4.25	.13	88.9	1.40	4.38	.06
25.4	11.56	5.38	.19	101.6	26.80	-.00	-.00
25.4	9.02	6.19	.40	101.6	24.26	-.00	-.00
25.4	6.48	6.44	.80	101.6	21.72	.56	0.
25.4	3.94	5.97	2.65	101.6	19.18	1.19	0.
25.4	1.40	-.00	-.00	101.6	16.64	2.25	0.
50.8	26.80	-.00	-.00	101.6	14.10	3.44	.06
50.8	24.26	.81	0.	101.6	11.56	4.65	.06
50.8	21.72	1.44	0.	101.6	9.02	5.25	.13
50.8	19.18	2.38	.06	101.6	6.48	5.38	.19
50.8	16.64	3.13	.19	101.6	3.94	4.88	.03
50.8	14.10	4.06	.19	101.6	1.40	4.00	0.
50.8	11.56	5.30	.13	114.3	26.80	-.00	-.00
50.8	9.02	5.40	.31	114.3	24.26	-.00	-.00
50.8	6.48	5.81	.50	114.3	21.72	.44	0.
50.8	3.94	6.00	2.00	114.3	19.18	1.00	0.
50.8	1.40	-.00	-.00	114.3	16.64	2.00	0.
63.5	26.80	-.00	-.00	114.3	14.10	3.50	0.
63.5	24.26	-.00	-.00	114.3	11.56	4.56	0.
63.5	21.72	1.13	0.	114.3	9.02	5.13	.15
63.5	19.18	1.94	.06	114.3	6.48	5.70	.25
63.5	16.64	2.50	.13	114.3	3.94	5.19	.06
63.5	14.10	3.56	.19	114.3	1.40	4.81	.06
63.5	11.56	4.81	.06	127.0	26.80	-.00	-.00
63.5	9.02	5.20	.15	127.0	24.26	-.00	-.00
63.5	6.48	6.25	.50	127.0	21.72	.25	0.
63.5	3.94	5.81	.80	127.0	19.18	.69	0.
63.5	1.40	-.00	-.00	127.0	16.64	1.50	0.
76.2	26.80	-.00	-.00	127.0	14.10	3.13	0.
76.2	24.26	-.00	-.00	127.0	11.56	4.53	.10
76.2	21.72	.90	0.	127.0	9.02	5.38	.22
76.2	19.18	1.75	0.	127.0	6.48	5.81	.27
76.2	16.64	2.38	0.	127.0	3.94	5.38	.19

TABLE D-1 (Continued)

Z(I)	R(J)	NOX	NO
127.0	1.40	5.00	.10
139.7	26.80	-.00	-.00
139.7	24.26	-.00	-.00
139.7	21.72	-.00	-.00
139.7	19.18	.15	0.
139.7	16.64	.56	0.
139.7	14.10	1.75	0.
139.7	11.56	3.56	.04
139.7	9.02	4.81	.31
139.7	6.48	5.50	.19
139.7	3.94	5.28	.25
139.7	1.40	4.44	.13
146.0	26.80	-.00	-.00
146.0	24.26	-.00	-.00
146.0	21.72	-.00	-.00
146.0	19.18	-.00	-.00
146.0	16.64	.19	0.
146.0	14.10	.50	0.
146.0	11.56	-.00	-.00
146.0	9.02	2.81	.03
146.0	6.48	3.75	.03
146.0	3.94	4.22	.03
146.0	1.40	3.75	.25
152.4	26.80	-.00	-.00
152.4	24.26	-.00	-.00
152.4	21.72	-.00	-.00
152.4	19.18	-.00	-.00
152.4	16.64	0.	0.
152.4	14.10	.19	0.
152.4	11.56	.28	0.
152.4	9.02	.52	0.
152.4	6.48	1.06	0.
152.4	3.94	1.63	.06
152.4	1.40	2.00	.38

TABLE D-1 (Continued)

DATA FOR CASE 3 TEMP= 600.0 EQIV= .6250 VEL=25.400

Z(I)	R(J)	NOX	NO	Z(I)	R(J)	NOX	NO
0.	26.80	6.00	.25	76.2	14.10	7.37	2.82
0.	24.26	6.00	.13	76.2	12.19	9.13	4.38
0.	21.72	7.00	1.00	76.2	9.65	10.13	4.63
0.	19.18	7.65	1.13	76.2	7.11	10.00	5.13
0.	16.64	8.30	1.63	76.2	4.57	10.30	5.88
0.	14.10	9.00	2.38	76.2	3.30	10.00	6.13
0.	12.19	10.75	3.80	88.9	26.80	-.00	-.00
0.	9.65	11.25	4.88	88.9	24.26	1.03	.25
0.	7.11	12.25	6.25	88.9	21.72	2.31	1.28
0.	4.57	12.50	6.88	88.9	19.18	3.21	.51
0.	3.30	11.75	7.38	88.9	16.64	4.87	1.41
25.4	26.80	4.75	.38	88.9	14.10	6.41	2.31
25.4	24.26	4.80	.80	88.9	12.19	7.75	1.13
25.4	21.72	5.63	1.13	88.9	9.65	9.75	4.00
25.4	19.18	7.50	1.63	88.9	7.11	10.25	4.50
25.4	16.64	8.38	2.00	88.9	4.57	10.13	4.88
25.4	14.10	9.25	2.63	88.9	3.30	9.88	4.00
25.4	12.19	11.00	4.75	101.6	26.80	-.00	-.00
25.4	9.65	11.75	5.50	101.6	24.26	.58	.12
25.4	7.11	11.38	5.88	101.6	21.72	1.41	.45
25.4	4.57	12.38	6.63	101.6	19.18	2.69	1.08
25.4	3.30	-.00	-.00	101.6	16.64	4.10	.51
50.8	26.80	-0.	-0.	101.6	14.10	5.51	.51
50.8	24.26	3.00	0.	101.6	12.19	7.25	.50
50.8	21.72	4.63	1.38	101.6	9.65	9.13	2.88
50.8	19.18	5.75	1.88	101.6	7.11	9.50	4.20
50.8	16.64	6.63	2.50	101.6	4.57	9.63	3.50
50.8	14.10	8.25	3.38	101.6	3.30	9.38	2.75
50.8	12.19	10.38	4.50	114.3	26.80	-.00	-.00
50.8	9.65	11.25	6.00	114.3	24.26	-.00	-.00
50.8	7.11	11.38	6.63	114.3	21.72	.90	.13
50.8	4.57	11.38	6.25	114.3	19.18	2.18	.51
50.8	3.30	-.00	-.00	114.3	16.64	3.33	.77
63.5	26.80	-.00	-.00	114.3	14.10	5.13	.39
63.5	24.26	2.44	1.03	114.3	12.19	6.63	.13
63.5	21.72	3.08	.13	114.3	9.65	8.38	2.00
63.5	19.18	5.50	1.92	114.3	7.11	9.00	3.25
63.5	16.64	6.92	2.56	114.3	4.57	9.00	3.13
63.5	14.10	7.43	3.08	114.3	3.30	-.00	-.00
63.5	12.19	10.13	4.38	127.0	26.80	-.00	-.00
63.5	9.65	10.88	5.25	127.0	24.26	-.00	-.00
63.5	7.11	10.63	5.75	127.0	21.72	-0.	-0.
63.5	4.57	10.88	6.13	127.0	19.18	1.43	.26
63.5	3.30	-.00	-.00	127.0	16.64	3.11	.78
76.2	26.80	-.00	-.00	127.0	14.10	-0.	-0.
76.2	24.26	2.31	1.54	127.0	12.19	5.50	0.
76.2	21.72	2.69	.77	127.0	9.65	8.00	.88
76.2	19.18	4.23	1.15	127.0	7.11	9.38	3.25
76.2	16.64	6.54	2.44	127.0	4.57	10.13	4.25

TABLE D-1 (Continued)

Z(I)	R(J)	NOX	NO
127.0	3.30	-.00	-.00
139.7	26.80	-.00	-.00
139.7	24.26	-.00	-.00
139.7	21.72	-.00	-.00
139.7	19.18	-0.	-0.
139.7	16.64	-0.	-0.
139.7	14.10	-0.	-0.
139.7	12.19	3.13	0.
139.7	9.65	5.63	0.
139.7	7.11	8.00	.63
139.7	4.57	9.00	3.00
139.7	3.30	-.00	-.00
146.0	26.80	-.00	-.00
146.0	24.26	-.00	-.00
146.0	21.72	-.00	-.00
146.0	19.18	.78	.13
146.0	16.64	1.92	.52
146.0	14.10	-0.	-0.
146.0	12.19	-.00	-.00
146.0	9.65	2.25	0.
146.0	7.11	4.50	0.
146.0	4.57	6.00	.38
146.0	3.30	-.00	-.00
152.4	26.80	-.00	-.00
152.4	24.26	-.00	-.00
152.4	21.72	-.00	-.00
152.4	19.18	.52	0.
152.4	16.64	1.23	.39
152.4	14.10	-.00	-.00
152.4	12.19	.25	0.
152.4	9.65	.63	0.
152.4	7.11	1.38	0.
152.4	4.57	2.25	.13
152.4	3.30	-.00	-.00

TABLE D-1 (Continued)

DATA FOR CASE 4 TEMP= 600.0 EQIV= .6250 VEL=13.590

Z(I)	R(J)	NOX	NO	Z(I)	R(J)	NOX	NO
0.	24.26	3.44	.65	76.2	3.94	9.13	2.50
0.	21.72	4.75	.25	88.9	24.26	-.00	-.00
0.	19.18	-.00	-.00	88.9	21.72	.25	0.
0.	16.64	-.00	-.00	88.9	19.18	.88	.05
0.	16.00	7.75	.13	88.9	16.64	2.31	.38
0.	13.46	8.81	.90	88.9	16.00	-.00	-.00
0.	10.92	10.12	1.60	88.9	13.46	3.88	0.
0.	8.38	10.75	2.13	88.9	10.92	5.63	0.
0.	5.84	11.35	2.75	88.9	8.38	7.50	.13
0.	3.94	10.25	4.50	88.9	5.84	8.88	2.13
25.4	24.26	1.75	.13	88.9	3.94	8.25	2.00
25.4	21.72	2.63	.54	101.6	24.26	-.00	-.00
25.4	19.18	5.38	.13	101.6	21.72	-.00	-.00
25.4	16.64	6.38	1.00	101.6	19.18	.63	0.
25.4	16.00	-.00	-.00	101.6	16.64	1.75	.13
25.4	13.46	8.50	.35	101.6	16.00	-.00	-.00
25.4	10.92	9.25	1.63	101.6	13.46	3.50	0.
25.4	8.38	9.63	2.25	101.6	10.92	5.38	0.
25.4	5.84	11.00	3.13	101.6	8.38	6.88	0.
25.4	3.94	10.40	4.25	101.6	5.84	8.38	1.50
50.8	24.26	.75	.06	101.6	3.94	8.38	1.00
50.8	21.72	1.40	.08	114.3	24.26	-.00	-.00
50.8	19.18	2.94	.70	114.3	21.72	-.00	-.00
50.8	16.64	4.81	.25	114.3	19.18	.31	0.
50.8	16.00	-.00	-.00	114.3	16.64	1.12	0.
50.8	13.46	6.75	0.	114.3	16.00	-.00	-.00
50.8	10.92	7.75	.25	114.3	13.46	2.75	0.
50.8	8.38	9.13	2.13	114.3	10.92	5.00	0.
50.8	5.84	10.13	3.25	114.3	8.38	6.50	0.
50.8	3.94	9.63	2.75	114.3	5.84	7.38	.75
63.5	24.26	.31	0.	114.3	3.94	8.13	1.50
63.5	21.72	.65	.06	127.0	24.26	-.00	-.00
63.5	19.18	1.50	.19	127.0	21.72	-.00	-.00
63.5	16.64	3.25	.69	127.0	19.18	-.00	-.00
63.5	16.00	-.00	-.00	127.0	16.64	-.00	-.00
63.5	13.46	5.88	0.	127.0	16.00	-.00	-.00
63.5	10.92	7.50	0.	127.0	13.46	.75	0.
63.5	8.38	8.20	1.25	127.0	10.92	1.80	0.
63.5	5.84	8.75	1.63	127.0	8.38	4.00	0.
63.5	3.94	9.13	1.50	127.0	5.84	5.50	0.
76.2	24.26	-.00	-.00	127.0	3.94	6.38	0.
76.2	21.72	.50	.03	133.3	24.26	-.00	-.00
76.2	19.18	1.25	.13	133.3	21.72	-.00	-.00
76.2	16.64	2.19	.38	133.3	19.18	-.00	-.00
76.2	16.00	-.00	-.00	133.3	16.64	-.00	-.00
76.2	13.46	4.88	0.	133.3	16.00	-.00	-.00
76.2	10.92	6.75	0.	133.3	13.46	-.00	-.00
76.2	8.38	7.75	.50	133.3	10.92	.38	0.
76.2	5.84	8.50	1.63	133.3	8.38	.88	0.

TABLE D-1 (Continued)

Z(I)	R(J)	NOX	NO
133.3	5.84	1.75	0.
133.3	3.94	2.63	0.
139.7	24.26	-.00	-.00
139.7	21.72	-.00	-.00
139.7	19.18	-.00	-.00
139.7	16.64	-.00	-.00
139.7	16.00	-.00	-.00
139.7	13.46	-.00	-.00
139.7	10.92	-.00	-.00
139.7	8.38	-.00	-.00
139.7	5.84	.50	0.
139.7	3.94	.25	0.

TABLE D-1 (Continued)

DATA FOR CASE 5 TEMP= 600.0 EQIV= .5500 VEL= 7.240

Z(I)	R(J)	NOX	NO	Z(I)	R(J)	NOX	NO
0.	26.80	2.38	.10	76.2	24.26	.63	.06
0.	24.26	2.63	.22	76.2	21.72	1.15	.20
0.	21.72	3.00	.22	76.2	19.18	1.75	.47
0.	19.18	3.63	.15	76.2	16.64	2.35	.47
0.	16.64	3.88	.13	76.2	14.10	3.00	.19
0.	14.10	-.00	-.00	76.2	13.46	-.00	-.00
0.	13.46	4.63	0.	76.2	10.92	3.94	0.
0.	10.92	4.94	.06	76.2	8.38	4.25	.13
0.	8.38	5.00	.20	76.2	5.84	4.56	.44
0.	5.84	5.50	.44	76.2	3.94	4.81	.63
0.	3.94	5.13	1.75	76.2	1.40	2.88	0.
0.	1.40	-.00	-.00	88.9	26.80	-.00	-.00
25.4	26.80	1.88	.10	88.9	24.26	.44	.04
25.4	24.26	2.20	.30	88.9	21.72	.81	.11
25.4	21.72	2.63	.44	88.9	19.18	1.44	.25
25.4	19.18	2.88	.25	88.9	16.64	2.06	.44
25.4	16.64	3.31	.13	88.9	14.10	2.63	.25
25.4	14.10	4.06	.30	88.9	13.46	2.88	0.
25.4	13.46	-.00	-.00	88.9	10.92	3.50	0.
25.4	10.92	-.00	-.00	88.9	8.38	4.13	.31
25.4	8.38	4.94	.06	88.9	5.84	4.25	.56
25.4	5.84	4.94	.19	88.9	3.94	4.10	.25
25.4	3.94	5.00	1.56	88.9	1.40	2.97	0.
25.4	1.40	-.00	-.00	101.6	26.80	-.00	-.00
50.8	26.80	1.25	.25	101.6	24.26	-.00	-.00
50.8	24.26	1.56	.44	101.6	21.72	.63	.04
50.8	21.72	2.00	.60	101.6	19.18	1.13	.07
50.8	19.18	2.38	.50	101.6	16.64	2.15	.31
50.8	16.64	3.19	.10	101.6	14.10	2.70	.31
50.8	14.10	3.44	.15	101.6	13.46	2.94	0.
50.8	13.46	3.69	0.	101.6	10.92	3.50	0.
50.8	10.92	4.30	0.	101.6	8.38	3.75	.06
50.8	8.38	4.63	.06	101.6	5.84	4.38	.31
50.8	5.84	4.88	.20	101.6	3.94	4.06	.10
50.8	3.94	4.75	1.13	101.6	1.40	3.13	0.
50.8	1.40	-.00	-.00	114.3	26.80	-.00	-.00
63.5	26.80	-.00	-.00	114.3	24.26	-.00	-.00
63.5	24.26	1.13	.19	114.3	21.72	.50	.04
63.5	21.72	1.63	.44	114.3	19.18	.94	.06
63.5	19.18	2.13	.56	114.3	16.64	1.69	.19
63.5	16.64	2.69	.31	114.3	14.10	2.44	.30
63.5	14.10	-.00	-.00	114.3	13.46	2.50	0.
63.5	13.46	3.19	0.	114.3	10.92	3.31	0.
63.5	10.92	3.81	0.	114.3	8.38	4.06	.19
63.5	8.38	4.63	.25	114.3	5.84	4.44	.63
63.5	5.84	4.81	.38	114.3	3.94	4.19	.44
63.5	3.94	4.50	.81	114.3	1.40	3.63	.19
63.5	1.40	-.00	-.00	127.0	26.80	-.00	-.00
76.2	26.80	-.00	-.00	127.0	24.26	-.00	-.00

TABLE D-1 (Continued)

Z(I)	R(J)	NOX	NO
127.0	21.72	.35	0.
127.0	19.18	.69	.02
127.0	16.64	1.38	.10
127.0	14.10	2.38	.30
127.0	13.46	2.19	0.
127.0	10.92	3.38	0.
127.0	8.38	4.06	.15
127.0	5.84	4.00	.50
127.0	3.94	3.94	.50
127.0	1.40	3.56	.40
139.7	26.80	-.00	-.00
139.7	24.26	-.00	-.00
139.7	21.72	.19	0.
139.7	19.18	.38	0.
139.7	16.64	.88	.05
139.7	14.10	1.69	.20
139.7	13.46	1.75	0.
139.7	10.92	2.75	0.
139.7	8.38	3.38	0.
139.7	5.84	3.56	.19
139.7	3.94	4.00	.44
139.7	1.40	4.06	.50
146.0	26.80	-.00	-.00
146.0	24.26	-.00	-.00
146.0	21.72	.13	0.
146.0	19.18	.19	0.
146.0	16.64	.44	0.
146.0	14.10	1.06	.13
146.0	13.46	-.00	-.00
146.0	10.92	1.56	0.
146.0	8.38	2.68	0.
146.0	5.84	3.13	0.
146.0	3.94	3.25	0.
146.0	1.40	3.63	.10
152.4	26.80	-.00	-.00
152.4	24.26	-.00	-.00
152.4	21.72	-.00	-.00
152.4	19.18	-.00	-.00
152.4	16.64	.19	0.
152.4	14.10	.55	.06
152.4	13.46	-.00	-.00
152.4	10.92	.63	0.
152.4	8.38	1.06	0.
152.4	5.84	1.69	0.
152.4	3.94	2.38	0.
152.4	1.40	2.56	.31

TABLE D-1 (Continued)

DATA FOR CASE 6 TEMP= 600.0 EQIV= .0450 VEL=25.400

Z(I)	R(J)	NOX	NO	Z(I)	R(J)	NOX	NO
0.	26.80	.31	0.	63.5	3.30	-.00	-.00
0.	24.26	.44	0.	63.5	2.03	-.00	-.00
0.	21.72	.56	0.	63.5	1.40	-.00	-.00
0.	19.18	.69	0.	76.2	26.80	-.00	-.00
0.	16.64	.81	0.	76.2	24.26	.19	0.
0.	14.10	1.00	0.	76.2	21.72	.25	0.
0.	11.56	1.13	0.	76.2	19.18	.41	0.
0.	10.92	-.00	-.00	76.2	16.64	.56	0.
0.	8.38	1.27	0.	76.2	14.10	.69	0.
0.	5.84	1.25	0.	76.2	11.56	-0.	-0.
0.	3.30	1.15	0.	76.2	10.92	.88	0.
0.	2.03	-.00	-.00	76.2	8.38	.98	0.
0.	1.40	-.00	-.00	76.2	5.84	1.00	0.
25.4	26.80	.19	0.	76.2	3.30	1.04	0.
25.4	24.26	.31	0.	76.2	2.03	-.00	-.00
25.4	21.72	.44	0.	76.2	1.40	-.00	-.00
25.4	19.18	.63	0.	88.9	26.80	-.00	-.00
25.4	16.64	.80	0.	88.9	24.26	.13	0.
25.4	14.10	.88	0.	88.9	21.72	.19	0.
25.4	11.56	-0.	-0.	88.9	19.18	.38	0.
25.4	10.92	.94	0.	88.9	16.64	.53	0.
25.4	8.38	1.06	0.	88.9	14.10	.69	0.
25.4	5.84	1.13	0.	88.9	11.56	.81	0.
25.4	3.30	-.00	-.00	88.9	10.92	.80	0.
25.4	2.03	-.00	-.00	88.9	8.38	.94	0.
25.4	1.40	-.00	-.00	88.9	5.84	1.05	0.
50.8	26.80	-.00	-.00	88.9	3.30	1.00	.06
50.8	24.26	.28	0.	88.9	2.03	.94	.25
50.8	21.72	.35	0.	88.9	1.40	.88	.15
50.8	19.18	.50	0.	101.6	26.80	-.00	-.00
50.8	16.64	.65	0.	101.6	24.26	-.00	-.00
50.8	14.10	-0.	-0.	101.6	21.72	.19	0.
50.8	11.56	-0.	-0.	101.6	19.18	.31	0.
50.8	10.92	.81	0.	101.6	16.64	.47	0.
50.8	8.38	.91	0.	101.6	14.10	.69	0.
50.8	5.84	1.06	0.	101.6	11.56	.85	0.
50.8	3.30	-.00	-.00	101.6	10.92	.88	.05
50.8	2.03	-.00	-.00	101.6	8.38	1.00	.05
50.8	1.40	-.00	-.00	101.6	5.84	1.05	.06
63.5	26.80	-.00	-.00	101.6	3.30	1.05	.10
63.5	24.26	.19	0.	101.6	2.03	.97	.20
63.5	21.72	.31	0.	101.6	1.40	.94	.20
63.5	19.18	.47	0.	114.3	26.80	-.00	-.00
63.5	16.64	.63	0.	114.3	24.26	-.00	-.00
63.5	14.10	-0.	-0.	114.3	21.72	.13	0.
63.5	11.56	.88	0.	114.3	19.18	.25	0.
63.5	10.92	-.00	-.00	114.3	16.64	.47	0.
63.5	8.38	.92	0.	114.3	14.10	.69	0.
63.5	5.84	.94	0.	114.3	11.56	.88	0.

TABLE D-1 (Continued)

Z(I)	R(J)	NOX	NO
114.3	10.92	.94	-0.
114.3	8.38	1.04	.07
114.3	5.84	1.06	.06
114.3	3.30	.95	.06
114.3	2.03	.94	.15
114.3	1.40	.94	.15

TABLE D-2 NO_x AND NO DATA

DATA FOR CASE 1 TEMP= 300.0 EQIV= .6250 VEL= 7.240

Z(I)	R(J)	H2O	O2	CO2	C3H8	N2	CO	TEMP
0.	26.80	.0161	.2122	0.	.0282	.7234	.0006	330.0
0.	24.26	.0214	.2165	.0038	.0258	.7174	.0011	450.0
0.	21.72	.0247	.1949	0.	.0257	.7447	.0016	610.0
0.	19.18	.0332	.1708	.0101	.0062	.7520	.0022	790.0
0.	16.64	.0390	.1429	.0170	.0113	.7737	.0029	1010.0
0.	14.10	.0504	.1278	.0350	.0093	.7776	.0034	1175.0
0.	13.46	.0441	.1473	.0279	.0104	.7864	-.0	-0.
0.	11.56	.0570	.1098	.0430	.0068	.7834	.0037	1290.0
0.	10.92	.0626	.0920	.0370	.0092	.7992	-.0	-0.
0.	9.02	.0719	.1210	.0491	.0105	.7474	.0036	-0.
0.	8.38	.0686	.1022	.0421	.0110	.7752	-.0	-0.
0.	6.48	.0747	.1033	.0411	.0119	.7590	.0035	1340.0
0.	5.84	.0751	.0951	.0460	.0111	.7827	-.0	-0.
0.	3.94	.0783	.1019	.0641	.0125	.7332	-.0	-0.
0.	1.40	-.0010	-.0010	-.0010	-.0010	-.0010	-.0010	-.0
25.4	26.80	.0119	.2103	.0037	.0248	.7323	.0001	-0.
25.4	24.26	.0135	.1908	.0023	.0285	.7649	.0007	360.0
25.4	21.72	.0181	.1993	.0034	.0280	.7513	.0011	475.0
25.4	19.18	.0203	.1649	.0065	.0158	.7125	.0018	650.0
25.4	16.64	.0362	.1405	.0248	.0098	.7987	.0026	850.0
25.4	14.10	.0518	.1514	.0344	.0074	.7549	.0031	1050.0
25.4	13.46	-.0010	-.0010	-.0010	-.0010	-.0010	-.0010	-.0
25.4	11.56	-.0010	-.0010	-.0010	-.0010	-.0010	.0035	-.0
25.4	10.92	.0669	.1267	.0378	.0122	.7564	-.0	-0.
25.4	9.02	-.0010	-.0010	-.0010	-.0010	-.0010	.0036	1365.0
25.4	8.38	.0711	.0997	.0539	.0170	.7584	-.0	-0.
25.4	6.48	-.0010	-.0010	-.0010	-.0010	-.0010	.0035	1375.0
25.4	5.84	.0733	.1017	.0511	.0100	.7639	-.0	-0.
25.4	3.94	.0741	.0965	.0608	.0042	.7664	.0047	-0.
25.4	1.40	-.0010	-.0010	-.0010	-.0010	-.0010	-.0010	-.0
50.8	26.80	.0146	.2018	0.	.0230	.7607	-.0	-0.
50.8	24.26	.0129	.1929	.0032	.0204	.7706	.0003	300.0
50.8	21.72	.0213	.1980	0.	.0289	.7518	.0008	400.0
50.8	19.18	.0204	.1609	.0021	.0176	.7790	.0015	560.0
50.8	16.64	.0292	.1690	.0050	.0186	.7572	.0024	775.0
50.8	14.10	-.0010	-.0010	-.0010	-.0010	-.0010	.0032	-.0
50.8	13.46	.0583	.1596	.0273	.0202	.7345	-.0	-0.
50.8	11.56	-.0010	-.0010	-.0010	-.0010	-.0010	.0037	1175.0
50.8	10.92	.0772	.1356	.0273	.0185	.7320	-.0	-0.
50.8	9.02	-.0010	-.0010	-.0010	-.0010	-.0010	.0039	1320.0
50.8	8.38	.0709	.1130	.0456	.0180	.7745	-.0	-0.
50.8	6.48	-.0010	-.0010	-.0010	-.0010	-.0010	.0037	1380.0
50.8	5.84	.0741	.0978	.0440	.0145	.7646	-.0	-0.
50.8	3.94	.0720	.0956	.0475	.0152	.7697	.0043	-0.
50.8	1.40	-.0010	-.0010	-.0010	-.0010	-.0010	-.0010	-.0
63.5	26.80	-.0010	-.0010	-.0010	-.0010	-.0010	-.0010	-.0
63.5	24.26	.0168	.1947	0.	.0264	.7702	-.0	-0.
63.5	21.72	.0210	.2079	0.	.0210	.7401	.0007	375.0
63.5	19.18	.0256	.1767	0.	.0218	.7660	.0016	510.0

TABLE D-2 (Continued)

Z(I)	R(J)	H2O	O2	CO2	C3H8	N2	CO	TEMP
63.5	16.64	.0334	.1710	.0166	.0177	.7813	.0024	710.0
63.5	14.10	-.0010	-.0010	-.0010	-.0010	-.0010	.0033	-.0
63.5	13.46	.0442	.1472	.0171	.0193	.7722	-.0	-0.
63.5	11.56	-.0010	-.0010	-.0010	-.0010	-.0010	.0039	1130.0
63.5	10.92	.0714	.1178	.0327	.0156	.7626	-.0	-0.
63.5	9.02	-.0010	-.0010	-.0010	-.0010	-.0010	.0042	1280.0
63.5	8.38	.0843	.1206	.0432	.0128	.7521	-.0	-0.
63.5	6.48	-.0010	-.0010	-.0010	-.0010	-.0010	.0039	1370.0
63.5	5.84	.0828	.1056	.0513	.0065	.6957	-.0	-0.
63.5	3.94	.0843	.0991	.0596	.0103	.7467	-.0	-0.
63.5	1.40	-.0010	-.0010	-.0010	-.0010	-.0010	-.0010	-.0
76.2	26.80	-.0010	-.0010	-.0010	-.0010	-.0010	-.0010	-.0
76.2	24.26	.0142	.2082	0.	.0230	.7546	-.0	-0.
76.2	21.72	.0182	.2118	0.	.0303	.7397	.0006	340.0
76.2	19.18	.0128	.2097	.0001	.0241	.7533	-.0	450.0
76.2	16.64	.0291	.1827	.0073	.0229	.6869	.0022	625.0
76.2	14.10	-.0010	-.0010	-.0010	-.0010	-.0010	.0033	-.0
76.2	13.46	.0411	.1516	.0274	.0128	.7670	-.0	-0.
76.2	11.56	-.0010	-.0010	-.0010	-.0010	-.0010	.0040	1100.0
76.2	10.92	.0606	.1376	.0299	.0161	.7558	-.0	-0.
76.2	9.02	-.0010	-.0010	-.0010	-.0010	-.0010	.0044	1290.0
76.2	8.38	.0645	.1182	.0502	.0162	.7508	-.0	-0.
76.2	6.48	-.0010	-.0010	-.0010	-.0010	-.0010	.0039	1425.0
76.2	5.84	.0732	.0960	.0435	.0154	.7719	-.0	-0.
76.2	3.94	.0870	.1076	.0592	.0123	.7239	.0035	-0.
76.2	1.40	.0771	.1227	.0437	.0092	.7473	-.0	-0.
88.9	26.80	-.0010	-.0010	-.0010	-.0010	-.0010	-.0010	-.0
88.9	24.26	-.0010	-.0010	-.0010	-.0010	-.0010	-.0010	-.0
88.9	21.72	-.0010	-.0010	-.0010	-.0010	-.0010	.0005	300.0
88.9	19.18	.0078	.1868	0.	.0215	.7839	.0011	410.0
88.9	16.64	.0237	.1835	.0173	.0150	.7104	.0022	580.0
88.9	14.10	-.0010	-.0010	-.0010	-.0010	-.0010	-.0010	-.0
88.9	13.46	.0499	.1591	.0220	.0187	.7503	-.0	-0.
88.9	11.56	-.0010	-.0010	-.0010	-.0010	-.0010	.0044	1115.0
88.9	10.92	-.0010	-.0010	-.0010	-.0010	-.0010	-.0010	-.0
88.9	9.02	-.0010	-.0010	-.0010	-.0010	-.0010	.0046	1300.0
88.9	8.38	.0693	.1258	.0430	.0102	.7326	-.0	-0.
88.9	6.48	-.0010	-.0010	-.0010	-.0010	-.0010	.0040	1435.0
88.9	5.84	-.0010	-.0010	-.0010	-.0010	-.0010	-.0010	-.0
88.9	3.94	.0840	.0802	.0528	.0095	.7735	.0047	-0.
88.9	1.40	.0546	.1047	.0420	.0109	.7879	.0123	-0.
101.6	26.80	-.0010	-.0010	-.0010	-.0010	-.0010	-.0010	-.0
101.6	24.26	-.0010	-.0010	-.0010	-.0010	-.0010	-.0010	-.0
101.6	21.72	-.0010	-.0010	-.0010	-.0010	-.0010	.0003	280.0
101.6	19.18	.0158	.2127	0.	.0190	.7825	.0009	360.0
101.6	16.64	.0189	.1932	.0078	.0227	.7675	.0020	540.0
101.6	14.10	-.0010	-.0010	-.0010	-.0010	-.0010	.0035	-.0
101.6	13.46	.0504	.1598	.0294	.0167	.7336	-.0	-0.
101.6	11.56	-.0010	-.0010	-.0010	-.0010	-.0010	.0046	1140.0

TABLE D-2 (Continued)

Z(I)	R(J)	H2O	O2	CO2	C3H8	N2	CO	TEMP
101.6	10.92	.0638	.1292	.0543	.0076	.7411	-.0	-0.
101.6	9.02	-.0010	-.0010	-.0010	-.0010	-.0010	.0047	1320.0
101.6	8.38	.0951	.1136	.0479	.0174	.7260	-.0	-0.
101.6	6.48	-.0010	-.0010	-.0010	-.0010	-.0010	.0047	1460.0
101.6	5.84	.0835	.0875	.0468	.0117	.7705	-.0	-0.
101.6	3.94	.0905	.0848	.0509	.0037	.7451	.0054	-0.
101.6	1.40	.0770	.1051	.0481	.0013	.7586	.0144	-0.
114.3	26.80	-.0010	-.0010	-.0010	-.0010	-.0010	-.0010	-.0
114.3	24.26	-.0010	-.0010	-.0010	-.0010	-.0010	-.0010	-.0
114.3	21.72	.0149	.1934	0.	.0270	.7647	-.0	295.0
114.3	19.18	.0196	.1908	.0008	.0241	.7616	.0007	325.0
114.3	16.64	.0190	.2068	0.	.0257	.7315	.0017	500.0
114.3	14.10	-.0010	-.0010	-.0010	-.0010	-.0010	.0033	-.0
114.3	13.46	-.0010	-.0010	-.0010	-.0010	-.0010	-.0010	-.0
114.3	11.56	-.0010	-.0010	-.0010	-.0010	-.0010	.0046	1150.0
114.3	10.92	.0652	.1314	.0525	.0044	.7108	-.0	-0.
114.3	9.02	-.0010	-.0010	-.0010	-.0010	-.0010	.0046	1375.0
114.3	8.38	.0863	.1009	.0595	.0076	.7456	-.0	-0.
114.3	6.48	-.0010	-.0010	-.0010	-.0010	-.0010	.0036	1475.0
114.3	5.84	.0880	.0101	.0537	.0080	.7813	-.0	-0.
114.3	3.94	.0859	.0991	.0518	.0090	.7382	.0039	-0.
114.3	1.40	.0874	.0814	.0601	.0098	.7513	.0066	-0.
127.0	26.80	-.0010	-.0010	-.0010	-.0010	-.0010	-.0010	-.0
127.0	24.26	-.0010	-.0010	-.0010	-.0010	-.0010	-.0010	-.0
127.0	21.72	.0118	.1865	0.	.0267	.7751	-.0	-0.
127.0	19.18	.0069	.1950	0.	.0271	.7710	-.0	300.0
127.0	16.64	.0109	.1953	.0001	.0249	.7888	.0009	375.0
127.0	14.10	-.0010	-.0010	-.0010	-.0010	-.0010	.0019	620.0
127.0	13.46	.0543	.1421	.0162	.0200	.7674	-.0	-0.
127.0	11.56	-.0010	-.0010	-.0010	-.0010	-.0010	.0032	-.0
127.0	10.92	.0656	.1316	.0415	.0044	.7569	-.0	-0.
127.0	9.02	-.0010	-.0010	-.0010	-.0010	-.0010	.0034	1340.0
127.0	8.38	.0802	.0909	.0527	.0021	.7571	-.0	-0.
127.0	6.48	-.0010	-.0010	-.0010	-.0010	-.0010	.0026	1470.0
127.0	5.84	.0991	.0724	.0733	.0001	.7552	-.0	-0.
127.0	3.94	.0764	.0803	.0729	.0010	.7814	.0021	-0.
127.0	1.40	.0951	.0823	.0701	.0012	.7512	.0026	-0.
139.7	26.80	-.0010	-.0010	-.0010	-.0010	-.0010	-.0010	-.0
139.7	24.26	-.0010	-.0010	-.0010	-.0010	-.0010	-.0010	-.0
139.7	21.72	-.0010	-.0010	-.0010	-.0010	-.0010	-.0010	-.0
139.7	19.18	-.0010	-.0010	-.0010	-.0010	-.0010	.0001	-.0
139.7	16.64	.0105	.2110	0.	.0257	.7528	.0001	-0.
139.7	14.10	-.0010	-.0010	-.0010	-.0010	-.0010	.0003	280.0
139.7	13.46	.0216	.1952	.0030	.0240	.7561	-.0	-0.
139.7	11.56	-.0010	-.0010	-.0010	-.0010	-.0010	-.0010	375.0
139.7	10.92	.0290	.1219	.0041	.0235	.7715	-.0	-0.
139.7	9.02	-.0010	-.0010	-.0010	-.0010	-.0010	.0011	600.0
139.7	8.38	.0355	.1501	.0234	.0121	.7599	-.0	-0.
139.7	6.48	-.0010	-.0010	-.0010	-.0010	-.0010	.0014	895.0

TABLE D-2 (Continued)

Z(I)	R(J)	H2O	O2	CO2	C3H8	N2	CO	TEMP
139.7	5.84	.0591	.1294	.0498	.0096	.7520	-.0	-0.
139.7	3.94	.0696	.1025	.0505	.0130	.7644	.0017	-0.
139.7	1.40	.0724	.1013	.0513	.0098	.7652	.0019	-0.
146.0	26.80	-.0010	-.0010	-.0010	-.0010	-.0010	-.0010	-.0
146.0	24.26	-.0010	-.0010	-.0010	-.0010	-.0010	-.0010	-.0
146.0	21.72	-.0010	-.0010	-.0010	-.0010	-.0010	-.0010	-.0
146.0	19.18	-.0010	-.0010	-.0010	-.0010	-.0010	-.0010	-.0
146.0	16.64	-.0010	-.0010	-.0010	-.0010	-.0010	-.0010	-.0
146.0	14.10	-.0010	-.0010	-.0010	-.0010	-.0010	-.0010	-.0
146.0	13.46	-.0010	-.0010	-.0010	-.0010	-.0010	-.0010	-.0
146.0	11.56	-.0010	-.0010	-.0010	-.0010	-.0010	-.0010	-.0
146.0	10.92	-.0010	-.0010	-.0010	-.0010	-.0010	-.0010	-.0
146.0	9.02	-.0010	-.0010	-.0010	-.0010	-.0010	-.0010	280.0
146.0	8.38	.0158	.2096	0.	.0234	.7713	-.0	-0.
146.0	6.48	-.0010	-.0010	-.0010	-.0010	-.0010	-.0010	325.0
146.0	5.84	.0128	.1937	.0023	.0258	.7655	-.0	-0.
146.0	3.94	.0211	.1711	.0077	.0178	.8023	.0003	-0.
146.0	1.40	.0341	.1639	.0180	.0155	.7135	.0004	-0.
152.4	26.80	-.0010	-.0010	-.0010	-.0010	-.0010	-.0010	-.0
152.4	24.26	-.0010	-.0010	-.0010	-.0010	-.0010	-.0010	-.0
152.4	21.72	-.0010	-.0010	-.0010	-.0010	-.0010	-.0010	-.0
152.4	19.18	-.0010	-.0010	-.0010	-.0010	-.0010	-.0010	-.0
152.4	16.64	-.0010	-.0010	-.0010	-.0010	-.0010	-.0010	-.0
152.4	14.10	-.0010	-.0010	-.0010	-.0010	-.0010	-.0010	-.0
152.4	13.46	-.0010	-.0010	-.0010	-.0010	-.0010	-.0010	-.0
152.4	11.56	-.0010	-.0010	-.0010	-.0010	-.0010	-.0010	-.0
152.4	10.92	-.0010	-.0010	-.0010	-.0010	-.0010	-.0010	-.0
152.4	9.02	-.0010	-.0010	-.0010	-.0010	-.0010	-.0010	-.0
152.4	8.38	.0149	.2085	0.	.0268	.7438	-.0	-0.
152.4	6.48	-.0010	-.0010	-.0010	-.0010	-.0010	-.0010	-.0
152.4	5.84	.0129	.2091	0.	.0241	.7940	-.0	-0.
152.4	3.94	.0090	.1922	0.	.0254	.7674	-.0	-0.
152.4	1.40	.0112	.2132	.0048	.0157	.7551	-.0	-0.

TABLE D-2 (Continued)

DATA FOR CASE 3 TEMP= 600.0 EQIV= .6250 VEL= 7.240

Z(I)	R(J)	H2O	O2	CO2	C3H8	N2	CO	TEMP
0.	26.80	.0956	.0771	.0713	.0086	.7524	.0016	-0.
0.	24.26	.0817	.0794	.0716	.0011	.7828	.0013	-0.
0.	21.72	.0743	.0763	.0749	.0023	.7903	.0013	1740.0
0.	19.18	.1011	.0724	.0801	.0028	.7396	.0011	1765.0
0.	16.64	.1003	.0806	.0742	.0031	.7628	.0008	1785.0
0.	14.10	.0973	.0848	.0718	.0025	.7358	.0005	1795.0
0.	11.56	.0872	.0755	.0713	.0001	.7659	.0003	1800.0
0.	9.02	.1060	.0828	.0800	.0004	.7309	.0003	1780.0
0.	6.48	.0949	.0949	.0767	.0009	.7326	.0002	1695.0
0.	3.94	.0954	.0706	.0803	.0010	.7437	-.0	-0.
0.	1.40	-.0010	-.0010	-.0010	-.0010	-.0010	-.0010	-.0
25.4	26.80	.1024	.0882	.0588	.0019	.7286	-.0	1570.0
25.4	24.26	.0864	.0725	.0548	.0093	.7990	.0022	1600.0
25.4	21.72	.0976	.0822	.0719	.0006	.7477	.0015	1695.0
25.4	19.18	.1017	.0933	.0723	.0012	.7226	.0009	1750.0
25.4	16.64	.1083	.0893	.0700	.0070	.7194	.0006	1785.0
25.4	14.10	.0827	.0694	.0577	.0081	.7771	.0005	1810.0
25.4	11.56	.0868	.0654	.0727	.0010	.7731	.0005	1800.0
25.4	9.02	.1071	.0808	.0789	.0010	.7321	.0004	-0.
25.4	6.48	.0849	.0689	.0634	.0090	.7837	.0003	1700.0
25.4	3.94	.0893	.0786	.0724	.0032	.7564	.0002	-0.
25.4	1.40	-.0010	-.0010	-.0010	-.0010	-.0010	-.0010	-.0
50.8	26.80	.0845	.0753	.0424	.0144	.7833	-.0	1275.0
50.8	24.26	.0916	.0829	.0478	.0087	.7689	-.0	1350.0
50.8	21.72	.0924	.0895	.0590	.0008	.7534	.0024	1575.0
50.8	19.18	.0882	.0855	.0587	.0084	.7642	.0016	1710.0
50.8	16.64	.1035	.0850	.0695	.0007	.7412	.0012	1775.0
50.8	14.10	.0826	.0751	.0692	.0034	.7696	.0008	-0.
50.8	11.56	.0994	.0815	.0675	.0005	.7510	.0005	1800.0
50.8	9.02	.0926	.0757	.0727	.0007	.7634	.0005	1780.0
50.8	6.48	.0859	.0868	.0659	.0017	.7598	.0003	1680.0
50.8	3.94	.0897	.0706	.0605	.0010	.7782	.0002	-0.
50.8	1.40	-.0010	-.0010	-.0010	-.0010	-.0010	-.0010	-.0
63.5	26.80	-.0010	-.0010	-.0010	-.0010	-.0010	-.0010	1110.0
63.5	24.26	.0914	.0908	.0492	.0010	.7676	.0048	1180.0
63.5	21.72	.0836	.0803	.0543	.0107	.7771	.0029	1445.0
63.5	19.18	.0887	.0738	.0563	.0069	.7863	-.0	-0.
63.5	16.64	.0954	.0843	.0768	.0097	.7118	.0012	1725.0
63.5	14.10	.0969	.0924	.0704	.0006	.7167	.0008	1790.0
63.5	11.56	.0953	.0831	.0586	.0090	.7341	.0005	1790.0
63.5	9.02	.0933	.0954	.0642	.0083	.7388	.0005	1785.0
63.5	6.48	.0905	.0844	.0653	.0040	.7558	.0004	1775.0
63.5	3.94	.0793	.0816	.0709	.0001	.7682	.0003	-0.
63.5	1.40	-.0010	-.0010	-.0010	-.0010	-.0010	-.0010	-.0
76.2	26.80	-.0010	-.0010	-.0010	-.0010	-.0010	-.0010	950.0
76.2	24.26	.0708	.1413	.0175	.0152	.7553	.0094	-0.
76.2	21.72	.0990	.0876	.0519	.0035	.7580	.0044	1320.0
76.2	19.18	.0910	.0807	.0554	.0090	.7639	.0023	1560.0
76.2	16.64	.0895	.0898	.0636	.0051	.7520	.0016	1700.0

TABLE D-2 (Continued)

Z(I)	R(J)	H2O	O2	CO2	C3H8	N2	CO	TEMP
76.2	14.10	.0945	.0842	.0630	.0066	.7447	-.0	1775.0
76.2	11.56	.0877	.0803	.0636	.0006	.7778	.0008	1780.0
76.2	9.02	.0678	.0779	.0515	.0015	.8213	.0005	1775.0
76.2	6.48	.0950	.0817	.0731	.0006	.6786	.0005	1770.0
76.2	3.94	.0935	.0772	.0698	.0014	.7580	.0005	-0.
76.2	1.40	-.0010	-.0010	-.0010	-.0010	-.0010	-.0010	-.0
88.9	26.80	-.0010	-.0010	-.0010	-.0010	-.0010	0.	810.0
88.9	24.26	.0585	.1979	.0140	.0143	.7153	.0200	860.0
88.9	21.72	.0867	.1063	.0358	.0016	.7616	.0087	1150.0
88.9	19.18	.0917	.0872	.0466	.0186	.7658	.0032	1440.0
88.9	16.64	.1098	.0943	.0675	.0043	.7241	.0017	1650.0
88.9	14.10	.0988	.0833	.0697	.0070	.7411	.0011	1760.0
88.9	11.56	.0914	.0786	.0631	.0128	.7851	-.0	1775.0
88.9	9.02	.0971	.0804	.0703	.0012	.7370	.0005	-0.
88.9	6.48	.0967	.0856	.0719	.0006	.7392	.0004	1750.0
88.9	3.94	.0954	.0909	.0627	.0045	.7536	-.0	-0.
88.9	1.40	.0981	.0880	.0556	.0083	.7500	.0020	-0.
101.6	26.80	-.0010	-.0010	-.0010	-.0010	-.0010	-.0010	710.0
101.6	24.26	.0294	.2109	.0100	.0351	.6866	.0030	770.0
101.6	21.72	.0438	.1787	.0263	.0020	.7492	.0190	1010.0
101.6	19.18	.0638	.1049	.0394	.0073	.7847	.0050	1360.0
101.6	16.64	.0898	.0872	.0612	.0008	.7611	.0019	1660.0
101.6	14.10	.0948	.0845	.0667	.0087	.7413	.0010	-0.
101.6	11.56	.0859	.0830	.0546	.0013	.7802	.0007	1745.0
101.6	9.02	.1010	.0667	.0669	.0033	.7421	.0003	1740.0
101.6	6.48	.0876	.0698	.0599	.0066	.7900	.0006	1730.0
101.6	3.94	.0927	.0678	.0547	.0062	.7687	.0012	-0.
101.6	1.40	.0925	.0769	.0562	.0070	.7574	.0020	-0.
114.3	26.80	-.0010	-.0010	-.0010	-.0010	-.0010	-.0010	640.0
114.3	24.26	-.0010	-.0010	-.0010	-.0010	-.0010	-.0010	680.0
114.3	21.72	.0310	.1860	.0116	.0215	.7499	.0028	940.0
114.3	19.18	.0573	.1222	.0186	.0136	.7683	.0150	-0.
114.3	16.64	.0799	.0850	.0576	.0071	.7704	.0027	1580.0
114.3	14.10	.1005	.0858	.0566	.0142	.7217	-.0	1720.0
114.3	11.56	.0872	.0824	.0494	.0115	.7696	.0008	1725.0
114.3	9.02	.0892	.0843	.0488	.0103	.7574	-.0	1720.0
114.3	6.48	.0832	.0718	.0654	.0048	.7848	-.0	1720.0
114.3	3.94	.0884	.0796	.0579	.0066	.7675	.0008	1710.0
114.3	1.40	.0964	.0757	.0579	.0126	.7574	.0011	-0.
127.0	26.80	-.0010	-.0010	-.0010	-.0010	-.0010	-.0010	-.0
127.0	24.26	-.0010	-.0010	-.0010	-.0010	-.0010	-.0010	620.0
127.0	21.72	.0225	.1907	.0041	.0221	.7906	-.0	-0.
127.0	19.18	.0386	.1619	.0144	.0197	.7954	.0230	1075.0
127.0	16.64	.0556	.1265	.0290	.0123	.7647	.0065	1450.0
127.0	14.10	.0849	.0962	.0481	.0153	.7457	-.0	1660.0
127.0	11.56	.0743	.0809	.0516	.0117	.7796	.0010	1700.0
127.0	9.02	.0826	.0682	.0538	.0097	.7857	-.0	1720.0
127.0	6.48	.0914	.0792	.0474	.0082	.7559	.0005	1720.0
127.0	3.94	.0905	.0651	.0588	.0085	.7691	.0003	-0.

TABLE D-2 (Continued)

Z(I)	R(J)	H2O	O2	CO2	C3H8	N2	CO	TEMP
127.0	1.40	.0921	.0703	.0587	.0069	.7719	.0005	-0.
139.7	26.80	-.0010	-.0010	-.0010	-.0010	-.0010	-.0010	-.0
139.7	24.26	-.0010	-.0010	-.0010	-.0010	-.0010	-.0010	-.0
139.7	21.72	-.0010	-.0010	-.0010	-.0010	-.0010	-.0010	645.0
139.7	19.18	.0272	.2000	0.	.0246	.7482	.0018	830.0
139.7	16.64	.0444	.1668	.0189	.0022	.7611	.0060	1135.0
139.7	14.10	.0629	.1342	.0408	.0118	.7910	.0065	1440.0
139.7	11.56	.0750	.1152	.0372	.0110	.7552	.0027	1600.0
139.7	9.02	.0964	.0998	.0373	.0174	.7393	-.0	1670.0
139.7	6.48	.0916	.0922	.0420	.0186	.7457	.0016	1680.0
139.7	3.94	.0970	.0868	.0551	.0104	.7407	.0005	-0.
139.7	1.40	.1138	.0855	.0546	.0161	.7201	.0010	-0.
146.0	26.80	-.0010	-.0010	-.0010	-.0010	-.0010	-.0010	-.0
146.0	24.26	-.0010	-.0010	-.0010	-.0010	-.0010	-.0010	-.0
146.0	21.72	-.0010	-.0010	-.0010	-.0010	-.0010	-.0010	-.0
146.0	19.18	-.0010	-.0010	-.0010	-.0010	-.0010	-.0010	-.0
146.0	16.64	-.0010	-.0010	-.0010	-.0010	-.0010	-.0010	-.0
146.0	14.10	.0418	.1896	.0200	.0219	.7428	-.0	975.0
146.0	11.56	.0374	.1652	.0132	.0156	.7586	.0250	1180.0
146.0	9.02	.0524	.1342	.0242	.0148	.7743	.0021	1375.0
146.0	6.48	.0666	.1242	.0480	.0096	.7416	.0028	1540.0
146.0	3.94	.0831	.1148	.0451	.0117	.7452	.0090	-0.
146.0	1.40	.0939	.0947	.0356	.0246	.7512	.0030	-0.
152.4	26.80	-.0010	-.0010	-.0010	-.0010	-.0010	-.0010	-.0
152.4	24.26	-.0010	-.0010	-.0010	-.0010	-.0010	-.0010	-.0
152.4	21.72	-.0010	-.0010	-.0010	-.0010	-.0010	-.0010	-.0
152.4	19.18	-.0010	-.0010	-.0010	-.0010	-.0010	-.0010	590.0
152.4	16.64	-.0010	-.0010	-.0010	-.0010	-.0010	-.0010	620.0
152.4	14.10	-.0010	-.0010	-.0010	-.0010	-.0010	-.0010	690.0
152.4	11.56	.0155	.1720	.0021	.0230	.7874	-.0	790.0
152.4	9.02	.0201	.1907	.0035	.0251	.7576	.0005	930.0
152.4	6.48	.0237	.1821	.0074	.0276	.7592	.0008	1075.0
152.4	3.94	.0322	.1616	.0204	.0124	.7735	.0015	-0.
152.4	1.40	.0570	.1987	.0284	.0201	.7157	.0243	-0.

TABLE D-2 (Continued)

DATA FOR CASE 6 TEMP= 600.0 EQIV= .0450 VEL= 7.240

Z(I)	R(J)	H2O	O2	CO2	C3H8	N2	CO	TEMP
0.	26.80	.0259	.2000	.0095	.0175	.7471	.0025	970.0
0.	24.26	.0351	.1906	.0178	.0158	.7407	.0024	1120.0
0.	21.72	.0413	.1725	.0211	.0156	.7455	.0023	-0.
0.	19.18	.0546	.1673	.0238	.0114	.7430	-.0	1275.0
0.	16.64	.0575	.1320	.0268	.0093	.7845	.0024	1330.0
0.	14.10	.0654	.1397	.0355	.0063	.7530	-.0	1420.0
0.	11.56	.0657	.1349	.0550	.0002	.7502	.0025	1450.0
0.	9.02	.0681	.1327	.0587	0.	.7045	.0020	1460.0
0.	6.48	.0653	.1284	.0593	.0001	.7298	.0020	1410.0
0.	3.94	.0757	.1085	.0 57	.0005	.7076	.0026	-0.
0.	1.40	-.0010	-.0010	-.0010	-.0010	-.0010	-.0010	-.0
25.4	26.80	.0177	.1907	.0036	.0223	.7752	-.0	-0.
25.4	24.26	.0337	.1980	.0128	.0210	.7345	.0021	1000.0
25.4	21.72	.0305	.1740	.0178	.0170	.7607	.0022	1120.0
25.4	19.18	.0535	.1747	.0212	.0076	.7330	.0025	1200.0
25.4	16.64	.0544	.1497	.0253	.0161	.7545	.0027	1300.0
25.4	14.10	.0533	.1521	.0384	.0070	.7392	-.0	1350.0
25.4	11.56	.0621	.1512	.0580	.0057	.7079	.0028	1410.0
25.4	9.02	.0615	.1468	.0526	0.	.7191	.0023	1420.0
25.4	6.48	.0691	.1207	.0613	.0006	.7484	.0019	-0.
25.4	3.94	.0601	.1167	.0552	.0007	.7673	.0028	-0.
25.4	1.40	-.0010	-.0010	-.0010	-.0010	-.0010	-.0010	-.0
50.8	26.80	-.0010	-.0010	-.0010	-.0010	-.0010	-.0010	-.0
50.8	24.26	.0140	.1888	.0041	.0154	.7776	-.0	910.0
50.8	21.72	.0287	.1903	.0140	.0178	.7492	.0020	1025.0
50.8	19.18	.0320	.1775	.0186	.0130	.7789	-.0	1125.0
50.8	16.64	.0508	.1585	.0212	.0122	.7213	-.0	1240.0
50.8	14.10	.0503	.1457	.0390	.0100	.7551	-.0	1325.0
50.8	11.56	.0553	.1512	.0437	.0113	.7185	.0033	-0.
50.8	9.02	.0588	.1407	.0578	.0096	.7301	.0025	1425.0
50.8	6.48	.0593	.1251	.0642	.0004	.7510	.0023	1420.0
50.8	3.94	.0766	.1267	.0641	.0016	.7011	.0030	-0.
50.8	1.40	-.0010	-.0010	-.0010	-.0010	-.0010	-.0010	-.0
63.5	26.80	-.0010	-.0010	-.0010	-.0010	-.0010	-.0010	-.0
63.5	24.26	.0236	.1889	.0024	.0187	.7663	.0015	875.0
63.5	21.72	.0302	.1866	.0052	.0155	.7625	.0020	975.0
63.5	19.18	.0366	.1795	.0130	.0115	.7513	.0024	1075.0
63.5	16.64	.0363	.1496	.0235	.0105	.7801	.0029	-0.
63.5	14.10	.0415	.1605	.0289	.0109	.7664	-.0	1280.0
63.5	11.56	.0548	.1318	.0402	.0084	.7649	.0034	1360.0
63.5	9.02	.0615	.1379	.0535	0.	.6871	.0034	1420.0
63.5	6.48	.0698	.1311	.0488	.0044	.7389	.0026	1425.0
63.5	3.94	-.0010	-.0010	-.0010	-.0010	-.0010	.0027	-.0
63.5	1.40	-.0010	-.0010	-.0010	-.0010	-.0010	-.0010	-.0
76.2	26.80	-.0010	-.0010	-.0010	-.0010	-.0010	-.0010	-.0
76.2	24.26	-.0010	-.0010	-.0010	-.0010	-.0010	-.0010	810.0
76.2	21.72	.0237	.1947	.0029	.0171	.7716	.0016	-0.
76.2	19.18	.0473	.1843	.0126	.0178	.7380	.0021	1040.0
76.2	16.64	.0441	.1658	.0262	.0148	.7091	-.0	1150.0

TABLE D-2 (Continued)

Z(I)	R(J)	H2O	O2	CO2	C3H8	N2	CO	TEMP
76.2	14.10	.0501	.1677	.0369	.0103	.7349	.0032	1270.0
76.2	11.56	.0494	.1486	.0440	.0100	.7612	.0035	1365.0
76.2	9.02	.0596	.1401	.0481	.0103	.7419	.0030	1410.0
76.2	6.48	.0640	.1383	.0568	.0004	.7316	.0027	1445.0
76.2	3.94	.0656	.1308	.0621	.0053	.7196	.0025	-0.
76.2	1.40	-.0010	-.0010	-.0010	-.0010	-.0010	-.0010	-.0
88.9	26.80	-.0010	-.0010	-.0010	-.0010	-.0010	-.0010	-.0
88.9	24.26	.0164	.2021	0.	.0199	.7815	.0009	775.0
88.9	21.72	.0221	.1949	.0020	.0180	.7751	.0014	890.0
88.9	19.18	.0348	.1956	.0044	.0247	.7405	-.0	1000.0
88.9	16.64	.0377	.1633	.0173	.0163	.7654	.0027	1130.0
88.9	14.10	.0509	.1656	.0233	.0175	.7426	.0034	1270.0
88.9	11.56	.0544	.1637	.0457	.0003	.7208	.0037	1365.0
88.9	9.02	.0571	.1357	.0446	.0036	.7530	.0031	1420.0
88.9	6.48	.0627	.1237	.0630	.0016	.7490	.0040	-0.
88.9	3.94	.0650	.1281	.0678	0.	.7390	-.0	-0.
88.9	1.40	.0531	.1517	.0478	.0000	.7414	.0063	-0.
101.6	26.80	-.0010	-.0010	-.0010	-.0010	-.0010	-.0010	-.0
101.6	24.26	-.0010	-.0010	-.0010	-.0010	-.0010	0.	740.0
101.6	21.72	.0188	.2031	.0016	.0214	.7551	.0012	840.0
101.6	19.18	.0309	.2038	.0085	.0212	.7356	.0019	950.0
101.6	16.64	.0421	.1613	.0167	.0138	.7660	-.0	1100.0
101.6	14.10	.0384	.1582	.0231	.0099	.7704	.0033	1245.0
101.6	11.56	.0589	.1385	.0511	.0105	.7433	.0036	-0.
101.6	9.02	.0671	.1336	.0443	.0074	.6996	.0033	1425.0
101.6	6.48	.0628	.1310	.0649	.0002	.7411	.0031	1440.0
101.6	3.94	.0846	.1329	.0588	0.	.7236	.0056	-0.
101.6	1.40	.0548	.1393	.0443	.0003	.7613	.0084	-0.
114.3	26.80	-.0010	-.0010	-.0010	-.0010	-.0010	-.0010	-.0
114.3	24.26	-.0010	-.0010	-.0010	-.0010	-.0010	.0053	700.0
114.3	21.72	.0215	.1955	0.	.0239	.7482	.0009	800.0
114.3	19.18	.0260	.2108	.0072	.0238	.7223	-.0	960.0
114.3	16.64	.0386	.1810	.0110	.0188	.7505	-.0	1125.0
114.3	14.10	.0530	.1642	.0144	.0176	.7507	.0033	-0.
114.3	11.56	.0656	.1585	.0583	.0067	.6789	.0037	1370.0
114.3	9.02	.0744	.1303	.0596	.0034	.7233	.0031	1430.0
114.3	6.48	.0614	.1279	.0580	.0051	.7476	.0030	1440.0
114.3	3.94	.0642	.1294	.0545	.0041	.7418	.0050	-0.
114.3	1.40	.0711	.1360	.0503	.0115	.7201	.0092	-0.
127.0	26.80	-.0010	-.0010	-.0010	-.0010	-.0010	-.0010	-.0
127.0	24.26	-.0010	-.0010	-.0010	-.0010	-.0010	-.0010	650.0
127.0	21.72	-.0010	-.0010	-.0010	-.0010	-.0010	.0008	770.0
127.0	19.18	.0299	.2035	.0014	.0217	.7435	.0150	910.0
127.0	16.64	.0350	.1827	.0033	.0154	.7417	.0022	-0.
127.0	14.10	.0510	.1540	.0197	.0207	.7746	-.0	1275.0
127.0	11.56	.0557	.1483	.0519	.0050	.7291	.0036	1400.0
127.0	9.02	.0523	.1303	.0468	.0104	.7603	.0031	1440.0
127.0	6.48	.0772	.1233	.0452	.0118	.7425	.0025	1460.0
127.0	3.94	.0744	.1265	.0609	0.	.7281	.0028	-0.

TABLE D-2 (Continued)

Z(I)	R(J)	H2O	O2	CO2	C3H8	N2	CO	TEMP
127.0	1.40	.0739	.1163	.0493	.0108	.7397	-.0	-0.
139.7	26.80	-.0010	-.0010	-.0010	-.0010	-.0010	-.0010	-.0
139.7	24.26	-.0010	-.0010	-.0010	-.0010	-.0010	-.0010	615.0
139.7	21.72	-.0010	-.0010	-.0010	-.0010	-.0010	.0049	700.0
139.7	19.18	.0175	.2044	0.	.0193	.7787	.0009	-0.
139.7	16.64	.0297	.1879	.0003	.0162	.7538	.0026	1000.0
139.7	14.10	.0481	.1693	.0088	.0188	.7531	.0024	1200.0
139.7	11.56	.0483	.1696	.0239	.0097	.7263	.0031	1330.0
139.7	9.02	.0651	.1514	.0572	.0012	.7251	.0028	1420.0
139.7	6.48	.0626	.1254	.0573	.0007	.7500	.0019	1445.0
139.7	3.94	.0711	.1045	.0587	.0006	.7579	.0015	-0.
139.7	1.40	.0781	.1216	.0535	.0064	.7312	.0017	-0.
152.4	26.80	-.0010	-.0010	-.0010	-.0010	-.0010	-.0010	-.0
152.4	24.26	-.0010	-.0010	-.0010	-.0010	-.0010	-.0010	575.0
152.4	21.72	-.0010	-.0010	-.0010	-.0010	-.0010	-.0010	-.0
152.4	19.18	-.0010	-.0010	-.0010	-.0010	-.0010	-.0010	650.0
152.4	16.64	-.0010	-.0010	-.0010	-.0010	-.0010	-.0010	750.0
152.4	14.10	-.0010	-.0010	-.0010	-.0010	-.0010	-.0010	875.0
152.4	11.56	.0269	.2144	.0116	.0232	.7038	-.0	1050.0
152.4	9.02	.0367	.1907	.0150	.0242	.7335	.0010	1175.0
152.4	6.48	.0515	.1815	.0319	.0171	.7081	.0012	1300.0
152.4	3.94	.0551	.1608	.0566	.0125	.7150	-.0	-0.
152.4	1.40	.0476	.1288	.0526	.0008	.7702	-.0	-0.
158.7	26.80	-.0010	-.0010	-.0010	-.0010	-.0010	-.0010	-.0
158.7	24.26	-.0010	-.0010	-.0010	-.0010	-.0010	-.0010	-.0
158.7	21.72	-.0010	-.0010	-.0010	-.0010	-.0010	-.0010	-.0
158.7	19.18	-.0010	-.0010	-.0010	-.0010	-.0010	-.0010	-.0
158.7	16.64	-.0010	-.0010	-.0010	-.0010	-.0010	-.0010	620.0
158.7	14.10	-.0010	-.0010	-.0010	-.0010	-.0010	-.0010	690.0
158.7	11.56	.0232	.2134	0.	.0181	.6903	-.0	785.0
158.7	9.02	.0164	.2128	.0084	.0180	.7443	0.	875.0
158.7	6.48	.0245	.2038	0.	.0169	.7248	-.0	1020.0
158.7	3.94	.0216	.1962	.0128	.0248	.7446	-.0	-0.
158.7	1.40	-.0010	-.0010	-.0010	-.0010	-.0010	-.0010	-.0

APPENDIX E

Numerical Computer Program

This appendix lists the numerical computer program used in this investigation to solve the governing differential equations for the opposed reacting jet flowfield. This program represents a modified version of the original program developed by Gosman, et al[44] and later used by Samuelsen[47]. Section E.1 defines the Fortran symbols used in the program and Section E.2 provides a complete listing of the program. The various subroutines are described in detail in the above mentioned references.

E.1. Fortran Symbols

Fortran Symbols	Meaning
A (I, J, 1 to 9), also AQ(I, J, 1 to 9)	Dependent variables
ACTE(I)	Activation energy
AGLOB(I)	See GLOB(I)
ANAME	Full names for dependent variables; for use in print-out
AQ(I, J, 1 to 13)	For convenience, some variables are assigned two variable-names, through an EQUIVALENCE statement, one of the two is AQ
AQ(I, J, 14)	Temporary storage locations
ASYMBL	Symbol array for dependent variables, e.g. STRM for stream function; for use in print-out
ATITLE	Title of problem to be input through this array
AU	The finite-difference approximation for the convection terms for the dependent variable ϕ is: ZU $\cdot$ ϕ_P-AU

BB	Coefficient in the quadratic representation of a -profile near an adiabatic boundary
BGLOB(I)	See GLOB(I)
CC	Convergence criterion
CPJ (1 to 3)	Specific heats of mixture components
CPREF	Reference specific heat
DCN, DN	Chamber dimensions
DC	Divergence driterion
DELX 1 (I)	Length of control volume in the z direction for nodes on grid-line I
DELX 2 (J)	Length of control volume in the r direction for noeds on grid-line J
G1(I,J), also AQ(I,J,10) G2(I,J), also AQ(I,J,11)	Mass velocities in directions z and r respectively
GC	Gravitational constant
GCPM	Universal gas constant
GM1E, GM1W GM2N, GM2S	Quantities used for evaluation of the convection terms
GLOB(I)	Preexponential factor in Equation 4.24; GLOB = AGLOB(I) · $10^{BGLOB(I)}$
HF	Heat of formation
IC, IN	Grid-line designations
IE	Number of partial differential equations to be solved
IN	Number of z = constant grid lines
INM	= IN - 1
IMIN(J), IMAX(J)	Respectively, value of I on Jth line at lefthand boundary and righthand boundary
INDG	Control index for geometry of flow: 1 for Cartesian coordinates, 2 for cylindrical coordinates

INDRO	Control index for density: 2 for non-uniform density, 1 for constant density
INDE(K)	Only when this index is put equal to 1 will the equation for the dependent variable having the ordering index equal to K be solved
INDZMU	Control index for viscosity: 2 for variable viscosity, 1 for constant viscosity
JN	Number of r constant grid lines
JC1, JC2, JC, JN	Grid-line designations
JJC2	JC2 + 1
JC2M	JC2 - 1
JC1M	JC1 - 1
JNM	JN - 1
KVORT	A control index used during calculation of vorticities on boundaries: when KVORT = 0, wall vorticities are not calculated when KVORT = 1, wall values calculated as well
NW	Vorticity/radius
NF	Stream function
NZML	Fuel mass fraction
NZMC Dependent-variable ordering	CO_2 mass fraction
NZMN and identifying index, respective-	NO mass fraction
NZMH ly for:	Stagnation enthalpy
NZMF	Mixture fraction
NVT	Swirl velocity
NP	Static pressure
NMAX	Maximum number of iterations to be performed
NPRIN	Results to be printed out, in display form, at intervals of NPRIN interations

NHOT	NHOT = 0, cold flow; NHOT = 1, hot flow
NPRES	NPRES = 0 static pressure not obtained; NPRES = 1 static pressure is obtained
NREAD	Number of dependent variable values to be read in from previous solution
PHIP	Primary stream equivalence ratio
PHIJ	Jet stream equivalence ratio
PR 91 to 9)	Prandtl or Schmidt numbers, i.e., $\sigma_{h,eff}$ or $\sigma_{fu,eff}$
PREF	Reference static pressure
R(J)	Value of r at the constant r grid-line J
RADC1, RADC2, RADN	Chamber radii
RO(I,J), also AQ(I,J,12)	Mixture density, ρ
ROP	Mixture density at primary or fuel inlet
ROREF	Reference density
ROJ	Mixture density at jet inlet
ROWF	Weighting factor (or under-relaxation factor) for density
RP (1 to 9)	Relaxation parameters for dependent variables
STC	Stoichiometric fuel/air ratio
SOURCE	The source term for the dependent variable Ψ is approximated by: source term = SOURCE + ZQ x ϕ_P
T(I,J)	Absolute temperature
TREF	Reference temperature
VINP	Axial velocity at primary inlet
VINJ	Axial velocity at jet inlet
X1(I)	Spatial length to grid-line I
X2(J)	Spatial length to grid-line J

ZEX	Exponential factor, Equation 4.24
ZJC	Joule's constant
AMU(I,J), also AQ(I,J,13)	Effective viscosity, μ_{eff}
ZMUK	Constant K in the effective-viscosity law
AMUREF	Reference viscosity
ZMW (1 to 3)	Molecular weights
ZU	See AU
ZQ	See SOURCE

E.2. Fortran Listing of Program OPJET

```
      BLOCK DATA
C  OPJET
      COMMON/CVP/A(33,15,9),G1(33,15),G2(33,15),RO(33,15),ZMU(33,15)
      COMMON/CGRID/IMIN(33),IMAX(33),IN,JN,INM,JNM,IE
      COMMON/CNUMBR/NW,NF,NZML,NZMH,NZMC,NZMF,NZMN,NP,NVT
      COMMON/CINDEX/INDE(9),INDG,INDRO,INDZMU
      COMMON/CCHECK/RSDU(9),RP(9),CC,DC,NMAX,NPRIN
      COMMON/CREFER/ROREF,PREF,ZMUREF,TREF,CPREF,TO
      COMMON/CCONST/PR(9),ZMW(3),CPJ(3),GCPM,GC,ZJC
      COMMON/CHEM/STC,STOX,HFP,HFCO,HFCO2,HFH2O,GLOB(3),ZEX(3)
      COMMON/CYLI/JC1,JC2,IC,RADC1,RADC2,RADN,DCN,DN,JJC2,ICM,JC2M,JC1M
      COMMON/CX1X2/X1(33),X2(15),DELX1(33),DELX2(15)
      COMMON/CVARY/NHOT,NPUNCH,NREAD,NPRES,NGRID
      COMMON/CIGNIT/ISTAG1,ISTAG2,JSTAG
      COMMON/CROWF/ROWF
      COMMON/CZMUK/ZMUK
      COMMON/CPARAM/VINJ,VINP(15),TP,PP,TJ,PJ,PHIP,PHIJ
      COMMON/CGLOB/AGLOB(3),BGLOB(3),ACTE(3)
      COMMON/CTIME/TMAX
      COMMON/CENTHL/NENTHL,NSTRM
      DIMENSION AQ(33,15,14)
      EQUIVALENCE (A(1,1,1),AQ(1,1,1))
C*********************************************************************
C
C
C*********************************************************************
      DATA NHOT,NPUNCH,NREAD,NPRES,NGRID,NENTHL,NSTRM /
     1  1,  1,  5,  0,  1,  1,  1/
C
      DATA  ISTAG1,ISTAG2,JSTAG  /
     1  11,  25,  8/
C
      DATA  ROWF,ZMUK/
     1  1.00,  0.012/
C    ACTE IS ACTIVATION ENERGY IN CAL/MOLE
      DATA  (AGLOB(I),I=1,3),(BGLOB(I),I=1,3),(ACTE(I),I=1,3)/
     1  2.6,  1.364,  3.95,
     2  2.0,  11.0,  10.0,
     3  9.195E03,  30.0E03,  68.869E03/
C
      DATA  (VINP(J),J=1,15),  PHIP,  VINJ,  PHIJ,  TJ,  TP /
     1  12*25.3,24.61,23.06,0.0,
     2  0.625,  -315.0,  0.625,  540.0,  1080.0/
C
      DATA NMAX,NPRIN,INDG,INDRO,INDZMU,TMAX  /
     1  299,  150,  2,  2,  2,  420.0/
C
      DATA  JN,  IN,  JC1,  JC2,  IC  /
     1   15,33,  3,  6,  27  /
C
      DATA ROREF,PREF,ZMUREF,TREF,CPREF,TO/
     1   0.076,      2116.0,      0.0111,      530.0,   0.294,   536.67  /
C
      DATA  (RP(L1),L1=1,9),(PR(L2),L2=1,9),(ZMW(L3),L3=1,3)/
     1  0.75,1.0, 0.2,0.2,5*1.0,9*1.0,44.09,32.0,  28.02/
C
      DATA (CPJ(L1),L1=1,3),CC,DC,GCPM,GC,ZJC/
     1   3*0.29, 0.0050, 1000.00, 1545.0, 32.2, 778.0 /
C
      DATA NW,NF,NZML,NZMC,NZMH,NZMN,NZMF,NP,NVT,IE/
     1  1,  2,  3,  4,  5,  6,  7,  8,  9,  6/
```

```
      DATA STC,HFP,HFCO,HFCO2,HFH2O/
     1  0.06409,  -1012.6,  -1696.4,  -3844.1,  -5770.8 /
      END
      PROGRAM CPJET (INPUT,PUNCH,TAPE6,OUTPUT)
      COMMON/CVP/A(33,15,9),G1(33,15),G2(33,15),RO(33,15),ZMU(33,15)
      COMMON/CPARAM/VINJ,VINP(15),TP,PP,TJ,PJ,PHIP,PHIJ
      COMMON/CX1X2/X1(33),X2(15),DELX1(33),DELX2(15)
      COMMON/CNAME/ATITLE(12),ASYMBL(12),ANAME(6,10)
      COMMON/CGRID/IMIN(33),IMAX(33),IN,JN,INM,JNM,IE
      COMMON/CINDEX/INDE(9),INDG,INDRO,INDZMU
      COMMON/CNUMBR/NW,NF,NZML,NZMH,NZMC,NZMF,NZMN,NP,NVT
      COMMON/CYLI/JC1,JC2,IC,RADC1,RADC2,RADN,DCN,DN,JJC2,ICM,JC2M,JC1M
      COMMON/CRAD/R(15)
      COMMON/CCONST/PR(9),ZMW(3),CPJ(3),GCPM,GC,ZJC
      COMMON/CREFER/ROREF,PREF,ZMUREF,TREF,CPREF,TO
      COMMON/CHEM/STC,STOX,HFP,HFCO,HFCO2,HFH2O,GLOB(3),ZEX(3)
      COMMON/CNITER/NITER
      COMMON/CVARY/NHOT,NPUNCH,NREAD,NPRES,NGRID
      COMMON/CCHECK/RSDU(9),RP(9),CC,DC,NMAX,NPRIN
      COMMON/CGLOB/AGLOB(3),BGLOB(3),ACTE(3)
      DIMENSION AQ(33,15,14)
      EQUIVALENCE (A(1,1,1),AQ(1,1,1))
C*********************************************************************
C
C
C*********************************************************************
      READ 101, ATITLE, ASYMBL, ANAME
      IF (NHOT.EQ.0)  GO TO 60
      GO TO 61
60    IE=2
      INDRO=1
      HC=0.0
61    CONTINUE
C**** COMPUTE KINETIC PARAMETERS
      DO 62 I=1,3
      GLOB(I)=AGLOB(I)*10.0**BGLOB(I)
      ZEX(I)=ACTE(I)*1.8/1.987
   62 CONTINUE
      INM=IN-1
      JNM=JN-1
      JJC2=JC2+1
      ICM=IC-1
      JC2M=JC2-1
      JC1M=JC1-1
C**** SPECIFYING INDE*S
      DO 8 L=1,IE
8     INDE(L)=1
      IE1=IE+1
      DO 9 L=IE1,9
9     INDE(L)=9
      IF  (NPRES.EQ.1)  INDE(NP)=1
      IF  (NHOT.NE.0)  GO TO 22
      DO 23 L=1,6
   23 ANAME(L,3)=ANAME(L,9)
      ASYMBL(3)=ASYMBL(9)
      GO TO 29
   22 NZ=IE+1
      DO 27 L=1,6
   27 ANAME(L,NZ)=ANAME(L,8)
      ASYMBL(NZ)=ASYMBL(8)
      IF(INDE(NP).NE.1) GO TO 29
```

```
      G2(I,J)=0.
      AO(I,J,14)=0.0
2     CONTINUE
C****READ NREAD VALUES OF DEP VAR FROM PREVIOUS SOLUTIONS
      IZ=IE
      IF  (NREAD.EQ.0)  GO TO 12
      IZ=NREAD
      READ 100,(((A(I,J,K),I=1,IN),J=1,JN),K=1,IZ)
      NITER=1
12    CONTINUE
C
      PP=PREF
      IF  (NHOT.EQ.0)  TJ=TP
      PJ=PREF
      VT=0.0
      IF(INDE(NVT).NE.1) GO TO 46
      DO 45 J=1,JC1
45    A(IC,J,NVT)=VT*R(J)
46    CONTINUE
      CALL INIT
      CALL HEADCT
      ITAB=IE+1
      IF  (NHOT.EQ.0)  ITAB=ITAB-1
      ITAB=8
      CALL SOLVCT (ITAB)
      IF(INDE(NP).EQ.1) CALL PRESCT
      IF  (NHOT.EQ.0)  GO TO 92
      GO TO 92
92    CONTINUE
      CALL PRINCT (ITAB)
      IZ=IE
      IF  (NPUNCH.EQ.0)  GO TO 16
      PUNCH 100,(((A(I,J,K),I=1,IN),J=1,JN),K=1,IZ)
16    CONTINUE
      IF(NITER.GE.NMAX) STOP
      ITAB=7
      CALL TABUCT (ITAB)
      CALL PLOTCT (ITAB)
1     CONTINUE
C CALCULATE MOLE FRACTIONS
C  SET NHOT =0 TO PREVENT T CALC IN PRINCT
      NHOT=0
      AFUI=A(1,1,NZML)
  203 DO 200 J=1,JN
  204 IL=IMIN(J)
  205 IH=IMAX(J)
  206 DO 200 I=IL,IH
  207 AFU=A(I,J,NZML)
  208 AFC=A(I,J,NZMC)
  209 AH=A(I,J,NZMH)
      ACO=1.9059*(AFUI-AFU)-0.636*AFC
      AH2O=1.634*(AFUI-AFU)+0.00151
      FOX=AFUI/(PHIP*STOX)-0.888*(AH2O-0.00151)-0.5712*ACO-0.727*AFC
  214 FN2=1.0-FOX-AFU-ACO-AH2O-AFC
  215 TEMP=TO+(AH-AFU*HFP-ACO*HFCO-AFC*HFCO2-AH2O*HFH2O)/CPREF
  216 ZMEAN=1.0/(AFU/ZMW(1)+FOX/ZMW(2)+FN2/ZMW(3)+ACO/28.011+AH2O/18.016
     1+AFC/44.011)
      A(I,J,1)=A(I,J,NZML)*ZMEAN/44.09
      A(I,J,2)=A(I,J,NZMC)*ZMEAN/44.011
      A(I,J,3)=AH2O*ZMEAN/18.016
      A(I,J,4)=ACO*ZMEAN/28.011
      A(I,J,5)=FOX*ZMEAN/32.0
```

```
      NZ=IE+2
      DO 28 L=1,6
   28 ANAME(L,NZ)=ANAME(L,9)
      ASYMBL(NZ)=ASYMBL(9)
   29 CONTINUE
      IF(NGRID.EQ.1) GO TO 21
      DO 999 I=1,IN
  999 X1(I)=0.05*FLOAT(I-1)
      DO 998 J=1,JN
  998 X2(J)=0.025*FLOAT(J-1)
      GO TO 24
   21 FCT=1.37
      X2(1)=0.0
      X2(2)=0.016/12.
      X2(3)=0.032/12.
      DO 900  J=4,JN
      IF  (J.GE.7)  FCT=1.195
  900 X2(J)=X2(J-1)+(X2(J-1)-X2(J-2))*FCT
      FCT=1.0
      X1(1)=0.0
      X1(2)=0.500/12.
      DO 910 I=3,IN
      IF (I.GE.6) FCT=1./1.36
      IF (I.GE.9) FCT=1.0
      IF (I.GE.28) FCT=1.33
      IF (I.GE.31) FCT=1.00
  910 X1(I)=X1(I-1)+(X1(I-1)-X1(I-2))*FCT
   24 DO 3 I=2,INM
    3 DELX1(I)=0.5*(X1(I+1)-X1(I-1))
      DO 4 J=2,JNM
    4 DELX2(J)=0.5*(X2(J+1)-X2(J-1))
      DO 5 J=1,JN
      IF(INDG.EQ.1) R(J)=1.0
      IF(INDG.EQ.2) R(J)=X2(J)
    5 CONTINUE
      IF(INDG.NE.1) GO TO 6
C    FOR PLANE FLOWS PUT THE CHAMBER RADII EQUAL UNITY
      RADC1=1.0
      RADC2=1.0
      RADN=1.0
      GO TO 7
C**** SPECIFYING CHAMBER DIMENSIONS
    6 RADC1=X2(JC1)
      RADC2=X2(JC2)
      RADN=X2(JN)
    7 DCN=X1(IC)
      DN=X1(IN)
C**** SPECIFYING IMIN=S AND IMAX=S
      DO 30 L=1,JN
   30 IMIN(L)=1
      DO 32 L=1,JC2M
   32 IMAX(L)=IC
      DO 33 L=JC2,JN
C****     SETTING INITIAL VALUES
   33 IMAX(L)=IN
      DO 2 J=1,JN
      DO 2 I=1,IN
      DO 13  K=1,IE
      A(I,J,K)=-1.0E-78
   13 CONTINUE
      A(I,J,NF)=-5.0E-03
      G1(I,J)=0.
```

```
      A(I,J,6)=A(I,J,NZMN)*ZMEAN/30.0
      A(I,J,7)=TEMP/1.8
  200 CONTINUE
      CALL PRINCT(8)
100   FORMAT (5(E16.9))
101   FORMAT(12A6)
      STOP
      END
      SUBROUTINE INIT
      COMMON/CPARAM/VINJ,VINP(15),TP,PP,TJ,PJ,PHIP,PHIJ
      COMMON/CVP/A(33,15,9),G1(33,15),G2(33,15),RO(33,15),ZMU(33,15)
      COMMON/CNUMBR/NW,NF,NZML,NZMH,NZMC,NZMF,NZMN,NP,NVT
      COMMON/CGRID/IMIN(33),IMAX(33),IN,JN,INM,JNM,IE
      COMMON/CHEM/STC,STOX,HFP,HFCO,HFCO2,HFH2O,GLOB(3),ZEX(3)
      COMMON/CYLI/JC1,JC2,IC,RADC1,RADC2,RADN,DCN,DN,JJC2,ICM,JC2M,JC1M
      COMMON/CCONST/PR(9),ZMW(3),CPJ(3),GCPM,GC,ZJC
      COMMON/CREFER/ROREF,PREF,ZMUREF,TREF,CPREF,TO
      COMMON/CIGNIT/ISTAG1,ISTAG2,JSTAG
      COMMON/CVARY/NHOT,NPUNCH,NREAD,NPRES,NGRID
      COMMON/CRAD/R(15)
      COMMON/CINDEX/INDE(9),INDG,INDRO,INDZMU
C*********************************************************************
C CALCULATES DENSITY, ENTHALPY, FUEL MASS FRACTION, AND MIXTURE FRACTION
C MASS FLOW RATE AT INLET PLANE OF APPROACH AND JET
C*********************************************************************
      AFUSTC=STC/(1.+STC)
      FIPSTC=AFUSTC/((28.966/(0.79*28.016))*STC)
      FOXSTC=1.0-AFUSTC-FIPSTC
      STOX=AFUSTC/FOXSTC
C
C FUEL MASS FRACTION A(I,J,NZML)
C
      XX=PHIP*STC
      AFUP=XX/(1.+XX)
      FN2=5.0*3.77*28.016/PHIP
      FN2P=FN2/(44.094+5.0*32.0/PHIP+FN2+5.0*0.012*18.016/PHIP)
      XX=PHIJ*STC
      AFUJ=XX/(1.+XX)
      FN2=5.0*3.77*28.016/PHIJ
      FN2J=FN2/(44.094+5.0*32.0/PHIJ+FN2+5.0*0.012*18.016/PHIJ)
      DO 4 J=1,JN
    4 A(1,J,NZML)=AFUP
      DO 8 J=1,JC1
    8 A(IC,J,NZML)=AFUJ
      IF(NREAD.GE.3) GO TO 22
      DO 2 J=1,JN
      III=IMIN(J)
      II2=IMAX(J)
      DO 2 I=III,II2
2     A(I,J,NZML)=AFUP
      DO 3 J=1,JC1
3     A(IC,J,NZML)=AFUJ
      IF  (NHOT.EQ.0)  GO TO 22
   75 DO 14 J=1,JSTAG
      DO 14 I=ISTAG1,ISTAG2
   14 A(I,J,NZML)=1.0E-07
22    CONTINUE
C
C DENSITY RO(I,J)
C
      HUMID=0.00151
      FH2O=HUMID
```

```
      FOXP=1.0-AFUP-FN2P-FH2O
      ZMEAN=1.0/(AFUP/ZMW(1)+FOXP/ZMW(2)+FN2P/ZMW(3)+FH2O/18.016)
      RO(1,1)=(PP*ZMEAN)/(TP*GCPM)
      DO 5 J=1,JN
      II1=IMIN(J)
      II2=IMAX(J)
      DO 5  I=II1,II2
5     RO(I,J)=RO(1,1)
      FOXJ=1.0-AFUJ-FN2J-FH2O
      ZMEAN=1.0/(AFUJ/ZMW(1)+FOXJ/ZMW(2)+FN2J/ZMW(3)+FH2O/18.016)
      RO(IC,1)=(PJ*ZMEAN)/(TJ*GCPM)
      DO 7 J=1,JC1
7     RO(IC,J)=RO(IC,1)
      IF  (NHOT.EQ.0)  GO TO 21
C
C   CO2 MASS FRACTION    A(I,J,NZMC)
C
      IF(NREAD.GE.4) GO TO 23
      DO 31 J=1,JN
      II1=IMIN(J)
      II2=IMAX(J)
      DO 31 I=II1,II2
   31 A(I,J,NZMC)=0.0
      DO 43 J=1,JSTAG
      DO 43 I=ISTAG1,ISTAG2
   43 A(I,J,NZMC)=0.115
23    CONTINUE
   70 CONTINUE
C
C ENTHALPY    A(I,J,NZMH)
C
      DO 50 J=1,JN
   50 A(1,J,NZMH)=CPREF*(TP-TO)+AFUP*HFP+FH2O*HFH2O
      DO 51 J=1,JC1
   51 A(IC,J,NZMH)=CPREF*(TJ-TO)+AFUJ*HFP+FH2O*HFH2O
      IF(NREAD.GE.5) GO TO 24
      A(1,1,NZMH)=CPREF*(TP-TO)+AFUP*HFP+FH2O*HFH2O
      DO 9 J=1,JN
      II1=IMIN(J)
      II2=IMAX(J)
      DO 9  I=II1,II2
9     A(I,J,NZMH)=A(1,1,NZMH)
      A(IC,1,NZMH)=CPREF*(TJ-TO)+AFUJ*HFP+FH2O*HFH2O
      DO 11 J=1,JC1
11    A(IC,J,NZMH)=A(IC,1,NZMH)
   24 CONTINUE
C  NO MASS FRACTION  A(I,J,NZMN)
      IF(NREAD.GE.6) GO TO 25
      DO 32 J=1,JN
      II1=IMIN(J)
      II2=IMAX(J)
      DO 32 I=II1,II2
   32 A(I,J,NZMN)=0.0
   25 CONTINUE
C
C
C MASS VELOCITY    G1(I,J)
C
21    CONTINUE
      IF(NREAD.GE.5) CALL DENSCT
      DO 17 J=1,JN
17    G1(1,J)=RO(1,J)*VINP(J)
```

```
      DO 19 J=1,JC1M
19    G1(IC,J)=PO(IC,J)*VINJ
      IF(NREAD.GE.2)  RETURN
C
C INLET VORTICITY
C
      JJ=J+1
      DO 30 J=JJ,JNM
      A(1,J,NW)=-ADF(1,J,2,15)/R(J)
30    IF  (ABS(A(I,J,NW)).LT.1.0)  A(I,J,NW)=0.0
C
C  SWIRL VELOCITY  A(I,J,NVT)
C
      RETURN
      END
      SUBROUTINE HEADCT
      COMMON/CINDEX/INDE(9),INDG,INDRO,INDZMU
      COMMON/CCHECK/RSDU(9),RP(9),CC,DC,NMAX,NPRIN
      COMMON/CREFER/ROREF,PREF,ZMUREF,TREF,CPREF,TO
      COMMON/CGRID/IMIN(33),IMAX(33),IN,JN,INM,JNM,IE
      COMMON/CCONST/PR(9),ZMW(3),CPJ(3),GCPM,GC,ZJC
      COMMON/CNAME/ATITLE(12),ASYMBL(12),ANAME(6,10)
      COMMON/CNUMBR/NW,NF,NZML,NZMH,NZMC,NZMF,NZMN,NP,NVT
      COMMON/CYLI/JC1,JC2,IC,RADC1,RADC2,RADN,DCN,DN,JJC2,ICM,JC2M,JC1M
      COMMON/CHEM/STC,STOX,HFP,HFCO,HFCO2,HFH2O,GLOB(3),ZEX(3)
      COMMON/CX1X2/X1(33),X2(15),DELX1(33),DELX2(15)
      COMMON/CPARAM/VINJ,VINP(15),TP,PP,TJ,PJ,PHIP,PHIJ
C*********************************************************************
C    **HEADING** SUBROUTINE
C    THIS SUBR. PRINTS OUT SOME OF THE INFORMATION FED IN
C*********************************************************************
      PRINT 101, ATITLE
      IF(INDG.EQ.2) GO TO 3
      PRINT 401
      GO TO 4
3     PRINT 402
4     IF(INDZMU.EQ.2) GO TO 5
      PRINT 105
      GO TO 6
5     PRINT 106
6     IF(INDRO.EQ.2) GO TO 7
      PRINT 107
      GO TO 8
7     PRINT 108
8     PRINT 109
      DO 10 K=1,IE
   10 IF(INDE(K).EQ.1) PRINT 110, (ANAME(L, K),L=1, 6)
      PRINT 111, JN, IN, (J,IMIN(J), IMAX(J), J = 1, JN)
      PRINT 201, JC1,JC2,IC,RADC1,RADC2,RADN,DCN,DN
      DO 20 I=1,IN
20    X1(I)=X1(I)*12.
      DO 21 J=1,JN
21    X2(J)=X2(J)*12.
      PRINT 202, (I,I = 1, 11)
      PRINT 203, (X1(I), I = 1, 11 )
      PRINT 204, (X2(J), J = 1, 11)
      IF (IN.GT.21) GO TO 50
      PRINT 205, (I,I=12,21)
      PRINT 203, (X1(I), I=12,21)
      GO TO 51
50    PRINT 205, (I, I = 12, 22)
      PRINT 203, (X1(I), I=12,22)
```

```
51    IF (JN.GT.11) PRINT 204, (X2(J), J = 12, JN)
      IF (IN.GT.22)  PRINT 205, (I,I=23,IN)
      IF (IN.GT.22) PRINT 203, (X1(I), I=23,IN)
      DO 22 I=1,IN
22    X1(I)=X1(I)/12.
      DO 23 J=1,JN
23    X2(J)=X2(J)/12.
      PRINT 112, (VINP(J),J=1,JN)
      PRINT 113,                          VINJ, TP, PP, TJ, PJ, ROREF, PREF,
     1 ZMUREF, TREF, CPREF, GC, ZJC
      PRINT 301,STC,STOX
      IF (INDE(NZMH).EQ.1) PRINT 114, CPJ(1)
      IM=NZMH-NZML+1
      IF (INDE(NZML).EQ.1) PRINT 115, IM, ZMW, CPJ, (PR(L),L=NZML, NZMH)
      PRINT 116, CC, DC, NMAX
      PRINT 230,GLOB(1),ZEX(1),GLOB(2),ZEX(2)
  230 FORMAT(1HO///,2X,*KINETIC REACTION RATES CONSIDERED ARE*,/,2X,*--
     1------ ----- ---------- ---*,//,10X,*RC3H8=*,E14.8,43H MC3H8**1.0*
     2MO2**0.5*MH2O**0.5*RO**2.0/EXP(,F9.3,*/T) LB/FT 3 SEC*,//,*RCO2=*,
     3E14.8,41H MCO**1.0*MO2**0.5*MH2O**0.5*RO**2.0/EXP(,F9.3,*/T) LB/FT
     4 3 SEC*)
101   FORMAT(1H1,35X,43HFINITE-DIFFERENCE  ITERATION  SOLUTION  FOR/
     236X,43H-----------------------------------------//
     320X,12A6)
105   FORMAT(1HO50X,15HFOR LAMINAR AND)
106   FORMAT(1HO50X,17HFOR TURBULENT AND)
107   FORMAT(1HO50X,20HINCOMPRESSIBLE FLOW )
108   FORMAT(1HO50X,24HNON-UNIFORM-DENSITY FLOW)
109   FORMAT(1HO//46H THE DEPENDENT VARIABLES BEING CONSIDERED ARE,/
     246H --- --------- --------- ----- ---------- --- )
110   FORMAT(1HO40X,6A6)
111   FORMAT(1HO24HTHE GEOMETRICAL DATA ARE/
     225H --- ---------- ---- ---/
     341X,44HJN,     THE NUMBER OF ROWS     (DIRECTION-2) =,I3/
     441X,44HIN,     THE NUMBER OF COLUMNS (DIRECTION-1) =,I3//
     441X,1HJ,11X,4HIMIN,10X,4HIMAX//(1H 39X,3(I2,11X)))
112   FORMAT(22H1THE PHYSICAL DATA ARE/
     222H --- -------- ---- ---/
     210X,50HVINP,    INLET VEL. OF THE PRIMARY STREAM,  FT/SEC=,15F5.1)
113   FORMAT (
     210X,50HVINJ,    INLET VEL. OF THE JET STREAM,      FT/SEC=,F10.2//
     210X,50HTP(R), PP(PSF), APPROACH INLET T AND P.....=,2F10.2//
     210X,50HTJ(R), PJ(PSF), JET INLET T AND P..........=,2F10.2//
     310X,50HROREF,  REFERENCE DENSITY FOR THE FLUID.....=,F10.4/
     410X,50HPREF,   REFERENCE PRESSURE FOR THE FLUID.....=,F10.4/
     510X,50HZMUREF, REFERENCE VISCOSITY FOR THE FLUID.....=,F10.8/
     610X,50HTREF,   REFERENCE TEMPRATURE FOR THE FLUID.....=,F10.4/
     710X,50HCPREF,  REFERENCE SPECIFIC-HEAT FOR THE FLUID....=,F10.4/
     610X,50HGC,     GRAVITATIONAL CONSTANT..............=,F10.4/
     710X,50HZJC,    JOULE'S MECH.EQUIVALENT FOR HEAT.....=,F10.4/)
114   FORMAT(1H  9X,50HREFERENCE SP.HEAT FOR FIRST MASS COMPONENT.....
     1=,F10.4)
115   FORMAT(1H  9X,50HIM,     NUMBER OF MASS SPECIES BEING CONSIDERED..
     1=,I6/
     210X,50HZMW*S   MOLECULAR WEIGHTS OF SPECIES 1,2,3 .....=,3F10.4/
     310X,50HCPJ*S   REFERENCE SP.HEATS FOR SPECIES 1,2,3 ....=,3F10.4/
     410X,50HPR*S    TURB.SCHMIDT NUMBERS FOR SPECIES 1,2,3 ..=,3F10.4)
116   FORMAT(1HO///24H OTHER DATA SUPPLIED ARE/
     224H ----- ---- -------- ---//
     310X,50HCC,     THE CONVERGENCY CRITERION.............=,F13.7/
     410X,50HDC,     THE DIVERGENCY  CRITERION.............=,F13.7/
     510X,50HNMAX,   THE MAXIMUM NUMBER OF ITERATIONS.....=,I6)
```

```
201   FORMAT(1HO,20X,22H          JC1,JC2,IC = ,3(I3,1H,),12HRESPECTIVELY
     1        /1HO,20X,28H          RADC1,RADC2,RADN = ,3(F6.3,1H,),5X,
     2        16HFT, RESPECTIVELY/
     3        1HO,20X,19H           DCN,DN = ,2(F6.3,1H,),5X,
     4        16HFT, RESPECTIVELY/)
202   FORMAT(1H1,10X,10H  I OR J  ,5X,11(3X,I2,3X))
203   FORMAT(1H ,10X,10H  X1(I)   ,5X,11(F8.4))
204   FORMAT(1H ,10X,10H  X2(J)   ,5X,11(F8.4))
205   FORMAT(1HO,10X,10H  I OR J  ,5X,11(3X,I2,3X))
301   FORMAT(10X,
     1 50HSTC,    (STC LB OF FUEL REACTS WITH 1 LB OF AIR),=,F10.4/10X,
     2 50HSTOX,   (STOX LB OF FUEL REACTS WITH 1 LB OF OX),=,F10.4)
401   FORMAT(1HO50X,24HIN CARTESIAN COORDINATES)
402   FORMAT(1HO50X,26HIN CYLINDRICAL COORDINATES)
      RETURN
      END
      SUBROUTINE SOLVCT (ITAB)
      COMMON/CVP/A(33,15,9),G1(33,15),G2(33,15),RO(33,15),ZMU(33,15)
      COMMON/CINDEX/INDE(9),INDG,INDRO,INDZMU
      COMMON/CCHECK/RSDU(9),RP(9),CC,DC,NMAX,NPRIN
      COMMON/CGRID/IMIN(33),IMAX(33),IN,JN,INM,JNM,IE
      COMMON/CNAME/ATITLE(12),ASYMBL(12),ANAME(6,10)
      COMMON/CNUMBR/NW,NF,NZML,NZMH,NZMC,NZMF,NZMN,NP,NVT
      COMMON/CNITER/NITER
      COMMON/CPARAM/VINJ,VINP(15),TP,PP,TJ,PJ,PHIP,PHIJ
      COMMON/CDI/DIFMAX(9),IPT(9),JPT(9),IPTR(9),JPTR(9)
      COMMON/CKVORT/KVORT
      COMMON/CYLI/JC1,JC2,IC,RADC1,RADC2,RADN,DCN,DN,JJC2,ICM,JC2M,JC1M
      COMMON/CTIME/TMAX
      COMMON/CVARY/NHOT,NPUNCH,NREAD,NPRES
      COMMON/CIGNIT/ISTAG1,ISTAG2,JSTAG
      COMMON/CENTHL/NENTHL,NSTRM
C*********************************************************************
C    **SOLVE** SUBROUTINE
C    THIS SUBR. CONTROLS THE ITERATION PROCEDURE
C*********************************************************************
      PRINT 101
      DO 10 K=1,IE
10     IF(INDE(K).EQ.1) PRINT 102, K, (ANAME(L,K),L = 1, 6)
      PRINT 103, (ASYMBL(K),K=1, IE)
      NITER=1
      NNN=NPRIN
      KVORT=0
      CALL  BOUNCT(NW)
1     CALL MVELCT(NF)
      IF((NITER.EQ.(NMAX-9)).AND.(NHOT.EQ.1)) NENTHL=1
      IF  ((NITER.EQ.(NMAX-1)).AND.(NHOT.EQ.1))  NSTRM=1
      IF((INDZMU.EQ.1).AND.(NITER.EQ.1))  CALL VISCCT
      IF(INDZMU.EQ.2) CALL VISCCT
      IF(INDRO.EQ.2) CALL DENSCT
      CALL MVBCCT
      DO 2 K=1,IE
      DIFMAX(K)=0.
      RSDU(K)=0.
      IF(IE.EQ.6.AND.K.LT.6) GO TO 2
      IPTR(K)=1
      JPTR(K)=1
      IF((NSTRM.EQ.2).AND.(K.EQ.2)) GO TO 2
      IF((NENTHL.EQ.2).AND.(K.EQ.NZMH)) GO TO 2
      DIFMAX(K)=0.
      RSDU(K)=0.
      IF(INDE(K).EQ.1) CALL FDEQCT(K,INDG)
```

```
    2 CONTINUE
      PRINT 104, NITER, (RSDU(K),IPTR(K),JPTR(K),K=1,IE)
      IF(IE.EQ.6) GO TO 300
      GO TO 34
      IF((NENTHL.GE.2).OR.(NHOT.EQ.0)) GO TO 30
      IF  (ABS(RSDU(NZMH)).GT..005)  GO TO 30
      NENTHL=2
      PRINT 61
   61 FORMAT(5X,*ENTHALPY HAS MET CONVERGENCE CRITERIA*)
30    CONTINUE
      IF((NSTRM.GE.2).OR.(NHOT.EQ.0)) GO TO 34
      IF  (ABS(RSDU(NF)).GT..005)  GO TO 34
      NSTRM=2
      PRINT 62
   62 FORMAT(5X,*STREAM FUNCTION HAS MET CONVERG CRITERIA*)
34    CONTINUE
      IPTRR=IPTR(NW)
      JPTRR=JPTR(NW)
      PRINT 109, A(IPTRR,JPTRR,NW)
  300 RES=RSDU(6)
      IF(NITER.GT.NMAX) GO TO 5
      IF(NITER-NNN)6,7,7
7     NNN=NNN+NPRIN
8     CONTINUE
      KVORT=1
      CALL  BOUNCT(NW)
      IF(INDE(NP).EQ.1) CALL PRESCT
      CALL PRINCT (ITAB)
      PRINT 103, (ASYMBL(K),K=1, IE)
6     CONTINUE
C****PRINT RESULTS OF FIRST ITERATION-IE VARIABLES
      IW=8
      NITER=NITER+1
      IF((ABS(RES).GT.CC).OR.(NITER.LE.2))  GO TO 1
      IF  (NHOT.EQ.0)  GO TO 33
      GO TO 33
      IF ((NENTHL.EQ.2).OR.(NSTRM.EQ.2))  GO TO 32
      IF ((ABS(RSDU(NZMH)).GT..005).OR.(ABS(RSDU(NF)).GT..005)) GO TO 1
33    CONTINUE
      KVORT=1
      CALL  BOUNCT(NW)
      RETURN
32    NENTHL=1
      NSTRM=1
      PRINT 121,  NITER
      NITER=NMAX-25
      NNN=(NITER/NPRIN)*NPRIN + NPRIN
      GO TO 1
5     PRINT 106, NITER
      KVORT=1
      CALL BOUNCT (NW)
100   FORMAT (8(E10.3))
101   FORMAT(1H1///10X,45HTHE FOLLOWING ARE MAXIMUM RESIDUES IN THE FIE,
     141HLD OF INTEGRATION AT EACH ITERATION FOR..//)
102   FORMAT(1H 40X,I2,3H.  ,6A6)
103   FORMAT    (1H1,30X,35H..NOTE.. PREFIX *R* DENOTES RESIDUE//
     1117HO....NOTE.....LEFT-HAND-COLUMNS FOR FRACTIONAL DIFFERENCES, RI
     1GHT-HAND-COLUMNS FOR CORRESPONDING ABSOLUTE DIFFERENCES///
     26X,5HNITER,9(7X,1HR,A6)//)
  104 FORMAT(1H ,6X,I3,6(1PE12.3,2I3))
106   FORMAT (32HOTHE PROCESS DID NOT CONVERGE IN,I5,13H   ITERATIONS)
107   FORMAT  (46X,4(1PE12.3,2I3))
```

```
  108   FORMAT (32HOTHE PROCESS DID NOT CONVERGE IN,F8.3,9H  SECONDS)
  109 FORMAT(1H+,105X,1(1PE12.3))
  121   FORMAT  (35HOVORT, STRM, PUMP HAVE CONVERGED IN,I5,
     1  13H   ITERATIONS)
      RETURN
      END
      SUBROUTINE FDEQCT(K,INDG)
      COMMON/CVP/A(33,15,9),G1(33,15),G2(33,15),RO(33,15),ZMU(33,15)
      COMMON/CCOEF/CE,CW,CN,CS,C(5)
      COMMON/CCHECK/RSDU(9),RP(9),CC,DC,NMAX,NPRIN
      COMMON/CGRID/IMIN(33),IMAX(33),IN,JN,INM,JNM,IE
      COMMON/CNUMBR/NW,NF,NZML,NZMH,NZMC,NZMF,NZMN,NP,NVT
      COMMON/CDI/DIFMAX(9),IPT(9),JPT(9),IPTR(9),JPTR(9)
      COMMON/CYLI/JC1,JC2,IC,RADC1,RADC2,RADN,DCN,DN,JJC2,ICM,JC2M,JC1M
      COMMON/CX1X2/X1(33),X2(15),DELX1(33),DELX2(15)
      COMMON/CZW/ZW,IL,IH
      COMMON/CRAD/R(15)
      COMMON/CPARAM/VINJ,VINP(15),TP,PP,TJ,PJ,PHIP,PHIJ
      WC1H(WK,DELF,ROP,DELRO,RAD)=  -DELF/(324.*DX2*DX2*(WK*DX2+RAD)*
     1   (ROP*(WK*DX2/37.+RAD/19.)+DELRO*(WK*DX2/55.+RAD/37.)))
      WC2H(WK,ROP,DELRO,RAD)=-(RAD+WK*DX2)*
     2                        (ROP*(RAD/6.+WK*DX2/8.)
     3                        +DELRO*(RAD/8.+WK*DX2/10.))
     4                  /(RAD*(ROP*(RAD/3.+5.*WK*DX2/24.)
     5                  +DELRO*(5.*RAD/24.+3.*WK*DX2/20.)))
      WC1V(DELF,ROP,DELRO,ETA2)=-DELF/(((ETA2*DX1)**2)*
     1                        (ROP/3.+5.*DELRO/24.))
      WC2V(ROP,DELRO)=-(ROP/6.+DELRO/8.)/(ROP/3.+5.*DELRO/24.)
C*************************************************************************
C    **FINITE-DIFFERENCE-EQUATION** SUBROUTINE
C*************************************************************************
      IPTR(K)=2
      JPTR(K)=2
      IPT(K)=2
      JPT(K)=2
      DO 10 J=2,JNM
      IL=IMIN(J)+1
      IH=IMAX(J)-1
      IF(J.EQ.JC2)IH=IC-1
      DO 10 I=IL,IH
      IF((K.EQ.NW).AND.((J.EQ.JC1).AND.(I.EQ.(IC-1))))  GO TO 100
      GO TO 110
  100 CALL CCEFCT (I,J,NF,INDG)
      YY=A(I,J,NF)*(CE+CW+CN+CS)
      YY=YY-(CE*A(I+1,J,NF)+CW*A(I-1,J,NF)+CN*A(I,J+1,NF)
     1 +CS*A(I,J-1,NF))
      Z=A(I,J,NW)
      A(I,J,NW)=YY/R(J)
      GO TO 222
  110 CONTINUE
      CALL SORCCT(I,J,K,SOURCE,ZQ)
      CALL CCEFCT(I,J,K,INDG)
      IF(K.NE.NW) GO TO 999
C***  INCORPORATING B.C. FOR VORTICITY IN THE FINITE DIFF. FORMULATION
C***  UP TO STATEMENT NUMBER 999
      ZW=0.
      ZWMU=0.0
      IF((I.EQ.IH).AND.((J.GE.JC1).AND.(J.LE.JC2)))   GO TO 600
      GO TO 700
  501 LJNS=J+1
      WKNS=FLOAT(1-INDG)
      RADNS=RADN
```

```
      CONS=CN
      GO TO 666
502   LJNS=J-1
      WKNS=FLOAT(INDG-1)
      RADNS=RADC2
      CONS=CS
      GO TO 666
600   LIEW=I+1
      CQEW=CE
      GO TO 555
700   IF(J.EQ.JNM) GO TO 501
      IF((J.EQ.(JC2+1)).AND.(I.GE.IC))  GO TO 502
      GO TO 999
555   DX1=ABS(X1(LIEW)-X1(I))
      A(LIEW,J,NW)=WC1V(A(I,J,NF)-A(LIEW,J,NF),RO(LIEW,J),
     1                  RO(I,J)-RO(LIEW,J), R(J))
      ZW=CQEW*WC2V(RO(LIEW,J),RO(I,J)-RO(LIEW,J))
      ZWMU=ZWMU+ZW*ZMU(LIEW,J)
      GO TO 999
666   DX2=ABS(X2(LJNS)-X2(J))
      A(I,LJNS,NW)=WC1H(WKNS,A(I,J,NF)-A(I,LJNS,NF),RO(I,LJNS),
     1                  RO(I,J)-RO(I,LJNS),RADNS)
      ZW=0.0
      ZWMU=ZWMU+ZW*ZMU(I,LJNS)
C***  END VORTICITY B.C. SPECIAL FORMULATION
999   CONTINUE
      IF(K.NE.NF) GO TO 1
      IF ((J.EQ.JC1).AND.(I.EQ.(IC-1)).AND.(VINJ.NE.0.0))  GO TO 223
      GO TO 1
223   A(I,J,NF)=A(IC,JC1,NF)
      GO TO 10
1     CONTINUE
      CALL  CONVEC(I,J,K,AU,ZU)
      IF(K.EQ.NW) AU=AU*R(J)*R(J)
      IF(K.EQ.NW) ZU=ZU*R(J)*R(J)
      ANUM=CE*C(2)*A(I+1,J,K)+CW*C(4)*A(I-1,J,K)
     1    +CN*C(3)*A(I,J+1,K)+CS*C(5)*A(I,J-1,K)+AU+SOURCE
      ADNM=(CE+CW+CN+CS)*C(1)+ZU+ZQ
      IF(K.EQ.NW) ADNM=ADNM-ZWMU
      IF((ADNM.EQ.0.0).OR.(ANUM.EQ.0.0)) GO TO 10
4     Z=A(I,J,K)
      A(I,J,K)=ANUM/ADNM
      IF(ABS(A(I,J,NZML)).LE.1.0E-210) A(I,J,NZML)=1.0E-210
      IF  (ABS(A(I,J,NF)).GT.2.0E-02)  A(I,J,NF)=-3.0E-03
222   CONTINUE
      DIF=A(I,J,K)-Z
      A(I,J,K)=Z+RP(K)*DIF
      AB=0.25*(ABS(A(I+1,J,K))+ABS(A(I-1,J,K))+ABS(A(I,J+1,K))
     1  +ABS(A(I,J-1,K)))
      IF((A(I,J,K).EQ.0.0).OR.(AB.EQ.0.0))  GO TO 10
      RS=DIF/A(I,J,K)
      RSM=DIF/AB
      IF(ABS(RSM).LT.ABS(RS)) RS=RSM
      IF(ABS(RS).GT.ABS(RSDU(K)))   GO TO 55
      GO TO 54
55    RSDU(K)=RS
      IPTR(K)=I
      JPTR(K)=J
54    CONTINUE
      IF(ABS(DIF).GT.ABS(DIFMAX(K)))  GO TO 52
      GO TO 10
52    DIFMAX(K)=DIF
```

```
      IPT(K)=I
      JPT(K)=J
10    CONTINUE
      CALL BCUNCT(K)
      RETURN
      END
      SUBROUTINE SORCCT(I,J,K,SOURCE,ZQ)
      COMMON/CNITER/NITER
      COMMON/CPARAM/VINJ,VINP(15),TP,PP,TJ,PJ,PHIP,PHIJ
      COMMON/CVP/A(33,15,9),G1(33,15),G2(33,15),RO(33,15),ZMU(33,15)
      COMMON/CNUMBR/NW,NF,NZML,NZMH,NZMC,NZMF,NZMN,NP,NVT
      COMMON/CX1X2/X1(33),X2(15),DELX1(33),DELX2(15)
      COMMON/CRAD/R(15)
      COMMON/CCONST/PR(9),ZMW(3),CPJ(3),GCPM,GC,ZJC
      COMMON/CHEM/STC,STOX,HFP,HFCO,HFCO2,HFH2O,GLOB(3),ZEX(3)
      COMMON/CINDEX/INDE(9),INDG,INDRO,INDZMU
      COMMON/CREFER/ROREF,PREF,ZMUREF,TREF,CPREF,TO
C*********************************************************************
C    **SOURCE** - TERMS SUBROUTINE
C    SOURCE TERMS IN FINITE DIFFERENCE FORM
C*********************************************************************
      GO TO (1,2,5,5,3,5,5,3,4),K
C*****  FOR VORTICITY
1     SOURCE=0.
      DEN=16.0*DELX1(I)*DELX2(J)/(R(J)**2)
      S1=RO(I,J+1)+RO(I,J)
      S1=S1*(VS2(I+1,J)-VS2(I-1,J)+VS2(I+1,J+1)-VS2(I-1,J+1))
      S2=RO(I,J-1)+RO(I,J)
      S2=S2*(VS2(I-1,J)-VS2(I+1,J)+VS2(I-1,J-1)-VS2(I+1,J-1))
      S3=RO(I+1,J)+RO(I,J)
      S3=S3*(VS2(I,J-1)-VS2(I,J+1)+VS2(I+1,J-1)-VS2(I+1,J+1))
      S4=RO(I-1,J)+RO(I,J)
      S4=S4*(VS2(I,J+1)-VS2(I,J-1)+VS2(I-1,J+1)-VS2(I-1,J-1))
      SOURCE=SOURCE+(S1+S2+S3+S4)/DEN
      IF(INDE(NVT).EQ.1) SOURCE=SOURCE+(RO(I+1,J)*(A(I+1,J,NVT)**2)
     1     -RO(I-1,J)*(A(I-1,J,NVT)**2))/((X1(I+1)-X1(I-1))*R(J))
      ZQ=0.
      RETURN
C*****  FOR STREAM FUNCTION
2     SOURCE=A(I,J,NW)*R(J)
      ZQ=0.
      RETURN
C*****  FOR MIXTURE FRACTION AND ENTHALPY
3     SOURCE=0.
      ZQ=0.
      RETURN
C*****  FOR SWIRL VELOCITY
4     ZQ=0.
      SOURCE=0.0
      RETURN
C*******  FOR MASS FRACTIONS
C
C    COMPUTE TEMP AND MOLEC WEIGHT
C
    5 AFU=A(I,J,NZML)
      IF(AFU.LT.0.0) AFU=0.0
      AFC=A(I,J,NZMC)
      IF(AFC.LT.0.0) AFC=0.0
      AH=A(I,J,NZMH)
      ACO=1.9059*(A(I,1,NZML)-A(I,J,NZML))-0.636*AFC
      IF(ACO.LT.-5.0E-05) ACO=-5.0E-05
      AH2O=1.634*(A(I,1,NZML)-A(I,J,NZML))+0.00151
```

```
      FOX=A(1,1,NZML)/(PHIP*STOX)-0.888*(AH2O-0.00151)-0.5712*ACO-0.727*
     1AFC
      IF(FOX.LE.0.0) FOX=0.0
      FIP=1.0-FOX-AFU-ACO-AH2O-AFC
      TEMP=TO*(AH-AFU*HFP-ACO*HFCO-AFC*HFCO2-AH2O*HFH2O)/CPREF
      IF (TEMP.LT.300.) TEMP=TREF
      ZMEAN=1.0/(AFU/ZMW(1)+FOX/ZMW(2)+FIP/ZMW(3)+ACO/28.011+AH2O/18.016
     1+AFC/44.011)
C    COMPUTE SOURCE TERMS
      SORC=(PREF*ZMEAN)/(TEMP*GCPM)
      IF(K.EQ.3) GO TO 10
      IF(K.EQ.4) GO TO 11
      IF(K.EQ.6) GO TO 12
C    FUEL MASS FRACTION
   10 CONTINUE
      IF(AFU.LE.0.0) GO TO 350
      SORC=SORC**0.5
      SORC=SORC*GLOB(1)*AFU**0.5
      SORC=-SORC/EXP(ZEX(1)/TEMP)
      ZQ=-(SORC/AFU)*R(J)
      SOURCE=0.0
      RETURN
C    CO2 MASS FRACTION
   11 CONTINUE
      IF(AH2O.LE.0.0.OR.FOX.LE.0.0) GO TO 350
      ACO=1.9059*(A(1,1,NZML)-A(I,J,NZML))-0.636*AFC
      SORC=SORC**2.0
      SORC=SORC*GLOB(2)*FOX**0.50*AH2O**0.50
      SORC=SORC/(EXP(ZEX(2)/TEMP))
      SORCS=1.9059*(A(1,1,NZML)-A(I,J,NZML))*SORC
      SOURCE=SORCS*R(J)
      SORCZ=0.636*AFC*SORC
      ZQ=(SORCZ/AFC)*R(J)
      A(I,J,7)=ACO
      A(I,J,8)=SORCS
      A(I,J,9)=SORCZ
      RETURN
C    NO MASS FRACTION
   12 CONTINUE
      IF(ACO.LE.0.0.OR.AFC.LT.0.000001) GO TO 350
      SORC=SORC**2.0
      SORC=SORC*GLOB(3)*FIP*FOX*ACO/AFC
      SORC=SORC/(EXP(ZEX(3)/TEMP))
      SOURCE=SORC*R(J)
      ZQ=0.0
      A(I,J,7)=SORC
      RETURN
      GO TO 450
350   ZQ=0.0
450   SOURCE=0.0
      IF(K.EQ.4) A(I,J,7)=0.0
      IF(K.EQ.4) A(I,J,9)=0.0
      IF(K.EQ.6) A(I,J,7)=0.0
      IF(K.EQ.4) A(I,J,8)=0.0
      RETURN
      END
      SUBROUTINE COEFCT(I,J,K,INDG)
      COMMON/CX1X2/X1(33),X2(15),DELX1(33),DELX2(15)
      COMMON/CVP/A(33,15,9),G1(33,15),G2(33,15),RO(33,15),ZMU(33,15)
      COMMON/CCOEF/CE,CW,CN,CS,C(5)
      COMMON/CCONST/PR(9),ZMW(3),CPJ(3),GCPM,GC,ZJC
      COMMON/CRAD/R(15)
```

```
      COMMON/CNUMBR/NW,NF,NZML,NZMH,NZMC,NZMF,NZMN,NP,NVT
      COMMON/CYLI/JC1,JC2,IC,RADC1,RADC2,RADN,DCN,DN,JJC2,ICM,JC2M,JC1M
C*************************************************************************
C    **COEFFICIENT** (FOR DIFFUSION TERMS) SUBROUTINE
C*************************************************************************
C*****  SUBSCRIPTS 1,2,3,4,5 REFER TO POINTS P,E,N,W,S RESPECTIVELY
      DIMENSION B(5)
      DO 16 L=1,5
16    C(L)=1.0
      IF((K.NE.NW).AND.(K.NE.NP))  GO TO 2
C*****  FOR VORTICITY
      B(1)=R(J)**3
      B(2)=B(1)
      B(3)=R(J+1)**3
      B(4)=B(1)
      B(5)=R(J-1)**3
      C(1)=ZMU(I,J)
      C(2)=ZMU(I+1,J)
      C(3)=ZMU(I,J+1)
      C(4)=ZMU(I-1,J)
      C(5)=ZMU(I,J-1)
      GO TO 20
2     IF(K.NE.NF) GO TO 3
C*****  FOR STREAM FUNCTION
      B(1)=1./(R(J)*RO(I,J))
      B(2)=1./(R(J)*RO(I+1,J))
      B(3)=8.0/((R(J)+R(J+1))*(RO(I,J)+RO(I,J+1)))-B(1)
      B(4)=1./(R(J)*RO(I-1,J))
      B(5)=8.0/((R(J)+R(J-1))*(RO(I,J)+RO(I,J-1)))-B(1)
      GO TO 20
3     IF(K.NE.NVT) GO TO 15
C*****  FOR SWIRL VELOCITY
      B(1)=ZMU(I,J)*R(J)**3
      B(2)=ZMU(I+1,J)*R(J)**3
      B(3)=ZMU(I,J+1)*R(J+1)**3
      B(4)=ZMU(I-1,J)*R(J)**3
      B(5)=ZMU(I,J-1)*R(J-1)**3
      C(1)=1./(R(J)*R(J))
      C(2)=C(1)
      C(3)=1./(R(J+1)*R(J+1))
      C(4)=C(1)
      IF(R(J-1).GT.0.0) C(5)=1./(R(J-1)*R(J-1))
      IF(R(J-1).EQ.0.0) C(5)=0.0
      GO TO 20
C**** FOR MIXTURE FRACTION AND ENTHALPY AND MASS FRACTIONS
15    B(1)=ZMU(I,J)*R(J)/PR(K)
      B(2)=ZMU(I+1,J)*R(J)/PR(K)
      B(3)=ZMU(I,J+1)*R(J+1)/PR(K)
      B(4)=ZMU(I-1,J)*R(J)/PR(K)
      B(5)=ZMU(I,J-1)*R(J-1)/PR(K)
20    CONTINUE
C*****  FOR ALL DEPENDENT VARIABLES
      CE=(B(2)+B(1))/((X1(I+1)-X1(I))*2.*DELX1(I))
      CW=(B(1)+B(4))/((X1(I)-X1(I-1))*2.*DELX1(I))
      CN=(B(3)+B(1))/((X2(J+1)-X2(J))*2.*DELX2(J))
      CS=(B(1)+B(5))/((X2(J)-X2(J-1))*2.*DELX2(J))
      RETURN
      END
      SUBROUTINE CONVEC(I,J,K,AU,ZU)
      COMMON/CVP/A(33,15,9),G1(33,15),G2(33,15),RO(33,15),ZMU(33,15)
      COMMON/CX1X2/X1(33),X2(15),DELX1(33),DELX2(15)
      COMMON/CNUMBR/NW,NF,NZML,NZMH,NZMC,NZMF,NZMN,NP,NVT
```

```
      COMMON/CYL1/JC1,JC2,IC,RADC1,RADC2,RADN,DCN,DN,JJC2,ICM,JC2M,JC1M
      COMMON/CRAD/R(15)
      COMMON/CZW/ZW,IL,IH
      COMMON/CCOEF/CE,CW,CN,CS,C(5)
      COMMON/CGRID/IMIN(33),IMAX(33),IN,JN,INM,JNM,IE
C*****************************************************************
C   **CONVECTION** - TERM  SUBROUTINE
C   TANK-AND-TUBE FORMULATION OF THE CONVECTION TERMS
C*****************************************************************
      AU=0.
      ZU=0.
      IF(K.EQ.NF) GO TO 12
      DX12=1./(4.*DELX1(I)*DELX2(J))
      GM1E=DX12*(A(I,J+1,NF)-A(I,J-1,NF)+A(I+1,J+1,NF)-A(I+1,J-1,NF))
      GM1W=DX12*(A(I,J+1,NF)-A(I,J-1,NF)+A(I-1,J+1,NF)-A(I-1,J-1,NF))
      GM2S=-DX12*(A(I+1,J,NF)-A(I-1,J,NF)+A(I+1,J-1,NF)-A(I-1,J-1,NF))
      GM2N=-DX12*(A(I+1,J,NF)-A(I-1,J,NF)+A(I+1,J+1,NF)-A(I-1,J+1,NF))
C
      IF(GM1W)1,3,2
1     ZU=-GM1W
      GO TO 3
2     AU=GM1W*A(I-1,J,K)
3     IF(GM2S)4,6,5
4     ZU=ZU-GM2S
      GO TO 6
5     AU=AU+GM2S*A(I,J-1,K)
      IF((K.EQ.NW).AND.(J.EQ.(JC2+1)).AND.(I.GE.IC))  GO TO 501
6     IF(GM1E)7,9,8
7     AU=AU-GM1E*A(I+1,J,K)
      GO TO 9
8     ZU=ZU+GM1E
9     IF(GM2N)10,11,11
10    AU=AU-GM2N*A(I,J+1,K)
      IF((K.EQ.NW).AND.(J.EQ.JNM))  GO TO 504
      RETURN
11    ZU=ZU+GM2N
12    RETURN
C
 501  ZU=ZU-GM2S*ZW/CS
      GO TO 6
 502  ZU=ZU+GM1E*ZW/CE
      GO TO 9
504   ZU=ZU+GM2N*ZW/CN
      RETURN
      END
      SUBROUTINE DENSCT
      COMMON/CPARAM/VINJ,VINP(15),TP,PP,TJ,PJ,PHIP,PHIJ
      COMMON/CVP/A(33,15,9),G1(33,15),G2(33,15),RO(33,15),ZMU(33,15)
      COMMON/CINDEX/INDE(9),INDG,INDRO,INDZMU
      COMMON/CREFEP/ROREF,PREF,ZMUREF,TREF CPREF,TO
      COMMON/CGRID/IMIN(33),IMAX(33),IN,JN,INM,JNM,IE
      COMMON/CCONST/PR(9),ZMW(3),CPJ(3),GCPM,GC,ZJC
      COMMON/CNITER/NITER
      COMMON/CNUMBR/NW,NF,NZML,NZMH,NZMC,NZMF,NZMN,NP,NVT
      COMMON/CHEM/STC,STOX,HFP,HFCO,HFCO2,HFH2O,GLOB(3),ZEX(3)
      COMMON/CROWF/RCWF
C*****************************************************************
C   **DENSITY** SUBROUTINE
C   MIXTURE DENSITY CALCULATION
C*****************************************************************
      DO 40 J=1,JN
      IL=IMIN(J)
```

```
      IH=IMAX(J)
      DO 40 I=IL,IH
      AFU=A(I,J,NZML)
      AFC=A(I,J,NZMC)
      ACO=1.9059*(A(1,1,NZML)-AFU)-0.636*AFC
      AH2O=1.634*(A(1,1,NZML)-A(I,J,NZML))+0.00151
      FOX=A(1,1,NZML)/(PHIP*STOX)-0.888*(AH2O-0.00151)-0.5712*ACO-0.727*
     1AFC
      FIP=1.0-FOX-AFU-ACO-AH2O-AFC
      IF(AFU.GT.1.)  AFU=1.0
      IF(AFC.GT.1.) AFC=1.0
      IF(ACO.GT.1.) ACO=1.0
      IF(FOX.GT.1.) FOX=1.0
      IF(AH2O.GT.1.) AH2O=1.0
      IF(AFU.GT.-1.0E-05) GO TO 15
      AFU=0.0
15    CONTINUE
      IF(AFC.GT.-1.0E-05) GO TO 17
      AFC=0.0
   17 CONTINUE
      IF (FOX.GT.-1.E-05) GO TO 20
      FOX=0.0
20    CONTINUE
      AH=A(I,J,NZMH)
      TEMP=TO+(AH-AFU*HFP-ACO*HFCO-AFC*HFCO2-AH2O*HFH2O)/CPREF
      IF(TEMP.GE.300.) GO TO 50
      TEMP=TREF
50    CONTINUE
      ZMEAN=1.0/(AFU/ZMW(1)+FOX/ZMW(2)+FIP/ZMW(3)+ACO/28.011+AH2O/18.016
     1+AFC/44.011)
      DENSTY=(ZMEAN*PREF)/(GCPM*TEMP)
      RO(I,J)=ROWF*DENSTY+(1.0-ROWF)*RO(I,J)
40    CONTINUE
      RETURN
      END
      SUBROUTINE VISCCT
      COMMON/CVP/A(33,15,9),G1(33,15),G2(33,15),RO(33,15),ZMU(33,15)
      COMMON/CINDEX/INDE(9),INDG,INDRO,INDZMU
      COMMON/CREFER/ROREF,PREF,ZMUREF,TREF,CPREF,TO
      COMMON/CGRID/IMIN(33),IMAX(33),IL,JN,INM,JNM,IE
      COMMON/CNUMBR/NW,NF,NZML,NZMH,NZMC,NZMF,NZMN,NP,NVT
      COMMON/CYLI/JC1,JC2,IC,RADC1,RADC2,RADN,DCN,DN,JJC2,ICM,JC2M,JC1M
      COMMON/CPARAM/VINJ,VINP(15),TP,PP,TJ,PJ,PHIP,PHIJ
      COMMON/CZMUK/ZMUK
      COMMON/CX1X2/X1(33),X2(15),DELX1(33),DELX2(15)
C*********************************************************************
C    **VISCOSITY** SUBROUTINE
C    MIXTURE VISCOSITY
C*********************************************************************
      IF(INDZMU.EQ.1) GO TO 20
      ZMP=2.*(A(1,JN,NF)-A(1,1,NF))
      ZMJ=-2.*(A(IC,JC1,NF)-A(IC,1,NF))
      IF(INDG.EQ.2) ZMP=ZMP*3.14162
      IF(INDG.EQ.2) ZMJ=ZMJ*3.14162
      VINPSUM=0.0
      DO 40 J=1,JN
40    VINPSUM=VINPSUM+VINP(J)
      VPMEAN=VINPSUM/FLOAT(JN)
      ZMVV=ZMP*VPMEAN**2+ZMJ*VINJ**2
      IF(INDE(NVT).EQ.1) ZMVV=ZMVV+ZMJ*(A(1,JC1-1,NVT)**2)
      ZMVV=ZMVV**0.33333
      AA=ZMUK*((2.*X2(JN))**0.666667)*ZMVV/((DCN)**0.33333)
```

```
      DO 10 J=1,JN
      IL=IMIN(J)
      IH=IMAX(J)
      DO 10 I=IL,IH
      ZMU(I,J)=AA*(RO(I,J)**0.666667)
10    CONTINUE
      GO TO 30
20    DO 21 J=1,JN
      IL=IMIN(J)
      IH=IMAX(J)
      DO 21 I=IL,IH
      ZMU(I,J)=ZMUREF
21    CONTINUE
30    CONTINUE
      RETURN
      END
      FUNCTION T(I,J)
      COMMON/CVP/A(33,15,9),G1(33,15),G2(33,15),RO(33,15),ZMU(33,15)
      COMMON/CNUMBR/NW,NF,NZML,NZMH,NZMC,NZMF,NZMN,NP,NVT
      COMMON/CCONST/PR(9),ZMW(3),CPJ(3),GCPM,GC,ZJC
      COMMON/CREFER/ROREF,PREF,ZMUREF,TREF,CPREF,TO
      COMMON/CHEM/STC,STOX,HFP,HFCO,HFCO2,HFH2O,GLOB(3),ZEX(3)
C*********************************************************************
C   TEMPERATURE CALCULATION
C*********************************************************************
      AFU=A(I,J,NZML)
      AFC=A(I,J,NZMC)
      ACO=1.9059*(A(1,1,NZML)-AFU)-0.636*AFC
      AH2O=1.634*(A(1,1,NZML)-A(I,J,NZML))+0.00151
      AH=A(I,J,NZMH)
      TEMP=TO*(AH-AFU*HFP-ACO*HFCO-AFC*HFCO2-AH2O*HFH2O)/CPREF
      T=TEMP
      RETURN
      END
      FUNCTION VS2(I,J)
      COMMON/CVP/A(33,15,9),G1(33,15),G2(33,15),RO(33,15),ZMU(33,15)
      VS2     =(G1(I,J)*G1(I,J)+G2(I,J)*G2(I,J))/(RO(I,J)*RO(I,J))
      RETURN
      END
      SUBROUTINE MVBCCT
      COMMON/CVP/A(33,15,9),G1(33,15),G2(33,15),RO(33,15),ZMU(33,15)
      COMMON/CGRID/IMIN(33),IMAX(33),IN,JN,INM,JNM,IE
      COMMON/CPARAM/VINJ,VINP(15),TP,PP,TJ,PJ,PHIP,PHIJ
      COMMON/CREFER/ROREF,PREF,ZMUREF,TREF,CPREF,TO
      COMMON/CNUMBR/NW,NF,NZML,NZMH,NZMC,NZMF,NZMN,NP,NVT
      COMMON/CYLI/JC1,JC2,IC,RADC1,RADC2,RADN,DCN,DN,JJC2,ICM,JC2M,JC1M
      COMMON/CCONST/PR(9),ZMW(3),CPJ(3),GCPM,GC,ZJC
      COMMON/CX1X2/X1(33),X2(15),DELX1(33),DELX2(15)
      COMMON/CRAD/R(15)
      COMMON/CINDEX/INDE(9),INDG,INDRO,INDZMU
      DIMENSION AQ(33,15,14)
      EQUIVALENCE (A(1,1,1),AQ(1,1,1))
C*********************************************************************
C   **MASS-VELOCITY-BOUNDARY-CONDITION** SUBROUTINE
C   THIS SUBR. CALCULATES G1, G2 ON THE BOUNDARIES
C*********************************************************************
C
C*********************************************************************
C   UNIFORM INLET-VELOCITY DISTRIBUTIONS...
C   ZERO AXIAL GRADIENTS OF STREAM FUNCTION AND VORTICITY AT EXIT
C   VEXIT IS THE MEAN VELOCITY AT EXIT
C*********************************************************************
```

```
      DO 31 J=JJC2,JNM
      G1(IN,J)=ADF(IN,J,2,NF)/R(J)
31    CONTINUE
      BB=1./(1.-((X2(2)-X2(1))/(X2(3)-X2(1)))**2)
      DO 10 I=2,ICM
   10 G1(I,1)=BB*G1(I,2)-(BB-1.)*G1(I,3)
      RETURN
      END
      SUBROUTINE MVELCT(NF)
      COMMON/CVP/A(33,15,9),G1(33,15),G2(33,15),RO(33,15),ZMU(33,15)
      COMMON/CRAD/R(15)
      COMMON/CGRID/IMIN(33),IMAX(33),IN,JN,INM,JNM,IE
      COMMON/CYLI/JC1,JC2,IC,RADC1,RADC2,RADN,DCN,DN,JJC2,ICM,JC2M,JC1M
      DIMENSION AQ(33,15,14)
      EQUIVALENCE (A(1,1,1),AQ(1,1,1))
C*****************************************************************************
C    **MASS-VELOCITY** SUBROUTINE
C    THIS SUBR. CALCULATES G1 AND G2 AT ALL POINTS  NOT ON THE BOUND.
C*****************************************************************************
      DO 10 J=2,JNM
      IL=IMIN(J)+1
      IH=IMAX(J)-1
      IF(J.EQ.JC2)  IH=IC-1
      DO 10 I=IL,IH
      G1(I,J)=ADF(I,J,2,NF)/R(J)
10    G2(I,J)=-(ADF(I,J,1,NF)/R(J))
      RETURN
      END
      SUBROUTINE PRINCT  (ITAB)
      COMMON/CX1X2/X1(33),X2(15),DELX1(33),DELX2(15)
      COMMON/CVP/A(33,15,9),G1(33,15),G2(33,15),RO(33,15),ZMU(33,15)
      COMMON/CINDEX/INDE(9),INDG,INDRO,INDZMU
      COMMON/CNUMBR/NW,NF,NZML,NZMH,NZMC,NZMF,NZMN,NP,NVT
      COMMON/CGRID/IMIN(33),IMAX(33),IN,JN,INM,JNM,IE
      COMMON/CNAME/ATITLE(12),ASYMBL(12),ANAME(6,10)
      COMMON/CNITER/NITER
      COMMON/CVEXIT/VEXIT
      COMMON/CPARAM/VINJ,VINP(15),TP,PP,TJ,PJ,PHIP,PHIJ
      COMMON/CREFER/ROREF,PREF,ZMUREF,TREF,CPREF,TO
      COMMON/CRAD/R(15)
      COMMON/CHEM/STC,STOX,HFP,HFCO,HFCO2,HFH2O,GLOB(3),ZEX(3)
      COMMON/CYLI/JC1,JC2,IC,RADC1,RADC2,RADN,DCN,DN,JJC2,ICM,JC2M,JC1M
      COMMON/CVARY/NHOT,NPUNCH,NREAD,NPRES
      DIMENSION W(33)
C*****************************************************************************
C    **PRINT** SUBROUTINE
C    THIS SUBR. PRINTS OUT PART OF THE RESULTS FOR EASY EXAMINATION
C*****************************************************************************
      PRINT 500
      IQ=ITAB
      IT=IE+1
      IF  (NHOT.EQ.0)  GO TO 80
      DO 70 J=1,JN
      IL=IMIN(J)
      IH=IMAX(J)
      DO 70 I=IL,IH
      A(I,J,IT)=T(I,J)
70    CONTINUE
80    IF(INDE(NP).EQ.1) IT=IT+1
      IF(INDE(NP).NE.1) GO TO 82
      IQ=IQ+1
      DO 50 J=1,JN
```

```
      IL=IMIN(J)
      IH=IMAX(J)
      DO 50 I=IL,IH
50    A(I,J,IT)=A(I,J,NP)
82    CONTINUE
      IX=1
      DO 10 K=1,IQ
      PRINT 100, (ANAME(L,K),L=1, 6), NITER
      DO 6 IP=1,3
      IF((IP.EQ.2).AND.(IN.LE.21)) GO TO 6
      II1=12
      IF (IN.GT.21) II1=23
      IF(IP.EQ.1) IEND=11
      IF(IP.EQ.2) IEND=22
      IF (IP.EQ.3) IEND=IN
      DO 5 JJ=1,JN
      J=JN+1-JJ
      IF(IP.EQ.1) II1=1
      IF(IP.EQ.2) II1=12
      II2=IMAX(J)
      IF (IP.EQ.1) II2=11
      IF (IP.EQ.2) II2=22
      IF((K.NE.NW).AND.((INDE(K).NE.1).OR.(K.NE.NVT)))  GO TO 4
      DO 40 I=II1,II2,IX
      W(I)=A(I,J,K)
      IF((K.EQ.NVT).AND.(R(J).GT.0.0))  A(I,J,NVT)=W(I)/R(J)
40    CONTINUE
4     CONTINUE
      PRINT 101, J, (A(I, J, K), I = II1, II2, IX)
      IF((K.NE.NW).AND.((INDE(K).NE.1).OR.(K.NE.NVT)))  GO TO 5
      DO 41 I=II1,II2,IX
41    A(I,J,K)=W(I)
5     CONTINUE
      IF (IP.EQ.1) PRINT 102, (I,I=1,IEND)
      IF (IP.EQ.2) PRINT 102, (I,I=12,IEND)
      IF (IP.EQ.3) PRINT 102, (I,I=II1,IEND)
      PRINT 103
6     CONTINUE
10    CONTINUE
      IF (NITER.EQ.1) RETURN
      RENO=-42.750*A(1,1,2)/ZMU(1,1)
      PRINT 401, RENO
      ROSUM=0.0
      DO 20 J=JC2,JN
20    ROSUM=ROSUM+RO(IN,J)
      ROMEAN=ROSUM/(FLOAT(JN)-FLOAT(JC2M1))
      IF(INDG.EQ.1) VEXIT=-A(IN,JC2,NF)/((X2(JN)-X2(JC2))*ROMEAN)
      IF(INDG.EQ.2)  VEXIT=-2.*A(IN,JC2,NF)/((RADN*RADN-RADC2*RADC2)*
     1                    ROMEAN)
      PRINT 301, VEXIT
100   FORMAT(1H1,35X,21HTHE DISTRIBUTION OF  ,6A6//
     223H NUMBER OF ITERATION = ,I5//)
101   FORMAT(1H ,I2,2X,11(1PE11.3))
102   FORMAT(1HO/11111///)
103   FORMAT(1HO///)
301   FORMAT(9H VEXIT = ,F8.3)
401   FORMAT (/// 10X,
     1       55HREYNOLDS NO BASED ON MEAN MASS FLOW RATE AND MAX DIA = ,
     2     OPF7.1)
500   FORMAT (1H7)
      RETURN
      END
```

```
      FUNCTION ADF(I,J,LX,KQ)
      COMMON/CVP/A(33,15,9),G1(33,15),G2(33,15),R0(33,15),ZMU(33,15)
      COMMON/CYLI/JC1,JC2,IC,RADC1,RADC2,RADN,DCN,DN,JJC2,ICM,JC2M,JC1M
      COMMON/CX1X2/X1(33),X2(15),DELX1(33),DELX2(15)
      COMMON/CGRID/IMIN(33),IMAX(33),IN,JN,INM,JNM,IE
      DIMENSION AQ(33,15,14)
      DIMENSION BENQ(20),BWSR(20),BP(20)
      EQUIVALENCE (A(1,1,1),AQ(1,1,1))
      DF(PN,BENQ,BWSR,BP,XENQ,XWSR)=((XENQ*XENQ-XWSR*XWSR)*BP+
     1       XWSR*XWSR*BENQ-XENQ*XENQ*BWSR)/(XENQ*XWSR*(PN*XENQ+XWSR))
C*************************************************************************
C   THIS FUNCTION EVALUATES FIRST DERVIATIVES ACCORDING
C   TO THE THREE-POINT QUADRATIC APPROXIMATION
C*************************************************************************
C
C****    DEPENDING ON THE POSITION OF THE POINT (I,J), THERE
C****    ARE FIVE DIFFERENT EXPRESSIONS FOR THE DERIVATIVE
C
      M=1
      IF((J.EQ.1).OR.((J.EQ.JC2).AND.(I.LE.IN).AND.(I.GE.IC))) GO TO 92
      IF(I.EQ.1)  GO TO 93
      IF ( J.EQ.JN)  GO TO 94
      IF(((I.EQ.IC).AND.(J.LE.JC2).AND.(J.GE.JC1)).OR.
     1   ((I.EQ.IN).AND.(J.LE.JN).AND.(J.GE.JC2))) M=5
      GO TO 99
92    M=2
      GO TO 99
93    M=3
      GO TO 99
94    M=4
99    CONTINUE
      GO TO (1,2,3,4,5),M
C****    M=1....FOR POINTS NOT ON ANY OF THE BOUNDARIES
1     PN=1.
      IF(LX.EQ.1) GO TO 12
13    IF((J.EQ.1).OR.(J.EQ.JC2))  GO TO 21
      IF(J.EQ.JN) GO TO 41
      DO 10 L=1,14
      BENQ(L)=AQ(I,J+1,L)
      BWSR(L)=AQ(I,J-1,L)
10    BP(L)=AQ(I,J,L)
      XENQ=X2(J+1)-X2(J)
      XWSR=X2(J)-X2(J-1)
      GO TO 100
12    IF(I.EQ.1) GO TO 31
      IF(((I.EQ.IC).AND.(J.EQ.1)).OR.(I.EQ.IN))  GO TO 51
      DO 11 L=1,14
      BENQ(L)=AQ(I+1,J,L)
      BWSR(L)=AQ(I-1,J,L)
11    BP(L)=AQ(I,J,L)
      XENQ=X1(I+1)-X1(I)
      XWSR=X1(I)-X1(I-1)
      GO TO 100
C****    M=2....FOR POINTS ON THE BOUNDARY J=1
2     IF(LX.EQ.1) GO TO 1
21    PN=-1.
      DO 20 L=1,14
      BENQ(L)=AQ(I,J+1,L)
      BWSR(L)=AQ(I,J+2,L)
20    BP(L)=AQ(I,J,L)
      XENQ=X2(J+1)-X2(J)
      XWSR=X2(J+2)-X2(J)
```

```
      GO TO 100
C****    M=3....FOR POINTS ON THE IAB-PLANE
3     IF(LX.NE.1) GO TO 1
31    PN=-1.
      DO 30 L=1,14
      BENQ(L)=AQ(I+1,J,L)
      BWSR(L)=AQ(I+2,J,L)
30    BP(L)=AQ(I,J,L)
      XENQ=X1(I+1)-X1(I)
      XWSR=X1(I+2)-X1(I)
      GO TO 100
C****    M=4....FOR POINTS ON ALL WALLS PARALLEL TO THE J-LINES,
C****    BEYONN THE IAB-PLANE
4     IF(LX.EQ.1) GO TO 1
41    PN=-1.
      DO 40 L=1,14
      PRINT 14,I,J,L,AQ(I,J-1,L)
   14 FORMAT(/,3(2X,I3),3X,E14.8)
      BENQ(L)=AQ(I,J-1,L)
      BWSR(L)=AQ(I,J-2,L)
40    BP(L)=AQ(I,J,L)
      XENQ=X2(J-1)-X2(J)
      XWSR=X2(J-2)-X2(J)
      GO TO 100
C****    M=5....FOR POINTS ON THE WALL OF I=IC AND THOSE ON THE EXIT
5     IF(LX.NE.1) GO TO 1
51    PN=-1.
      DO 50 L=1,14
      BENQ(L)=AQ(I-1,J,L)
      BWSR(L)=AQ(I-2,J,L)
50    BP(L)=AQ(I,J,L)
      XENQ=X1(I-1)-X1(I)
      XWSR=X1(I-2)-X1(I)
100   CONTINUE
      IF(KQ.LT.15) GO TO 101
C****    EVALUATION OF DERIVATIVES FOR V1  (KQ=15) AND V2  (KQ=16)
      BENQ(15)=BENQ(10)/BENQ(12)
      BENQ(16)=BENQ(11)/BENQ(12)
      BWSR(15)=BWSR(10)/BWSR(12)
      BWSR(16)=BWSR(11)/BWSR(12)
      BP(15)=BP(10)/BP(12)
      BP(16)=BP(11)/BP(12)
C****
101   CONTINUE
      ADF=DF(PN,BENQ(KQ),BWSR(KQ),BP(KQ),XENQ,XWSR)
      RETURN
      END
      SUBROUTINE BOUNCT(K)
      COMMON/CVP/A(33,15,9),G1(33,15),G2(33,15),RO(33,15),ZMU(33,15)
      COMMON/CGRID/IMIN(33),IMAX(33),IN,JN,INM,JNM,IE
      COMMON/CNUMBR/NW,NF,NZML,NZMH,NZMC,NZMF,NZMN,NP,NVT
      COMMON/CPARAM/VINJ,VINP(15),TP,PP,TJ,PJ,PHIP,PHIJ
      COMMON/CREFER/ROREF,PREF,ZMUREF,TREF,CPREF,TO
      COMMON/CCONST/PR(9),ZMW(3),CPJ(3),GCPM,GC,ZJC
      COMMON/CYLI/JC1,JC2,IC,RADC1,RADC2,RADN,DCN,DN,JJC2,ICM,JC2M,JC1M
      COMMON/CX1X2/X1(33),X2(15),DELX1(33),DELX2(15)
      COMMON/CHEM/STC,STOX,HFP,HFCO,HFCO2,HFH2O,GLCB(3),ZEX(3)
      COMMON/CRAD/R(15)
      COMMON/CKVORT/KVORT
      COMMON/CNITER/NITER
      COMMON/CINDEX/INDE(9),INDG,INDRO,INDZMU
      FP(ROP,Y,XI2)= -ROP*VINP(J)*(Y-XI2)*((0.5*(Y+XI2))**(INDG-1))
```

```
      FJ(ROJ,Y,XI2)=FBASE+ROJ*VINJ*(Y-XI2)*((0.5*(Y+XI2))**(INDG-1))
      WP(XI2)=0.0*XI2
      WJ(XI2)=0.0*XI2
      WVW(   DELF,WQ,ROP,DELRO,ETA2)= -(    DELF/((ETA2*DX1)**2)
     1                                   +WQ*(ROP/6.+DELRO/8.))
     2                                  /(ROP/3.+5.*DELRO/24.)
      WHW(WK,DELF,WQ,ROP,DELRO,RAD)=  -(    DELF/(DX2*DX2)
     1                                 +WQ*(RAD+WK*DX2)*
     2                                  (ROP*(RAD/6.+WK*DX2/8.)
     3                                  +DELRO*(RAD/8.+WK*DX2/10.)))
     4                            /(RAD*(ROP*(RAD/3.+5.*WK*DX2/24.)
     5                            +DELRO*(5.*RAD/24.+3.*WK*DX2/20.)))
      YY(YN,YP)=1./(1.-(YP/YN)**2)
C*********************************************************************
C    **BOUNDARY** - CONDITONS SUBROUTINE
C    BOUNDARY VALUES FOR ALL THE DEPENDENT VARIABLES
C*********************************************************************
C
C
C*********************************************************************
C    UNIFORM INLET-VELOCITY DISTRIBUTIONS...
C    ZERO AXIAL GRADIENTS FOR ALL DEPENDENT VARIABLES AT EXIT
C    QUADRATIC PROFILE NEAR *ADIABATIC* BOUNDARIES
C*********************************************************************
      GO TO (1,2,3,3,3,3,3),K
C*********************************************
C    FOR STREAM FUNCTION..... A(I,J,NF)
C*********************************************
2     CONTINUE
      IF(NITER.GE.2) GO TO 211
      DO 205 J=1,JN
      IF(INDG.EQ.2) A(1,J,NF)=FP(RO(1,J),RADN,R(J))
  205 IF(INDG.EQ.1)  A(1,J,NF)=FP(RO(1,J),X2(JN),X2(J))
      DO 204 I=1,IC
204   A(I,1,NF)=A(1,1,NF)
      FBASE=A(IC,1,NF)
      DO 207  J=2,JC1
      IF(INDG.EQ.2)  A(IC,J,NF)=FJ(RO(IC,J),R(J),R(1))
  207 IF(INDG.EQ.1)  A(IC,J,NF)=FJ(RO(IC,J),X2(J),X2(1))
      DO 201  I=1,IN
201   A(I,JN,NF)=0.
      DO 208  J=JC1,JC2
  208 A(IC,J,NF)=A(IC,JC1,NF)
      DO 202  I=IC,IN
  202 A(I,JC2,NF)=A(IC,JC2,NF)
211   CONTINUE
      BB=YY(2.*DELX1(IN-1),X1(IN)-X1(IN-1))
      DO 210  J=JJC2,JN
210   A(IN,J,NF)=BB*A(IN-1,J,NF)-(BB-1.)*A(IN-2,J,NF)
299   RETURN
C*********************************************
C FOR MASS FRACTION, ENTHALPY, AND MIXTURE FRACTION
C*********************************************
C
3     BB=YY(2.*DELX2(JNM),X2(JN)-X2(JNM))
      DO 816  I=2,INM
  816 A(I,JN,K)=BB*A(I,JNM,K)-(BB-1.)*A(I,JN-2,K)
      IF  ((JC2-JC1).EQ.1)  GO TO 51
      JJC1=JC1+1
      BB=YY(2.*DELX1(IC-1),X1(IC)-X1(IC-1))
      DO 817  J=JJC1,JC2M
      IF(K.EQ.NZMH) GO TO 301
```

```
      A(IC,J,K)=BB*A(IC-1,J,K)-(BB-1.)*A(IC-2,J,K)
      GO TO 817
  301 AFU=A(IC,J,NZML)
      AH2O=1.634*(A(1,1,NZML)-AFU)+0.00151
      AFC=A(IC,J,NZMC)
      ACO=1.9059*(A(1,1,NZML)-AFU)-0.636*AFC
      A(IC,J,NZMH)=CPREF*(1260.-TO)+AFU*HFP+AH2O*HFH2O+AFC*HFCO2+ACO*HFC
     1O
  817 CONTINUE
51    BB=YY(2.*DELX2(2),X2(2)-X2(1))
      DO 819 I=2,ICM
      A(I,1,K)=BB*A(I,2,K)-(BB-1.)*A(I,3,K)
      IF (K.EQ.NZMF) GO TO 819
      IF(A(I,1,K).LT.0.0) A(I,1,K)=0.5*(A(I,1,K)+A(I,2,K))
      IF(A(I,1,K).LT.0.0) A(I,1,K)=A(I,2,K)
819   CONTINUE
      BB=YY(2.*DELX2(JC2+1),X2(JC2+1)-X2(JC2))
      DO 843  I=IC,INM
      IF(K.EQ.NZMH) GO TO 302
      A(I,JC2,K)=BB*A(I,JC2+1,K)-(BB-1.)*A(I,JC2+2,K)
      GO TO 843
  302 AFU=A(I,JC2,NZML)
      AH2O=1.634*(A(1,1,NZML)-AFU)+0.00151
      AFC=A(I,JC2,NZMC)
      ACO=1.9059*(A(1,1,NZML)-AFU)-0.636*AFC
      A(I,JC2,NZMH)=CPREF*(1260.-TO)+AFU*HFP+AH2O*HFH2O+AFC*HFCO2+ACO*HF
     1CO
  843 CONTINUE
      BB=YY(2.*DELX1(IN-1),X1(IN)-X1(IN-1))
      DO 820 J=JC2,JN
820   A(IN,J,K)=BB*A(IN-1,J,K)-(BB-1.)*A(IN-2,J,K)
      RETURN
C*************************************************
C   FOR VORTICITY.... A(I,J,NW)
C*************************************************
1     CONTINUE
      WK=FLOAT(INDG-1)
      IF(KVORT.NE.1) GO TO 111
      DX2=X2(JN)-X2(JN-1)
      DO 11  I=1,INM
11    A(I,JN,NW)=WHW(-WK,A(I,JN-1,NF),A(I,JN-1,NW),RO(I,JN),
     1               RO(I,JN-1)-RO(I,JN),RADN)
      DX2=X2(JC2+1)-X2(JC2)
      DO 101  I=IC,INM
101   A(I,JC2,NW)= WHW(WK,A(I,JC2+1,NF)-A(I,JC2,NF),A(I,JC2+1,NW),
     1               RO(I,JC2),RO(I,JC2+1 )-RO(I,JC2),RADC2)
      IF ((JC2-JC1).EQ.1)  GO TO 111
      DX1=X1(IC)-X1(IC-1)
      JJC1=JC1+1
      DO 15  J=JJC1,JC2M
15    A(IC,J,NW)=WVW(    A(IC-1,J,NF),A(IC-1,J,NW),
     1               RO(IC,J),RO(IC-1,J)-RO(IC,J), R(J))
111   DO 10 I=1,IC
      IF(INDG.EQ.1) A(I,1,NW)=0.0
      IF(INDG.EQ.2) A(I,1,NW)=
     1          A(I,2,NW)+(X2(2)/(X2(3)-X2(2)))*(A(I,2,NW)-A(I,3,NW))
10    CONTINUE
      DO 17  J=2,JC1
17    A(IC,J,NW)=WJ(X2(J))/R(J)
      BB=YY(2.*DELX1(IN-1),X1(IN)-X1(IN-1))
      DO 18  J=JC2,JN
18    A(IN,J,NW)=BB*A(IN-1,J,NW)-(BB-1.)*A(IN-2,J,NW)
```

```
100   CONTINUE
      RETURN
C*********************************************
C   FOR SWIRL VELOCITY
C*********************************************
4     CONTINUE
      BB=YY(2,*DELX1(IN-1),X1(IN)-X1(IN-1))
      DO 41  J=JC2,JN
41    A(IN,J,NVT)=BB*A(IN-1,J,NVT)-(BB-1.)*A(IN-2,J,NVT)
      RETURN
      END
      SUBROUTINE TABUCT    (ITAB)
      COMMON/CVP/A(33,15,9),G1(33,15),G2(33,15),RO(33,15),ZMU(33,15)
      COMMON/CGRID/IMIN(33),IMAX(33),IN,JN,INM,JNM,IE
      COMMON/CNAME/ATITLE(12),ASYMBL(12),ANAME(6,10)
      COMMON/CRAD/R(15)
      COMMON/CHEM/STC,STOX,HEP,HFCO,HFCO2,HFH2O,GLOB(3),ZEX(3)
      COMMON/CYLI/JC1,JC2,IC,RADC1,RADC2,RADN,DCN,DN,JJC2,ICM,JC2M,JC1M
      COMMON/CNUMBR/NW,NF,NZML,NZMH,NZMC,NZMF,NZMN,NP,NVT
      COMMON/CINDEX/INDE(9),INDG,INDRO,INDZMU
      COMMON/CVARY/NHOT,NPUNCH,NREAD,NPRES
C*****************************************************************************
C   **TABULATE** SUBROUTINE
C   THIS SUBR. TABULATES THE COMPLETE SET OF RESULTS
C*****************************************************************************
      IT=ITAB
      IQ=IT
      IF (INDE(NP).EQ.1) IQ=IT+1
      IF  ((NHOT.EQ.0).AND.(INDE(NP).EQ.1))  IT=IQ
      IF (IE.EQ.5) IQ=IT
      IF ((IE.EQ.6).OR.(NHOT.EQ.0))  GO TO 21
      PRINT 101, (ASYMBL(K),K=1,IE),(ASYMBL(K),K=IT,IQ)
      GO TO 20
21    PRINT 101, (ASYMBL(K),K=1,IE)
20    CONTINUE
      ILINE=0
      DO 1 J=1,JN
      IL=IMIN(J)
      IH=IMAX(J)
      DO 1 I=1,IN
      ILINE=ILINE+1
      IF((I.LT.IL).OR.(I.GT.IH))  PRINT 104, I, J
      IF((I.LT.IL).OR.(I.GT.IH))  GO TO 10
      W=A(I,J,1)*R(J)
      V1=G1(I,J)/RO(I,J)
      V2=G2(I,J)/RO(I,J)
      IF(INDE(NVT).EQ.1) V3=A(I,J,NVT)
      IF(INDE(NVT).EQ.1.AND.R(J).GT.0.0) A(I,J,NVT)=V3/R(J)
      IF  ((IE.EQ.6).OR.(NHOT.EQ.0))  GO TO 22
      PRINT 102, I, J, V1, V2, RO(I,J), ZMU(I,J),W,(A(I,J,K),K=2,IE),
     1 (A(I,J,K),K=IT,IQ)
      GO TO 23
22    PRINT 102, I, J, V1, V2, RO(I,J), ZMU(I,J),W,(A(I,J,K),K=2,IE)
23    CONTINUE
      IF(INDE(NVT).EQ.1) A(I,J,NVT)=V3
10    CONTINUE
      IF (ILINE/IN*IN.EQ.ILINE) PRINT 103
      IF(IE.EQ.6.OR.NHOT.EQ.0) GO TO 24
      IF((IN.LT.33).AND.(ILINE/(2*IN)*(2*IN).EQ.ILINE))  PRINT 101,
     2(ASYMBL(K),K=1,IE),(ASYMBL(K),K=IT,IQ)
      IF((IN.EQ.33).AND.(ILINE/(  IN)*(  IN).EQ.ILINE))  PRINT 101,
     2(ASYMBL(K),K=1,IE),(ASYMBL(K),K=IT,IQ)
```

```
      GO TO 25
24    IF((IN.LT.33).AND.(ILINE/(2*IN)*(2*IN).EQ.ILINE))  PRINT 101,
     2(ASYMBL(K),K=1,IE)
      IF((IN.EQ.33).AND.(ILINE/(  IN)*(  IN).EQ.ILINE))  PRINT 101,
     2(ASYMBL(K),K=1,IE)
25    CONTINUE
1     CONTINUE
101   FORMAT(10H1    I     J,48H          V1            V2        DENSITY
     1VISC   ,6(6X,A6))
102   FORMAT(1H ,2I5,10(1PE12.3))
103   FORMAT(1H )
104   FORMAT(1H ,2I5)
      RETURN
      END
      SUBROUTINE PLOTCT  (ITAB)
      COMMON/CVP/A(33,15,9),G1(33,15),G2(33,15),RO(33,15),ZMU(33,15)
      COMMON/CGRID/IMIN(33),IMAX(33),IN,JN,INM,JNM,IE
      COMMON/CNUMBR/NW,NF,NZML,NZMH,NZMC,NZMF,NZMN,NP,NVT
      COMMON/CINDEX/INDE(9),INDG,INDRO,INDZMU
      COMMON/CNAME/ATITLE(12),ASYMBL(12),ANAME(6,10)
      COMMON/CYLI/JC1,JC2,IC,RADC1,RADC2,RADN,DCN,DN,JJC2,ICM,JC2M,JC1M
      COMMON/CHEM/STC,STOX,HFP,HFCO,HFCO2,HFH2O,GLOB(3),ZEX(3)
      COMMON/CRAD/R(15)
      DIMENSION X(120),XA(9),VJ(9),C(11),Y(41)
      DATA INTVAL,NVJ1/3,7/
      DATA XEMTY,XBOUN,(XA(L),L=1,9)/1H ,1H.,1H1,1H2,1H3,1H4,1H5,1H6,
     1                                1H7,1H8,1H9/
C*************************************************************************
C    **PLOTTING** SUBROUTINE
C    THIS SUBR. GIVES APPROX. CONTOUR-PLOTS OF THE DEPENDENT VAR.
C    ALSO OF TEMPERATURE
C*************************************************************************
C
C****     INTVAL=NUMBER OF LINE-SPACING BETWEEN TWO J-LINES
C****     NVJ=NUMBER OF CONTOUR-LINES TO BE PLOTTED FOR EACH VARIABLE
C
      DO 20 J=1,JN
      DO 20 I=1,IN
      A(I,J,NW)=A(I,J,NW)*R(J)
      IF((INDE(NVT).EQ.1).AND.(R(J).GT.0.0))  A(I,J,NVT)=A(I,J,NVT)/R(J)
20    CONTINUE
      IX=IN/10
      JX=JN/10
      IF(IN.LT.10) IX=1
      IF(JN.LT.10) JX=1
      IQ=ITAB
      DO 900 K=1,IC
      IF(K.EQ.NF)  GO TO 30
      NVJ=NVJ1
      IF  (K.EC.NW)  NVJ=5
      IF(NVJ.EQ.1) NVJ=NVJ1
C****    FINDING MAX., MIN. AND MEAN VALUES IN THE FIELD AND
C****    HENCE DETERMINING THE INTERVALS
      VMIN=A(5,5,K)
      VMAX=A(8,8,K)
      SUM=0.
      NSUM=0
      DO 1 J=1,JN,JX
      II1=IMIN(J)
      II2=IMAX(J)
      DO 1 I=II1,II2,IX
      IF(A(I,J,K).GT.VMAX) VMAX=A(I,J,K)
```

```
      IF(A(I,J,K).LT.VMIN) VMIN=A(I,J,K)
      SUM=SUM+A(I,J,K)
1     NSUM=NSUM+1
      VMEAN=SUM/FLOAT(NSUM)
      VSTEP1=(VMEAN-VMIN)/3.
      VSTEP2=(VMAX-VMEAN)/3.
      VJ(1)=VMIN+VSTEP1
      VJ(2)=VJ(1)+VSTEP1
      VJ(3)=VMEAN
      VJ(4)=VMEAN+VSTEP2
      VJ(5)=VJ(4)+VSTEP2
      VJ(6)=0.95*VMAX
      VJ(7)=1.05*VMIN
C
C SPECIAL VJ VALUES FOR OPPOSED JET PROBLEM
C
      GO TO 8
30    VJ(1)=A(1,3,NF)
      VJ(2)=A(1,(JN-6),NF)
      VJ(3)=A(1,(JN-4),NF)
      VJ(4)=A(1,(JN-2),NF)
      VJ(5)=A(1,(JN-1),NF)
      VJ(6)=A(1,1,NF)
      VJ(7)=A(IC,JC1,NF)
      VJ(8)=1.02*A(IC,JC1,NF)
      VJ(9)=1.05*A(IC,JC1,NF)
      NVJ=9
      GO TO 8
7     NVJ=1
      VJ(1)=STC/(1.+STC)
8     CONTINUE
C  END SPECIAL VJ VALUES FOR C-T PROBLEM
C
C****    PRINT OUT CONSTANT VALUES TO BE PLOTTED
      PRINT 101,ASYMBL(K)
      PRINT 102,(VJ(L),L=1,NVJ)
      PRINT 202
      DO 90 JJ=1,JN,JX
      J=JN+1-JJ
      II1=IMIN(J)
      II2=IMAX(J)
      L1=(IMIN(J)/IX-1/IX)*10+1
      L2=(IMAX(J)/IX-1/IX)*10+1
      L3=(IC/IX)*10-3
      IF (IN.LE.21) L3=(IC/IX)*10
      L4=(IN/IX-1/IX)*10 + 1
      IB=IX-1/IX+IMIN(J)
C****    BOUNDARIES FOR THE PROBLEM
      DO 80 JJN=1,INTVAL
      DO 100 L=1,101
100   X(L)=XEMTY
      X(L1)=XBOUN
      IF  ((J.LE.JC1).AND.(J.GT.1))  L2=L3
      X(L2)=XBOUN
      IF((J.EQ.JN).AND.(JJN.EQ.1))  GO TO 200
      IF((J.EQ.1).AND.(JJN.EQ.1))  GO TO 200
      GO TO 300
200   DO 201 L=L1,L4
201   X(L)=XBOUN
      GO TO 390
300   CONTINUE
C
```

```
C****    SPECIAL BOUNDARIES FOR THE COMBUSTION-CHAMBER PROBLEM
C
      IF (((J.LE.JC2).AND.(J.GT.JC1)).OR.((J.EQ.JC1).AND.(JJN.EQ.1)))
     1  GO TO 405
      GO TO 400
405   DO 406 L=L3,L4
406   X(L)=XBOUN
400   CONTINUE
390   CONTINUE
C****    INTERPOLATION BETWEEN TWO CONSECUTIVE J-LINES
      J1=J-JX
      IF((J.EQ.JC2).AND.(JJN.NE.1)) II2=IC
      DO 70 I=II1,II2
      IF ((J.EQ.1).OR.((J.EQ.JC2).AND.(I.GT.IC)))  GO TO 65
      DELAJ=(A(I,J1,K)-A(I,J,K))/FLOAT(INTVAL)
      GO TO 70
65    DELAJ=0.
70    Y(I)=A(I,J,K)+FLOAT(JJN-1)*DELAJ
C****    INTERPOLATION BETWEEN TWO I-LINES
      DO 60 I=IB,II2,IX
      IMARK=0
      I1=I-IX
      IF(IX.EQ.2) GO TO 71
      GO TO 79
71    DELY1=(Y(I1+1)-Y(I1))/5.
      DO 72   IJK=1,6
72    C(IJK)=Y(I1)+FLOAT(IJK-1)*DELY1
      DELY2=(Y(I)-Y(I1+1))/5.
      DO 73 IJK=7,11
73    C(IJK)=Y(I1+1)+FLOAT(IJK-6)*DELY2
      GO TO 74
79    CONTINUE
      DELY=(Y(I)-Y(I1))/10.
      DO 50 IJK=1,11
50    C(IJK)=Y(I1)+FLOAT(IJK-1)*DELY
74    CONTINUE
      DO 40 KL=1,NVJ
      DO 40 IJK=1,10
      IF((IX.EQ.2).AND.(IJK.LT.6))  DELY=DELY1
      IF((IX.EQ.2).AND.(IJK.GE.6))  DELY=DELY2
      NN=0
      IF((VJ(KL).GE.C(IJK)).AND.(VJ(KL).LE.(C(IJK)+DELY/2.))) NN=IJK
      IF((VJ(KL).GE.(C(IJK)+DELY/2.)).AND.(VJ(KL).LE.C(IJK+1))) NN=IJK+1
      IF((VJ(KL).LE.C(IJK)).AND.(VJ(KL).GE.(C(IJK)+DELY/2.))) NN=IJK
      IF(NN.EQ.0) GO TO 44
      GO TO 41
44    IF((IMARK.EQ.0).AND.(JJN.NE.1).AND.(IJK.EQ.10))  GO TO 45
      GO TO 40
45    DELAJ=(A(I,J1,K)-A(I,J,K))/FLOAT(INTVAL)
      CTOP =A(I,J,K)+FLOAT(JJN-2)*DELAJ
      IF((VJ(KL).LE.(CTOP+DELAJ/2.)).AND.(VJ(KL).GE.(C(11)+DELAJ/2.)))
     1   NN=11
      IF((VJ(KL).GE.(CTOP+DELAJ/2.)).AND.(VJ(KL).LE.(C(11)+DELAJ/2.)))
     1   NN=11
      IF(NN.EQ.0) GO TO 40
41    N1=(I1/IX)*10
      N2=N1+NN
      X(N2)=XA(KL)
      IMARK=1
40    CONTINUE
C****    PLOTTING OF ALL POINTS ON ONE J-LINE
60    CONTINUE
```

```
      IF((JJN.EQ.1).AND.(J.NE.JN))   GO TO 61
      GO TO 62
61    IF((K.EQ.NF).AND.(J.EQ.1))  GO TO 67
802   DO 63 L5=L1,L2,10
63    X(L5)=XBOUN
      IF((K.EQ.NF).AND.(J.EQ.JC2))  GO TO 64
      GO TO 62
64    DO 66 L5=L3,L4,2
66    X(L5)=XBOUN
      GO TO 62
67    DO 69  L5=L1,L3,2
69    X(L5)=XBOUN
62    CONTINUE
      IF (JJN.EQ.1) PRINT 104, J,(X(IP),IP=1, 101)
      IF (JJN.NE.1) PRINT 105, (X(IP),IP=1, 101)
      IF(J.EQ.1)  GO TO 90
80    CONTINUE
90    CONTINUE
      PRINT 302, (IZ,IZ=1,IN,IX)
900   CONTINUE
101   FORMAT(25H1CONSTANT-VALUE PLOT OF  ,A6//23H NUMBERS REFER TO THE
     139HCONSTANT-VALUES PLOTTED,VALUES BEING.../)
102   FORMAT(1H ,3H1= ,1PE12.4,   1H,,3X,
     1           3H2= ,1PE12.4,   1H,,3X,
     2           3H3= ,1PE12.4,   1H,,3X,
     3           3H4= ,1PE12.4,   1H,,3X,
     4           3H5= ,1PE12.4/
     5          4H 6= ,1PE12.4,   1H,,3X,
     6           3H7= ,1PE12.4,   1H,,3X,
     7           3H8= ,1PE12.4,   1H,,3X,
     8           3H9= ,1PE12.4)
103   FORMAT(1H1)
104   FORMAT(1H ,I2,10X,101A1)
105   FORMAT(1H ,12X,101A1)
202   FORMAT(1H0///)
302   FORMAT(1H7//12X,11(I2,8X)/)
      RETURN
      END
      SUBROUTINE PRESCT
      RETURN
      END
```

*U.S. GOVERNMENT PRINTING OFFICE: 1976 - 735-004/19